ASSOCIATIVE ION-MOLECULE REACTIONS AND ION TRAPPING WITH A TRIPLE QUADRUPOLE MASS SPECTROMETER

By

ANTHONY PETER ANNACCHINO, JR.

A DISSERTATION PRESENTED TO THE GRADUATE SCHOOL
OF THE UNIVERSITY OF FLORIDA IN PARTIAL FULFILLMENT
OF THE REQUIREMENTS FOR THE DEGREE OF
DOCTOR OF PHILOSOPHY

UNIVERSITY OF FLORIDA

1993

To my family with love.

ACKNOWLEDGEMENTS

I would like to extend my sincere gratitude to my research advisor, Dr. Richard A. Yost. Had it not been for his support, guidance and patience (and a couple of well-timed lunches at Joe's Deli), I am certain that this work would not have been realized. I would also like to thank the members of my graduate committee, Drs. James D. Winefordner, David H. Powell, John R. Eyler, and Charles L. Beatty.

I would like to acknowledge the U.S. Environmental Protection Agency-Environmental Research Laboratory/Duluth (U.S. EPA-ERL/D) for providing financial support for much of this work. Additionally, I would like to thank Dr. Douglas W. Kuehl of the U.S. EPA-ERL/D for helpful discussions.

I would like to thank all the members of the Yost group, past and present, with whom I have had the pleasure to work during my time here in Gainesville. In particular, I would like to acknowledge two of my office mates and close friends, Uli Bernier and Rafael Vargas. In their company, I was able to enjoy this period of my life and experience such wonders as the "foul towel" and the Bayou Plaza. Fond memories, indeed. I would also like to thank all the friends that I have gained in this community through music. More than once, these friends, and the music that

I shared with them, reinvigorated me when I needed it the most. Also, I was always reminded that there is more to life than graduate school.

I would like to thank my family, Mom, Dad, and Ken, who supported me throughout my studies and always had confidence in me, even during the rough times.

Finally, I would like to express my sincere thanks and love to my fiancée, Jennifer Buckingham. Her companionship and understanding allowed me to devote more time to school than was fair to her. But, then again, she said I would pay later.

TABLE OF CONTENTS

Abstract of Dissertation Presented to the Graduate School
of the University of Florida in Partial Fulfillment of the
Requirements for the Degree of Doctor of Philosophy

ASSOCIATIVE ION-MOLECULE REACTIONS AND ION TRAPPING WITH A TRIPLE QUADRUPOLE MASS SPECTROMETER

By

Anthony Peter Annacchino, Jr.

December 1993

Chairperson: Dr. Richard A. Yost
Major Department: Chemistry

Gas-phase reactions of ionized DNA/RNA bases and nucleosides with electrophilic allyl halides in the collision cell of a triple quadrupole mass spectrometer have been demonstrated. Reactions of this type are important because of their correspondence with the reactions of mutagenic electrophiles with biological macromolecules in vivo. Relative reactivities of the DNA/RNA base and nucleoside ions toward the allyl halides were determined based on the production of allyl-nucleophile adduct ions, P^+. Side reaction products due to charge exchange processes were also observed for many of the reagent combinations. Significant intensities of side reaction products were typically observed only when allyl iodide was used as the electrophile; in many cases the abundance of side reaction products distorted the relative reactivity as measured by P^+ production. Calibration curves for

reactions of each DNA/RNA base ion with allyl halides were generally not linear; limits of detection for the most reactive DNA/RNA base ion, uracil, were on the order of 10-100 femtomoles of allyl halide.

A system for trapping ions in the collision cell of a triple quadrupole mass spectrometer has been developed and characterized. Mass-selected ions are injected into the collision cell and trapped within Q2 for a variable period of time. Subsequently, the ions are gated out of Q2 and mass-analyzed by Q3. Ion optical parameters significant for effective ion trapping have been detailed and optimized. Moreover, the importance of helium buffer gas to Q2 ion trapping has been demonstrated via calculations of ion trapping efficiencies. It has been determined that buffer gas can enhance ion confinement and detection by over 2000%.

Utilizing the Q2 ion trapping system, applications have been demonstrated that illustrate the power and utility of the technique. It has been shown that large numbers of ions can be stored in the collision cell for several hours or more. Furthermore, it was demonstrated that Q2 ion trapping can be used to study ion-molecule reactions. In particular, the method was utilized to enhance formation of product ions resulting from reactions of DNA/RNA base ions with allyl chloride.

CHAPTER 1
INTRODUCTION

In this dissertation studies are presented that demonstrate the utility of associative ion-molecule reactions and ion trapping with a triple quadrupole mass spectrometer (TQMS). Gas-phase reactions of DNA/RNA base and nucleoside ions with electrophilic allyl halides have been studied as an extension of previous work [1] done in our laboratory involving ion-molecule reactions of various electrophiles with small model bases such as pyridine and piperidine. The studies presented here have shown that, while the reactions are often complex, characteristic product ions can signal the presence of potential carcinogens. Furthermore, the method can be used to roughly estimate the relative reactivities of these potential carcinogens. Also, a technique for ion trapping in the collision cell of the TQMS has been developed and characterized. The method allows execution of experiments that are normally impractical, or impossible, to perform on standard tandem quadrupole instruments. In particular, the technique is useful for the study of kinetically slow ion-molecule reactions.

This introductory chapter begins with a review of various analytical techniques that have been utilized for the determination of mutagenic compounds. It continues with a short discussion of ion-molecule reactions in the collision cell of the TQMS. A summary of previous research involving ion trapping with linear RF-only

quadrupoles is then presented and the general mechanism of the trapping method is described. The chapter concludes with an overview of the dissertation.

Methods for the Determination of Mutagenic Compounds

The detection of adducts that result when biological macromolecules such as DNA react with potentially hazardous chemicals such as mutagenic electrophiles is of great importance. These adducts signal modification of DNA molecules and may ultimately lead to carcinogenesis. Several methods have been utilized for the study of modified DNA or model DNA molecules. Via determination of the potential that electrophiles have to form covalent bonds with small DNA models, various analytical techniques have been utilized to study the potential mutagenicities of electrophiles toward DNA [2-6]. Of these, methods involving mass spectrometric characterization of DNA adducts have been particularly significant. Fast atom bombardment (FAB) [7-12], secondary ion mass spectrometry [13] and laser desorption [14] have all been utilized to study modified DNA. Continuous flow-fast atom bombardment (CF-FAB) mass spectrometry has been used to identify DNA adducts [15] as well as water-soluble hydrocarbon conjugates that indicate exposure to carcinogens [16]. Mass spectrometry has also been employed to detect DNA adducts formed via offline electrochemical oxidation [17-19], used to simulate metabolic activation. In addition, gas-phase reactions of pyridine and guanine with polynuclear aromatic hydrocarbons (PAHs) have been conducted in a mass spectrometer ion source [20].

Although many groups have clearly shown that analysis of modified DNA via mass spectrometry is practical, these methods still require batch preparation of the adducts in vitro. This does not allow for rapid analyses and makes the simultaneous determination of mutagenicities for several compounds impossible. To alleviate these limitations a method has been developed, as is described in the following section, that allows for the real-time determination of potential carcinogens via ion-molecule reactions in the collision cell of a TQMS.

Ion-Molecule Reactions in the Collision Cell of a Triple Quadrupole Mass Spectrometer

Certainly, the most frequently utilized type of ion-molecule process that takes place in the collision cell of a triple quadrupole mass spectrometer (TQMS) is collision-induced dissociation (CID). The pioneering research of Yost et al. [21] showed that CID can be accomplished with high efficiency in the collision cell of a TQMS and spawned the development of several commercially available triple quadrupole mass spectrometers, including the Finnigan MAT TSQ70. In turn, CID has been utilized by many researchers [22-24] in analytical tandem mass spectrometry (MS/MS) to fragment ions for mixture analysis or structure elucidation.

Although CID in the collision cell of a TQMS is a widely used technique, the study of other types of ion-molecule reactions performed in the collision cell has become increasingly common as researchers realize the potential utility of the method [25-32]. Charge exchange mass spectra have been obtained on a double quadrupole mass spectrometer [33] via mass-selection of appropriate reagent ions by

the first quadrupole (Q1) and reaction with neutral cyclohexene and benzene molecules in the interquadrupole region. Similar studies have been performed with a triple quadrupole mass spectrometer [34-35] in which various reactant ions were mass-selected by Q1 for subsequent charge exchange, proton transfer and hydride abstraction chemical ionization reactions in the collision cell. This research demonstrated that control of the energetics of the charge exchange and proton transfer processes could be achieved, facilitating the interpretation of the resulting mass spectra. Ion-molecule reactions in the collision cell have also been utilized to synthesize covalently bonded adduct ions between protonated esters and ammonia [36]. Reactions between both the neutral and ionic species of vinylmethylether and propene have been investigated with a triple quadrupole mass spectrometer [37] in order to elucidate the mechanism of the reaction under CI conditions in the ion source. Furthermore, the dependence of the protonation of neutral ammonia on the translational energy of protonated reactant ions has been studied in the gas phase inside the collision cell of a TQMS [38]. The ion-molecule reaction of the tolyl cation with dimethyl ether has also been investigated using triple quadrupole mass spectrometry [39].

In this dissertation, results from investigations of mass-selected reactions in the collision cell between DNA/RNA base and nucleoside ions and allyl halides are presented. These studies allowed for the determination of the relative reactivities of the nucleophilic base and nucleoside ions toward the allyl halides. Furthermore, predominant side reactions were systematically identified and correlated, as their

presence frequently caused the measured reactivities of the nucleophiles to be much lower than expected. The ability to detect gas-phase ion-molecule reaction products between mutagenic/carcinogenic electrophiles and simple base ions (e.g., the molecular ion of pyridine) which model DNA has been demonstrated previously in our laboratory [1,40]. The technique is unique in that electrophilic mutagens may be separated and characterized on a chromatographic time scale. Thus, the method allows samples to be rapidly screened for the presence of mutagens. Furthermore, the results of the investigations compared well to those for other methods used to estimate mutagenicities, such as the Ames test [41-42].

Trapping Ions with Linear RF-only Multipole Devices

The motivation to study ion trapping in the collision cell of a triple quadrupole mass spectrometer (TQMS) was partly due to the general popularity of other types of ion trapping apparatus. Quadrupole ion trap mass spectrometers (QITMS) and Fourier-transform ion-cyclotron resonance (FT-ICR) instruments are the two most common types of ion trapping devices. The quadrupole ion trap mass spectrometer [43-45] is essentially the three-dimensional analogue of the quadrupole mass filter [46-48]. Ions over a range of m/z values are trapped by appropriately selected RF and DC voltages applied to the two endcap electrodes and a doughnut-shaped ring electrode. A mass spectrum is produced by ramping the RF potential such that ions of successively higher m/z values become unstable and strike the electron multiplier detector behind the endcap. The ICR instrument [49-50]

operates on the principle that ions in a magnetic field move in circular orbits at frequencies characteristic of their m/z values. Ion detection is achieved via image currents that are generated in the receiver plates due to ions excited by a frequency-swept excitation signal. Because this signal contains all the excitation frequencies, the ions transmit a complex RF signal that contains the frequency components characteristic of all the ions. The resulting time-dependent image current is subjected to Fourier transformation, which produces the data for the mass spectrum.

Ion trapping in the collision cell (Q2) of a triple quadrupole mass spectrometer was first demonstrated by Yost [51] in 1982. It was proposed that the trapping of ions in the center quadrupole would provide a way to study the energetics of the CID process, as well as provide enhanced fragmentation patterns for particularly stable ions. Since then, only a few research groups have performed ion trapping experiments with linear RF-only devices. Beaugrand et al. [52-53] performed the first definitive work utilizing Q2 ion trapping for studies of collision-induced dissociation, decomposition of metastable ions, and ion-molecule reactions. It was shown that ion storage time can dramatically affect the relative abundances of the resulting product ions for each of these processes. Further investigations by Beaugrand et al. [54-55] demonstrated the utility of the technique for the study of the kinetic and, in some cases, thermodynamic parameters of gas-phase reactions resulting from the interaction of ammonium ions with a mixture of piperidine and pyrrolidine. Similar instrumentation and procedures required for Q2 ion trapping have been developed independently by Dolnikowski et al. [56]. The technique has

been utilized by this group to study acetone dimerization and protonation [56] reactions as well as ion-molecule reactions between protonated acetaldehyde and methanol [57].

Ions are trapped in a linear RF-only quadrupole (or octopole) by a combination of two mechanisms. Ions are confined in two dimensions by the RF potential applied to the rods of the quadrupole, as defined by the stability diagram (Figure 1-1). As is shown in Figure 1-1, ion trajectories within a quadrupole device can be either stable or unstable depending on the values of the Mathieu parameters q_u and a_u, which are related to the applied RF and DC potentials, respectively. The values of the parameters are defined by

$$q_u = \frac{4V_{RF}\,e}{mr_o^2\omega^2} \tag{1-1}$$

$$a_u = \frac{8V_{DC}\,e}{mr_o^2\omega^2} \tag{1-2}$$

where V_{RF} is the zero-to-peak RF voltage with an angular frequency of ω, V_{DC} is the DC potential, e is the charge of the ion, m is the mass of the ion, and r_o is the inscribed radius of the quadrupole. Ions that have Mathieu parameters within the triangular envelope of the stability diagram have stable trajectories and are transmitted through the device. When operated as a mass filter, RF and DC potentials are applied to the rods (in addition to a supplemental DC voltage, the offset potential, which determines the translational energy of the ions) such that only

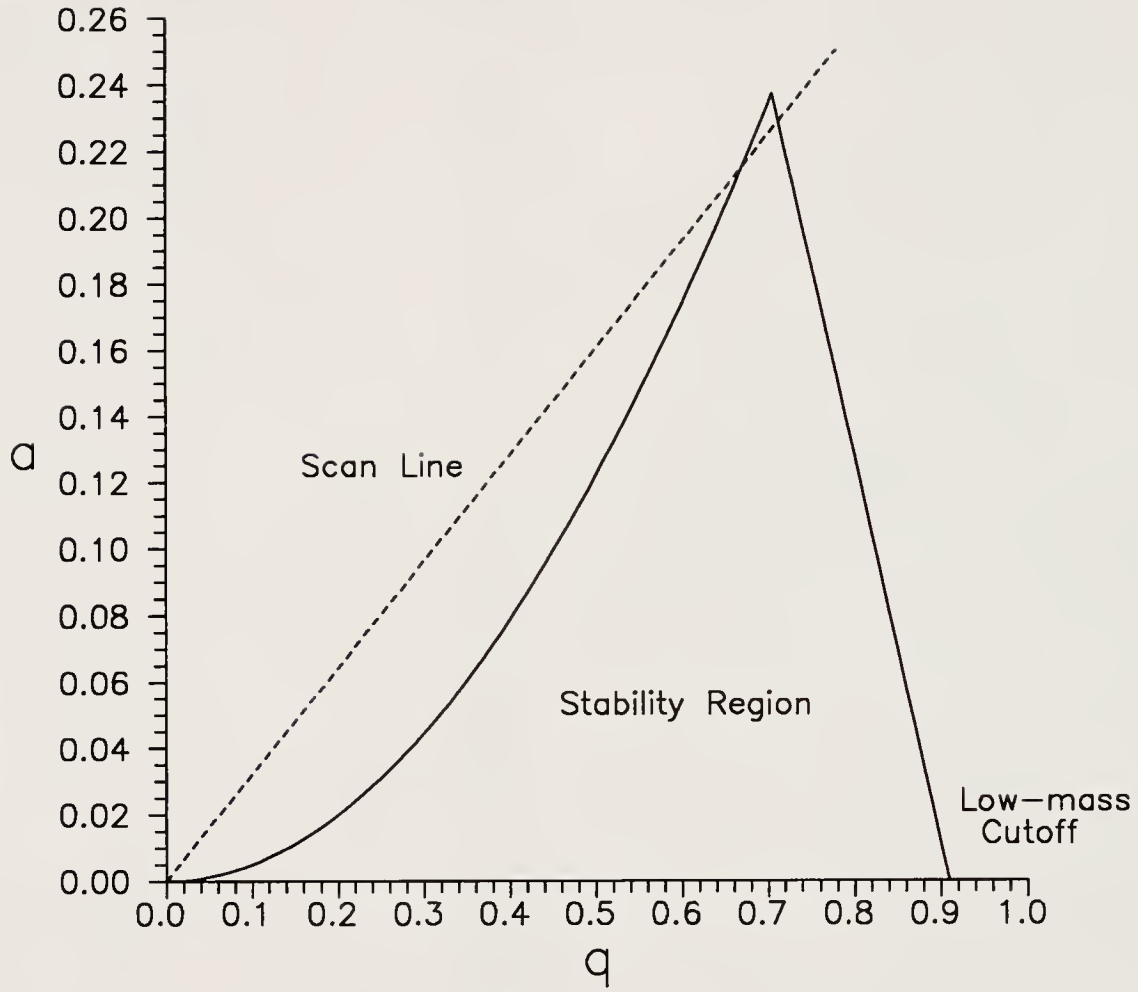

Figure 1-1: Stability diagram for the quadrupole mass filter.

masses in a narrow band are stable at one time. This is achieved by operating the device over a scan line that intersects the apex of the stability diagram that defines the RF/DC ratio. This ratio, in turn, determines the range of masses that are stable. By continually increasing the RF and DC potentials linearly with time (but at a constant RF/DC ratio), ions of increasing m/z are brought within the window of stability and a mass scan is obtained.

Operation of the quadrupole mass filter as an RF-only device (such as the collision cell in a TQMS) is a much simpler proposition since no DC potentials (other than the offset voltage) are applied to the quadrupole rods. Looking at Figure 1-1, this means that ions are stable all along the x-axis up until a value of q=0.908 where low masses become unstable (see Equation 1-1). This point is termed the low-mass cutoff of the device. By carefully selecting an appropriate RF potential, however, a wide range of masses can be stable within an RF-only quadrupole, making it suitable for applications such as a collision cell.

It should be noted that the collision cell of the TSQ70 used for the studies presented here is an RF-only octopole. Nonetheless, in general the basic operating principles of the RF-only quadrupole presented above are also applicable to the RF-only octopole. Even though a stability diagram cannot be explicitly defined for an octopole mass filter due to nonlinear and coupled ion motions [58], a stability envelope still exists, as does the low-mass cutoff. This, in effect, allows the RF-only octopole to be operated similarly to an RF-only quadrupole.

While the time-varying electric field produced by the RF potential confines the ions radially in two dimensions, the DC potentials applied to the lenses immediately before and after the collision cell can be employed to trap ions axially (in the third dimension). In this way, Q2 ion trapping can be likened to the trapping mechanism of a Fourier-transform ion-cyclotron resonance (FT-ICR) mass spectrometer [49-50] where ions are confined magnetically in two dimensions while DC potentials applied to the trapping plates trap ions in the third dimension.

Organization of Dissertation

This dissertation is organized into six individual chapters. Chapter 1 has presented a general overview of the topics to be discussed in the bulk of the dissertation and has also provided an overall perspective of the research. To begin with, various methods used in the determination of mutagenic compounds were described, focusing primarily on mass spectrometric techniques. Additionally, previous studies involving ion-molecule reactions in the collision cell were discussed. Furthermore, a discussion of ion trapping in the collision cell of a triple quadrupole mass spectrometer was presented along with a review of previous ion trapping studies performed using linear quadrupoles.

Chapter 2 presents research involving reactions of nucleophilic DNA/RNA base and nucleoside ions with electrophilic allyl halides in the collision cell of the triple quadrupole mass spectrometer (TQMS). A brief description of the technique of performing ion-molecule reactions in the collision cell is provided. The main part

of the chapter focuses on characterization of the reaction products that are observed for the electrophile/nucleophile reactions. In addition, the relative reactivities of the DNA/RNA base and nucleoside ions are reported and compared. These relative reactivities can provide a rough estimate for the mutagenicities of the allyl halides, even though side reactions often predominate for these processes and subsequently render the relative reactivity measurements inaccurate.

Chapter 3 describes several practical aspects that must be considered when studying collision cell reactions of DNA/RNA base and nucleoside ions with allyl halides. In particular, the effects of allyl halide pressure on reaction products are described and characterized. Also, calibration studies of reactions of DNA/RNA base ions with allyl halides are presented. Some nucleophiles are much more sensitive (due to higher reactivities) towards allyl halides than others and thus provide lower limits of detection.

Chapter 4 describes the development and characterization of a system for trapping ions in the collision cell of the TSQ70 triple quadrupole mass spectrometer. The unique ion optical design of the TSQ70, particularly the octopole collision cell, is discussed. The mechanism of the Q2 ion trapping technique is described, and key ion optical parameters that are important for efficient Q2 ion trapping are noted. Furthermore, studies are presented that show that helium buffer gas greatly improves Q2 ion trapping performance. Also, the various methods that were utilized during the development of the Q2 ion trapping system are discussed in detail. Finally, specially written Instrument Control Language (ICL) procedures used to control ion

trapping experiments and tune the instrument for Q2 ion trapping are described, with details provided in Appendix B.

Chapter 5 reports several investigations that utilized the Q2 ion trapping system described in Chapter 4. The section begins with a discussion of the mass scanning parameters (scan time, scan range, etc.) required when acquiring Q2 trapping data. Several examples of ion accumulation in the collision cell are then presented. If precautions are not taken, ions can amass in Q2 from cycle to cycle and cause erroneous results for ion-molecule reaction studies. Examples are then shown that indicate the maximum number of ions that the collision cell can accommodate. Also, investigations concerning ion trapping efficiencies for long confinement times are discussed. A method to obtain full scan data under ion trapping conditions is demonstrated, and the accompanying ICL procedures are described. The chapter concludes by evaluating several ion-molecule reactions using the Q2 ion trapping system. In particular, enhanced product ion formation is demonstrated for reactions of DNA/RNA base ions with allyl chloride.

Chapter 6 draws general conclusions about the research presented in the dissertation. In addition, several ideas for future studies are suggested.

CHAPTER 2
REACTIONS OF DNA/RNA BASE AND NUCLEOSIDE IONS WITH ALLYL HALIDES

This chapter describes studies of ion-molecule reactions in the collision cell of a triple quadrupole mass spectrometer to evaluate the reactivities of a series of mutagenic allyl halides toward DNA/RNA base and nucleoside ions. In performing these studies, the method initially developed with small model nucleophiles [1,40] has been substantiated via the use of actual DNA/RNA bases and nucleosides. Additionally, performing these ion-molecule reactions for four DNA/RNA bases and their corresponding nucleosides has allowed the determination of their relative reactivities toward the allyl halides. Also, predominant side reactions have been systematically identified and correlated. As these reactions were often extensive, their occurrence frequently caused the measured reactivities of the nucleophiles to be much lower than expected. Thus, the ability to understand and predict these side reactions is important for the results to be meaningfully interpreted.

Introduction

Ionization of DNA/RNA Bases and Nucleosides

Previous studies [1] have demonstrated that, in contrast to the molecular ions of nucleophiles produced by electron ionization (EI), $N^{+\cdot}$, protonated nucleophiles,

$[N+H]^+$, generally have little or no reactivity toward these mutagenic allyl halides. This lack of reactivity reflects the protonation of the (most) basic site of the nucleophile, reducing or eliminating the neutral's nucleophilicity. Whereas the DNA and RNA bases, with the exception of guanine, are thermally stable and volatile enough to produce $N^{+\cdot}$ ions by EI, the nucleosides are thermally labile, producing primarily the base ion due to loss of the ribose moiety. Commonly used soft ionization techniques such as chemical ionization (CI) [59], fast-atom bombardment (FAB) [60-62], electrospray (ESI) [63-65], and matrix-assisted laser desorption ionization (MALDI) [66-68] produce abundant protonated molecules, $[N+H]^+$, as well as adducts such as $[N+Na]^+$ and $[N+K]^+$, and are thus inappropriate for these studies.

Because of the problems with the ionization methods described above, benzene charge exchange [69-71] ionization was utilized to produce nucleoside $N^{+\cdot}$ ions. Chemical ionization via charge exchange can be a relatively soft ionization method if an appropriate reagent is selected [34-35,72]. Typically, charge exchange ionization will occur if the recombination energy (RE) of the reactant ion, $R^{+\cdot}$, is greater than the ionization energy (IE) of the sample molecule, N. The degree of fragmentation is determined by the difference between the RE of the reactant ion and the IE of the sample molecule. As indicated in Table 2-1, when performing charge exchange using benzene reagent gas very little energy is transferred to the sample molecules because of the relatively low recombination energy of $C_6H_6^{+\cdot}$ ions (RE=9.25 eV) compared to the ionization energies of the nucleosides (e.g.,

Table 2-1: Relevant properties of compounds used in these studies.

Compound	Ionization Energy, eV[a,b]	Proton Affinity, kcal/mol[a]	Gas Phase Basicity, kcal/mol[a]
Benzene	9.25	181.3	NF[c]
Allyl chloride	9.90	NF	NF
Allyl bromide	10.06	NF	NF
Allyl iodide	9.30	NF	NF
Pyridine	9.25	220.8	213.1
Adenine	7.80	223.5	215.7
Cytosine	8.45	223.8	216.0
Thymine	8.80	208.8	201.0
Uracil	9.20	208.0	200.0
Adenosine	NF	NF	NF
Cytidine	NF	NF	NF
Thymidine	NF	208.0	NF
Uridine	9.00	208.0	NF

[a] Values taken from reference 73.
[b] Recombination energies for the associated molecular ions are approximately equal in magnitude to the ionization energies of the neutral molecules.
[c] NF = no literature reference was found.

$IE_{uridine}$=9.00 eV). This minimizes fragmentation and provides the maximum intensity of molecular ion ($N^{+\cdot}$) for subsequent reactions in the collision cell.

Technique of Performing Ion-Molecule Reactions in Q2

The technique of performing such ion-molecule reactions in the second quadrupole (collision cell, Q2) of a triple quadrupole mass spectrometer has been described previously [40]. Also, the concepts and instrumentation required for GC introduction into the collision cell were reported [35]. A brief discussion of the method is offered here. The technique involves ionization of a nucleophile (DNA/RNA base or nucleoside) and mass-selection of nucleophile ions (normally molecular ions, $N^{+\cdot}$) with the first quadrupole (Q1). These ions then pass into the collision cell at low energies (1-2 eV) and subsequently react with volatile electrophiles (the allyl halides) eluting from a gas chromatograph (GC) into the collision cell (Q2). The third quadrupole (Q3) then scans over a mass range such that any product or fragment ions that may result are detected. The resultant mass chromatograms thus identify product ions with m/z values that correspond to formation of particular adduct ions. Figure 2-1 illustrates a typical ion-molecule reaction involving a DNA base ion and an allyl halide. In this case, radical molecular ions ($N^{+\cdot}$) of the nucleophile cytosine are mass selected to react in the collision cell with neutral allyl chloride to yield product ions of m/z 152. The product ions are formed by nucleophilic substitution of the allyl chloride and loss of the neutral $Cl^{\cdot}$ radical.

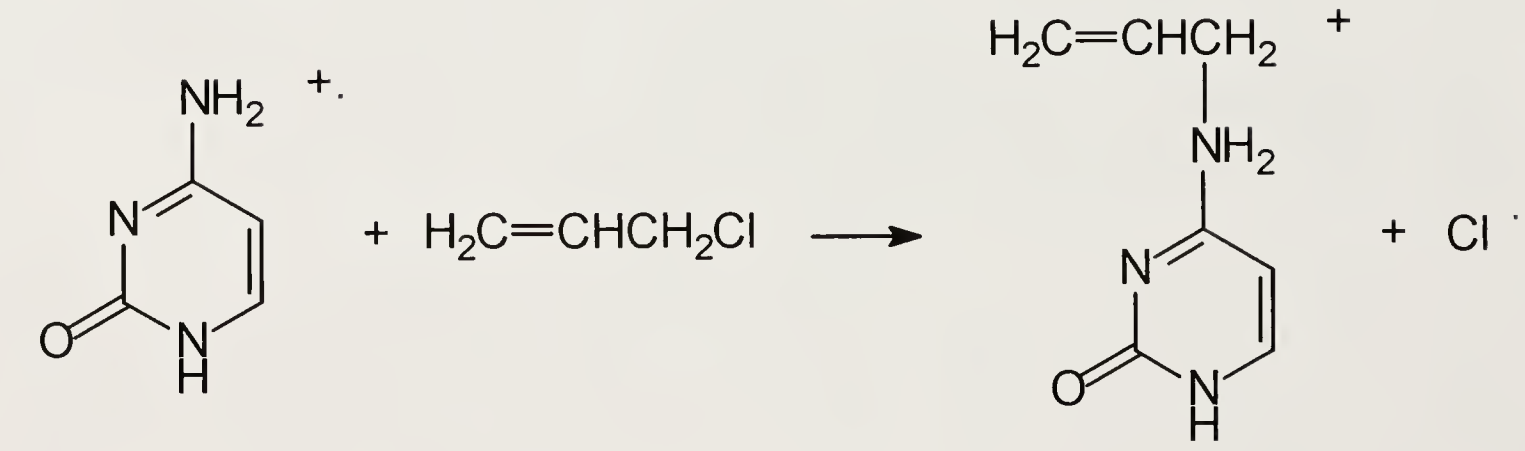

Cytosine Ion (N^+) m/z 111

Allyl Chloride

Product Ion (P^+) m/z 152

Figure 2-1: Collision cell reaction of mass-selected cytosine ions and neutral allyl chloride.

Experimental

Chemicals

Nucleophiles investigated included pyridine and the DNA/RNA bases (adenine, cytosine, guanine, thymine and uracil) and nucleosides (adenosine, cytidine, thymidine and uridine), which were purchased from Sigma Chemical Company (St. Louis, MO). The structures of these bases and nucleosides are shown in Figures 2-2 and 2-3, respectively. Allyl bromide, allyl chloride and allyl iodide were acquired from Aldrich Chemical Company (Milwaukee, WI). HPLC grade pentane solvent and benzene, utilized for charge exchange ionization of the nucleosides, were obtained from Fischer Scientific (Fairlawn, NJ). High purity helium carrier gas and nitrogen collision gas were purchased from Liquid Air Corporation (Walnut Creek, CA). Argon was acquired from Matheson Gas Products (East Rutherford, NJ).

Instrumentation

All experiments were performed on a Finnigan MAT (San Jose, CA) TSQ70 triple quadrupole mass spectrometer modified with an octopole collision cell and a 20 kV dynode. The mass spectrometer was equipped with a Varian (Walnut Creek, CA) 3400 gas chromatograph, interfaced to the collision cell, Q2, via a resistively heated transfer line [35]. Experiments were performed at an emission current of 200 μA, an electron energy of 70 eV (100 eV for CI conditions), a manifold temperature of 100°C, and an ion source temperature of 170°C (150°C for CI conditions). The

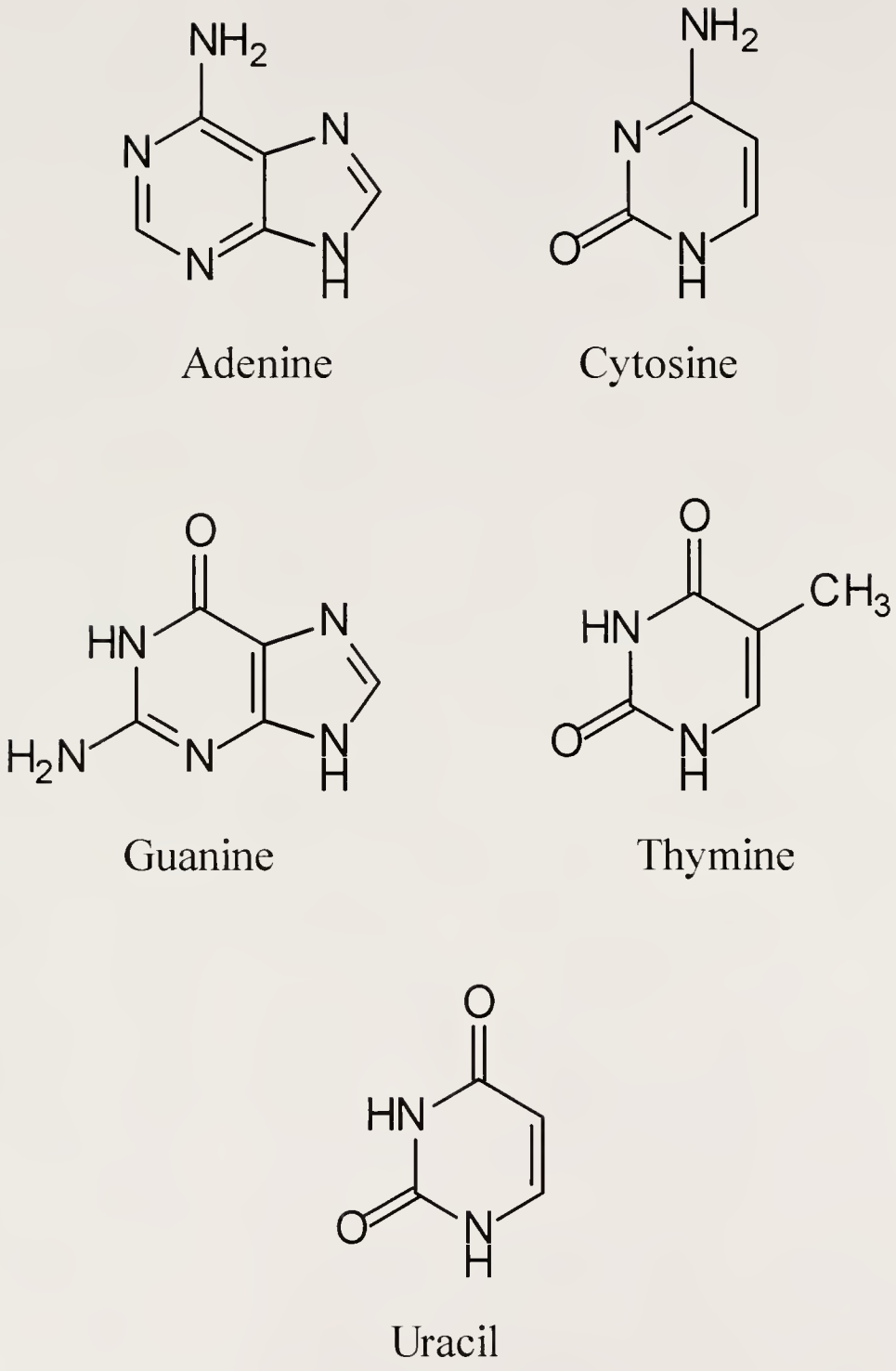

Figure 2-2: DNA/RNA bases used in these studies.

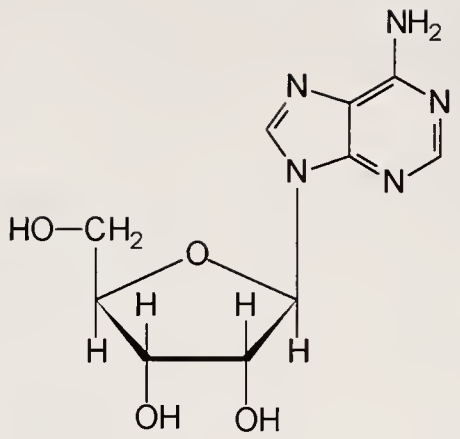

Adenosine

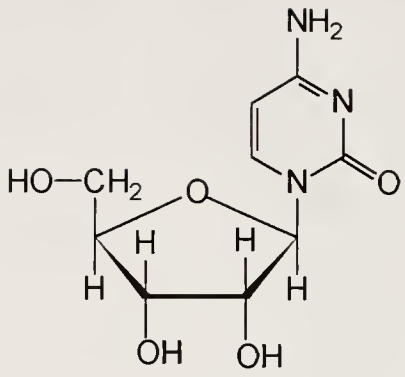

Cytidine

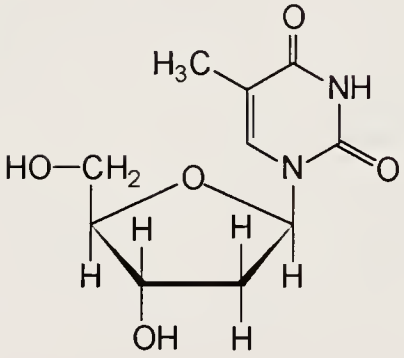

Thymidine

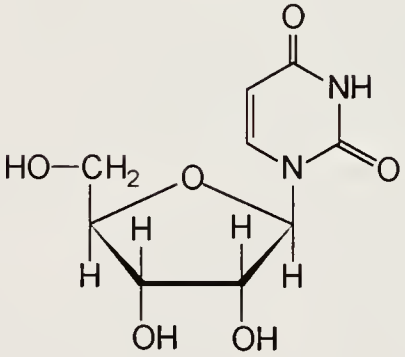

Uridine

Figure 2-3: Nucleosides used in these studies.

mass spectrometer was mass-calibrated using perfluorotributylamine (PFTBA) and then tuned to maximize product ion formation for low-energy ion-molecule reactions in the collision cell. The details involved in these tuning optimizations are presented in Appendix A.

For all studies, gas chromatography was carried out on a J & W Scientific DB-5 (17 m long, 0.178 mm i.d., 0.4 μm film thickness) capillary column in the split mode (split ratio = 100:1) with helium carrier gas at an inlet pressure of 5 psig. The GC oven was temperature programmed from 50°C to 100°C at 20°C/min with an injection port temperature of 200°C and a transfer line temperature of 200°C. One microliter injections were made in triplicate of mixtures containing equimolar amounts of allyl chloride, allyl bromide and allyl iodide in pentane ranging in concentrations from 40 pmol/μL to 3 μmol/μL.

Procedures

Bases and nucleosides contained in capped aluminum vials were introduced into the ion source via a heated solids probe. The solids probe temperature was precisely adjusted in each case to give a steady ion current of constant intensity. The DNA/RNA bases were ionized by electron ionization (EI), and the nucleosides were ionized under CI conditions using benzene charge exchange at an ion source pressure of approximately 100 mTorr, indicated by a Granville Phillips (Boulder, CO) Convectron gauge. Investigations to determine the relative reactivities of guanine and guanosine ions were not pursued due to the inability to achieve the sufficient,

and constant, ion intensities needed for reaction with the allyl halides as they elute from the GC. At the solids probe temperatures required for vaporization of guanine and guanosine (>300°C), sample decomposition readily occurs, thus the quantities of molecular ion needed for the experiments were not attainable. However, using a direct exposure probe (DEP), it was possible to produce brief intensities of guanine molecular ions that could then react separately with each of the allyl halides introduced into the collision cell via a leak valve.

Reference electron ionization (EI) spectra were taken of all the DNA/RNA bases and nucleosides used in the study. Also, reference spectra using benzene charge exchange ionization were acquired for the nucleosides. MS/MS daughter ion spectra were obtained for the molecular ions (either $N^{+\cdot}$ or $[N+H]^+$) of each of the DNA/RNA bases and nucleosides in order to help decipher the complicated product ion spectra. In an attempt to predict what charge exchange products may be observed, daughter ion spectra were taken when allowing mass selected argon ions (I.E.=15.76 eV) to react with the allyl halides in the collision cell. For all of these studies, instrumental conditions, including collision energy, collision gas pressure and reagent gas pressure, were optimized for maximum sensitivity of the ions of interest.

Reactions of DNA/RNA Base and Nucleoside Ions with Allyl Halides

Selection of Molecular Ions or Protonated Molecules for Reactions

As was stated earlier, protonated molecules, $[N+H]^+$, of many small DNA/RNA models are quite unreactive toward the allyl halides. In particular, it has

been demonstrated [1] that, while the $[N+H]^+$ ion of piperidine is reactive toward the allyl halides, the protonated molecule of pyridine is not. Therefore, in all cases except reactions performed with cytidine, $N^{+\cdot}$ molecular ions were mass-selected for subsequent reactions with allyl halides in Q2. Cytidine, however, produced a much higher intensity of $[N+H]^+$ than $N^{+\cdot}$ under benzene charge exchange conditions, and only the $[N+H]^+$ ions were reactive toward the allyl halides. Indeed, cytidine was the only nucleoside that produced a reactive $[N+H]^+$ species. The reason for the unusual reactivity of cytidine $[N+H]^+$ ions is unclear, but it may be that cytidine has a higher gas-phase basicity (or proton affinity) than any of the other nucleosides. Values of gas-phase basicities for the nucleosides are not recorded in the literature; but to the extent that the basicities of the corresponding DNA/RNA bases are an indication of the basicities of the related nucleosides, then this theory may be correct. Table 2-1 shows that cytosine, which also produces a reactive $[N+H]^+$ species, has the highest gas-phase basicity (and proton affinity) of the DNA/RNA bases used in this study. This suggests that cytidine would also have a proportionately large gas-phase basicity compared to the other nucleosides and would explain why cytidine forms almost exclusively $[N+H]^+$ ions under benzene charge exchange ionization.

Cytidine $[N+H]^+$ ions retain reactivity toward the electrophilic allyl halides because there are three potentially basic amine sites on the neutral molecule. Even with one site protonated to form $[N+H]^+$, the ion evidently still is basic enough to react with the allyl halides. Given that some basicity remains when the cytidine molecule is protonated, one might expect that the other nucleosides would produce

reactive $[N+H]^+$ species as well, since they too each have more than one basic site. One way to roughly estimate the basicities of the potentially reactive sites on each DNA/RNA base or nucleoside is to examine their acid dissociation constants (pK_{a1}, pK_{a2}, and pK_{a3}) in aqueous solution, as listed in Table 2-2. Although none of the DNA/RNA bases or nucleosides are basic enough to exist as diprotonated ions in solution, the pK_{a1} values for the association of one proton can provide some insight into the relative basicities of the free protonated molecules. It is clear that cytidine is the most basic of the nucleosides in solution and that only cytidine and adenosine exist primarily as protonated molecules at low pH. Furthermore, of the DNA/RNA bases, adenine and cytosine are the most basic. This suggests that the $[N+H]^+$ ions of adenine and adenosine, as well as those of cytosine and cytidine, might be reactive toward the allyl halides. Indeed, experiments have shown that adenine $[N+H]^+$ ions do react slightly with allyl iodide to produce the $[N+H+41]^+$ species, although protonated molecules of adenosine do not show any reactivity at all. The lack of reactivity of the adenosine $[N+H]^+$ species may be due to the intrinsically low reactivity of adenosine, in general, as is discussed below. Moreover, the somewhat lower pK_{a1} value of adenosine may indicate that the protonated molecule of adenosine is less basic, and less reactive, than that of cytidine.

It is surprising that, unlike the $[N+H]^+$ species, cytidine $N^{+\cdot}$ ions are not reactive toward the allyl halides. One would expect $N^{+\cdot}$ ions to always be more reactive than $[N+H]^+$ ions since, presumably, the $N^{+\cdot}$ species is more basic than the protonated molecule. The lack of reactivity of the cytidine $N^{+\cdot}$ species is probably

Table 2-2: Acid dissociation constants for DNA/RNA bases and nucleosides.

Base or Nucleoside (B)	pK_{a1}[a,b]	pK_{a2}[a,c]	pK_{a3}[a,d]
Adenine	4.15	9.8	NF[e]
Cytosine	4.45	12.2	NF
Thymine	0	9.9	>13.0
Uracil	0.5	9.5	13.0
Adenosine	3.63	12.5	NF
Cytidine	4.22	12.5	NF
Thymidine	NF	9.8	>13.0
Uridine	NF	9.17	12.5

[a] Values taken from reference 74.
[b] For the reaction $BH^+ \rightleftharpoons B + H^+$.
[c] For the reaction $B \rightleftharpoons [B\text{-}H]^- + H^+$.
[d] For the reaction $[B\text{-}H]^- \rightleftharpoons [B\text{-}2H]^{2-} + H^+$.
[e] NF = no literature reference was found.

a reflection of cytidine's very high proton affinity; the $N^{+\cdot}$ ion may preferentially add a hydrogen atom from allyl halide to form $[N+H]^+$ instead of adding the allyl group. In other words, the side reaction that forms $[N+H]^+$ may be so favorable that P^+ ($[N+41]^+$) is not observed. This argument is supported by the fact that cytidine produces much more $[N+H]^+$ than $N^{+\cdot}$ when ionized under benzene charge exchange conditions, while the other nucleosides readily form $N^{+\cdot}$ ions.

Relative Reactivities of DNA/RNA Base and Nucleoside Ions

Results of a typical experiment are shown in Figures 2-4 and 2-5. In this case, uracil $N^{+\cdot}$ ions (m/z 112) were allowed to react with allyl halides (5.6 nmol each) eluting from a GC column into Q2. Upon inspection of the m/z 153 mass chromatogram in Figure 2-4, it is clear that product ions, P^+, corresponding to $[N+41]^+$ ions were easily detected as the three allyl halides eluted from the GC. Relative reactivities of the individual DNA/RNA base and nucleoside ions toward the allyl halides were calculated using peak areas from mass chromatograms such as those in Figure 2-4. Looking at Figure 2-4, negative peaks in the m/z 112 chromatogram correspond to elution of the three allyl halides to form m/z 153. The large negative peak at a retention time of 1.1 minutes coincides with the elution of the n-pentane solvent, which causes extensive ion scattering. Due to probable column overload, some allyl halide also elutes with the solvent and gives rise to a corresponding peak in the m/z 153 chromatogram. The mass spectrum of this peak shows that m/z 113 is produced as well as a small amount of m/z 153. The shoulders

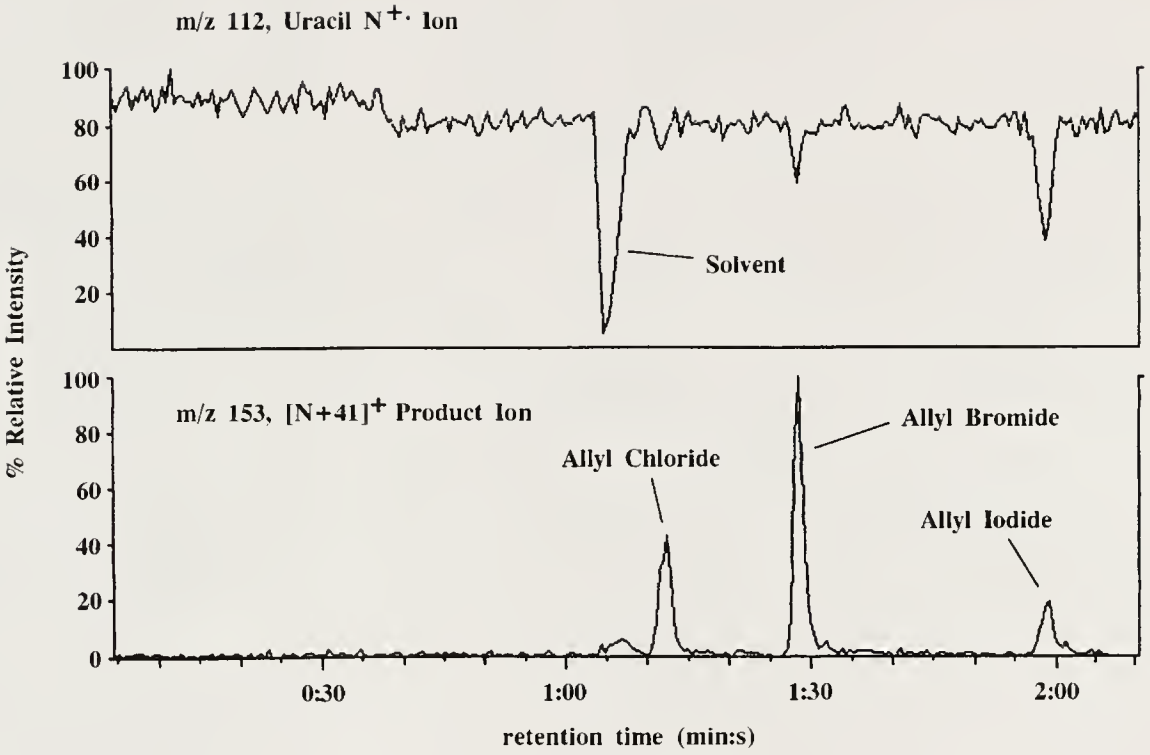

Figure 2-4: Mass chromatograms for uracil $N^{+\cdot}$ ions (m/z 112) reacting with allyl halides in the collision cell to form product ions of m/z 153.

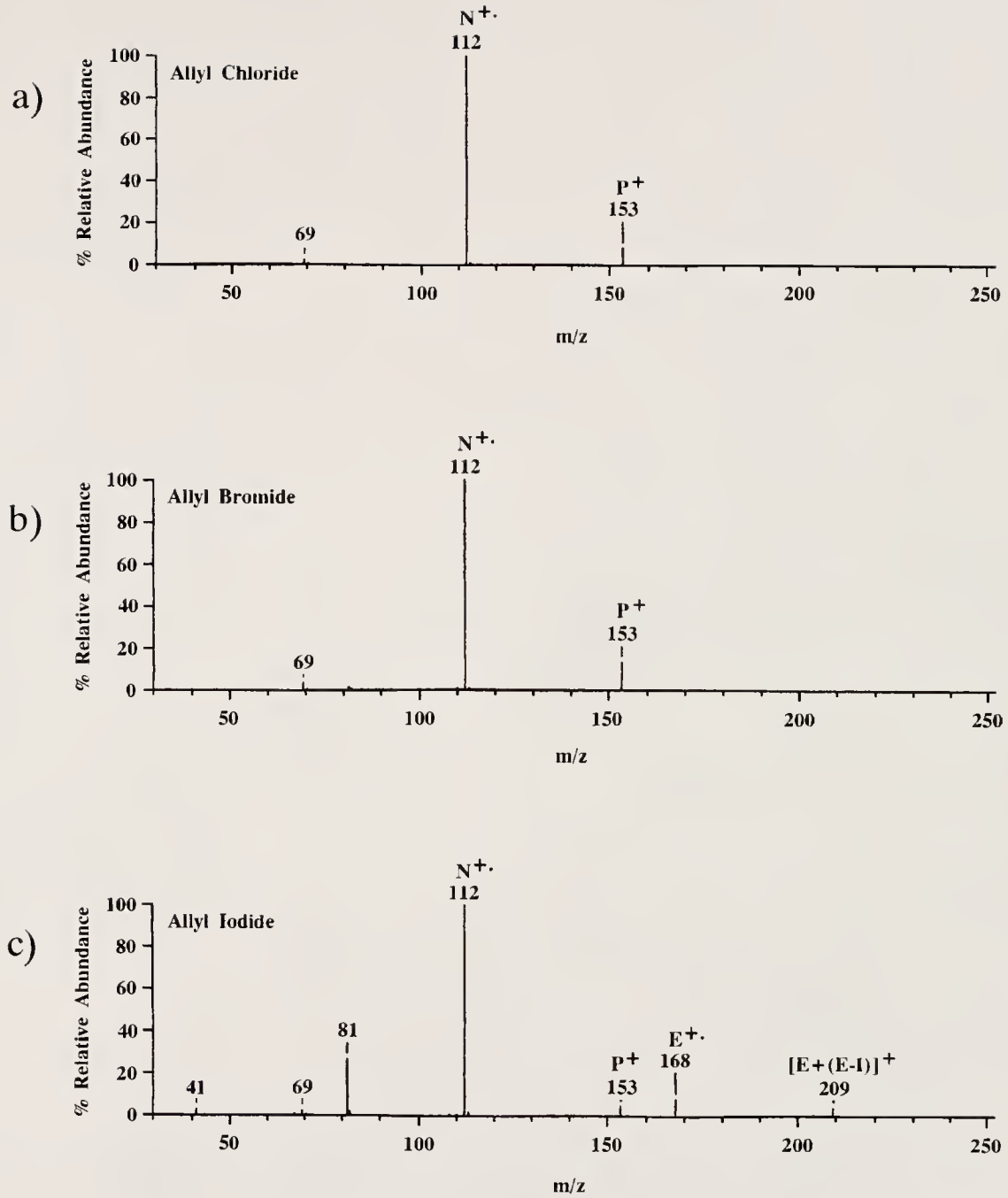

Figure 2-5: Product ion spectra (corresponding to the retention times of the three allyl halides in Figure 2-4) of uracil $N^{+\cdot}$ ions (m/z 112) reacting with a) allyl chloride, b) allyl bromide and c) allyl iodide in the collision cell.

on the allyl bromide and allyl iodide peaks can also be attributed to column overload and poor chromatography.

Figure 2-5 shows the spectra derived from the chromatograms in Figure 2-4. Each spectrum is an average of several scans over the tops of each allyl halide chromatographic peak and is not background subtracted. In all three spectra, it is clear that the expected product ion, P^+ (m/z 153), is observed as well as some unreacted $N^{+\cdot}$ ion at m/z 112 and a low abundance of ion at m/z 69 arising from CID of the $N^{+\cdot}$ ion (loss of CONH). In the case of allyl iodide, a number of products of other reactions are also observed, as discussed below.

Figures 2-6 and 2-7 show the calculated relative reactivities for the DNA/RNA base and nucleoside ions utilized in these studies. Relative reactivities were calculated by first determining the P^+ areas (for at least three individual trials for each reaction) from the appropriate mass chromatograms. These areas were then normalized for the flux of $N^{+\cdot}$ ions passing through Q1 into the collision cell by dividing by the average (over several scans) $N^{+\cdot}$ intensities immediately before the pentane solvent eluted (preceding any allyl halide elution) from the GC into the collision cell. The different concentrations of the allyl halide solutions were then accounted for by dividing by the individual solution concentrations (in mol/L) that were used for each particular experiment. For example, for one trial of the reaction of uracil $N^{+\cdot}$ ions with allyl bromide, the GC peak area of 1533939 counts for the m/z 153 product ion is divided by the average incident $N^{+\cdot}$ ion intensity of 4789373 counts/scan to get a ratio of 0.320280. Dividing this by the concentration of the allyl

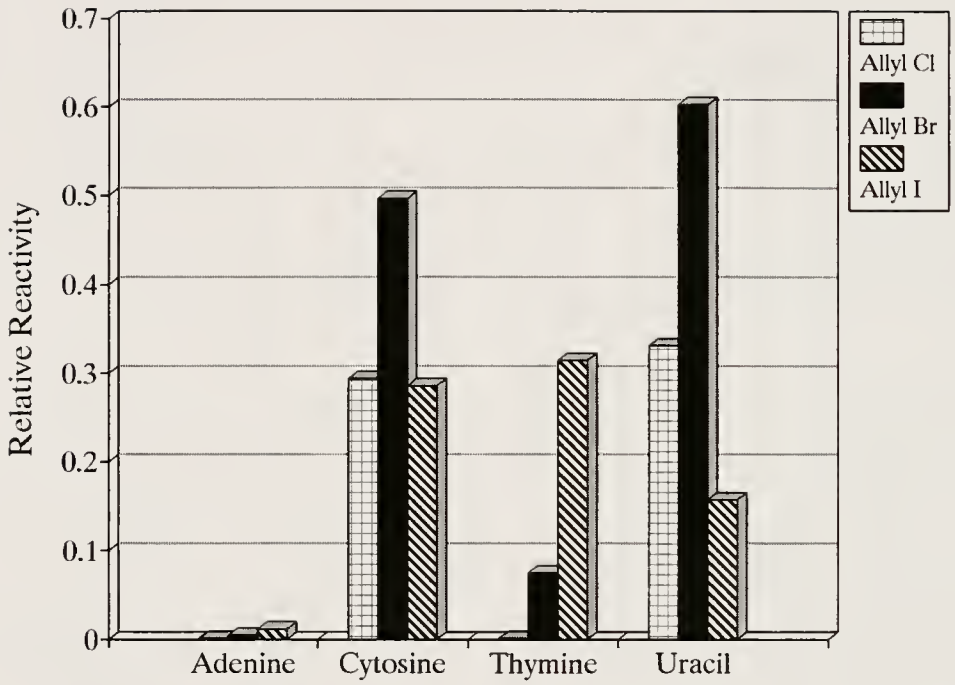

Figure 2-6: Relative reactivities of DNA/RNA base ions with allyl halides.

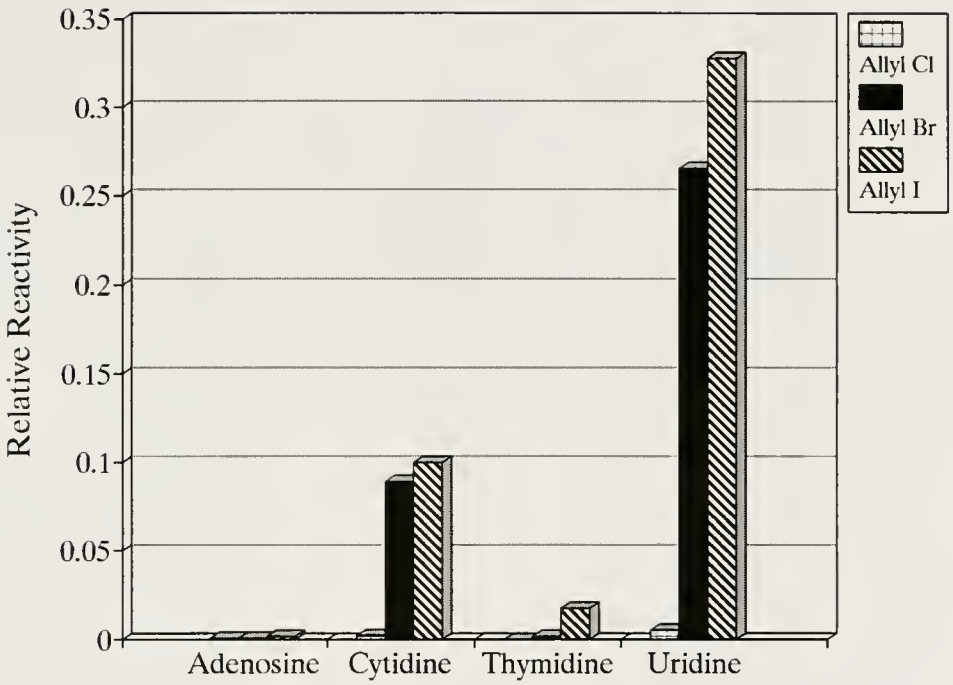

Figure 2-7: Relative reactivities of nucleoside ions with allyl halides.

bromide solution injected (0.558 mol/L) yields a relative reactivity of 0.574. Averaging this value with the results calculated for the other trials generates the relative reactivity shown in Figure 2-6 of 0.601. No corrections for the amount of allyl halide introduced on the column were necessary since 1 μL injections were always made with the same split ratio of 100:1.

As was previously stated, relative reactivities with the allyl halides were calculated by measuring the production of one specific product ion, $[N+41]^+$. In some instances, however, it may make more sense to include several product ions to evaluate nucleophile reactivities, particularly those that contain both the nucleophile and electrophile groups or fragments there of. Although this was not done in these studies, several other product ions listed in Tables 2-3 and 2-4, such as $[N+X]^+$ (X=halide) and $[BH+(E-X)]^+$ (see Table 2-4) could have been included for calculations of relative reactivities. The goal of this work, however, was to evaluate the reactivities of these nucleophiles with allyl halides based on production of the $[N+41]^+$ ion exclusively. Thus, no other product ions were considered for the determination of reactivities.

Comparing Figures 2-6 and 2-7, it is evident that the nucleoside ions are consistently less reactive (by a factor of 2-10, with the sole exception of uracil/uridine with allyl iodide) towards the allyl halides than the corresponding DNA/RNA base ions. In large part, the major reason for the lower apparent reactivities of the nucleoside $N^{+\cdot}$ ions is their lower stability, and therefore their greater tendency to undergo collision-induced dissociation (CID) in Q2, even at the low collision energy

Table 2-3: Adduct ions observed for the reactions of DNA/RNA base and nucleoside ions with allyl halides. Ion m/z (% relative abundance)

Nucleophile Ion, $N^{+\cdot}$ [a]	Electrophile, E	P^{+} [b]	$[P+H]^{+}$	$[N+X]^{+}$	Other Products that Contain N[c]
Adenine	Allyl Cl	176 (<0.1)	-	-	-
	Allyl Br	176 (0.1)	-	-	-
	Allyl I	176 (0.4)	177 (<0.1)[d]	262 (0.5)	-
Cytosine	Allyl Cl	152 (7.3)	153 (0.1)[d]	-	-
	Allyl Br	152 (22.4)	153 (0.4)[d]	-	-
	Allyl I	152 (9.4)	153 (0.1)[d]	238 (10.3)	320 (0.5), 406 (0.5)
Thymine	Allyl Cl	167 (<0.1)	-	-	-
	Allyl Br	167 (2.6)	168 (<0.1)[d]	-	-
	Allyl I	167 (8.5)	168 (0.8)[e]	253 (0.2)	-
Uracil	Allyl Cl	153 (8.8)	154 (0.3)[d]	-	-
	Allyl Br	153 (20.9)	154 (0.5)[d]	-	-
	Allyl I	153 (5.9)	154 (<0.1)[d]	239 (<0.1)	-
Adenosine	Allyl Cl	-	-	-	-
	Allyl Br	308 (0.2)	-	-	-
	Allyl I	308 (0.6)	-	394 (5.3)	-

Table 2-3: continued

Nucleophile Ion, $N^{+\cdot}$ [a]	Electrophile, E	P^+ [b]	$[P+H]^+$	$[N+X]^+$	Other Products that Contain N[c]
Cytidine[f]	Allyl Cl	-	285 (0.1)	-	-
	Allyl Br	-	285 (3.5)	-	-
	Allyl I	284 (0.1)	285 (3.1)	371 (<0.1)[g]	-
Thymidine	Allyl Cl	-	-	-	-
	Allyl Br	283 (0.2)	-	-	-
	Allyl I	283 (0.4)	-	-	-
Uridine	Allyl Cl	285 (0.2)	-	279 (<0.1)	-
	Allyl Br	285 (11.6)	286 (0.4)[d]	-	-
	Allyl I	285 (14.7)	286 (0.2)[d]	371 (0.6)	-

[a] The molecular ion ($N^{+\cdot}$) is mass-selected by Q1 for reaction in the collision cell.
[b] P^+ is the $[N+41]^+$ product ion (addition of the allyl group) and is equivalent to $[N+E-X]^+$.
[c] Ions of at least 0.1% relative abundance are listed.
[d] The majority of the ion intensity is most probably due to ^{13}C isomers.
[e] m/z 168 corresponds to both the $[P+H]^+$ ion and the $E^{+\cdot}$ ion of allyl iodide.
[f] The protonated molecule ($[N+H]^+$) of cytidine was mass selected by Q1 for reaction in the collision cell.
[g] This is the $[N+H+X]^+$ ion, not $[N+X]^+$.

Table 2-4: Adduct ions of CID products observed for the reactions of nucleoside ions with allyl halides.
Ion m/z (% relative abundance)

Nucleophile Ion, $N^{+\cdot}$ [a]	Electrophile, E	$[BH+(E-X)]^+$ [b]	$[BH_2+(E-X)]^+$ [b]	Other Products of $N^{+\cdot}$ Fragment Ions Reacting with Electrophiles[c]
Adenosine	Allyl Cl	-	-	219 (0.1)
	Allyl Br	176 (<0.1)	177 (0.1)	219 (1.1), 278 (0.2)
	Allyl I	176 (0.4)	-	219 (0.5), 220 (0.2), 262 (1.0), 278 (0.1), 304 (0.1), 306 (0.5), 322 (0.2), 346 (0.4), 364 (16.2)
Cytidine[d]	Allyl Cl	-	-	302 (0.4), 304 (0.1)
	Allyl Br	-	153 (0.9)	267 (3.3)
	Allyl I	-	153 (2.2)	267 (0.8), 353 (1.1)
Thymidine	Allyl Cl	-	-	-
	Allyl Br	167 (0.3)	-	139 (0.3)
	Allyl I	167 (0.4)	-	139 (1.8)

Table 2-4: continued

Nucleophile Ion, $N^{+\cdot}$ [a]	Electrophile, E	$[BH+(E-X)]^+$ [b]	$[BH_2+(E-X)]^+$ [b]	Other Products of $N^{+\cdot}$ Fragment Ions Reacting with Electrophiles[c]
Uridine	Allyl Cl	-	154 (<0.1)	267 (0.3), 302 (2.8), 304 (0.9)
	AMwyl Br	153 (1.0)	154 (0.1)	267 (10.6), 268 (0.3)
	Allyl I	153 (10.9)	154 (0.2)	267 (8.4), 268 (0.1)

[a] The molecular ion ($N^{+\cdot}$) is mass-selected by Q1 for reaction in the collision cell.
[b] B is the fragment formed by cleavage of the glycosidic bond of a nucleoside, representing the aglycone (base) portion of the molecule.
[c] Ions of at least 0.1% relative abundance are listed.
[d] The protonated molecule ($[N+H]^+$) of cytidine was mass selected by Q1 for reaction in the collision cell.

(1-2 eV) employed here. This competing reaction, in effect, reduces the number of intact molecular ions that are available for reactions and decreases the number of P^+ ions ($[N+41]^+$) that are ultimately formed. As is discussed below, other ion-molecule reactions involving the nucleoside fragment ions do occur, but were not included in the calculation of relative reactivities.

Correlation of Reactivities to Mutagenicities

The relative reactivities of each individual DNA/RNA base or nucleoside ion can, in some cases, roughly approximate the mutagenicity of each allyl halide. Table 2-5 lists the mutagenicities of the three allyl halides used in this study, as determined by the Ames test [41-42], a bacteriological assay. Allyl chloride is much less mutagenic than allyl bromide, and allyl bromide is substantially less mutagenic than allyl iodide. Since the mechanism of mutagenicity for electrophiles such as the allyl halides is direct modification of nucleophilic sites on DNA [75-76], one would expect to observe increasing relative reactivities, from allyl chloride to allyl iodide, upon reaction with DNA/RNA base and nucleoside ions, as has been previously observed upon reaction with pyridine ions [40]. Figures 2-6 and 2-7 show that, for reactions of six of the eight DNA/RNA base and nucleoside ions, this is what is observed. However, for the reactions of cytosine and uracil ions, the quantity of product ion, P^+, formed upon reaction with allyl iodide is less than that which would be expected. In fact, it is even lower than the product ion intensity obtained in the reaction with allyl chloride, which is over two orders of magnitude less mutagenic than allyl iodide.

Table 2-5: Mutagenicities of allyl halides as determined by the Ames Test.

Allyl Halide	Mutagenicity[a]
Allyl chloride	9
Allyl bromide	700
Allyl iodide	2000

[a] Values were taken from reference 41. Mutagenicity in rev/μmol without metabolic activation.

This phenomenon is apparent in the relatively small chromatographic peak observed for allyl iodide in the m/z 153 mass chromatogram in Figure 2-4 from reaction with uracil $N^{+\cdot}$ ions. This apparent contradiction is explained by noting (Figure 2-5c) that extensive side reactions occur when uracil $N^{+\cdot}$ ions react with allyl iodide. In this case, among other ions, allyl iodide molecular ions ($E^{+\cdot}$, m/z 168) and dimer ions ($[E_2\text{-I}]^+$, m/z 209 and $[E_2\text{-I-HI}]^+$, m/z 81) are produced along with the expected P^+ ions. Products of such side reactions are often observed in the product ion spectra; frequently the most intense ion is a product ion other than the expected P^+ ion.

Identification and Correlation of Side Reaction Products

It is immediately apparent upon inspection of Tables 2-3, 2-4, 2-6 and 2-7 that the number and variety of side reactions that take place for these ion-molecule reactions is significant. However, many product ions that may initially appear to be unrelated can be grouped into different categories, with analogs for each of the reactions for the different DNA/RNA base and nucleoside ions. A large fraction of the side reaction products arise directly from the allyl halides (Table 2-6), including allyl ions, $[E\text{-X}]^+$, allyl halide ions, $E^{+\cdot}$, allyl dimer ions, $[E_2\text{-HX-X}]^+$, and halide-bound allyl dimers, $[E_2\text{-X}]^+$. These ions arise from charge exchange reactions in competition with the desired associative ion-molecule reactions to form $E^{+\cdot}$ ions and $[E\text{-X}]^+$ (allyl) ions (from dissociative charge exchange or collision-induced dissociation (CID) of $E^{+\cdot}$ ions or allyl-containing adduct ions). Further reactions of these $E^{+\cdot}$ and $[E\text{-X}]^+$ ions with neutral electrophile produce the dimer ions observed.

Table 2-6: Charge exchange products observed for the reactions of DNA/RNA base and nucleoside ions with allyl halides. Ion m/z (% relative abundance)

Nucleophile Ion, $N^{+\cdot}$ [a]	Electrophile, E	$[E\text{-}X]^+$	$E^{+\cdot}$ [b]	$[E_2\text{-}HX\text{-}X]^+$	$[E_2\text{-}X]^+$	Other Products due to Charge Exchange of E[c]
Adenine	Allyl Cl	-	-	-	-	-
	Allyl Br	41 (<0.1)	-	81 (<0.1)[d]	-	-
	Allyl I	41 (0.1)	168 (<0.1)	81 (0.2)[d]	209 (<0.1)	-
Cytosine	Allyl Cl	41 (<0.1)	-	-	-	-
	Allyl Br	41 (<0.1)	-	81 (0.1)	-	-
	Allyl I	41 (0.1)	168 (0.2)	81 (0.9)	209 (0.3)	-
Thymine	Allyl Cl	-	-	-	-	82 (0.1)
	Allyl Br	41 (<0.1)	-	81 (<0.1)	-	-
	Allyl I	41 (0.2)	168 (0.8)[e]	81 (2.1)	209 (0.2)	82 (0.3), 210 (1.1)

Table 2-6: continued

Nucleophile Ion, $N^{+\cdot}$ [a]	Electrophile, E	$[E\text{-}X]^+$	$E^{+\cdot}$ [b]	$[E_2\text{-}HX\text{-}X]^+$	$[E_2\text{-}X]^+$	Other Products due to Charge Exchange of E[c]
Uracil	Allyl Cl	41 (<0.1)	-	81 (<0.1)	-	-
	Allyl Br	41 (0.4)	-	81 (2.6)	-	82 (0.5)
	Allyl I	41 (3.6)	168 (9.2)	81 (35.6)	209 (5.6)	82 (2.6), 169 (0.4), 210 (0.5)
Adenosine	Allyl Cl	-	-	-	-	-
	Allyl Br	-	-	-	-	-
	Allyl I	41 (<0.1)	-	-	209 (0.1)	-
Cytidine[f]	Allyl Cl	-	-	-	-	-
	Allyl Br	-	-	-	-	-
	Allyl I	-	168 (0.1)	-	209 (<0.1)	-

Table 2-6: continued

Nucleophile Ion, $N^{+\cdot}$ [a]	Electrophile, E	$[E\text{-}X]^+$	$E^{+\cdot}$ [b]	$[E_2\text{-}HX\text{-}X]^+$	$[E_2\text{-}X]^+$	Other Products due to Charge Exchange of E[c]
Thymidine	Allyl Cl	-	-	-	-	-
	Allyl Br	-	-	-	-	-
	Allyl I	-	168 (0.1)	-	-	-
Uridine	Allyl Cl	-	-	-	-	-
	Allyl Br	-	-	-	-	-
	Allyl I	-	168 (0.1)	81 (0.4)	209 (0.3)	-

[a] The molecular ion ($N^{+\cdot}$) is mass-selected by Q1 for reaction in the collision cell.
[b] $E^{+\cdot}$ is the molecular ion of the electrophile.
[c] Ions of at least 0.1% relative abundance are listed.
[d] m/z 81 is also a CID fragment of the $N^{+\cdot}$ ion of adenine.
[e] m/z 168 also corresponds to the $[P+H]^+$ ion.
[f] The protonated molecule ($[N+H]^+$) of cytidine was mass selected by Q1 for reaction in the collision cell.

Table 2-7: Collision-induced dissociation products of the nucleophile observed for the reactions of DNA/RNA base and nucleoside ions with allyl halides.

		Ion m/z (% relative abundance)		
Nucleophile Ion, $N^{+\cdot}$ [a]	Electrophile, E	$N^{+\cdot}$	$[N+H]^+$	CID Products of the Nucleophile Ion[b]
Adenine	Allyl Cl	135 (100)	136 (<0.1)	107 (0.1), 108 (2.1)
	Allyl Br	135 (100)	-	108 (2.9)
	Allyl I	135 (100)	136 (<0.1)	81 (0.2)[c], 108 (3.7)
Cytosine	Allyl Cl	111 (100)	112 (0.5)	68 (0.2), 69 (0.2), 83 (3.4)
	Allyl Br	111 (100)	112 (0.6)	68 (0.1), 69 (0.1), 83 (4.8)
	Allyl I	111 (100)	112 (2.1)	68 (0.3), 69 (0.2), 83 (6.0)
Thymine	Allyl Cl	126 (100)	127 (0.1)	55 (0.3), 83 (3.3)
	Allyl Br	126 (100)	127 (0.1)	55 (0.5), 83 (4.7)
	Allyl I	126 (100)	127 (0.6)	55 (0.5), 83 (3.4), 98 (0.1)
Uracil	Allyl Cl	112 (100)	113 (1.3)	69 (2.7), 70 (0.9)
	Allyl Br	112 (100)	113 (1.3)	69 (4.2), 70 (1.4)
	Allyl I	112 (100)	113 (2.0)	69 (3.3), 70 (1.6)
Adenosine	Allyl Cl	267 (100)	268 (<0.1)	136 (2.1), 164 (25.5), 178 (1.1), 237 (92.6)
	Allyl Br	267 (99.3)	268 (0.1)	135 (1.0), 136 (6.9), 164 (41.6), 178 (5.1), 179 (1.3), 194 (1.2), 237 (100), 250 (1.2)

Table 2-7: continued

Nucleophile Ion, $N^{+\cdot}$ [a]	Electrophile, E	$N^{+\cdot}$	$[N+H]^+$	CID Products of the Nucleophile Ion[b]
Adenosine	Allyl I	267 (57.9)	-	135 (1.6), 136 (9.6), 164 (75.1), 178 (8.0), 179 (1.2), 194 (1.6), 237 (100), 250 (1.2)
Cytidine[d]	Allyl Cl	243 (0.1)	244 (100)	112 (1.4), 113 (1.8), 226 (8.4)
	Allyl Br	243 (0.1)	244 (100)	112 (4.4), 113 (2.9), 132 (1.6), 226 (9.3)
	Allyl I	243 (0.2)	244 (100)	112 (4.0), 113 (2.9), 226 (8.6)
Thymidine	Allyl Cl	242 (100)	243 (0.1)	98 (5.6), 117 (1.6), 127 (2.6), 206 (1.2)
	Allyl Br	242 (100)	243 (0.2)	98 (6.7), 117 (6.1), 127 (4.7), 206 (1.2)
	Allyl I	242 (100)	243 (0.1)	98 (10.2), 117 (9.2), 126 (1.4), 127 (7.3), 206 (2.0)
Uridine	Allyl Cl	244 (100)	245 (<0.1)	113 (9.3), 132 (3.6), 226 (40.6)
	Allyl Br	244 (100)	245 (<0.1)	113 (12.4), 132 (4.9), 226 (42.5)
	Allyl I	244 (100)	245 (0.2)	86 (1.2), 113 (19.5), 132 (7.4), 133 (1.3), 171 (1.6), 226 (42.6)

[a] The molecular ion ($N^{+\cdot}$) is mass-selected by Q1 for reaction in the collision cell.
[b] Ions of at least 0.1% (DNA/RNA bases) or 1.0% (nucleosides) relative abundance are listed.
[c] m/z 81 also corresponds to $[E_2\text{-HX-X}]^+$.
[d] The protonated molecule ($[N+H]^+$) of cytidine was mass selected by Q1 for reaction in the collision cell.

The greater intensity and variety of these ions with allyl iodide are due to it's much lower ionization energy compared to the other allyl halides, as shown in Table 2-1. Similarly, the DNA/RNA bases with the highest ionization energies (and thus the base ions with the highest recombination energies) result in the most abundant electrophile ions. Figure 2-8, for example, illustrates the charge exchange reaction that occurs extensively between uracil $N^{+\cdot}$ ions and allyl iodide.

Figure 2-6 shows that, upon reaction with the most reactive of the base and nucleoside ions, uracil and cytosine, the relative gas phase reactivities of allyl bromide and allyl iodide are opposite to those that would be expected. This may point to another reason, in addition to excessive side reactions, for decreases in observed product ion formation upon reaction with allyl iodide. Simply put, reactivity can't increase *ad infinitum*. For reactions involving uracil and cytosine ions, the nucleophile is certainly highly reactive with both allyl bromide and allyl iodide. However, since it is apparent that side reactions are prominent when allyl iodide is used as the electrophile, these additional products may decrease $[N+41]^+$ formation by using up some of the nucleophile ions that would otherwise be available.

In addition to associative ion-molecule reactions, collision-induced dissociation (CID) of the DNA/RNA base or nucleoside ions may also take place when the allyl halides elute from the GC into the collision cell. That this process occurs is evident upon inspection of Table 2-7. In all cases except the reaction of adenosine $N^{+\cdot}$ ions with allyl bromide or iodide, the base peak is the ion that was mass-selected by the first quadrupole (Q1) for reaction in the collision cell. However, for many of the

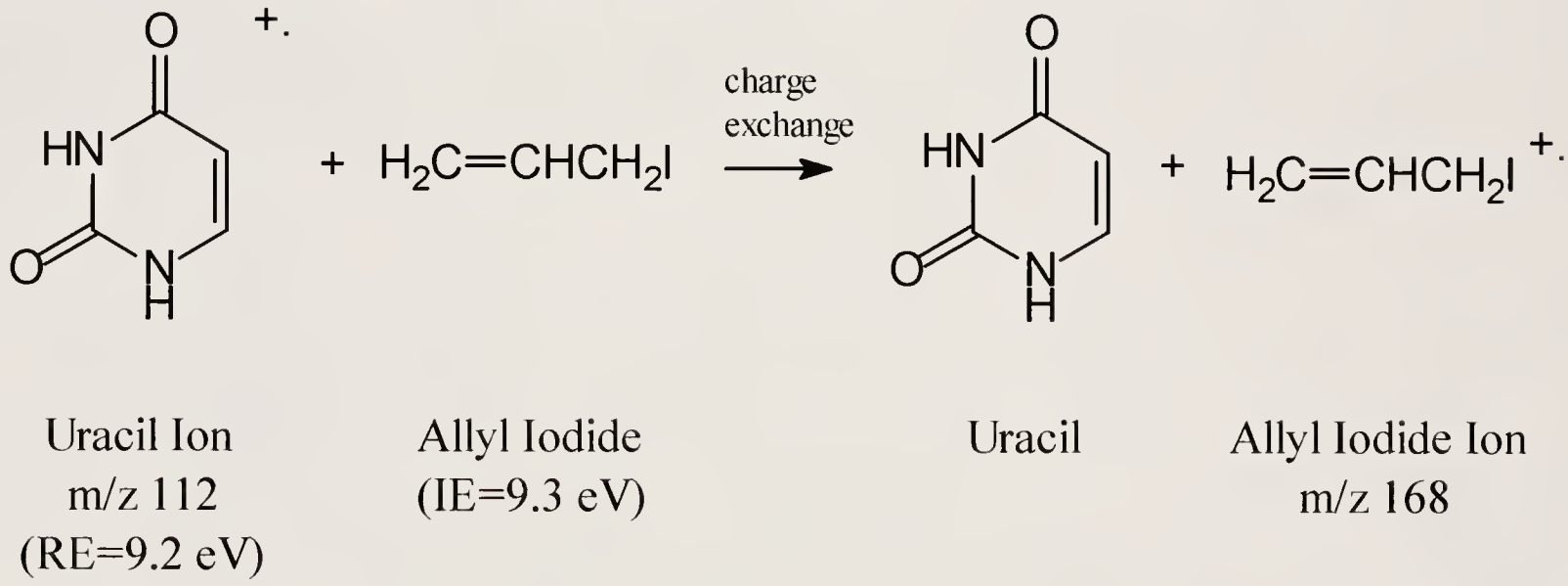

Figure 2-8: Charge exchange reaction of mass-selected uracil ions and neutral allyl iodide.

nucleophile ions, significant CID occurs due to the presence of allyl halide neutrals in Q2. CID product ions are more prominent in the daughter spectra of the nucleoside ions than of the corresponding DNA/RNA base ions. This difference in extent of CID is due to the intrinsic stability of the base ions compared to the nucleoside ions.

Daughter ions arising from CID of the nucleoside molecular ions include the aglycone, or base, fragment ions $[B+H]^+$ and $[B+2H]^+$. These ions are formed by cleavage of the glycosidic bonds of the nucleoside ions with transfer of one or two hydrogens and are analogous to the corresponding DNA/RNA base ions, $N^{+\cdot}$ and $[N+H]^+$. It is not surprising, then, to find that many of these nucleoside CID product ions go on to react with the allyl halides in the collision cell to produce either $[BH+(E-X)]^+$ or $[BH_2+(E-X)]^+$ ions, as shown in Table 2-4. In the case of uridine, the $[B+H]^+$ fragment goes on to react with allyl iodide to produce a $[BH+(E-X)]^+$ ion (m/z 153) with a relative abundance 2/3 as large as that of the P^+ ($[N+41]^+$) ion. Similarly, the uridine $N^{+\cdot}$ ion loses H_2O to form a daughter at m/z 226 which then goes on to react with all three allyl halides via addition of allyl to form m/z 267. Reaction of adenine molecular ions with the allyl halides yields the largest number of product ions due to reactions of CID product ions of the nucleoside, due to the significant extent of CID of the adenosine $N^{+\cdot}$ ion (Table 2-4). In the case of the reaction with allyl iodide, no less than nine significant product ions can be attributed to these types of processes. The most abundant of these, m/z 364, can be attributed to addition of iodine to the most abundant CID product ion,

$[N-30]^+$ at m/z 237, of adenosine. The $[BH+(E-X)]^+$ ion is also observed for the reaction of adenosine ions with allyl iodide, albeit with much less intensity than for the corresponding uridine reactions.

The previous discussion implies that the formation of ions such as $[BH+(E-X)]^+$ always occurs stepwise, via CID of the nucleoside ion to form a $[B+H]^+$ or $[B+2H]^+$ species which subsequently reacts to form the adduct. It should be pointed out, however, that it is probably just as likely that a single collision yields an $[N+E]^+$ adduct which can then fragment not just by loss of X to form P^+, but also by a coinciding loss of the sugar moiety (minus one or two hydrogens) to form the $[BH+(E-X)]^+$ or $[BH_2+(E-X)]^+$ species.

In summary, the lower reactivities of the nucleoside ions compared to those of the DNA/RNA bases (see Figures 2-6 and 2-7) reflect the greater ease with which the nucleoside $N^{+\cdot}$ ions can undergo CID. Although the CID products of the nucleoside $N^{+\cdot}$ ions can react with the allyl halides to form side reaction products (Table 2-4), the decrease in the number of $N^{+\cdot}$ ions remaining to undergo charge exchange with the allyl halides reduces the number of charge exchange side products observed (Table 2-6). The typically most abundant CID product ions of the nucleosides, $[B+2H]^+$ (corresponding to the protonated DNA/RNA base) are unlikely to charge exchange with the allyl halides. Although ionization energies have not been reported for three of the four nucleosides, they are probably all lower than those for the corresponding bases, as noted in Table 2-1 for uridine (with an IE 0.2

eV less than uracil). This may also account for the fewer charge exchange side reaction products observed for the nucleosides (Table 2-6).

Reactions of Guanine Ions with Allyl Halides

Because of guanine's very low volatility, it is impractical to achieve the constant flux of molecular ions required for Q2 ion-molecule reactions with allyl halide introduction via gas chromatography. Furthermore, when using the solids probe, temperatures in excess of 300°C are required for vaporization of guanine, and this leads to sample decomposition and reduced molecular ion intensities. Also, a dramatic decrease in sensitivity (over several scans) was noted when solids probe vaporization of guanine was attempted. It is unclear as to why this occurred, but it is speculated that vaporized guanine molecules may have rapidly cooled and coated the mass analyzer (Q1), thus impeding its operation due to field aberrations.

For these reasons, a direct exposure probe (DEP) has been utilized to vaporize guanine. DEP vaporization is accomplished by coating a fine wire on the end of the probe with a small amount of analyte. By increasing the current which flows through the wire, it is rapidly heated, causing the substance to be vaporized with much less sample decomposition as compared to solids probe vaporization. Electron ionization (EI) is then used for ion production. Since the temperature of the filament of the DEP is ramped (due to increasing current), the method is characterized by vaporization of the analyte as a distinct peak. Thus, reactions in the collision cell of guanine molecular ions formed by DEP ionization with allyl halides

eluting from a GC are not practical since a constant flux of guanine ions is not available.

Nonetheless, it has been demonstrated that guanine molecular ions are reactive toward the allyl halides. This was accomplished by using a leak valve to provide a constant pressure of each allyl halide separately in the collision cell while guanine was vaporized and ionized using the DEP. Unfortunately, this method does not allow relative reactivities (such as those shown in Figure 2-6) to be calculated since, unlike GC introduction of the allyl halides, it is impossible to accurately know how much allyl halide is present in the collision cell for each reaction. Thus, the products resulting from these reactions have not been included in any of the tabulated data presented in this chapter since the method used for guanine ion reactions was quite different from the technique used for the other reactions.

Product ion spectra resulting from reactions of guanine molecular ions (m/z 151) with allyl chloride, allyl bromide and allyl iodide are shown in Figure 2-9. It is clear that the $[N+41]^+$ product ion (P^+, m/z 192) is observed for all three reactions. Furthermore, the lowest P^+ intensity is observed in the allyl chloride reaction while the allyl iodide reaction produces the largest intensity of P^+, indicating that the order of reactivity follows the relative mutagenicities of the three allyl halides (see Table 2-5). This conclusion, however, may be erroneous since the absolute amounts of each allyl halide that were allowed to react in the collision cell are not known. Thus, it can not be said with certainty how the relative reactivities of each allyl halide toward guanine molecular ions compare. It can also be noted that several side

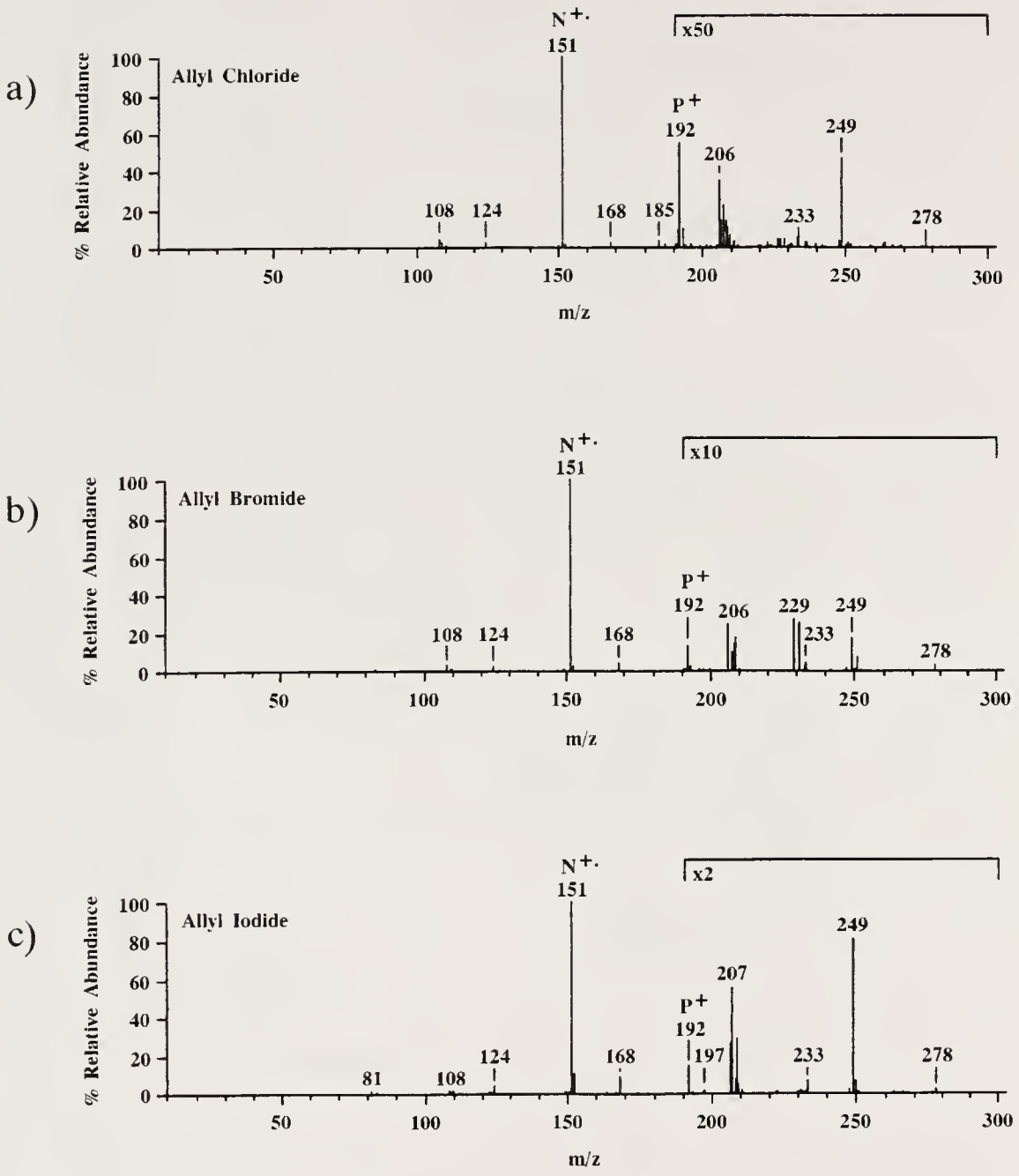

Figure 2-9: Product ion spectra of guanine $N^{+\cdot}$ ions (m/z 151) reacting with a) allyl chloride, b) allyl bromide and c) allyl iodide in the collision cell.

reaction products are present in each of the spectra. In particular, Figure 2-9c shows that the side reaction products $[E_2\text{-HX-X}]^+$ (m/z 81) and $E^{+\cdot}$ (m/z 168) are formed upon reaction of guanine molecular ions with allyl iodide. However, m/z 168 (corresponding to the allyl iodide ion) is observed for the allyl chloride and allyl bromide reactions as well (Figure 2-9a,b). This unusual result can be attributed to contamination by each allyl halide of the leak valve and plumbing used for allyl halide introduction into Q2; the allyl halides are only slightly volatile and tend to condense in the conduit leading to the collision cell. Other side reaction products that are observed in the spectra such as m/z 206 (or 207), 233, 249 and 278 do not correlate to any of the side reaction products listed in Tables 2-3 and 2-6 and are probably due to contamination of the plumbing as well, since they are common to all three spectra.

Comparison of Reactivities of DNA/RNA Base and Nucleoside Ions Towards Allyl Halides to Those of Pyridine Ions

Figure 2-10 compares the relative reactivities of the small model base (pyridine) ion to those of the most reactive DNA/RNA base (uracil) and nucleoside (uridine) ions toward the allyl halides. The relative reactivities were calculated as described previously.

Looking at Figure 2-10, it may initially appear surprising that both uracil and uridine ions are, in general, more reactive toward the allyl halides than pyridine ions, since previous research [1] indicated that small DNA model ions (such as pyridine) were typically more reactive than the DNA/RNA base and nucleoside ions. In the

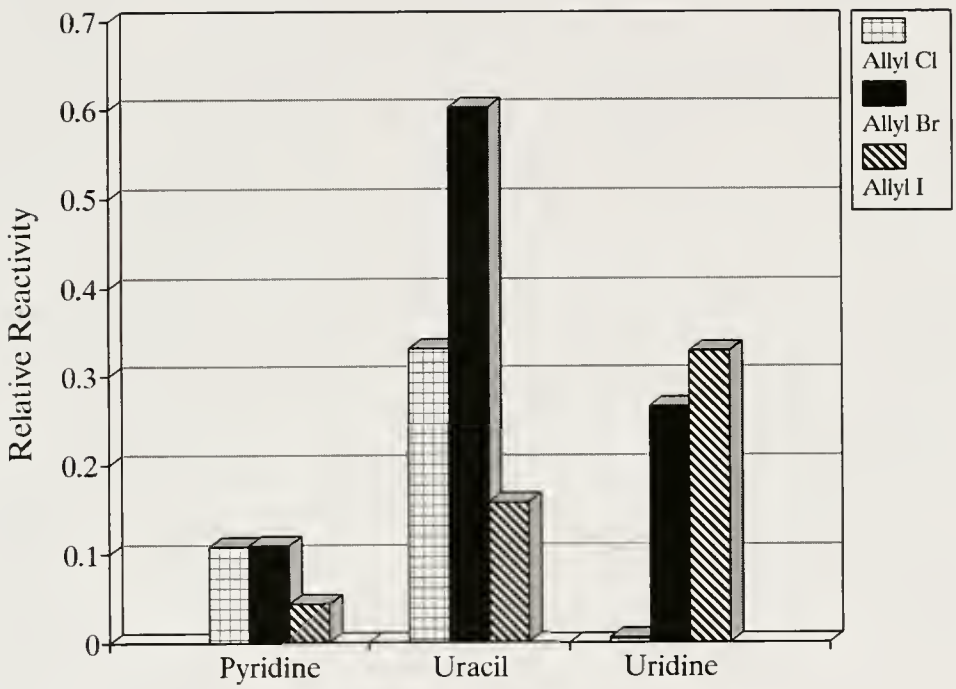

Figure 2-10: Relative reactivities of pyridine (a model base), uracil (a DNA/RNA base) and uridine (a nucleoside) ions with allyl halides.

previous studies [1] conditions for pyridine reactions with allyl halides were such that a pyridine pressure of 0.15 mTorr in the ion source resulted in maximum product ion (P^+, m/z 120) formation. The results reported here, however, were obtained using just enough pyridine in the ion source to obtain a sufficient ion intensity for subsequent reaction in Q2. Thus, it is clear that pyridine ion relative reactivities appear much greater at higher ion source pressures due to a much larger number of neutral pyridine molecules in the collision cell which subsequently react with electrophile charge exchange products such as $[E\text{-}X]^+$ and $E^{+\cdot}$ to form the P^+ species.

The observation that pyridine ions are less reactive toward the allyl halides than uracil and uridine ions (except for the reaction of uridine ions with allyl chloride) can be at least partially attributed to side reactions in the collision cell. Similarly to the results obtained for uracil, pyridine ions produce the least amount of P^+ ions upon reaction with allyl iodide due to excessive side reaction products arising from charge exchange processes. In fact, one would expect that pyridine ions are more prone to excessive side reactions via charge exchange since pyridine's ionization energy (9.25 eV) is higher than any of the DNA/RNA bases or nucleosides (see Table 2-1). Furthermore, pyridine's somewhat high ionization energy may allow it to charge exchange more readily with allyl bromide and allyl chloride than the DNA/RNA base or nucleoside ions. This would account for the overall lower reactivities of pyridine ions compared to the reactivities of uracil, and in some cases, uridine ions.

Conclusions

The ability to perform gas-phase ion-molecule reactions of DNA/RNA base and nucleoside ions with allyl halides has been demonstrated. Relative reactivities of the base and nucleoside ions toward the allyl halides were also calculated. In general, the DNA/RNA base ions were much more reactive than the corresponding nucleosides. This effect can be attributed to the fact that the nucleoside ions tend to fragment upon collision with the allyl halides to a larger degree than do the base ions, inhibiting product ion formation. Also, presumably due to their higher recombination energies, the DNA/RNA base ions tended to induce significant side reactions with the electrophiles, and, in particular with allyl iodide. These side reactions, arising from charge exchange between the base ions and the allyl halides, often distorted the measured relative reactivities by effectively decreasing the number of nucleophile ions that were available for reaction.

CHAPTER 3
PRACTICAL ASPECTS OF REACTIONS OF DNA/RNA BASE AND NUCLEOSIDE IONS WITH ALLYL HALIDES

Introduction

The characteristics of ion-molecule reactions for analytical determinations must be considered differently from typical analyses performed using mass spectrometric methods (e.g., GC/MS). Ion-molecule reactions can offer significant improvements in selectivity (as in being highly selective for reactive electrophiles here) compared to GC/MS due to the specific nature of the reactions themselves. Furthermore, the sensitivity of the ion-molecule reaction method depends on more parameters than does a GC/MS experiment. Whereas the sensitivity of a GC/MS analysis depends entirely on the properties of the instrument and the behavior of the analyte, an analysis performed using a particular ion-molecule reaction as the method of determination also depends on the characteristics of the reaction itself. These aspects, in turn, can lead to unexpected or unwanted results that often hinder the analysis.

Chapter 2 illustrated that associative ion-molecule reactions in the collision cell of a triple quadrupole mass spectrometer are useful for studies of reactions of ionized DNA/RNA bases and nucleosides with neutral allyl halides. In particular, it was pointed out that relative reactivity measurements can be correlated (with

varying accuracy) to the mutagenicities of the three allyl halides. Furthermore, it was demonstrated that product ions due to undesired side reactions often overshadow the product ions of interest, causing erroneous relative reactivity measurements.

In an attempt to more fully understand the processes that take place for the ion-molecule reactions described in Chapter 2, studies have been performed which address how the reaction products are altered under different circumstances, and also demonstrate the analytical utility of the method. The effects of varying allyl halide pressure in the collision cell on the formation of product ions upon reaction with ions of the DNA/RNA base uracil have been studied. Also, calibration curves have been determined for the reactions of each of the DNA/RNA base ions with the allyl halides. Furthermore, the effect of nucleophile ion (uracil) flux on reactions with allyl halides has been investigated.

Pressure Effects of Allyl Halides on Formation of Product Ions upon Reaction with DNA/RNA Base Ions

Experimental

Experiments were performed on a Finnigan MAT (San Jose, CA) TSQ70 triple quadrupole mass spectrometer modified with an octopole collision cell and a 20 kV dynode. The mass spectrometer was equipped with a Varian (Walnut Creek, CA) 3400 gas chromatograph, interfaced to the collision cell, Q2, via a resistively heated transfer line [35]. Experiments were performed at an emission current of 200 μA, an electron energy of 70 eV for EI (100 eV for CI), a manifold temperature of

100°C, and an ion source temperature of 170°C for EI (150°C for CI). The mass spectrometer was mass-calibrated using perfluorotributylamine (PFTBA), and then tuned to maximize product ion formation for low-energy ion-molecule reactions in the collision cell, as detailed in Appendix A. For studies involving the pressure effects of allyl halides on the reactivity of uracil ions, introduction of the allyl halides into Q2 was accomplished via a Negretti (Hampshire, England) fine-metering valve to provide constant and precise pressures. Allyl halide pressures within Q2 were indicated by a Granville Phillips (Boulder, CO) Convectron gauge, calibrated for nitrogen.

Reactions of Uracil Ions with Allyl Halides

As an example of the effect of allyl halide pressure in the collision cell on product ion formation, uracil molecular ions, $N^{+\cdot}$, were allowed to react with allyl chloride, allyl bromide and allyl iodide introduced individually via a variable leak valve into the collision cell at various pressures. Figures 3-1 through 3-3 show that the allyl halide pressure has a profound effect on the relative abundances of the various product ions that are formed for each reaction (note the logarithmic intensity scale). In particular, as the allyl halide pressure increases for each case, the intensities of all the ions start to decrease at indicated pressures above 1.5-2.0 mTorr. This is due to increased ion scattering losses in the collision cell, resulting in a smaller percentage of ions that are ultimately detected.

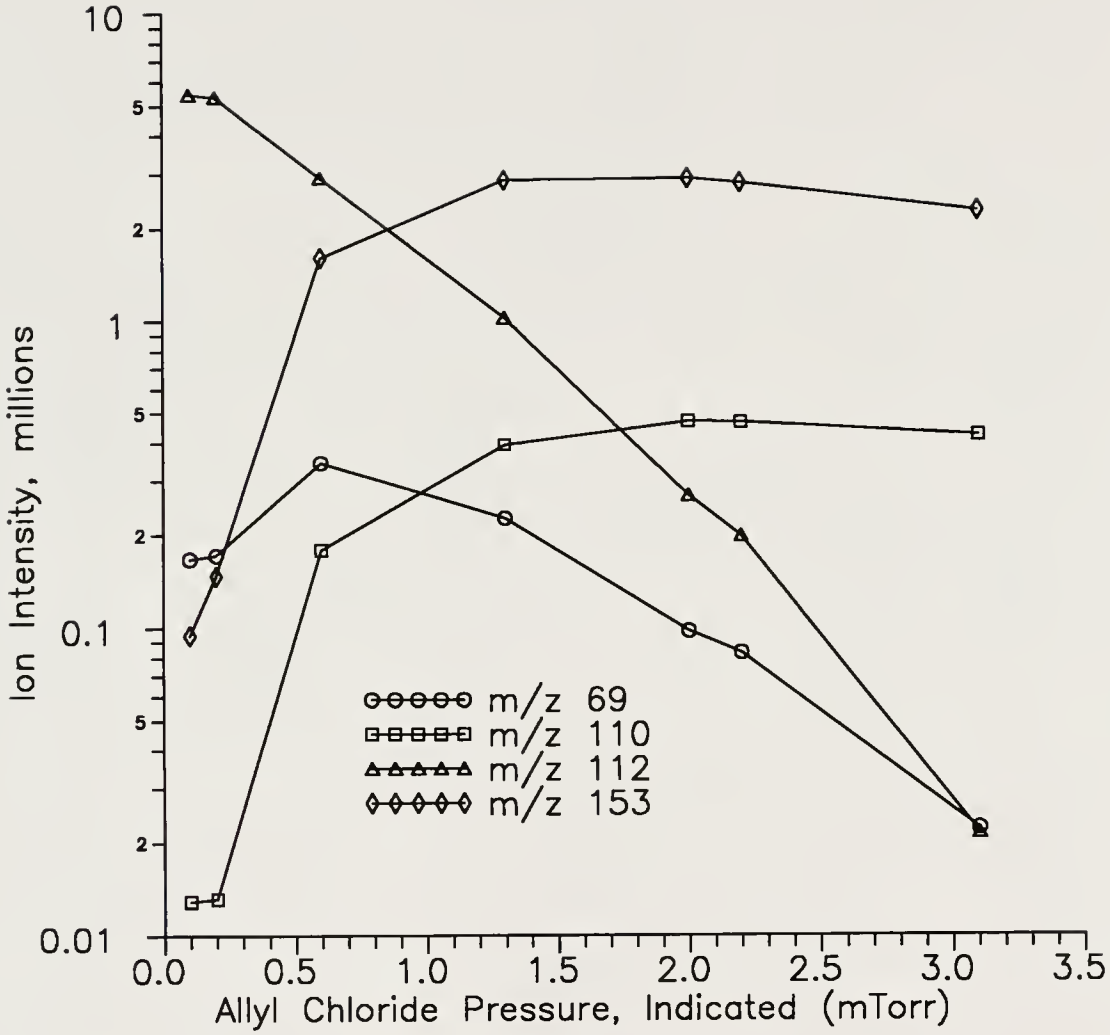

Figure 3-1: Effect of allyl chloride pressure on product ion distribution for the reaction of uracil $N^{+\cdot}$ ions, m/z 112, with allyl chloride.

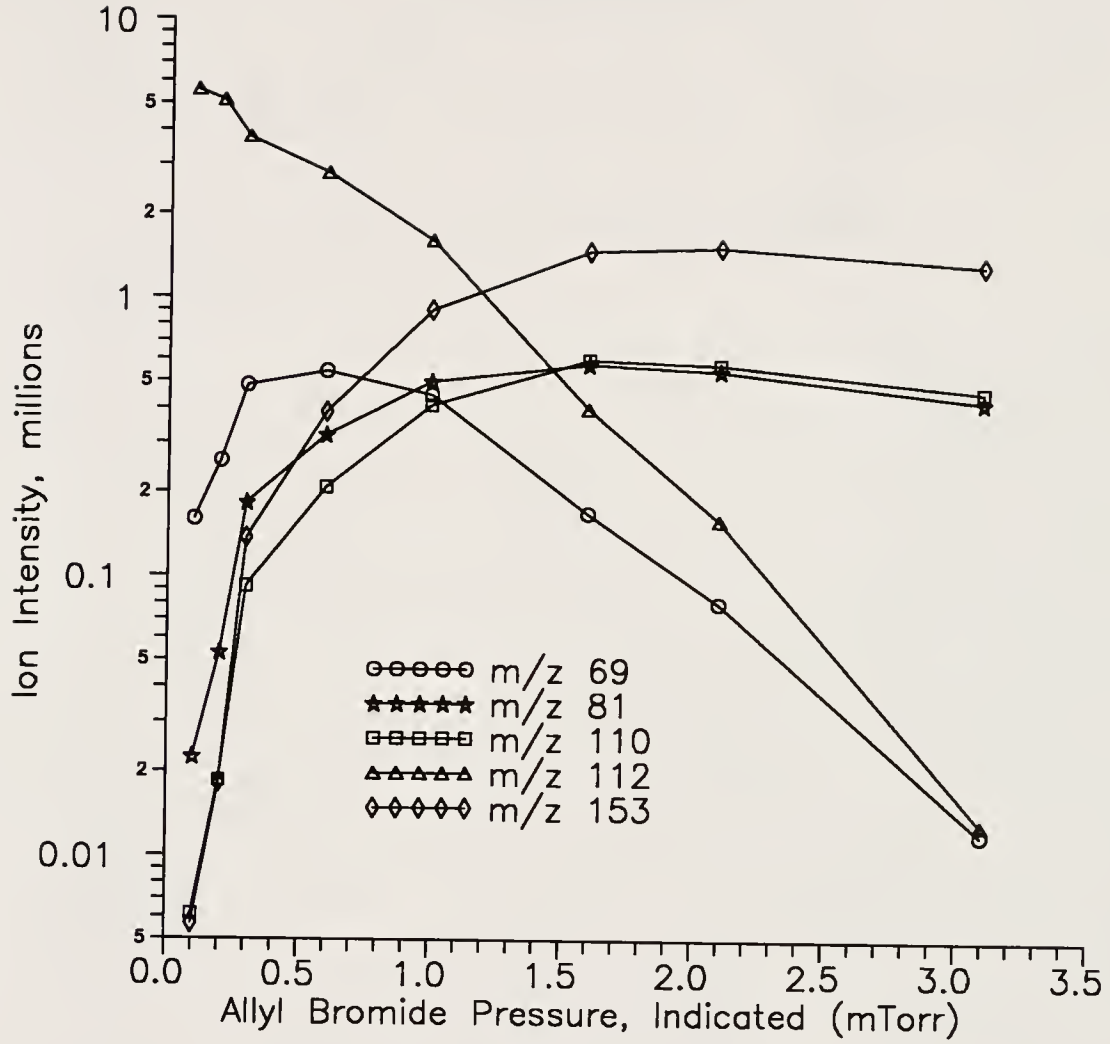

Figure 3-2: Effect of allyl bromide pressure on product ion distribution for the reaction of uracil $N^{+\cdot}$ ions, m/z 112, with allyl bromide.

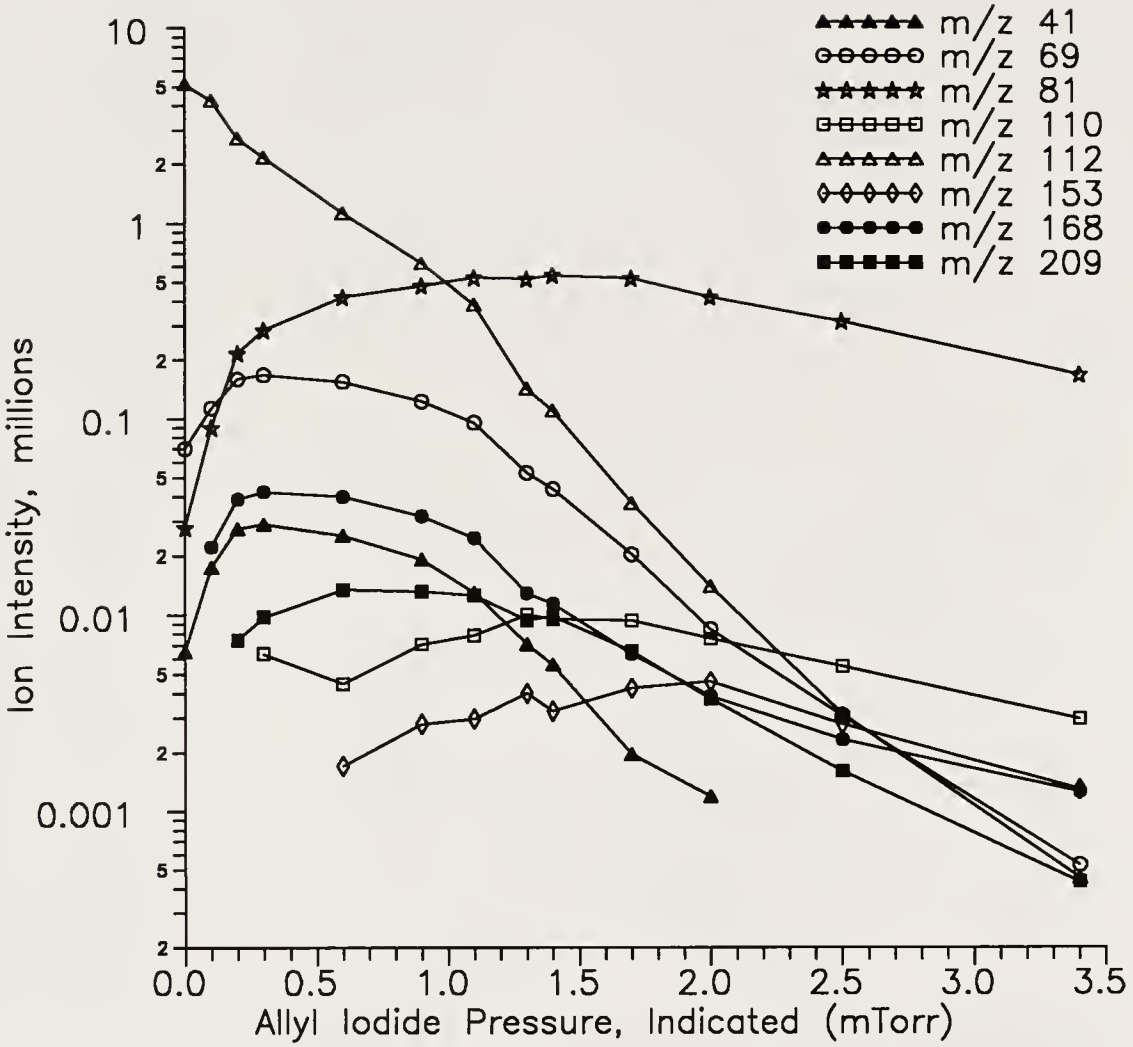

Figure 3-3: Effect of allyl iodide pressure on product ion distribution for the reaction of uracil $N^{+\cdot}$ ions, m/z 112, with allyl iodide.

Upon inspection of Figure 3-1, it is clear that the reactions that take place between uracil molecular ions and allyl chloride are relatively simple and few in number. As $N^{+\cdot}$ (m/z 112) is depleted, the intensity of the product ion, P^+ (m/z 153), increases until scattering begins to occur. The P^+ intensity then decreases gradually at higher allyl chloride pressures. The reaction that occurs between the major CID daughter ion of the uracil $N^{+\cdot}$ ion, m/z 69, and allyl chloride behaves similarly. As the pressure of allyl chloride in the collision cell increases, m/z 69 initially increases in intensity due to CID, and then decreases due to reaction with allyl chloride to form m/z 110, which is analogous to m/z 153 (P^+). Indeed, the curves for m/z 110 and m/z 153 mirror one another, as do the curves for m/z 69 and m/z 112 at higher pressures.

Examination of Figure 3-2 shows similar behavior for the reaction of uracil $N^{+\cdot}$ ions and allyl bromide. In addition to the ions depicted in Figure 3-1, a significant amount of m/z 81 is also formed at indicated pressures above 1 mTorr. This species, presumed to be the 3-methylcyclopentenyl ion, $[E_2\text{-HX-X}]^+$, evolves from reaction of an allyl bromide ion (formed via charge exchange with uracil $N^{+\cdot}$ ions) with an allyl bromide molecule. It is somewhat surprising that allyl bromide ions would form via charge exchange with uracil molecular ions since the ionization energy of allyl bromide (10.06 eV) is higher than the recombination energy of uracil $N^{+\cdot}$ ions (9.2 eV). However, small intensities of the allyl bromide ions 120^+ and 122^+ are observed in the product ion spectra (not shown in Figure 3-2), maximizing at an indicated allyl bromide pressure between 0.5 and 1.0 mTorr. Other research in our

laboratory [77] has substantiated that m/z 81 arises via the reaction between allyl bromide ions and allyl bromide neutrals. Not surprisingly, m/z 81 reaches a maximum intensity at about the same allyl bromide pressure as does P^+ (m/z 153). Then, at increasing allyl bromide pressures, all the ion intensities decrease due to scattering losses.

The reaction of uracil $N^{+\cdot}$ ions with allyl iodide (Figure 3-3) produces a somewhat different reaction profile than the reactions with either allyl chloride or allyl bromide, with many more side reaction products observed. In particular, m/z 81 dominates the spectra at pressures of allyl iodide greater than 1 mTorr, eventually surpassing the intensity of m/z 153 (P^+) by almost two orders of magnitude. Other product ions are also formed that can be directly related to charge exchange between uracil $N^{+\cdot}$ ions and allyl iodide neutrals. In addition to m/z 81, ions at m/z 41, 168 and 209 are also produced via the charge exchange process, corresponding to the allyl ion, $[E\text{-}X]^+$, the allyl iodide ion, $E^{+\cdot}$, and the iodine-bound allyl dimer ion, $[E_2\text{-}X]^+$, respectively. The intensities of both m/z 41 and m/z 168 can be observed to increase at indicated allyl iodide pressures below approximately 0.3 mTorr. At higher pressures, the intensities of m/z 41 and m/z 168 decrease while m/z 81 and 209 production continues to increase due to further reactions of the allyl and/or allyl iodide ions with neutral allyl iodide.

Calibration Studies of Reactions of DNA/RNA Base Ions with Allyl Halides

Experimental

Calibration studies of reactions of the DNA/RNA base ions with allyl halides were conducted under the identical mass spectrometric conditions as those employed for the experiments described previously. Introduction of the allyl halides into Q2, however, was accomplished via gas chromatography, instead of a fine-metering valve, so that precise amounts of each allyl halide could be allowed to react with the nucleophile ions. Gas chromatography was carried out on a J & W Scientific (Folsom, CA) DB-5 (20 m long, 0.25 mm i.d., 0.5 μm film thickness) capillary column in the split mode (split ratio = 100:1) with helium carrier gas at an inlet pressure of 5 psig. The GC oven was temperature programmed from 50°C to 100°C at 20°C/min, yielding retention times for allyl chloride, allyl bromide, and allyl iodide of 45 s, 55 s, and 75 s, respectively. Injection port and transfer line temperatures were maintained at 200°C. One microliter injections were made in triplicate of mixtures containing equimolar amounts of allyl chloride, allyl bromide and allyl iodide in pentane. The solutions utilized ranged in concentration from 9.8 fmol/μL to 980 nmol/μL.

Evaluation of Sensitivity Measurements

There are several processes that must be considered when evaluating the overall sensitivities of the reactions of nucleophile ions toward the allyl halides.

These critical issues affect the shapes and linearities of calibration curves and ultimately determine the apparent limits of detection of three allyl halides. The various parameters can be broken down into the following general events or categories:

1. The partial pressure of neutral nucleophile molecules available for ionization in the ion source.
2. The ionization efficiency of the nucleophile which determines the number of ions in the source.
3. The percentage of ions in the source that are the ion of interest, normally the molecular ion, $N^{+\cdot}$.
4. Ion transmission from the ion source through the first mass analyzer into the collision cell; all four of these factors determine the flux of $N^{+\cdot}$ ions available for reaction.
5. The gas-phase reactivity of the $N^{+\cdot}$ ion to form the desired product ion, $P^{+\cdot}$.
6. The variety and extent of competing side reactions that may take place as well; in the studies to date, most of these side reactions involve the formation and further reaction of electrophiles ionized by charge exchange, making the difference in ionization energies between the nucleophile and electrophile the most critical parameter.
7. The pressure of the electrophile, or other species, in Q2, which affects the extent of CID and scattering losses.
8. The pressure of helium in Q2 (carrier gas from the GC).

9. Ion transmission out of the collision cell and through the second mass analyzer to the detector, which determines the number of product ions that are detected by the electron multiplier.

Effect of Uracil $N^{+\cdot}$ Ion Intensity on Product Ion Formation

The effect of uracil $N^{+\cdot}$ ion intensity (i.e., the amount that is available for reaction) on product ion (P^+, m/z 153) formation via reaction with the allyl halides has been studied. Figure 3-4 shows the single reaction monitoring (SRM) curves for the collision cell reactions of uracil $N^{+\cdot}$ ions with allyl halides. Linear log-log curves are obtained over two orders of magnitude when varying the number of uracil $N^{+\cdot}$ ions that are allowed to react with 9770 pmol of each allyl halide introduced separately into the collision cell via GC. Furthermore, the slopes of the three curves are all approximately equal to one, indicating that the curves (when plotted using linear axes) are truly linear throughout the range of $N^{+\cdot}$ fluxes utilized. The results indicate that, in this case, uracil ion is the "limiting reagent" for each of the ion molecule reactions. The fact that the product ion intensity is directly proportional to the amount of $N^{+\cdot}$ available for reaction suggests that there is always a surplus of allyl halide in the collision cell. Also, the results point out that the absolute amount of nucleophile available for reaction should be as large as possible for quantitative determinations so that maximum sensitivity is realized, as previously shown for reactions with pyridine ions [40].

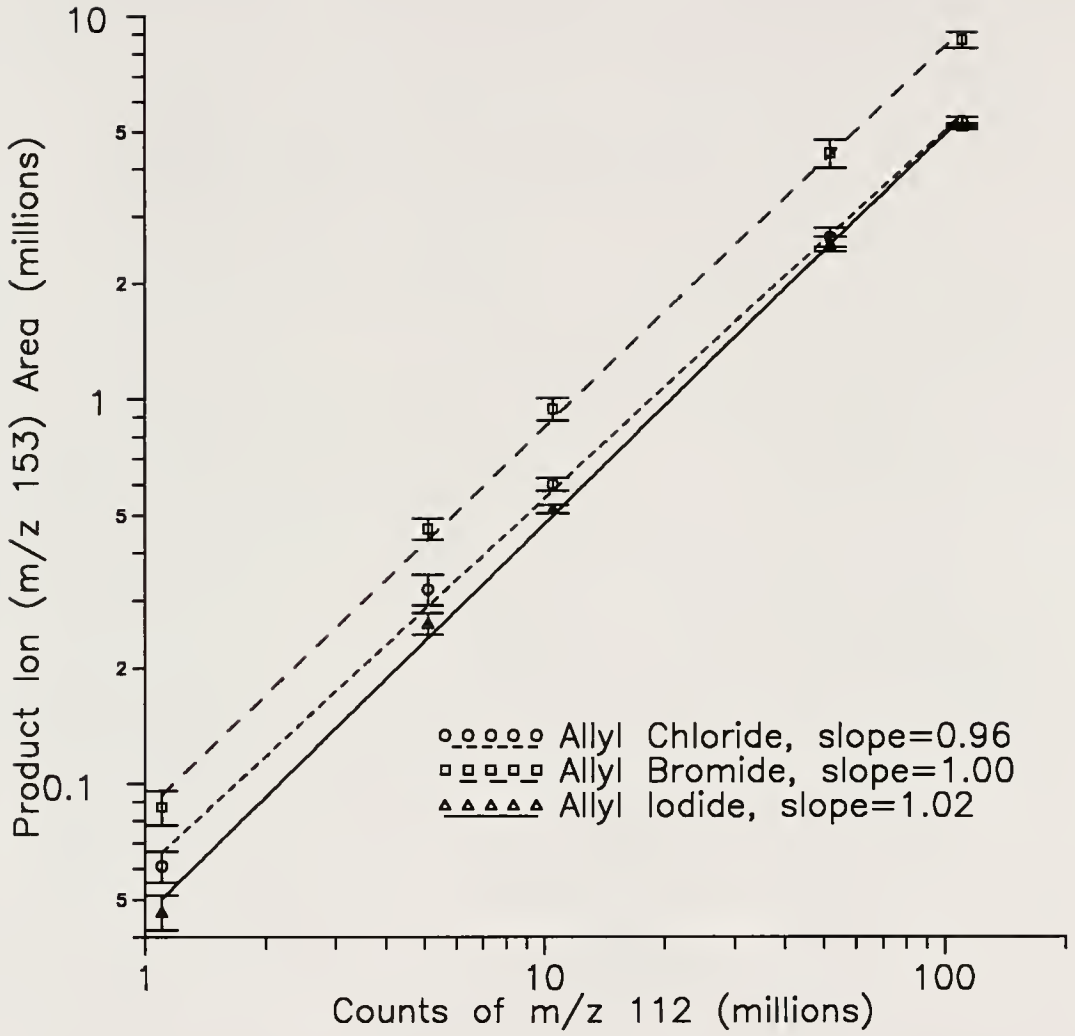

Figure 3-4: Single reaction monitoring (SRM) curves for the collision cell reactions of uracil $N^{+\cdot}$ ions with allyl halides (varying flux of $N^{+\cdot}$ that enters Q2; 9770 pmol of each allyl halide on column).

It is also interesting to note that, for each of these studies, product ions that indicate the presence of neutral uracil in the collision cell (i.e., $[N_2+H]^+$ or $[N_2+X]^+$) were never observed. Other studies [1] of reactions of the more volatile model DNA bases pyridine and piperidine with allyl halides have shown that products resulting from reactions of neutral nucleophile molecules in the collision cell are common. These observations can be attributed to the very high pressures of pyridine and piperidine that were utilized in the ion source for ion production. Invariably, at higher pressures some neutral pyridine or piperidine would migrate into the collision cell where it could take part in unwanted side reactions. The partial pressure of the DNA base uracil (a solid at room temperature), however, is much lower than those of either pyridine or piperidine (both liquids at room temperature). Therefore, for the studies performed here insignificant amounts of neutral nucleophile (uracil) entered the collision cell and no product ions that contain two or more nucleophile species were observed.

Calibration Studies of Allyl Halides

Calibration curves have been produced for the reactions of the DNA/RNA base ions with the allyl halides. Figures 3-5 through 3-8 show the single reaction monitoring curves obtained for the collision cell reactions of each DNA/RNA base ion while varying the amount of each allyl halide introduced into the collision cell for reaction. It is clear that the range of allyl halide concentrations that can be detected depends intrinsically on the nucleophile used for the reaction. As the

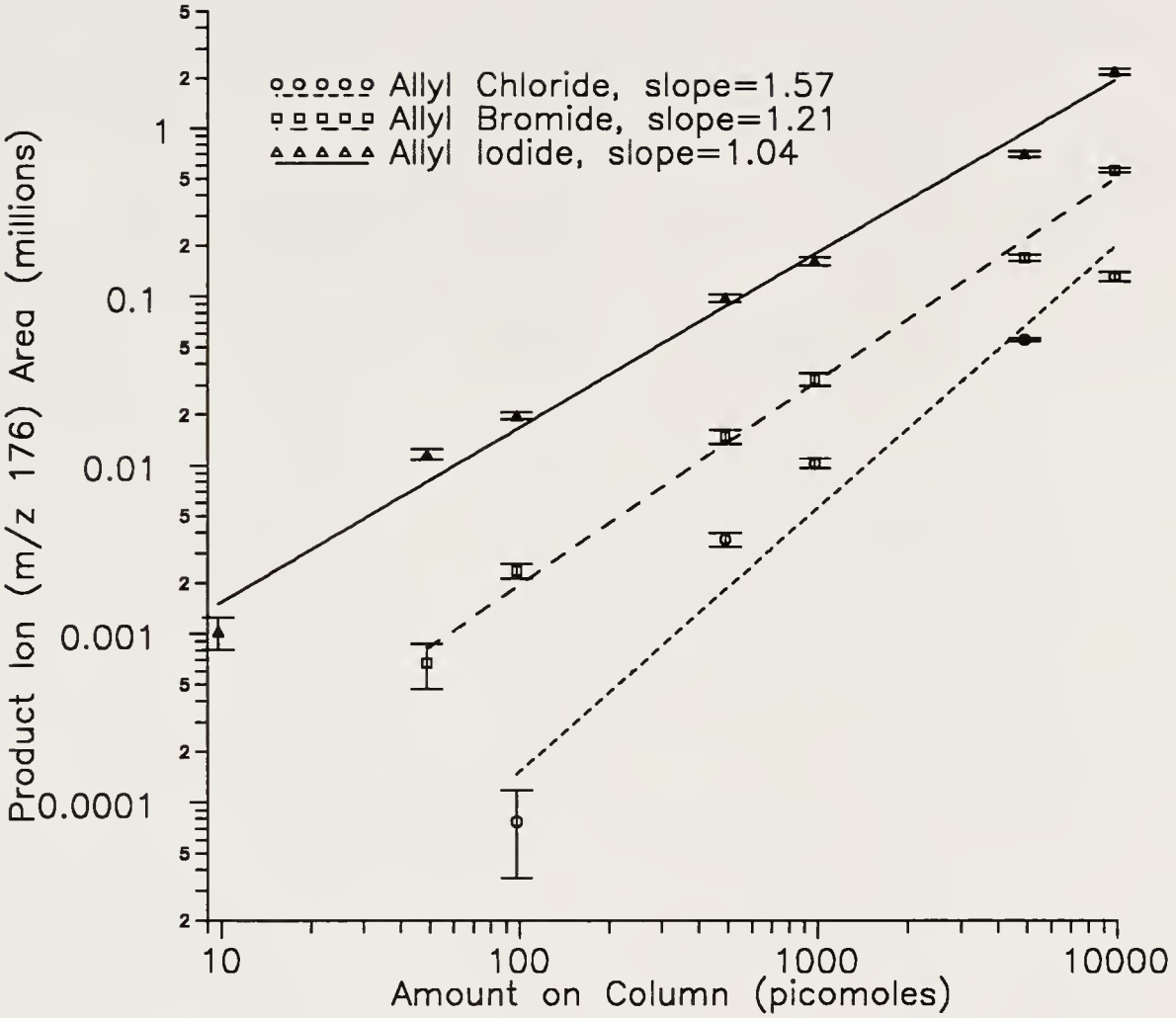

Figure 3-5: Single reaction monitoring (SRM) calibration curves for the collision cell reactions of adenine $N^{+\cdot}$ ions with allyl halides.

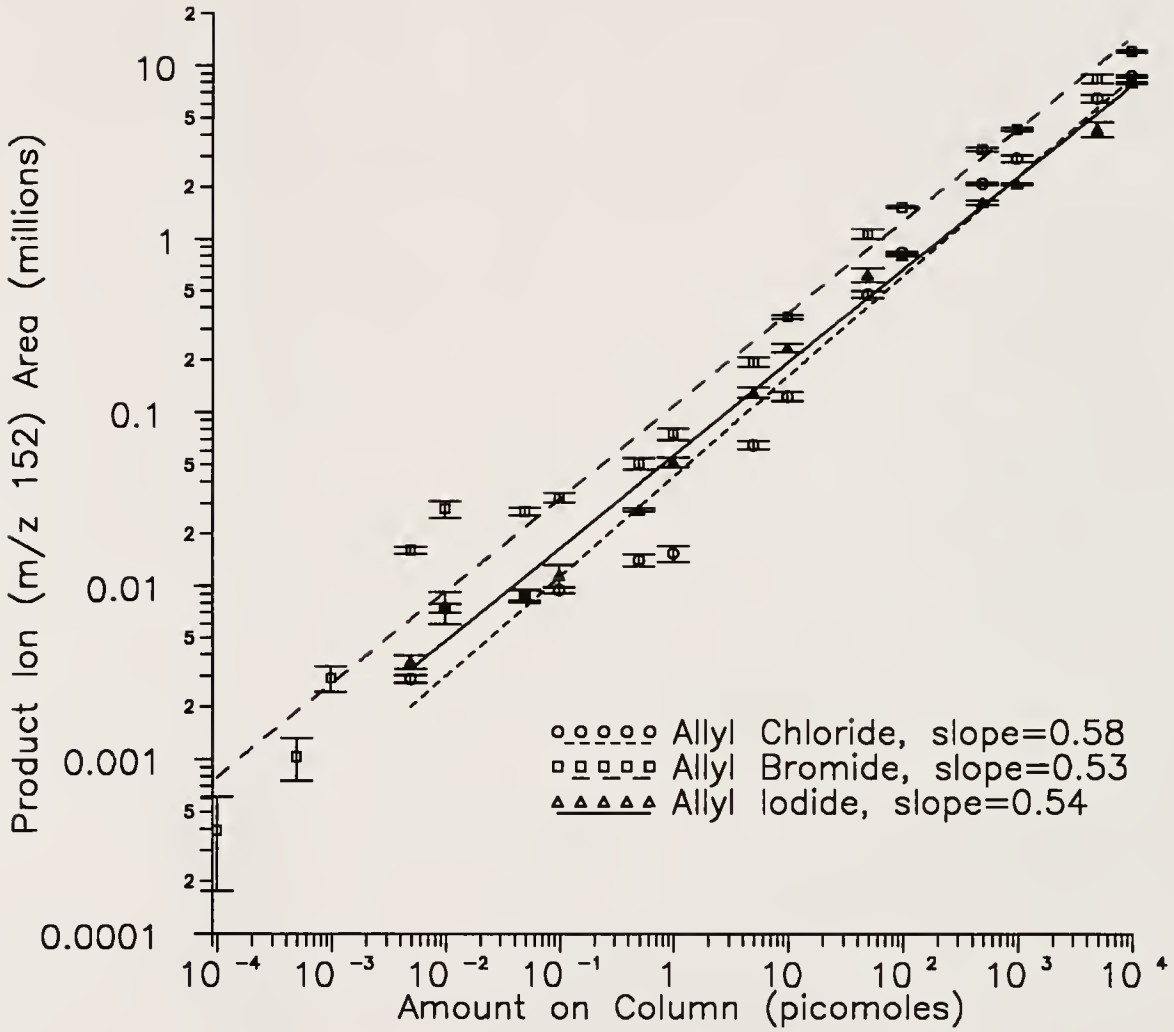

Figure 3-6: Single reaction monitoring (SRM) calibration curves for the collision cell reactions of cytosine $N^{+\cdot}$ ions with allyl halides.

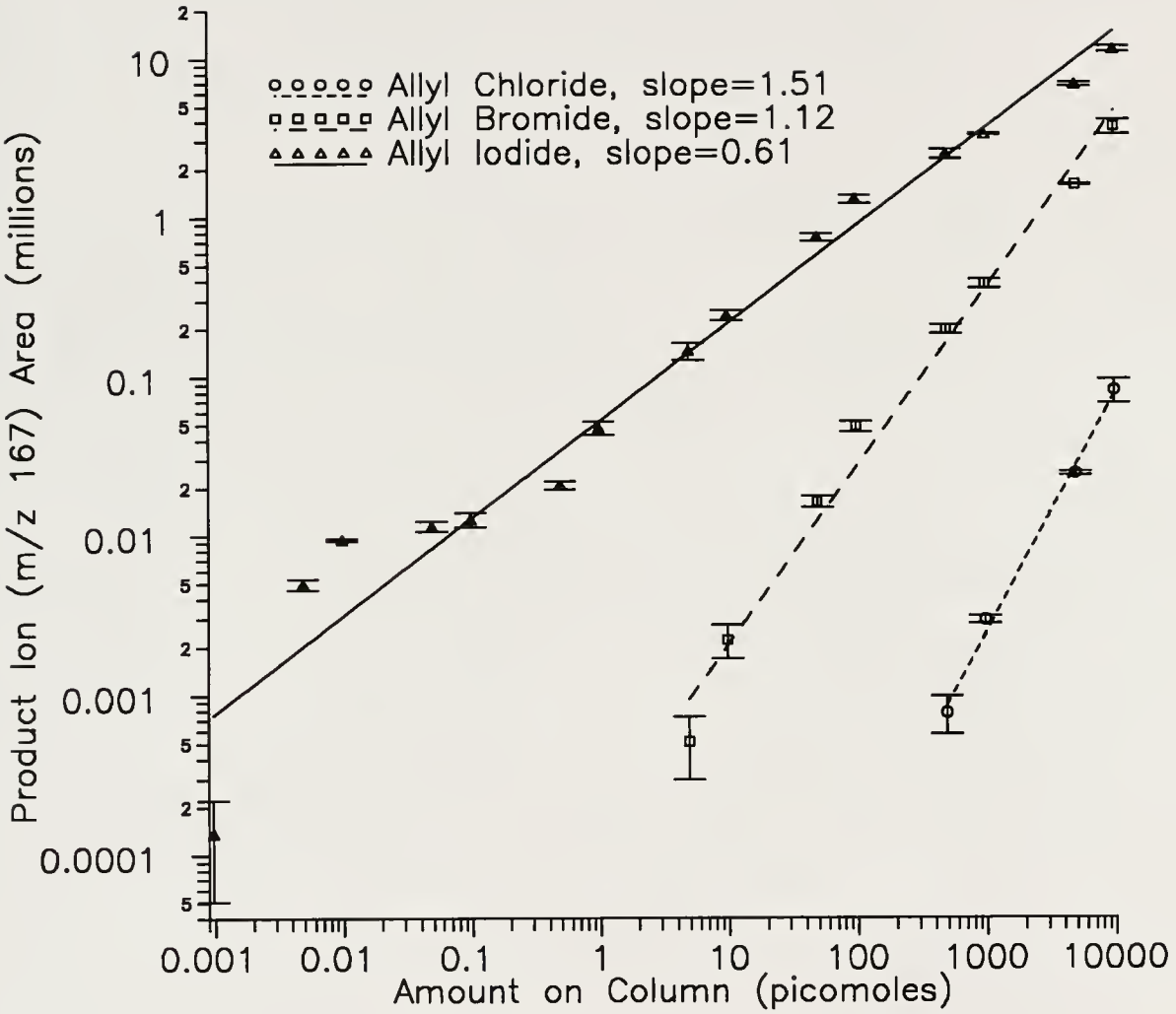

Figure 3-7: Single reaction monitoring (SRM) calibration curves for the collision cell reactions of thymine $N^{+\cdot}$ ions with allyl halides.

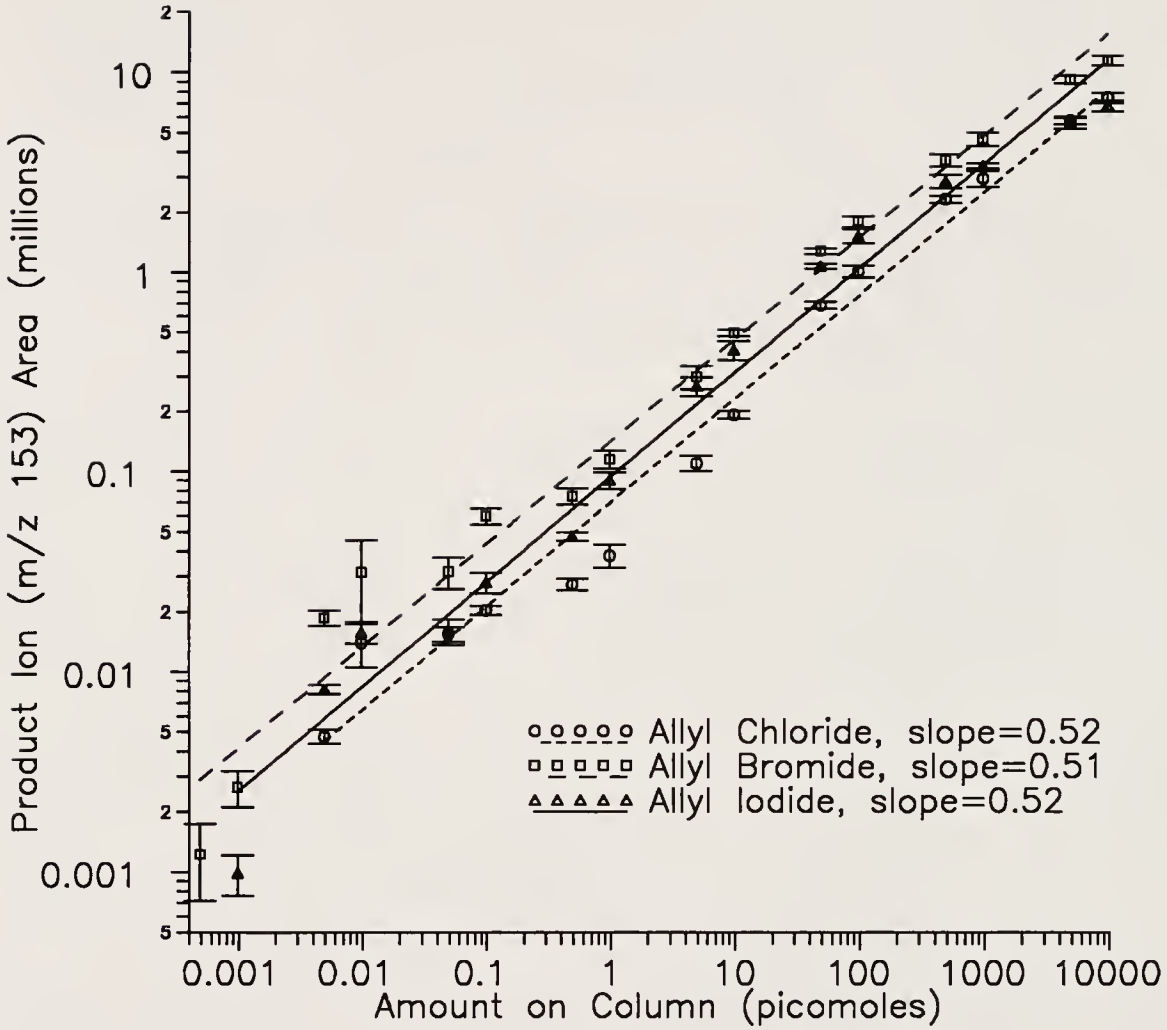

Figure 3-8: Single reaction monitoring (SRM) calibration curves for the collision cell reactions of uracil $N^{+\cdot}$ ions with allyl halides.

relative reactivities reported in Figure 2-6 would indicate, a very reactive combination such as uracil ions with allyl bromide produces detectable intensities of product ions over a wide range of concentrations (over seven orders of magnitude), as shown in Figure 3-8. In contrast, an only slightly reactive combination such as adenine ions with allyl chloride (see Figure 2-6) produces detectable intensities of product ions over only two orders of magnitude, as shown in Figure 3-5.

Looking at Figures 3-5 through 3-8, it is obvious that the log-log slopes of the calibration curves vary substantially depending on the nucleophile/electrophile combination used for each reaction. Slopes between 0.51 for the reaction of uracil ions with allyl bromide (Figure 3-8) and 1.57 for the reaction of adenine ions with allyl chloride (Figure 3-5) have been observed. Log-log slopes for each of the calibration curves are tabulated along with the relative reactivities of each DNA/RNA base ion toward the allyl halides (as calculated in Chapter 2) in Table 3-1. It is clear that there is a correlation between the relative reactivities of each nucleophile/electrophile pair and the log-log slope of the corresponding calibration curve. In general, reaction pairs that are quite unreactive (small relative reactivities) have slopes larger than one, maximizing at around 1.6, whereas reaction pairs that are very reactive (large relative reactivities) have slopes much less than one, minimizing around 0.5.

It should be pointed out that log-log slopes not equal to one indicate curves that are non-linear when plotted on linear axes; curves with log-log slopes less than one level off horizontally at increasing amounts on column, while curves with log-log

Table 3-1: Comparison of the relative reactivities of the DNA/RNA base ions and the log-log slopes of their calibration curves.

Nucleophile Ion, $N^{+\cdot}$	Electrophile, E	Relative Reactivity[a]	Log-Log Slope of Calibration Curve[b]
Adenine	Allyl Cl	0.001	1.57
	Allyl Br	0.005	1.21
	Allyl I	0.011	1.04
Cytosine	Allyl Cl	0.293	0.58
	Allyl Br	0.496	0.53
	Allyl I	0.285	0.54
Thymine	Allyl Cl	0.001	1.51
	Allyl Br	0.075	1.12
	Allyl I	0.313	0.61
Uracil	Allyl Cl	0.330	0.52
	Allyl Br	0.601	0.51
	Allyl 1	0.157	0.52

[a] Relative reactivities calculated as outlined in Chapter 2 and reported in Figure 2-6.
[b] Log-log slopes as indicated in Figures 3-5 through 3-8.

slopes greater than one skew upward as the amount on column increases. This means that, for the curve generated by the reactions of uracil ions with allyl bromide, product ion intensities increase by successively smaller proportions as the amount of allyl bromide introduced into the collision cell is increased. This behavior is probably due to the high reactivity of uracil ions toward allyl bromide. Since uracil ions are highly reactive, they are consumed more quickly (whether it be to form side reaction products or the desired product ion) when a larger quantity of allyl bromide is available for reaction. This same argument can be applied for the other reaction pairs (i.e., cytosine ions with the three allyl halides) that have log-log calibration curve slopes less than one. Conversely, for the curve generated by a quite unreactive pair (i.e., adenine ions and allyl chloride), product ion intensities increase by successively larger proportions as the amount of allyl chloride introduced into the collision cell is increased, as indicated by a log-log slope greater than one.

Conclusions

Several important considerations when performing reactions of ionized DNA/RNA bases with allyl halides in the collision cell of a triple quadrupole mass spectrometer have been addressed. It has been shown that allyl halide pressure can have a great effect on the relative intensities of the various product ions observed upon reaction with uracil ions. In particular, when allyl iodide is used as the electrophile many side reactions are observed due to charge exchange between the ionic uracil species and neutral allyl iodide. These side reaction products often

dominate the spectra at higher allyl iodide pressures, overshadowing the desired allyl adduct ion, P^+. Furthermore, it has been observed that at high pressures of allyl halide, ion losses due to scattering begin to occur, decreasing the sensitivity of the technique.

The technique of using Q2 ion-molecule reactions for quantitative analysis is much more involved than typical mass spectrometric techniques such as GC/MS. While the sensitivity of a technique such as GC/MS is determined primarily by the characteristics of the instrument and the properties of the analyte, the sensitivity of analytical ion-molecule reactions also depends on the attributes of the reaction itself, as well as those of possible competing reactions. With this in mind, calibration curves for reactions of DNA/RNA base ions with allyl halides have been obtained. Varying the nucleophile ion intensity for the reaction of uracil ions with allyl halides resulted in linear log-log plots with slopes of one. Upon variation of the amount of allyl halide neutral available for reaction with nucleophile ions, however, log-log calibration curves were observed to be linear, but with slopes ranging from 0.51 to 1.57 depending on the particular nucleophile ion. The individual slopes are related to the relative reactivities of each specific nucleophile/electrophile reactant couple, with higher slopes resulting from less reactive species, and more reactive pairs producing curves with lower slopes.

CHAPTER 4
DEVELOPMENT AND CHARACTERIZATION OF A SYSTEM FOR TRAPPING IONS IN THE COLLISION CELL OF A TRIPLE QUADRUPOLE MASS SPECTROMETER

Introduction

As will be demonstrated in this chapter and the next, trapping ions in the collision cell of a linear quadrupole instrument can be useful for studies of ion-molecule reactions. The technique, however, is not very common, having been implemented by only a few research groups [51-57]. This lack of utilization can be attributed, in part, to the unique designs of the many tandem quadrupole instruments in use today. The ion optical layouts, instrumental hardware, instrument control software and data system configurations are different for each commercial design. Additionally, "home-made" instruments that have unique designs of their own are being used in several laboratories. Moreover, many groups have found it necessary to further modify their instruments to successfully implement ion trapping in the linear quadrupole devices. Therefore, it is clear that a particular ion trapping scheme cannot be universally applied to every type of tandem quadrupole instrument, and that each kind of device must be considered individually. This points out that each instrument must be characterized before successful ion trapping is accomplished. With this in mind, this chapter will focus on the characterization

of the TSQ70 triple quadrupole mass spectrometer used in these studies and its development for use as an ion trapping device.

The Finnigan MAT TSQ70 Triple Quadrupole Mass Spectrometer

The Finnigan MAT TSQ70 triple quadrupole mass spectrometer (and its successor, the TSQ700) is certainly one of the most popular tandem quadrupole instruments in use today. This, and the fact that it is a highly complex and powerful computer controlled instrument, make it a good choice for development of a Q2 ion trapping system. A system developed for the instrument in our lab could be easily applied to other TSQ70 instruments worldwide. Additionally, the instrument is ideal for methods such as Q2 ion trapping since all instrumental parameters are under microprocessor control, and can be changed in real time. Control of the instrument by the user is accomplished using Instrument Control Language (ICL) procedures. This unique interface allows for computer control of any number of instrumental parameters during an experiment. Furthermore, ICL is structured similarly to many common computer programming languages, such as BASIC, which allows the instrument to receive incoming data and react accordingly. When performing ion trapping in the collision cell, this means that many operations that would be controlled by hardware modifications on other instruments can be regulated by software programmed on the TSQ70.

Figure 4-1 shows a diagram of the mass analyzer assembly of the TSQ70. As can be seen in the figure, the TSQ70 consists of an ion source, two quadrupole mass

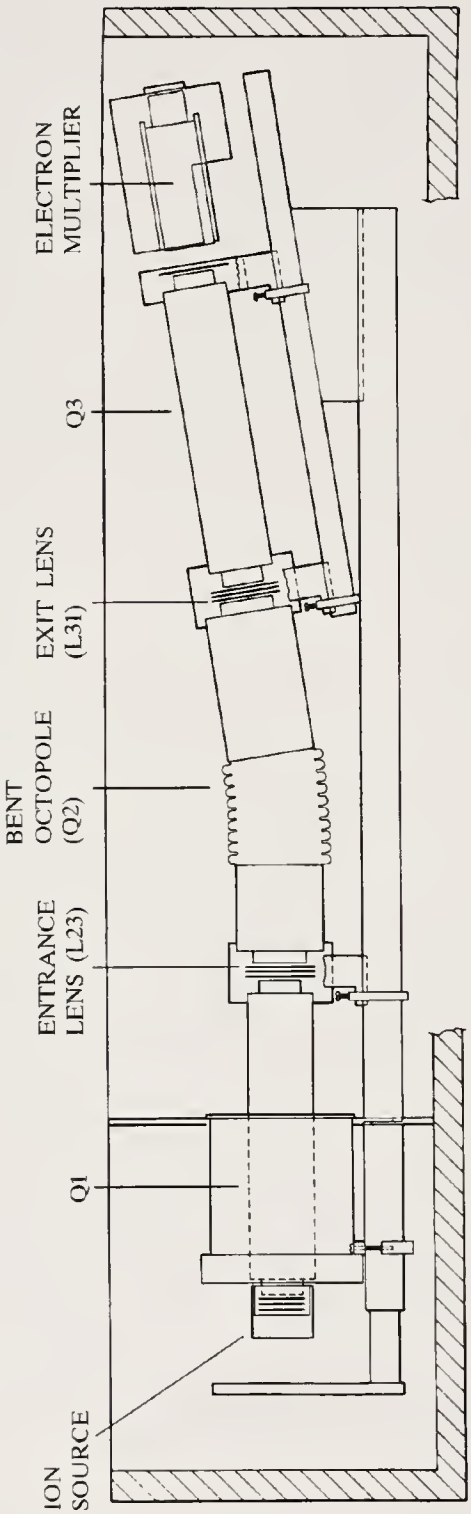

Figure 4-1: The mass analyzer assembly of the Finnigan MAT TSQ70 triple quadrupole mass spectrometer.

filters (Q1 and Q3), an enclosed bent octopole collision cell (Q2) and several focusing lenses mounted on an optical rail. To avoid confusion, only the lenses (L23 and L31) utilized for trapping ions in the collision cell have been labelled. One component of the TSQ70 that is quite different from all other triple quadrupole mass spectrometers is the bent collision cell. The bent design allows improved signal-to-noise ratios compared to linear collision cells, without a compromise in ion transmission [78-79]. The benefits are most apparent when using ionization methods which produce an abundance of excited neutrals, such as fast atom bombardment (FAB) ionization. The bent design reduces the number of neutrals that traverse the length of the instrument and reach the detector, and thus decreases the noise from the electron multiplier.

The collision cell of the TSQ70 used in these studies is, in fact, different from that in most other TSQ70 mass spectrometers in use. Typical TSQ70 instruments have a quadrupole collision cell, but the instrument in our laboratory was upgraded to the octopole design used in the newer TSQ700 mass spectrometers. Under normal operating conditions, almost no noticeable changes in spectral quality have been observed. However, many groups that have studied multipole devices with two-dimensional electric fields [58,80-84] have found that, in some cases, higher-order multipoles may be advantageous when used as RF-only collision cells. Through theoretical treatments and simulations, Hägg and Szabo [58,81-82] determined that octopoles are not best suited to operating as mass filters in the RF/DC mode. They pointed out that the diffuse stability diagrams of higher-order multipoles, due to

inherent nonlinearities, give rise to mass resolution too low for the purpose of mass analysis. However, they did state that octopoles can be more effective than quadrupoles in the RF-only mode for guiding and transporting low-energy ions, such as in a collision cell. In a related study, Syka and Szabo [83] evaluated the ion transmission characteristics of quadrupole, hexapole and octopole collision cells in the RF-only mode on a TSQ70 mass spectrometer. They suggested that octopole collision cells are modestly advantageous in comparison to quadrupole collision cells due to somewhat extended stability regions, leading to wider mass ranges, and more uniform transmission qualities. It was also pointed out that RF-only octopoles would be useful in studies where correct ion kinetic energies must be known, due to the flat-bottomed pseudo-potential wells generated by higher-order multipole fields. A representation of this concept, generated using the SIMION ion simulation program [85] and the exact measurements of the two commercially available TSQ70 collision cells, is shown in Figure 4-2. Davis and Wright [84] have also studied multipole collision cells, using a computer modelling technique. In their work, calculations were made to determine factors affecting transmission of ions through higher-order multipoles under more extreme entry conditions. It was determined that, under these circumstances, the trajectories may be less stable in an octopole than in a quadrupole. It was also noted, however, that if a well-ordered beam enters the octopole, the higher-order multipole may be advantageous in that it restricts transverse kinetic energy and causes an overall smearing of the parent ion oscillations. Effectively, this is the case for the TSQ70 collision cell. The focussing

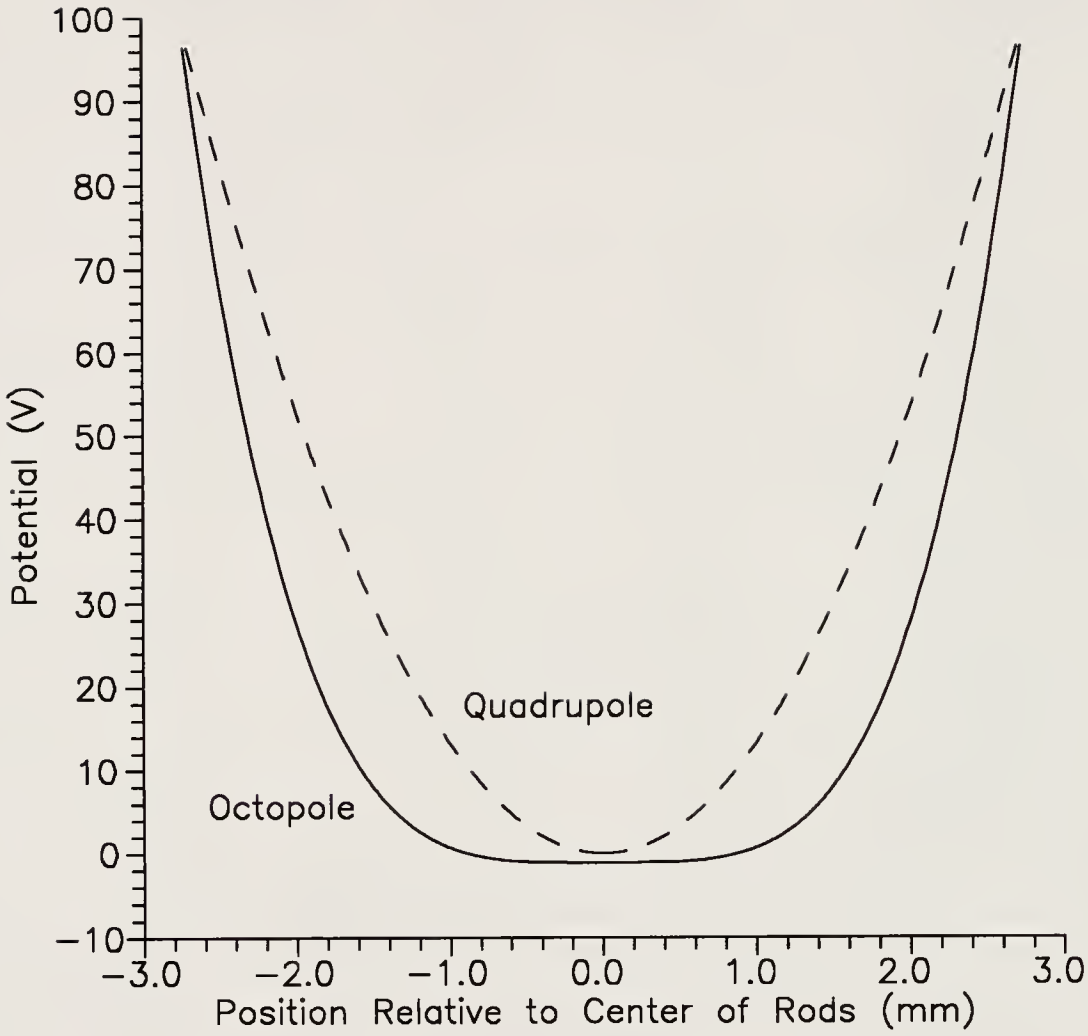

Figure 4-2: Comparison of pseudo-potential wells of the quadrupole and octopole collision cells of the TSQ70. Data generated using the SIMION ion simulation program with offset potentials of 0 V and RF potentials of ±100 V applied to opposite rods.

lenses immediately before the collision cell constrict the ion beam so that it enters the collision cell close to the central axis. This allows the octopole to act as an efficient ion containment device.

Trapping Ions in the Collision Cell of the TSQ70

The concept behind trapping ions in the RF-only octopole collision cell is relatively simple. The technique involves utilizing the lenses immediately before and after Q2 as electrostatic mirrors, trapping ions within the cell. The ions are then held within the octopole field for a variable time period, allowing ion-molecule reactions to occur, and subsequently scanned out via the third quadrupole.

Figure 4-1 shows the configuration of the TSQ70 triple quadrupole mass spectrometer used for trapping ions in Q2. Essentially, ions are trapped in Q2 by varying the potentials applied to the entrance (L23) and exit (L31) lenses in a specific and repetitive manner. An illustration of the time profiles of the voltages applied to the entrance and exit lenses is depicted in Figure 4-3. The lens potentials are changed according to Instrument Control Language procedures specifically designed to facilitate ion trapping in Q2. Additionally, these procedures allow for control of variables significant to the trapping process such as ion trapping time and Q2 fill time, as discussed below.

Inspection of Figure 4-3 shows that there are three distinct stages in a Q2 ion trapping cycle. The first stage, called the fill time, allows ions to be gated into the collision cell from Q1. In this interval, the entrance lens, L23, is held at an open

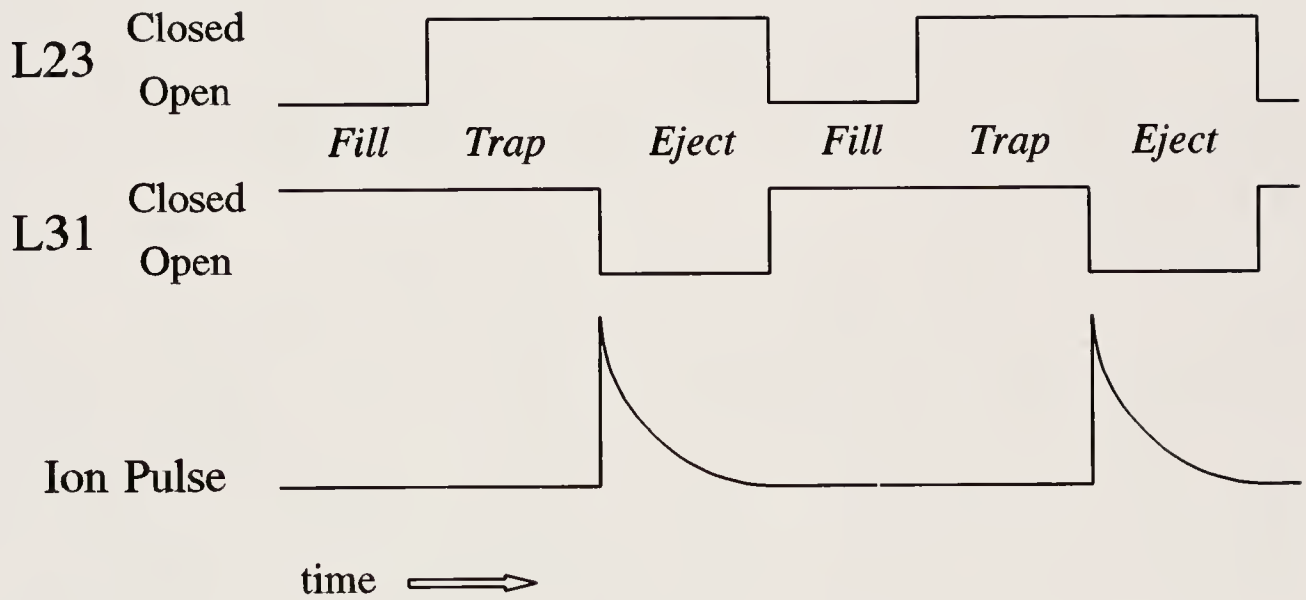

Figure 4-3: Time profile of the potentials applied to the entrance, L23, and exit, L31, lenses during the course of a Q2 ion trapping experiment.

potential while the exit lens, L31, is closed. In other words, to fill the collision cell with positive ions, lens L23 is held at a negative voltage while lens L31 is held positive. Through careful selection of the potentials applied to L23 and L31, ions are permitted to enter Q2 but not allowed to exit out the back. Thus, the collision cell is filled with ions. In the second phase of the cycle, the trapping time, lenses L23 and L31 are both closed so that ions may neither enter nor exit the collision cell. During this variable time period processes such as ion-molecule reactions or collision-induced dissociation are allowed to take place. In the last stage of the cycle, the exit lens, L31, is opened allowing the trapped ions to pass through Q3 and be detected my the electron multiplier. During this time, the entrance lens, L23, is still closed so that ions continually formed in the ion source do not pass through Q2 and Q3 and are not detected. An ion pulse typical of what is normally observed is shown in Figure 4-4.

Although the basic Q2 ion trapping scheme is very simple, many parameters must be carefully adjusted to achieve optimum trapping performance. In particular, the potential applied to the entrance lens, L23, when filling the collision cell with ions is of the utmost importance. Additionally, it was discovered that the DC offset voltage applied to the collision cell greatly affects ion trapping efficiency. Also, it was determined that the presence of helium buffer gas in the collision cell dramatically improves the ion trapping ability of the system. These and other parameters will be discussed in detail in the chapter.

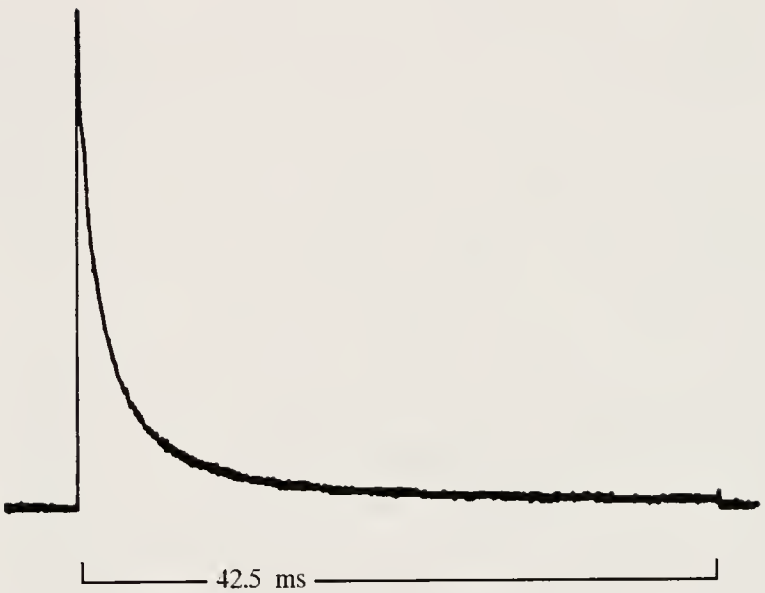

Figure 4-4: Trace of a typical ion pulse detected by a digital storage oscilloscope upon opening of the exit lens, L31, during a trap and pulse cycle.

Experimental

Experimental Conditions

All experiments were performed on a Finnigan MAT (San Jose, CA) TSQ70 triple quadrupole mass spectrometer modified with an octopole collision cell and a 20 kV conversion dynode. Optimization studies were performed using perfluorotributylamine (PFTBA) calibration compound. PFTBA was introduced into an EI ion volume in the ion source via a specially designed probe, constructed in house, which allowed for precise metering of the PFTBA vapor pressure. The probe consisted of a 1/2" o.d. hollow stainless steel probe connected to a variable leak solenoid valve under computer control. PFTBA pressure within the probe was indicated by a Granville Phillips (Boulder, CO) Convectron gauge. Studies were performed under EI conditions at an electron energy of 70 eV and an emission current of 200 μA. The manifold was maintained at temperatures ranging from 70-100 °C while the ion source was held at 170°C.

For the Q2 ion trapping optimization studies, electron multiplier potentials ranging from -600 to -1400 V were utilized. As is discussed in this and the next chapter, several experimental parameters greatly affect the number of ions that ultimately strike the electron multiplier. Among these, the mode in which the second mass analyzer, Q3, is operated, and the presence or absence of helium buffer gas in the collision cell have the largest effects. In general, experiments that were conducted with helium in the collision cell and Q3 in the RF-only mode used

electron multiplier voltages on the order of 700 V. On the other hand, studies that were performed without helium buffer gas in Q2 or with Q3 in the RF/DC mode required electron multiplier voltages upward of -1000 V. In all cases, the preamplifier gain was set at 10^8 V/A and the conversion dynode was held at -5 kV.

The mass spectrometer was tuned with PFTBA to optimize ion transmission and to calibrate the mass assignment using tuning procedures written by Hail [71]. Additionally, further tuning operations were performed using either of the two sets of tuning guidelines recommended in Appendix A.

Experiments involving Q2 ion trapping were regulated by several of the Instrument Control Language procedures listed in Appendix C. These programs were specifically written to perform the atypical operations of dynamically controlling the various ion optical devices needed to effect ion trapping in the collision cell. In addition to utilizing these specially written procedures, several other parameters were optimized for Q2 ion trapping. For all studies, the prescan voltage settling time, SETTIM, was set to its minimum value, 0.1 ms, to minimize the time that the trapping cycles took to execute. Also, the DC offset potential applied to the octopole collision cell was optimized at -6 or -2 V, respectively, depending on whether or not helium buffer gas was employed. For experiments where helium was utilized as a buffer gas, it was introduced into Q2 via a Negretti (Hampshire, England) fine-metering valve to an indicated pressure of approximately 6.0 mTorr. Furthermore, the mode in which Q3 was operated was varied. For experiments where the entire ion pulse was to be detected, Q3 was operated in the RF-only mode

by turning off the Q3 DC potential using the DDOFF command. If, however, mass analysis was to be performed on the pulse of ions as it exited the collision cell, Q3 was operated in the normal RF/DC mass filter mode.

Parameters defined by the Q2 ion trapping process were also carefully controlled. The period of time that the collision cell was allowed to fill with ions, the fill time, was typically on the order of 0.1 to 1 second. However, trapping times ranged from several hundred milliseconds to several minutes or more, depending on the particular experiment. In any case, specific values for fill times and trapping times are stated in the main text when the situation warrants.

Determination of Ion Trapping Efficiencies

In order to evaluate the effectiveness of the octopole collision cell as an ion trapping device, studies were performed to determine the number of ions that are ultimately detected as a percentage of those ions that are initially injected into Q2. For the sake of brevity, this quantity is referred to as %(Out/In). The procedures required to determine %(Out/In) are not intuitively obvious. In particular, calculations of the absolute numbers of ions that enter and exit the collision cell during a typical trapping cycle are difficult. Fortunately, calculation of the percentage of ions that are ultimately detected does not require that the absolute numbers of ions be known. For this reason, absolute quantities were not determined. In place of these, relative ion currents were used for %(Out/In) calculations.

There are several instrumental considerations that must be taken into account when performing %(Out/In) studies. Ideally, the instrument should have 100% transmission through Q2 and Q3 for these experiments, to facilitate the calculations. This is not the case, however. Fortunately, even though there is not 100% transmission, the net effects are canceled. Comparisons of the number of ions injected to the number of ions detected are valid because imperfect transmission characteristics equally affect both processes. Additionally, the Q1 and Q3 mass analyzers must be static (i.e., not scanning) for all the experiments so that a valid comparison of ion intensities can be made. Since ions are gated into the collision cell under static conditions in a trapping experiment, ion current determinations for both the number of ions injected and the number of ions detected must be made under these same conditions. Normally, the TSQ70 does not allow for data acquisition when the instrument is not scanning. However, by using a "DAC scan" one analyzer can be set to pass a chosen m/z while a lens voltage digital-to-analog converter (DAC) is varied over a small range. This, in effect, allows for detection of a continuous ion signal under static conditions.

DAC scans were used in studies to determine the relative number of ions injected into the collision cell. The instrument was set to scan over the ion of interest in the daughter mode while Q3 was operated as an RF-only device with a low-mass cutoff well below the m/z of the particular ion. Thus, ions formed in the ion source entered Q1 where a specific m/z was mass selected. The ions were then allowed to pass unobstructed through Q2 and Q3 and be detected by the electron

multiplier. In order to observe the ion currents, DAC scans were executed where lens L41 was varied over a small range. In fact, due to the nature of operation of the TSQ70 mass spectrometer, lens L41 was never varied at all since, in the daughter mode, the instrument does not permit ion optical components after the collision cell to be changed. At constant electron multiplier voltages and preamplifier gains, potentials representing ion currents were then measured from the SIG1 test point on the electrometer board of the TSQ70 using a LeCroy (Chestnut Ridge, NY) 9400 Digital Storage Oscilloscope (DSO). These values were then multiplied by the fill times used for the trapping experiments to obtain quantities, I_{in}, related to the total number of ions (charge) that were gated into the collision cell.

Determinations of the number of ions detected after being trapped were conducted at electron multiplier voltages and preamplifier gains identical to those used in the corresponding experiments where the relative numbers of ions injected into Q2 were determined. This was done so that additional factors were not introduced. For these experiments, the ICL trapping procedure TQ2FILL5K (Appendix C) was utilized to perform ion trapping, with and without helium buffer gas, in Q2. Using the same fill times as were utilized for the other studies, the TSQ70 parameter TIC read back the total ion currents, A, for the ion pulses as they exited the collision cell. These values provided a measure of the relative areas of the ion pulses. Additionally, the HEIGHT's of the peaks were recorded and converted to TIC's, B, that would have been expected had the signals been square pulses. Division of A by B gives the percentage of the entire area that was the actual pulse,

C. Concurrently, the digital storage oscilloscope was employed to measure the peak potentials of the ion pulses from the SIG1 test point on the electrometer board. Quantities that represent the total number of ions that were detected after being trapped in Q2, I_{out}, were then calculated by multiplying C by the scan time and the peak voltage as measured by the DSO. Finally, the numbers of ions that were ultimately detected as a percentage of those ions that were initially injected into Q2, %(Out/In), were calculated by dividing I_{out} by I_{in}.

TSQ70 Timing Studies

In order to gain some insight as to how the TSQ70 mass spectrometer operates with respect to acquisition timing, studies were performed to determine how scan time depends on several instrumental parameters. Changes in apparent scan time were noted upon variation of mass range. Additionally, the type of data acquired (profile or centroid) and whether or not the data were written to disk also affected the actual scan time. In addition to the fundamental understanding this work provided, these studies also contributed some knowledge useful in developing the procedures for Q2 ion trapping.

By far, the parameter which most affects the actual scan time is the mass scanning range. As shown in Figure 4-5, it is clear that the time required for a scan is affected greatly by the mass range that the instrument is scanning over. Although the requested scan time for these studies was set at 0.1 s, the actual time required for a single scan varied from approximately 115 to 124 ms, depending on the mass

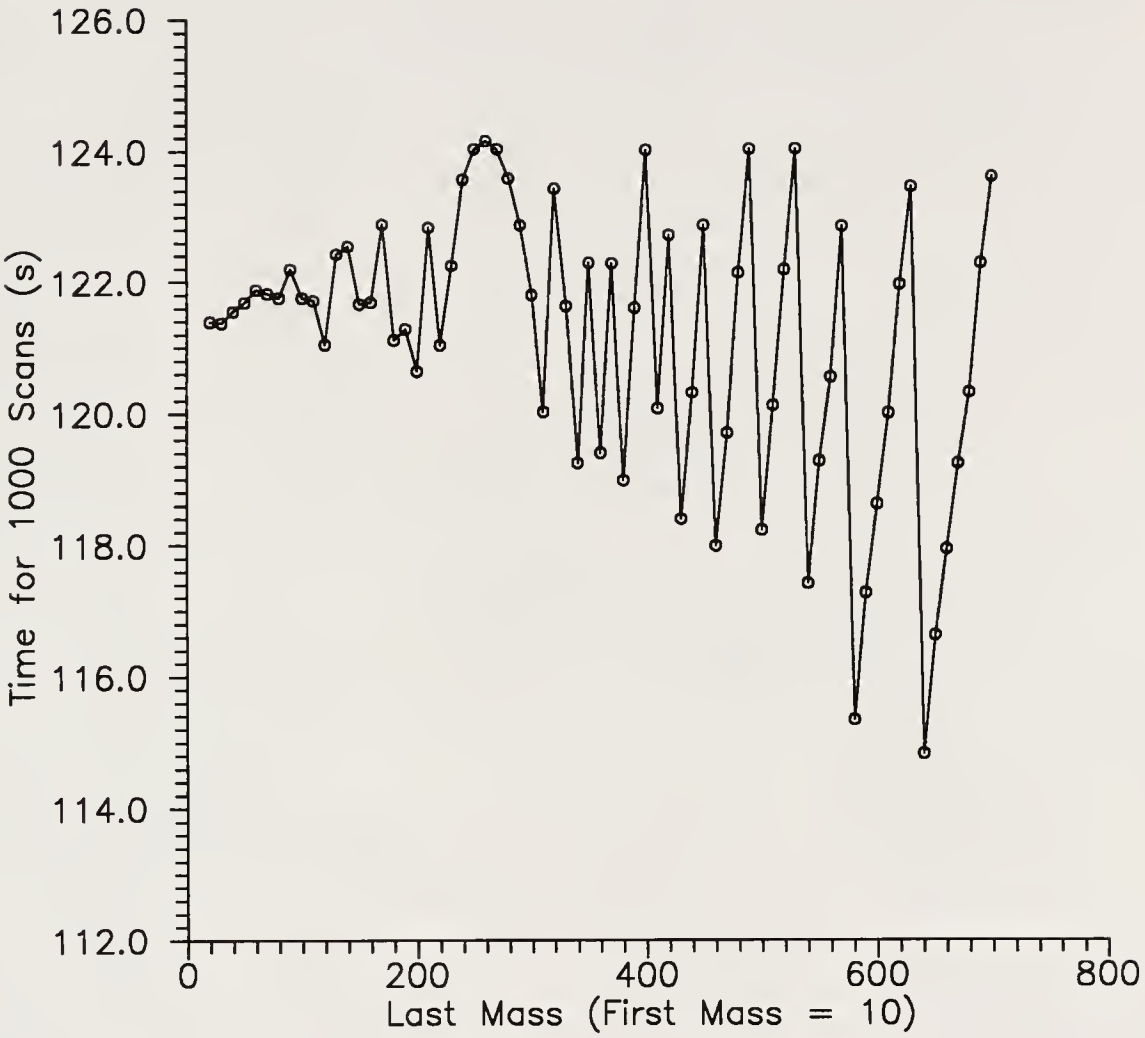

Figure 4-5: Dependence of observed scan time on mass range. Q1MS, profile data, scan time = 0.1 s.

range. Some of this extra time can be attributed to interscan overhead time, but a large part of it is due to real increases in the time required to perform the scan itself. Furthermore, it is easy to see that the graph follows a sawtooth form at higher masses and that the actual length of time that a scan takes cannot be directly related to the width of the mass range the instrument is scanning over. These observations are explained by considering the manner of operation of the TSQ70. The actual scan time that the instrument uses is limited by the clock rate and resolution of the 16-bit mass scan digital-to-analog converter (DAC). Additionally, the algorithm that is used to calculate the scan rate often causes the real scan rate to be somewhat different from that which was requested. Thus, the instrument always scans at a rate which is as close as possible to the requested rate, but often it is off by a substantial amount for wide mass ranges and fast scan times, due to quantization noise. Another prominent characteristic of the graph is the large hump between last masses of approximately 200-300 amu. This bulge is misleading, as it is actually due to an insufficient number of data points at the lower masses. Had data been taken that provided more resolution on the left side of the graph, the sawtooth form of the plot would have been apparent throughout the range of masses.

Figures 4-6, 4-7 and 4-8 show the effects that some other instrumental parameters have on the actual scan time. Figure 4-6 demonstrates that the absolute mass that is scanned over has a only small effect on the actual scan time. It is unclear why this occurs, but the effect is minute and much less important than the effect of the scan range width, described above. Figure 4-7 illustrates that the type

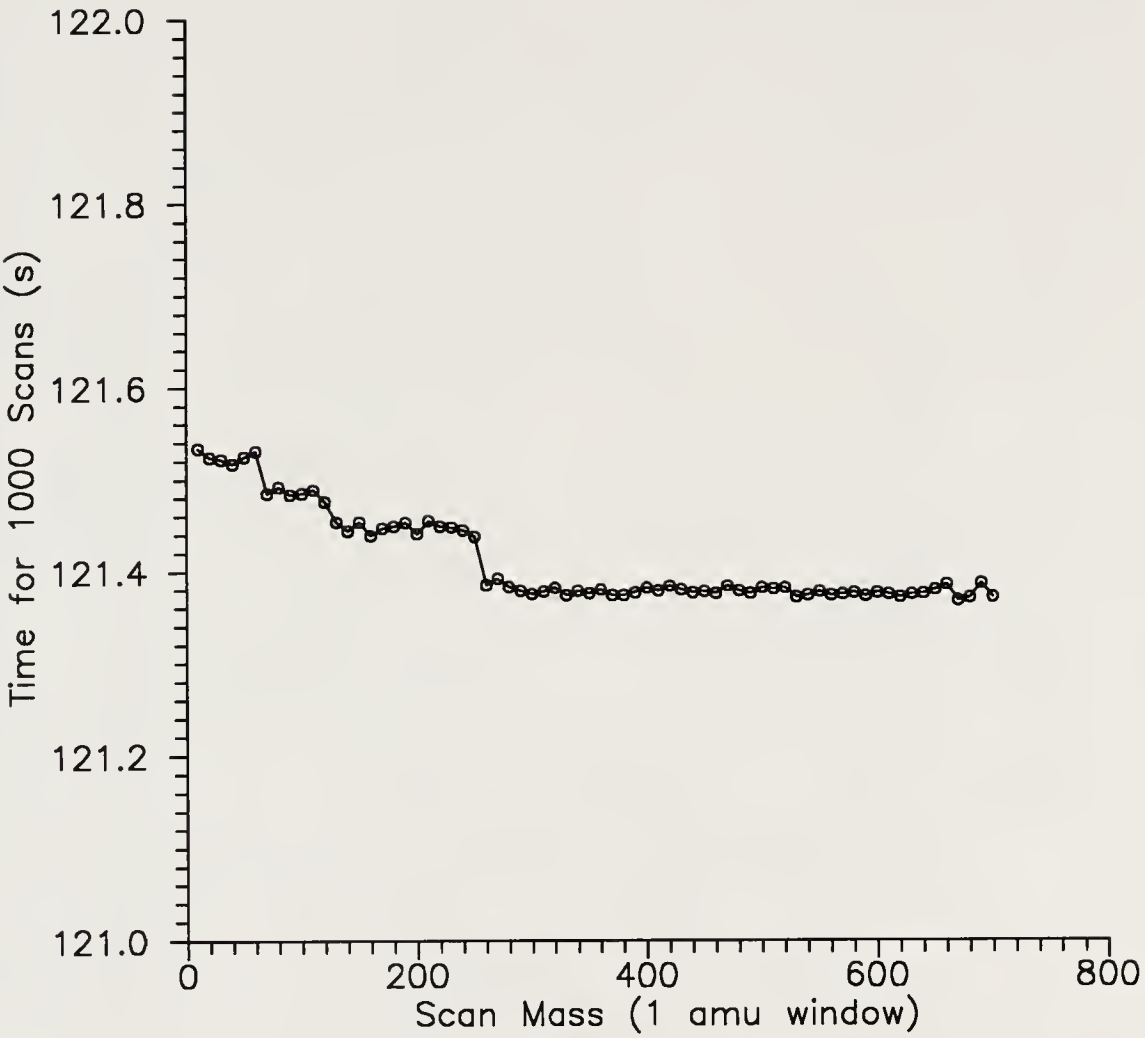

Figure 4-6: Dependence of observed scan time on mass window scanned over. Q1MS, profile data, scan time = 0.1 s.

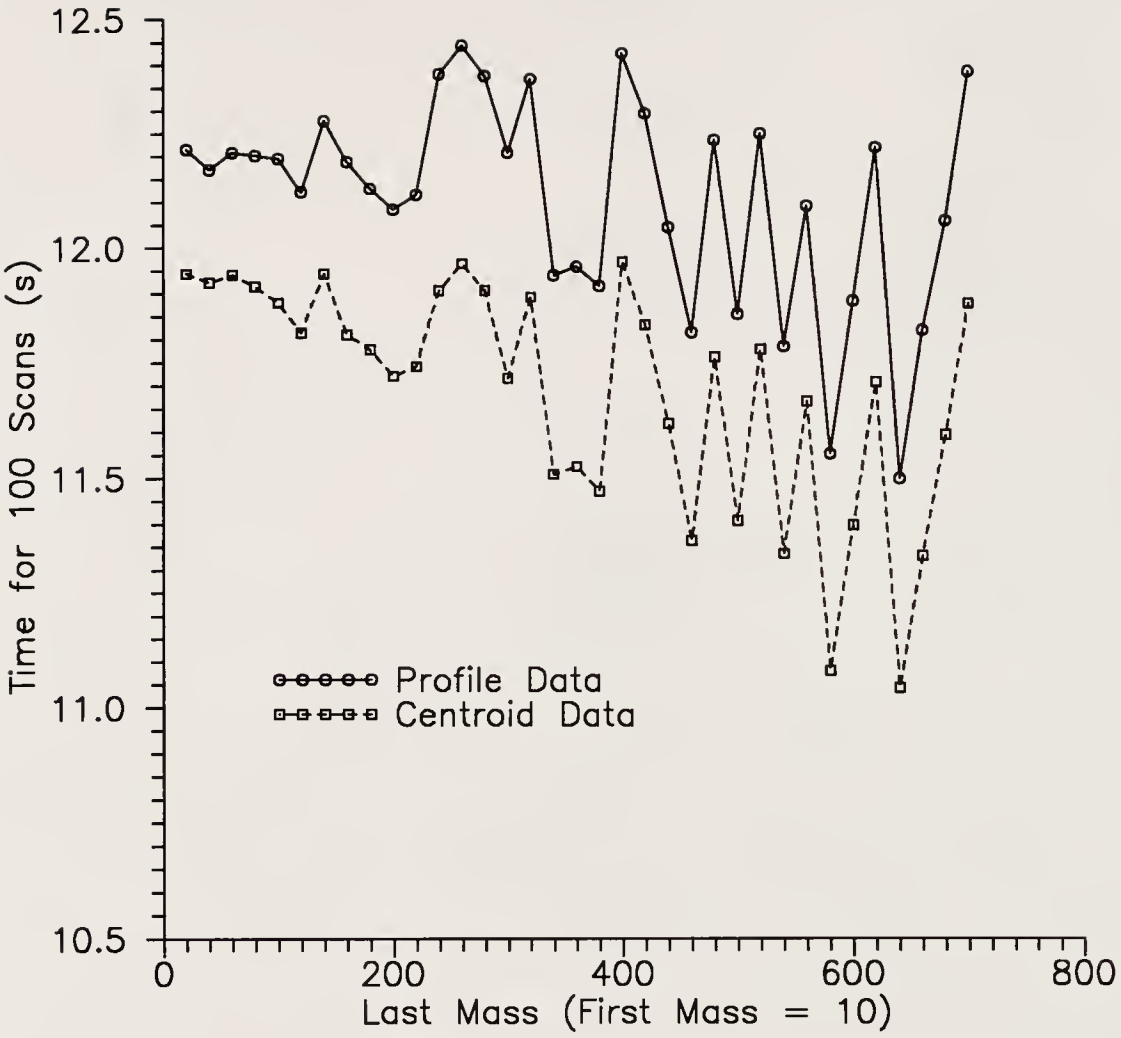

Figure 4-7: Effect of data acquisition mode on observed scan time. Q1MS, scan time = 0.1 s.

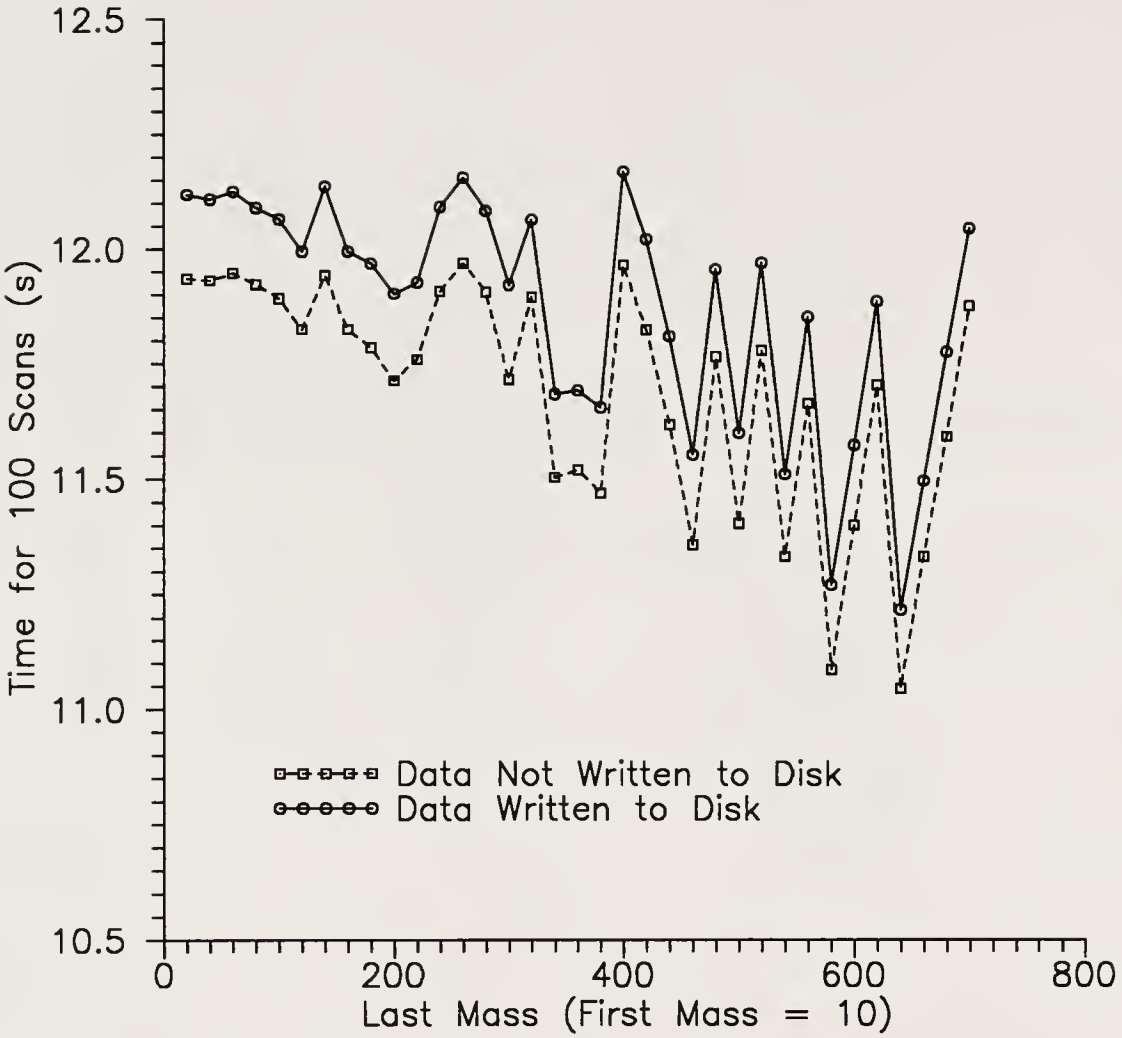

Figure 4-8: Dependence of observed scan time on whether or not data is written to disk. Q1MS, scan time = 0.1 s.

of data that is acquired (without writing to disk) also affects the absolute scan time. It is clear that scans that occur when acquiring profile spectra consistently take approximately 3 ms longer than equivalent scans acquired with centroided peaks. This result is somewhat surprising in that the instrument must perform centroiding algorithms when acquiring centroid data, and one would assume that this would take longer. Apparently, however, there is a tradeoff between the time it takes to centroid the data versus the time needed to handle the larger profile data set (even if it is not written to disk). Similarly, Figure 4-8 shows that spectra acquired to the data system have longer scan times than similar data which are not acquired. Presumably, this increase in scan time is due to the additional time that is required for the instrument to write the data to various files.

Methods for Trapping Ions in Q2

Several stages of improvement took place before a practical experimental design was established for Q2 ion trapping. Although many of the revisions actually enhanced the method, some of the modifications proved to be unworkable and were abandoned. In this section, some of the more important phases in the development of the Q2 ion trapping technique are described.

Precursory Techniques

The first pragmatic experiments involving Q2 ion trapping were performed using the ICL procedure TQ2FILL5F, listed in Appendix C. This program allows

for real-time computer control of all the parameters significant to the Q2 ion trapping process. Furthermore, most of these parameters, such as fill time, trapping time, and lens and offset potentials, can be changed while the procedure is running. This allows diagnostic studies to be easily accomplished. Additionally, no instrumental modifications to the TSQ70 are required when using this procedure. Looking at the listing in Appendix C, it is apparent that the program is relatively simple. Basically, the entrance lens, L23, is held open for a length of time, permitting ions to fill the collision cell. It is then closed so that ions can neither enter nor exit Q2, and the instrument is allowed to idle for a time equivalent to the trapping time. Subsequently, the exit lens, L31, is opened to allow the pulse of ions to exit the collision cell and be detected. The seemingly unnecessary ISOURCE statements in the program are present so that the data system can easily filter the mass chromatograms obtained when running the procedure. Likewise, all the other Q2 ion trapping programs listed in Appendix C utilize ISOURCE statements for the same reason.

As illustrated in Figure 4-9a, the main disadvantage of Q2 ion trapping using TQ2FILL5F is that lens L31 does not close simultaneously with the start of the data acquisition scan. It is clear that lens L31 opens approximately 5.3 ms before the data acquisition scan begins. In fact, 5.3 ms is the minimum delay time allowed by the instrument; if the prescan settling time (SETTIM) is not minimized to 0.1 ms, the time lag can be significantly greater. The real problem becomes apparent upon inspection of Figure 4-9b. Since the data acquisition scan starts much later than the

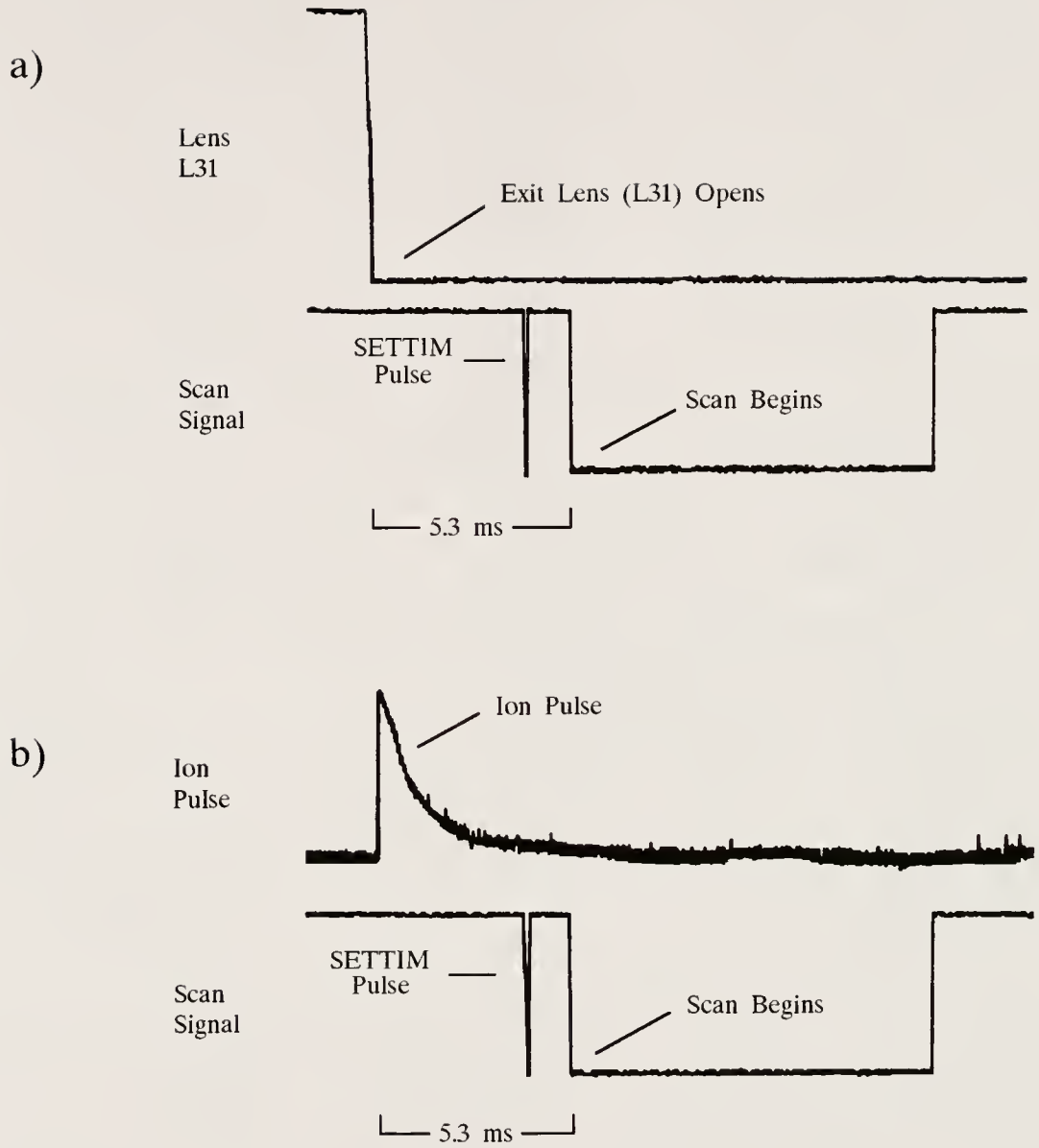

Figure 4-9: DSO traces showing that a) the exit lens opens approximately 5.3 ms before the data acquisition scan begins and b) most of the ion pulse is not detected due to the delay. The ICL procedure TQ2FILL5F was used for the studies.

opening of lens L31, more than 90% of the ions that are pulsed out of the collision cell as lens L31 opens go undetected. This causes the sensitivity of the technique to suffer irreparably. Since this is clearly unacceptable, other techniques were investigated in an attempt to circumvent this limitation.

The ICL procedure TQ2FILL5H, listed in Appendix C, is essentially similar to TQ2FILL5F except for the mechanism in which the exit lens, L31, is regulated. While TQ2FILL5F controls lens L31 directly by assigning specific voltages to the lens when open and closed, TQ2FILL5H uses a specially constructed tune table to control lens L31 indirectly. A tune table is simply a tabulation of voltage vs. m/z which allows for mass-dependent tuning of any ion optical parameter on the TSQ70. As a mass scan is performed, the instrument varies the potential applied to the particular ion optical device according to the tune table. The profile of a typical tune table used with TQ2FILL5H is shown in Figure 4-10. The tune table is characterized by a sharp break in the potential applied to lens L31. Before the break, the voltage is held at +25 V so that positive ions can not pass through lens L31. However, the lens potential after the break, -15 V, allows transmission of ions. Using TQ2FILL5H, ion trapping is effected by scanning Q3 over a mass range before the break when filling and trapping ions in the collision cell, permitting lens L31 to remain positive (closed). Ion detection is achieved by scanning over a mass range that encompasses the break. This means that the time that lens L31 opens depends on the mass range that Q3 scans over. This also ensures that the data acquisition scan begins before lens L31 opens and that the beginning of the ions pulse is

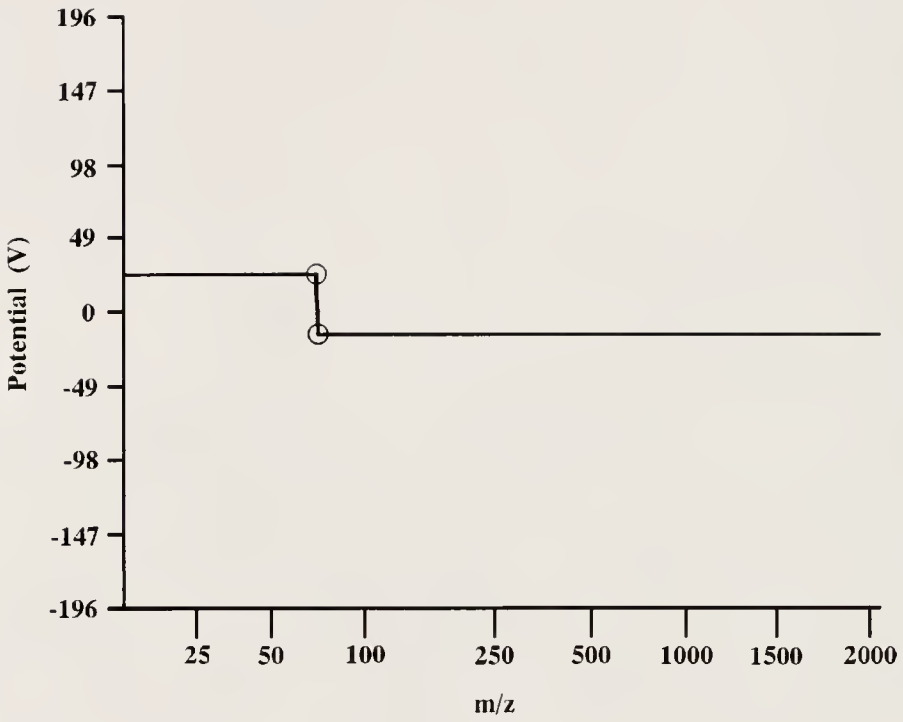

Figure 4-10: Profile of a typical tune table (for lens L31) used for Q2 ion trapping via the method utilizing the ICL procedure TQ2FILL5H.

detected. Thus, by using TQ2FILL5H and the special tune table to control lens L31, the data acquisition scan always begins before the ion pulse exits Q2, and the problem encountered with TQ2FILL5F is avoided.

Although this manner of trapping permits the entire ion pulse to be detected via the mass scan, there are several other problems with the method that make it much less practical than the technique utilizing TQ2FILL5F. The major limitation is directly related to the fact that the opening and closing of lens L31 is controlled by the tune table. Since only one tune table is available for lens L31 within a tune table file, mass scanning of trapped ions is facilitated for ions of only one m/z. This is not a problem when Q3 is in the RF-only mode as long as it is operated at a low-mass cutoff below any ions of interest. However, if Q3 is operated in the mass-selective RF/DC mode, the tune table for lens L31 must be successively modified so that the break encompasses each different m/z that corresponds to the ion of interest. This is tremendously time consuming and is impractical to implement. Furthermore, tune tables of this type must be constructed by hand so that the break is as close as possible to the mass of interest. This means that set points must be carefully positioned around the break; they should be as close as possible so that the break is sharp, but must not be too close so that the instrument does not recognize the break. This point is illustrated in Figure 4-11. It is clear that the minimum mass range between two set points needed to observe a break in the lens voltage is not constant throughout the mass range of the instrument. In fact, this minimum mass range broadens dramatically as the absolute mass range increases. This makes

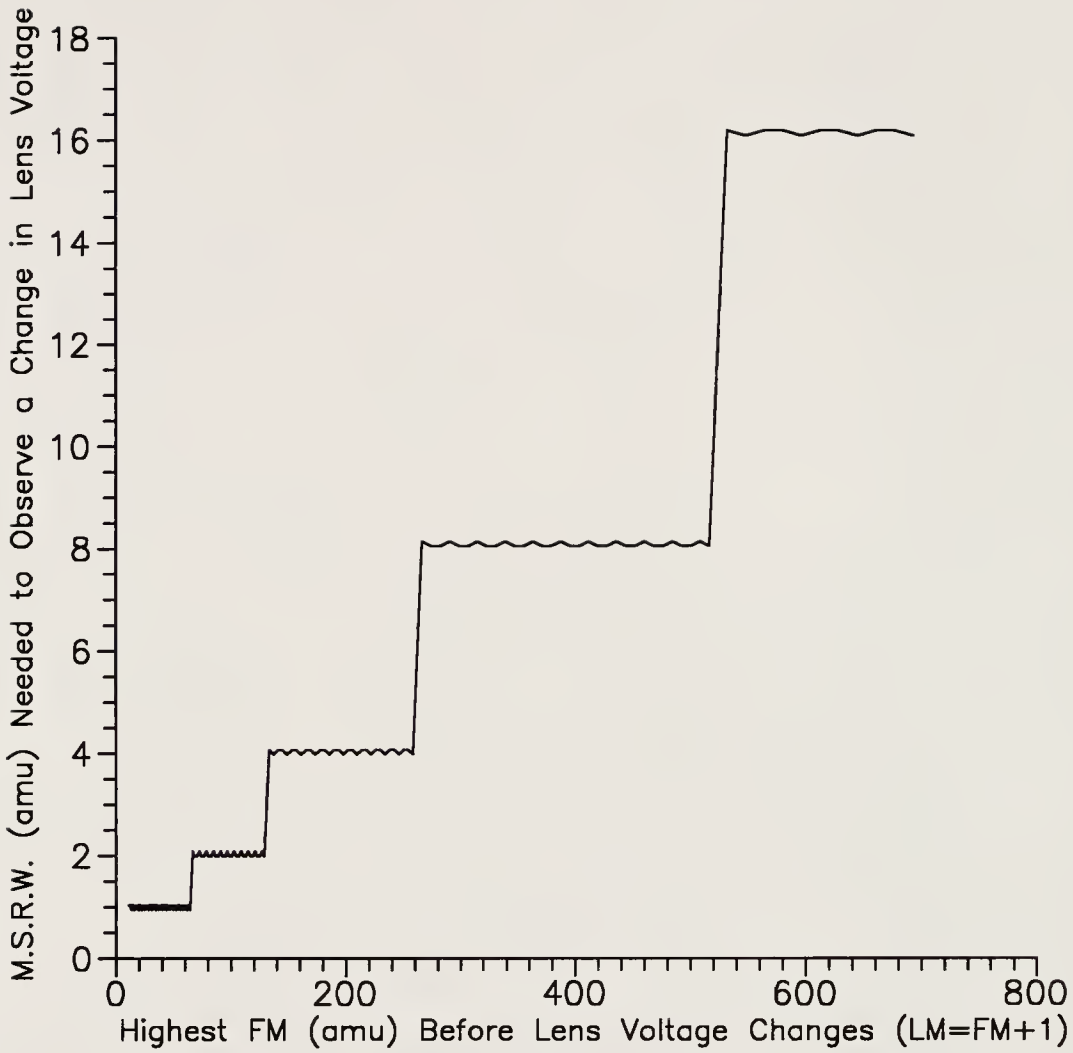

Figure 4-11: Effect of absolute scan range (defined by first mass, FM, and last mass, LM) on the minimum scan range width (M.S.R.W.) needed to observe a change in lens voltage.

construction of these special tune tables even more complex and effectively makes the technique futile.

As was stated earlier, TQ2FILL5H permits the data acquisition scan to start before the exit lens, L31, opens, and thus allows for detection of the entire ion pulse peak. However, the data acquisition scan still does not begin simultaneously with the opening of lens L31, and this causes additional problems. As shown in Figure 4-12, the scan actually starts several milliseconds before lens L31 opens and emits the ion pulse. The actual delay time depends on the mass range that Q3 is scanned over, the placement of the break in the lens L31 tune table, and the scan time. This causes several adverse effects when trapping is attempted using this method. When Q3 is operated as a mass filter, mass calibration will always be off since ions are not continually transmitted through Q3. The pulse of ions may exit the collision cell after Q3 has scanned past the m/z that primarily makes up the ions in the pulse. Sensitivity suffers greatly for this same reason. By the time lens L31 opens, the mass filter (Q3) may be scanning over a m/z higher than that which is predominant in the ion pulse. Thus, most of the ions in the pulse become unstable and are not detected.

External Control of the Exit Lens (L31) for Enhanced Ion Detection

In order to avoid the problems encountered with the two previous trapping methods, another approach to Q2 ion trapping and control of the exit lens was investigated. Unlike the other methods, where software is exclusively used to control the trapping experiment, this strategy involves regulation of lens L31 by simple

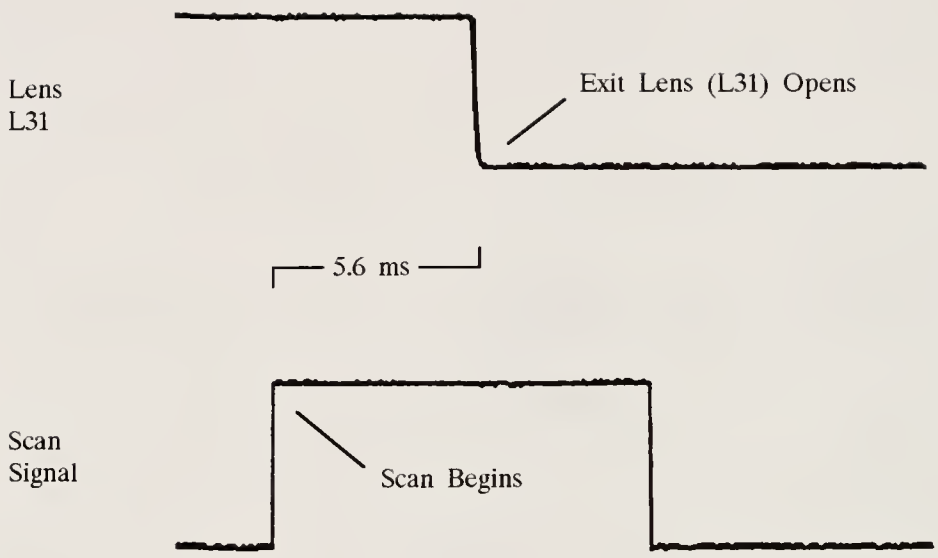

Figure 4-12: DSO traces illustrating that, when trapping using TQ2FILL5H, the data acquisition scan begins several milliseconds before the exit lens opens.

instrumental modifications in conjunction with software control. The ICL procedures that manage the Q2 ion trapping experiment are TQ2FILL5I and T5ISUB, and are listed in Appendix C. These procedures operate in much the same fashion as does TQ2FILL5F except that lens L31 is controlled by an external circuit. This circuit, in turn, is regulated by user outputs 1 and 2 (UO1 and UO2) within the procedures.

A diagram of the lens L31 control circuit is shown in Figure 4-13. The circuit replaces the resistor between pins 2 and 15 of connector RP1 on the 200 V Lens Driver printed circuit board assembly (PCBA). In order to have lens L31 open simultaneously as the data acquisition scan begins, a low-level signal, representing the start of a scan, is drawn from TP1-1 on the Electrometer PCBA as a trigger. This signal then enters a 4011 NAND gate along with the output from UO2, which is controlled by TQ2FILL5I. Under normal circumstances, when either UO2 or the scan signal (or both) are LO, the instrument operates as is would without the circuit; the 4016 analog switch allows the potential at pin 2 of RP1 on the 200 V Lens Driver PCBA to determine the voltage applied to lens L31. However, if both the scan signal and the output from UO2 are HI, the 4016 analog switch shifts control of the lens L31 potential to UO1. Thus, a change in the voltage applied to lens L31 is triggered off of the scan signal when UO2 is HI. TQ2FILL5I utilizes this circumstance by raising UO2 to +5 V (HI) only when the next scan is that which detects the ion pulse as it exits the collision cell. When this occurs, lens L31 control is switched to UO1. By selecting an appropriate voltage for UO1, the actual

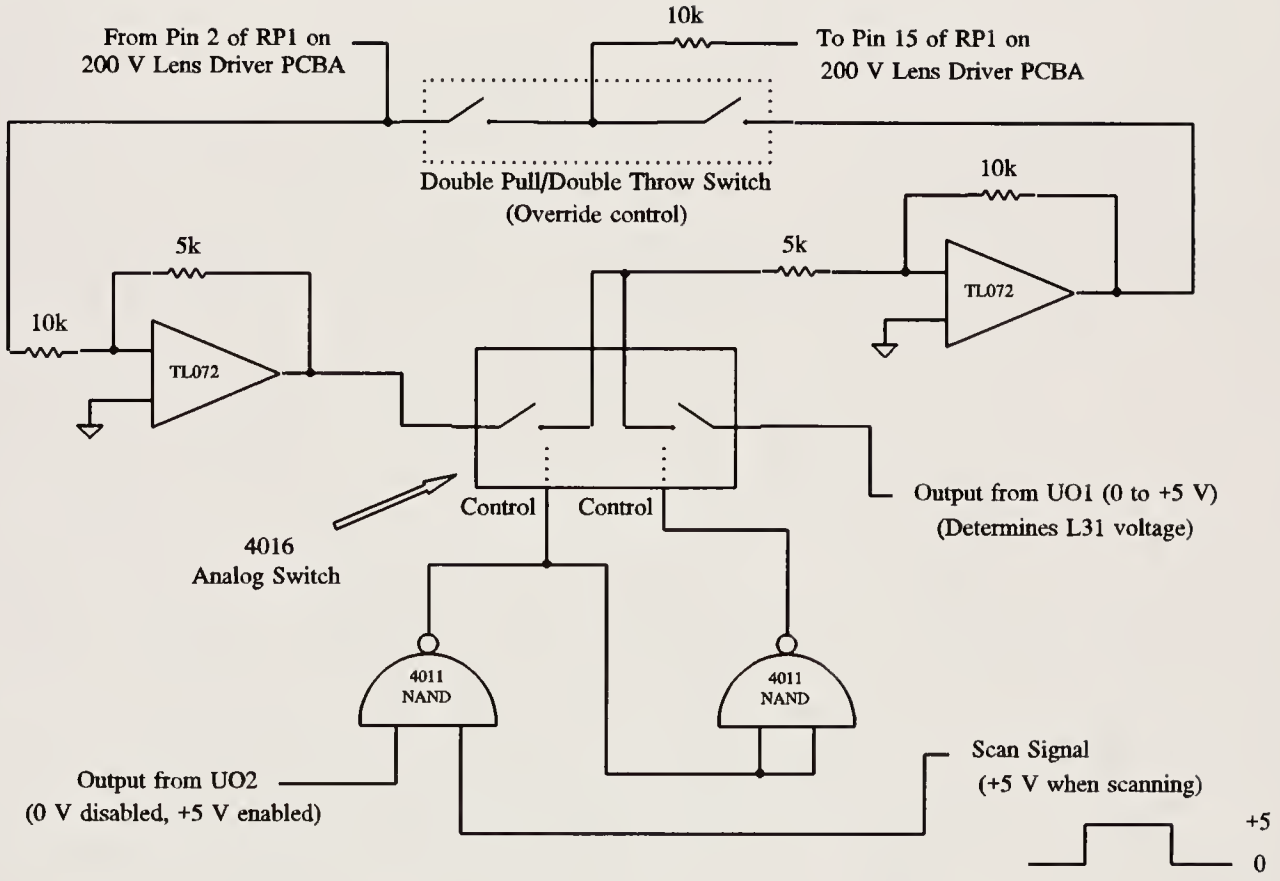

Figure 4-13: Diagram of lens L31 control circuit.

potential applied to lens L31 is pulsed to a negative value, thus allowing ions to exit Q2 and be detected as the scan begins.

The TL072 operational amplifiers in the circuit are used as inverters with gain. The voltage from pin 2 of RP1 on the 200 V Lens Driver PCBA, which is between 0 V and -10 V, must be inverted and halved so that the 4016 analog switch may operate correctly. Analogously, the output from the analog switch, whether or not it is from UO1, must be inverted and doubled so that the correct potential is applied to pin 15 of RP1 on the 200 V Lens Driver PCBA. The use of these inverting amplifiers, while necessary, means that the potentials from UO1 and pin 2 of RP1 must be calibrated to the observed voltage of lens L31. These calibration curves are shown in Figure 4-14. Since the 4016 analog switch is not a perfect device, it has some amount of resistance when closed. This translates into the nonlinear calibration curves that are observed. Furthermore, if the circuit is altered by replacement of any of its components, especially the 4016 analog switch, pin 2 of RP1 and UO1 must be recalibrated to the actual lens L31 potentials, since the resistance of the circuit will have changed. Also note in Figure 4-14a that the actual output of UO1 is half of that which is requested. This is due to changes in the jumper configuration for UO1 so as to allow it to put out potentials between 0 V and 5 V. The jumpers for UO2 were configured in the same fashion, so that UO2 puts out 5 V when 10 V is requested.

As has been implied, the sole purpose of the lens control circuit is to synchronize the times that lens L31 opens and the data acquisition scan begins. The

a)

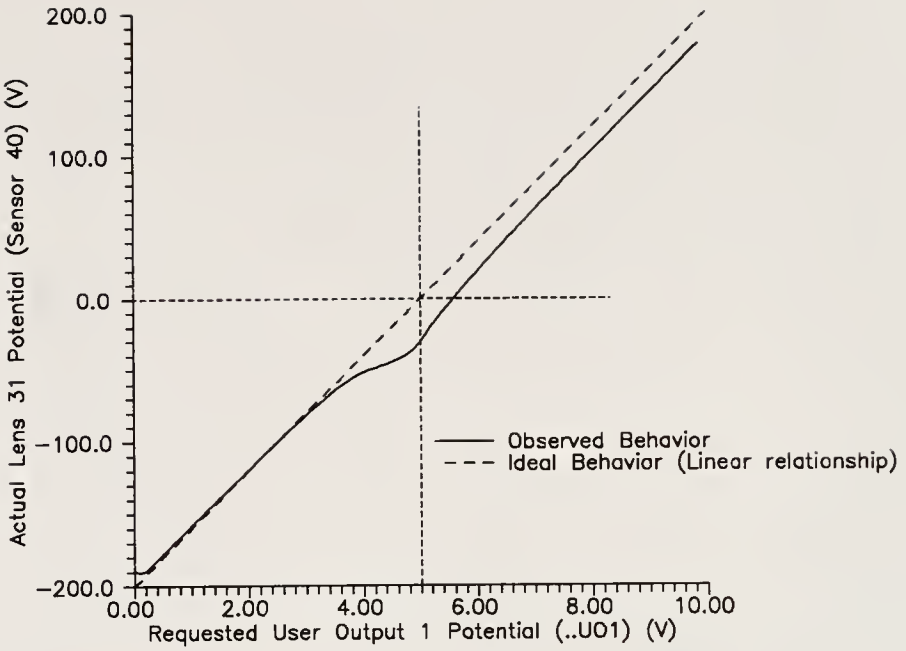

b)

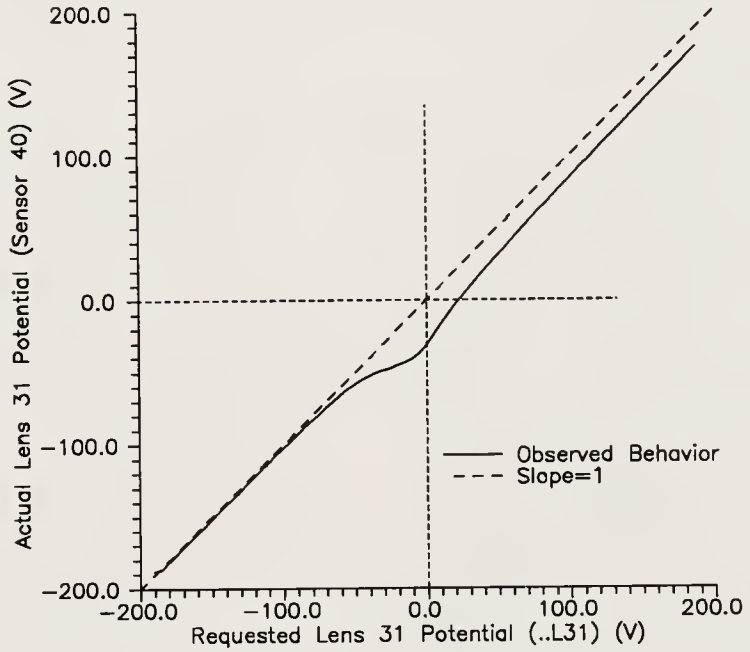

Figure 4-14: Calibration of lens L31 control circuit for a) user output 1 (UO1) and b) the requested lens L31 voltage. Note in a) that $UO1_{actual} = (1/2)UO1_{requested}$ due to the jumper configuration.

DSO trace shown in Figure 4-15 confirms that this is what happens when using TQ2FILL5I in combination with the lens control circuit. Figure 4-16 depicts why it is beneficial to do this. It is clear that the percentage of ions that are ultimately detected increases dramatically when the acquisition scan occurs at the same time that lens L31 is open. This, in turn, increases the sensitivity of the technique.

Helium Buffer Gas Effects

The advantages of using buffer gas in three-dimensional quadrupole ion traps have been known for some time [43,86]. The collisional damping of the ion motions to the center of the trap enhances ion containment which results in improved sensitivity and increased resolution. Similarly, it has been reported [87-88] that the use of buffer gas in two-dimensional RF-only devices results in enhanced ion transmission due to collisional focusing effects. In some cases, the improvement in ion transmission is dramatic, with gains as high as 7000% reported under certain circumstances [88].

In this section, the effects of buffer gas when trapping ions in the collision cell will be described. It has been determined that the use of helium in the collision cell can significantly improve the performance of the Q2 ion trapping system. In particular, much better ion trapping efficiencies are observed when helium buffer gas is employed.

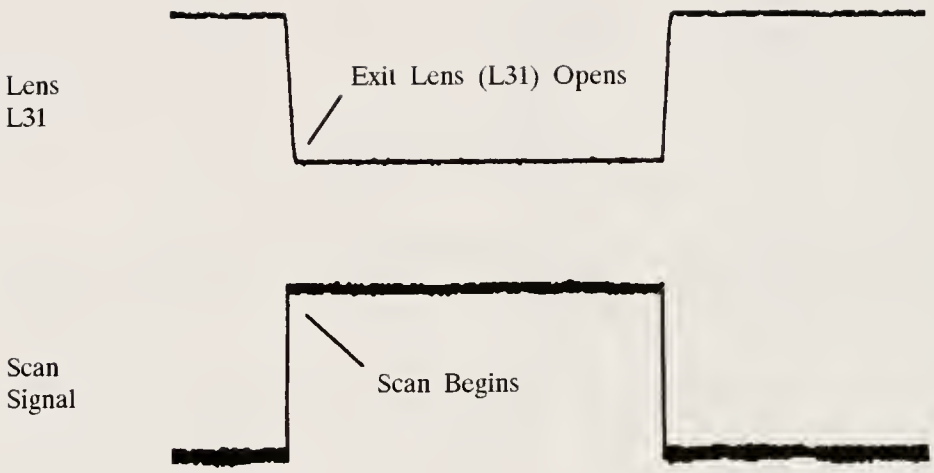

Figure 4-15: DSO traces showing that, when Q2 ion trapping is performed using the L31 lens control circuit, the exit lens opens simultaneously with the start of the data acquisition scan.

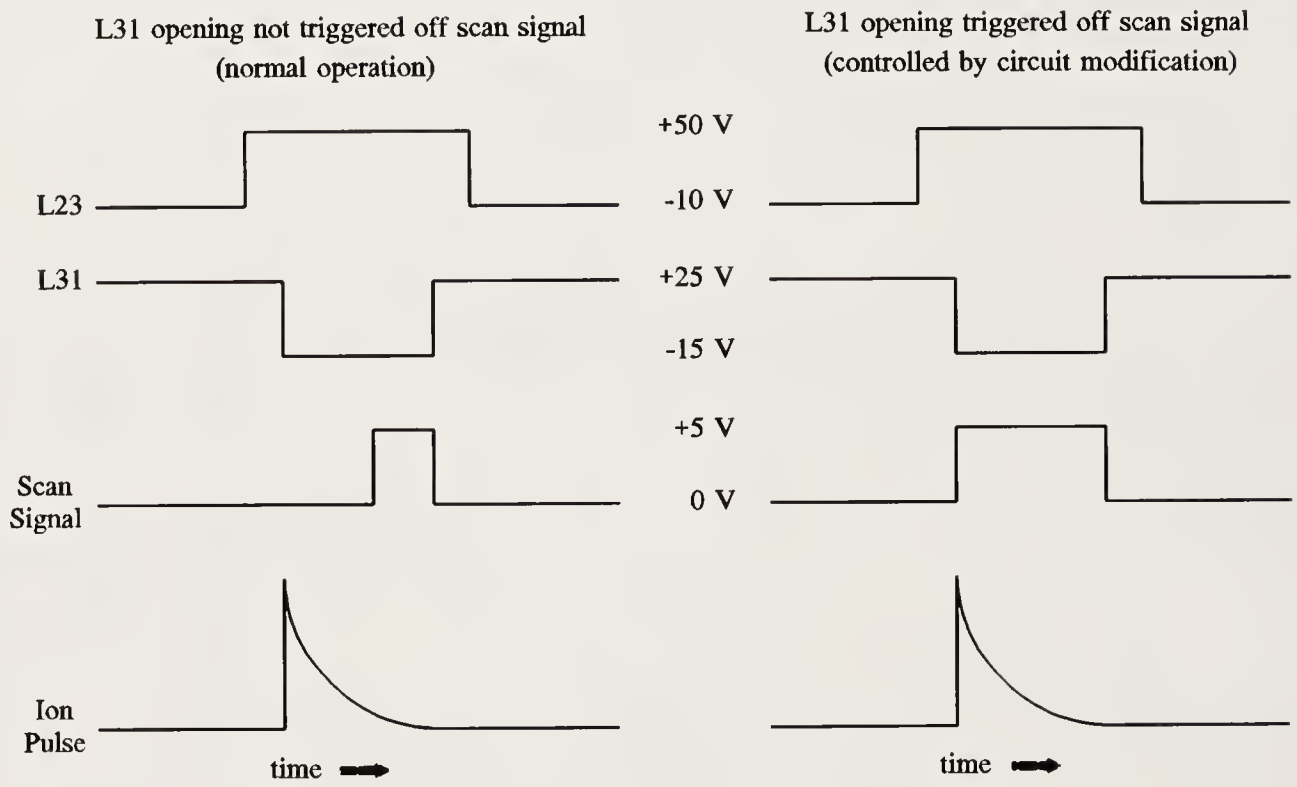

Figure 4-16: Illustration showing that enhanced ion detection is achieved through circuit control of the lens L31 potential.

Pressure Studies

Helium buffer gas effects two major functions that enhance the performance of the Q2 ion trapping system. Firstly, the helium acts to decelerate the ions through multiple collisions as they enter Q2. This allows the ions to be efficiently captured in the RF field generated by the collision cell, thus reducing ion losses due to instability. Secondly, the helium buffer gas tends to dampen the orbits of the ions to the center of the octopole. Since the octopole field is more uniform in this region, ions are less likely to become unstable, and ion trapping efficiency is increased. This is directly analogous to the mechanism in which helium buffer gas enhances the performance of the quadrupole ion trap.

Figure 4-17 shows the effect of collision cell pressures of helium on trapping three different ions of PFTBA. It is clear that the optimum buffer gas pressure is independent of the m/z of the ions being trapped. Ion trapping is always most effective at indicated helium pressures between 6 mTorr and 8 mTorr. The shapes of the curves in Figure 4-17 can be explained as follows. At lower pressures, the ions are not slowed down enough to be confined to the trapping field, while at pressures above 6-8 mTorr collision-induced dissociation (CID) and ion scattering processes begin to predominate. CID processes also explain why the curves for m/z 219 and m/z 414 decrease more rapidly at higher pressures than does the plot for m/z 69. PFTBA fragment ions of m/z 69 are much more stable than ions of m/z 219 and m/z 414. Thus, ion losses due to CID are more prevalent for the 219 and 414 ions at higher collision cell pressures.

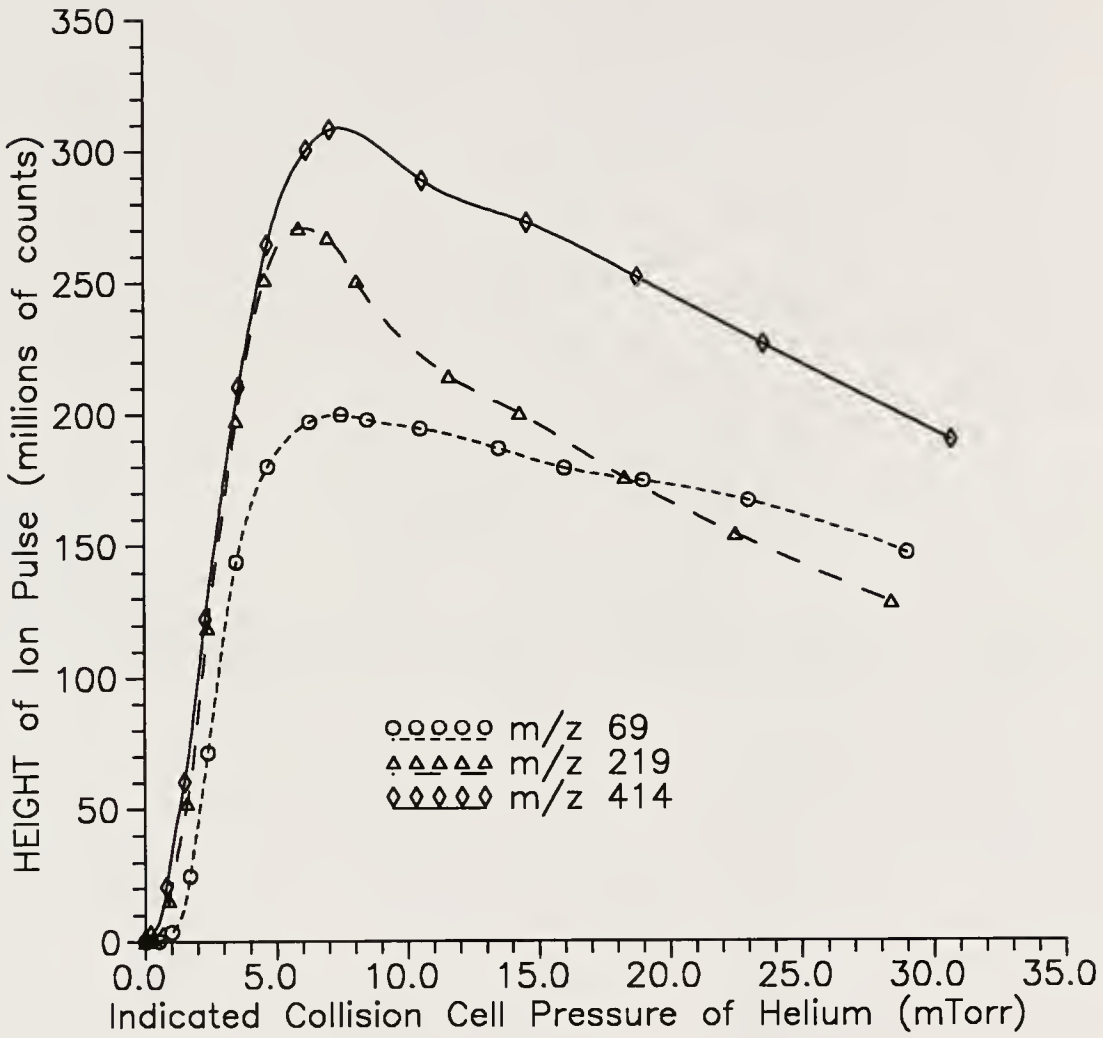

Figure 4-17: Optimization of helium pressure in the collision cell for ion trapping and detection. Trapping time = 0.05 s.

Ion Trapping Efficiencies

A dramatic improvement in ion trapping efficiency is the effect that is most apparent when helium buffer gas is utilized. Table 4-1 shows the ion trapping efficiencies, calculated as described in the Experimental section, observed when trapping several prominent fragment ions of PFTBA calibration compound. In order to distinguish any effects that may be due to different quantities of ions entering the collision cell, the studies were also performed at various ion fluxes into Q2. For comparison, ion trapping efficiencies observed under similar conditions, but without helium buffer gas in the collision cell, are listed in Table 4-2.

Comparing Tables 4-1 and 4-2, it is immediately apparent that much higher trapping efficiencies, as measured by %(Out/In), are possible when helium buffer gas is used in the collision cell. Ion confinement and detection are enhanced by almost 2000% for m/z 219, 3300% for m/z 414, and as much as 45,000% for m/z 69. Clearly, utilization of helium buffer gas is imperative if ultimate sensitivity is desired when trapping ions in Q2.

Another observation which is evident looking at Table 4-1 is that the number of ions that are injected into Q2 does have an effect on the overall trapping efficiency, when helium is used. It is clear that %(Out/In) increases as the number of ions that enter Q2 is increased, and then decreases at very high ion fluxes. This observation can be explained as follows. At very low ion fluxes, the collision cell is only partially filled with ions (i.e., there is a low density of ions in Q2), and ion-ion repulsions are insignificant. Thus, when the exit lens, L31, opens under these

Table 4-1: Comparison of trapping efficiencies of common fragment ions of PFTBA at various ion fluxes for the Q2 ion trapping system using helium buffer gas.

m/z[a]	Ion Flux into Q2[b]	%(Out/In)[c]
69	6	39.8
69	30	48.8
69	120	33.3
219	7	33.2
219	30	55.1
219	130	51.7
414	1.1	23.9
414	11	84.3
414	45	91.2

[a] Ions of this m/z were mass selected by Q1 and injected into the collision cell to be trapped.

[b] Millions of counts observed in the profile spectrum of the ion in Q1MS mode at an electron multiplier setting of 1000 V.

[c] The number of ions that are ultimately detected as a percentage of those ions that are initially injected into Q2, calculated as described in the Experimental section.

Table 4-2: Comparison of trapping efficiencies of common fragment ions of PFTBA at various ion fluxes for the Q2 ion trapping system without using helium buffer gas.

m/z[a]	Ion Flux into Q2[b]	%(Out/In)[c]
69	5.2	0.14
69	33	0.11
69	128	0.12
219	8	3.02
219	30	3.14
219	137	3.18
414	1.2	2.79
414	11.3	2.97
414	46	3.16

[a] Ions of this m/z were mass selected by Q1 and injected into the collision cell to be trapped.

[b] Millions of counts observed in the profile spectrum of the ion in Q1MS mode at an electron multiplier setting of 1000 V.

[c] The number of ions that are ultimately detected as a percentage of those ions that are initially injected into Q2, calculated as described in the Experimental section.

conditions, only the slight fringing field of the lens acts to draw out ions from the collision cell. Moreover, diffusion is the major mechanism in which ions exit Q2. This results in long, diffuse ion pulses when a low density of ions is trapped in Q2, as illustrated in Figure 4-18a. Since the time that lens L31 is open and ions are detected is fixed, many of the ions that are actually trapped in Q2 are not detected. Thus, %(Out/In) measurements are low at low ion fluxes.

At higher ion fluxes, the density of ions in the collision cell increases and ion-ion repulsions become important. Under these conditions, the collision cell is "saturated" with ions; the maximum number of ions are held in Q2 without significant ion losses due to space charge effects. The ions act like a compressed spring and, consequently, when lens L31 is opened ion-ion repulsions cause the ions to exit Q2 as a sharp pulse with an exponential decay, as shown in Figure 4-18b. This allows for a higher percentage of ions to be detected since most of the ions have been expelled from Q2. It follows that larger %(Out/In) measurements, as reflected in Table 4-1, are observed. At very high ion fluxes, the collision cell is physically unable to contain the number of ions injected into it. Consequently, ion losses due to ion-ion repulsions become pronounced and this, in turn, results in decreased ion trapping efficiencies as measured by %(Out/In).

Ion flux when trapping without helium in Q2, in contrast, seems to have little effect on measurements of %(Out/In), as indicated in Table 4-2. It is unclear why this is, but it may be due to the nature of the ion-ion repulsions when helium buffer gas is not used. In this instance, any increase in ion trapping efficiency that may be

a)

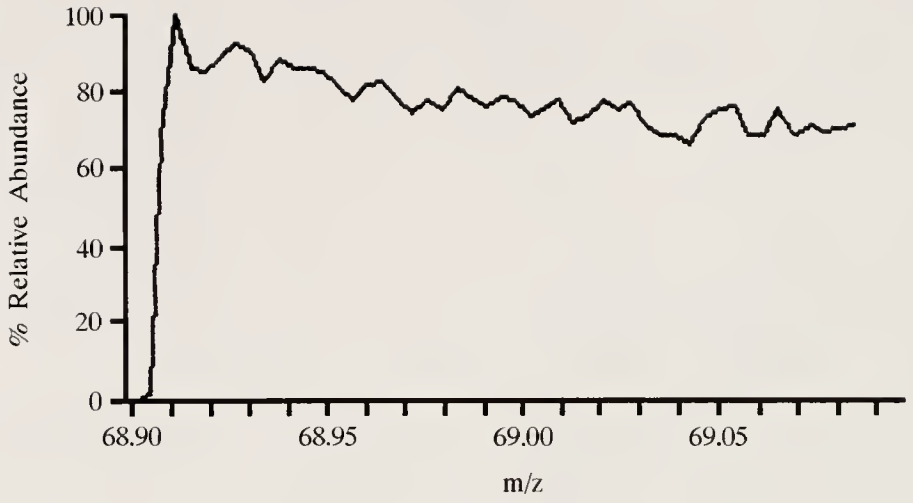

b)

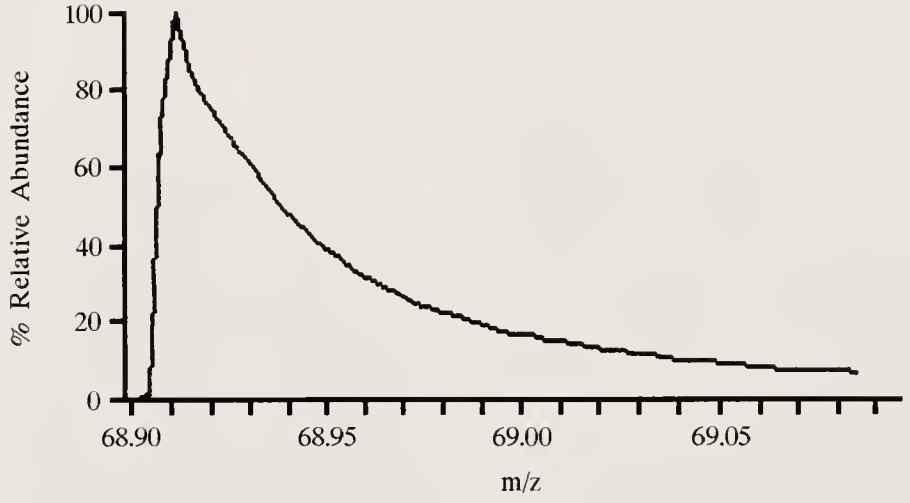

Figure 4-18: a) Ion pulse observed when a small number of ions is trapped in Q2 (electron multiplier = 1700 V). b) Ion pulse observed when a large number of ions is trapped in Q2 (electron multiplier = 750 V). In both cases, scan rate is 0.02 u/ms.

obtained via collimation of the ion pulse may be offset by profound ion losses at higher ion fluxes.

The m/z of the ions trapped in Q2 also seems to have an effect on the ultimate ion trapping efficiency. It can be seen in Table 4-1 that the maximum calculated %(Out/In) for m/z 69 was 48.8%, whereas %(Out/In) values were measured as high as 91.2% for m/z 414. It is unlikely that experimental errors can account for such a wide range of ion trapping efficiencies; therefore, the observations must have real significance. It is thought that collisions with the buffer gas, causing damping of the ion trajectories, is more effective for ions of higher mass. This leads to lower ion losses and higher values of %(Out/In). This theory is consistent with what others have observed. It has been reported [88] that collisional focusing in a linear RF-only quadrupole is dependent on the mass of the ion, not its mass-to-charge ratio. Furthermore, higher masses show significantly greater collisional focusing effects, presumably because the ratio of the mass of the ion to the buffer gas mass determines the kinematics of the collisions. Similar results have been noted in studies using a quadrupole ion trap mass spectrometer [43] with helium buffer gas, with more pronounced improvements in mass resolution and sensitivity for ions of higher masses when helium was utilized.

Optimization of Ion Optics for Q2 Trapping

Entrance Lens, L23

Although it is important to optimize all the ion optical components of the TSQ70 mass spectrometer, some parameters are of particular significance when conducting Q2 ion trapping experiments. Specifically, the entrance lens, L23, potential when filling Q2 with ions has a profound effect on ion trapping ability. Figure 4-19 shows that the height of the ion pulse peak, as measured by the DSO, depends greatly on the voltage applied to lens L23 when filling Q2 with ions. It can be seen that ion intensity decreases rapidly as the potential deviates from the optimum of approximately -2 V. The curve illustrated in Figure 4-19 actually represents a compromise between two competing processes. On one hand, the potential applied to lens L23 must be negative enough so that, when filling Q2 with positive ions, the ions have enough translational energy to make it into the collision cell. However, lens L23 must not be so negative so that ions, as they are filling Q2, are allowed to be forced back out the front of the collision cell (towards Q1) due to ion-ion repulsions. Concurrently, it is important that lens L23 be more positive than the Q2 offset voltage so that the lens acts as a hump in the potential gradient keeping ions, after losing some kinetic energy due to collisions in Q2, from leaving the collision cell. Figure 4-20 shows a typical DC potential gradient profile of the ion optics in the TSQ70 as Q2 is being filled with ions. The potential gradient was calculated with the SIMION ion simulation program [85] using the exact dimensions

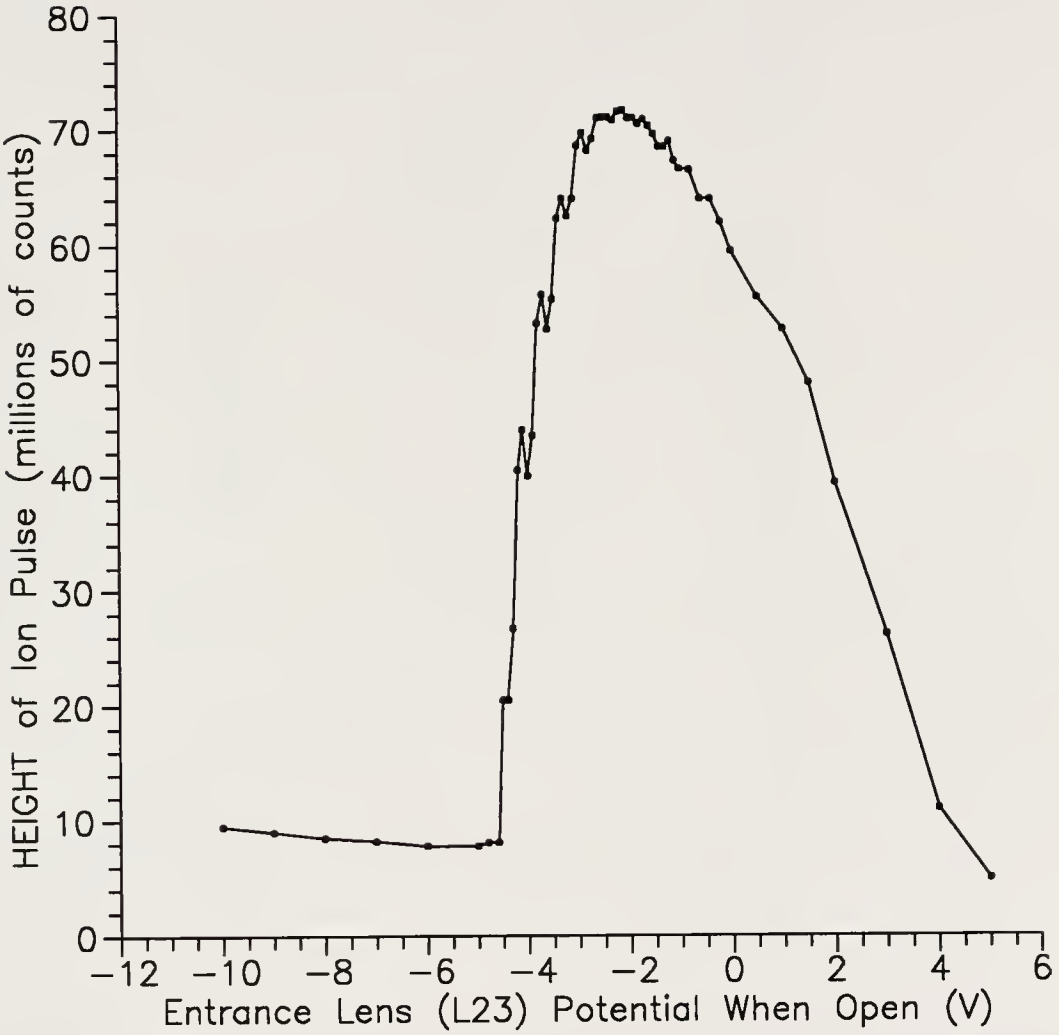

Figure 4-19: Effect of entrance lens, L23, potential (when injecting ions into Q2) on ion trapping ability. 6.0 mTorr indicated pressure of helium in the collision cell. Q1 offset = -2 V, Q2 offset = -6 V.

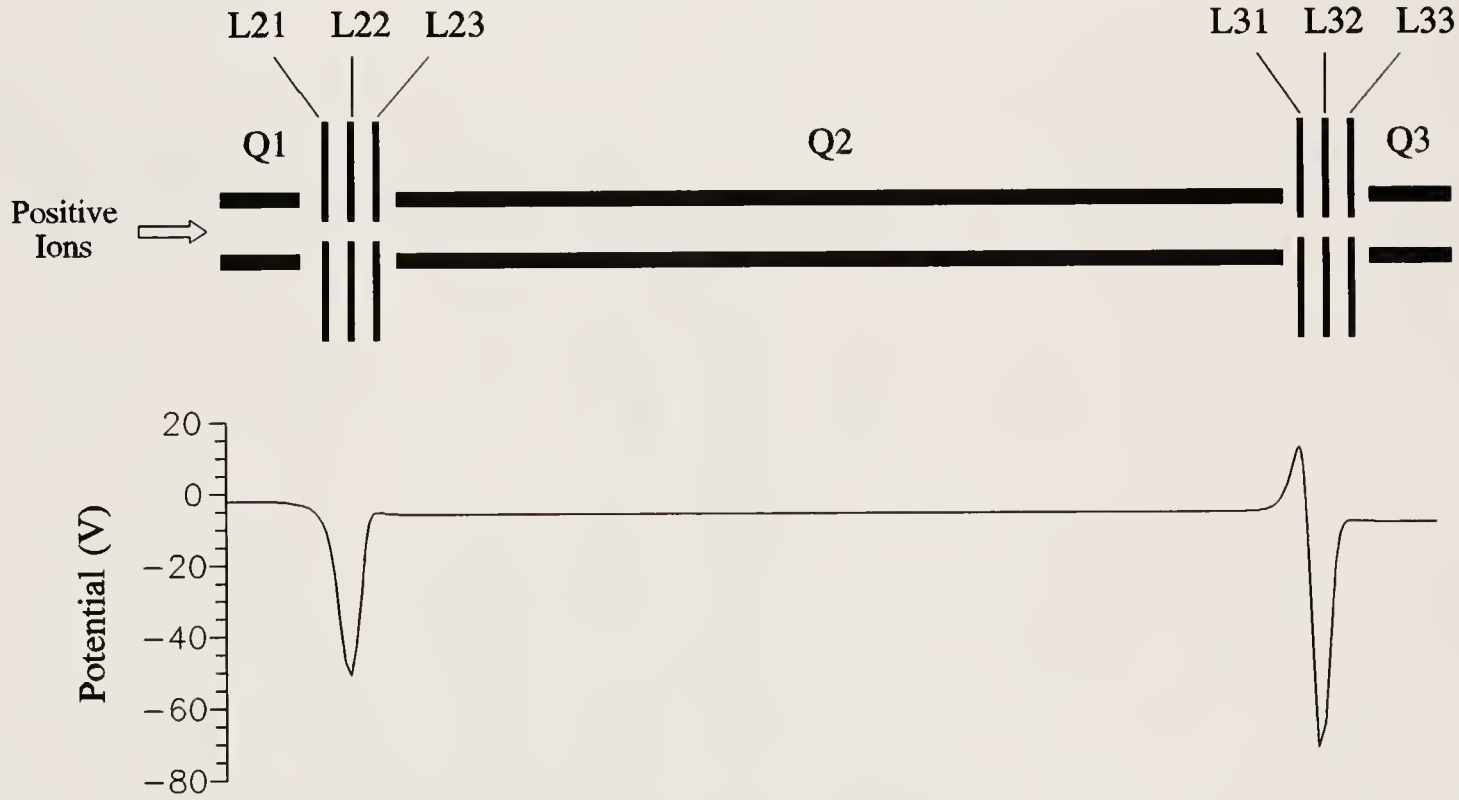

Figure 4-20: The potential gradient observed by ions as they are injected into the collision cell. Calculated using the exact dimensions of the TSQ70 octopole collision cell, using the SIMION ion simulation program. Q1 offset = -2 V, Q2 offset = -6 V.

of the TSQ70 ion optical components. It is clear that the ions experience a small increase in the potential at lens L23 as they travel toward the collision cell. This hump causes Q2 to act as a potential well and allows the ions to be confined to Q2 and not be forced out by ion-ion repulsions.

Other conditions also affect the optimum value of lens L23 when filling Q2 with ions. As Figure 4-21 illustrates, the ideal lens L23 voltage is intrinsically related to the potential applied to lens L22. The optimum lens L23 voltage becomes more positive as the lens L22 potential becomes more negative. This is intuitively apparent, as the potential gradient that the ion observes is a combination of both lens voltages. Whether or not helium buffer gas is utilized also affects the optimum lens L23 voltage. Figure 4-22 shows that maximum ion pulse intensity is achieved at a lens L23 potential of approximately +1 V, when no helium is used. This value is somewhat more positive than the optimum of -2 V indicated in Figure 4-19, where helium was used. Helium may act to help slow down and thermalize ions as they enter Q2, decreasing ion-ion repulsions and allowing for a more negative lens L23 potential. In the absence of helium (i.e., no collisions), however, the barrier to the ions leading back out the front of Q2 has to be at a positive voltage with respect to the grounded ion source where ions were formed. The differences in collision offset voltages that were utilized for each of the studies are likely to be more significant in the determination of the discrete optima since, for ion confinement in Q2, the potential gradient between lens L23 and the Q2 offset is most important. As will be discussed in the next section, optimum collision offset potentials for Q2 ion trapping

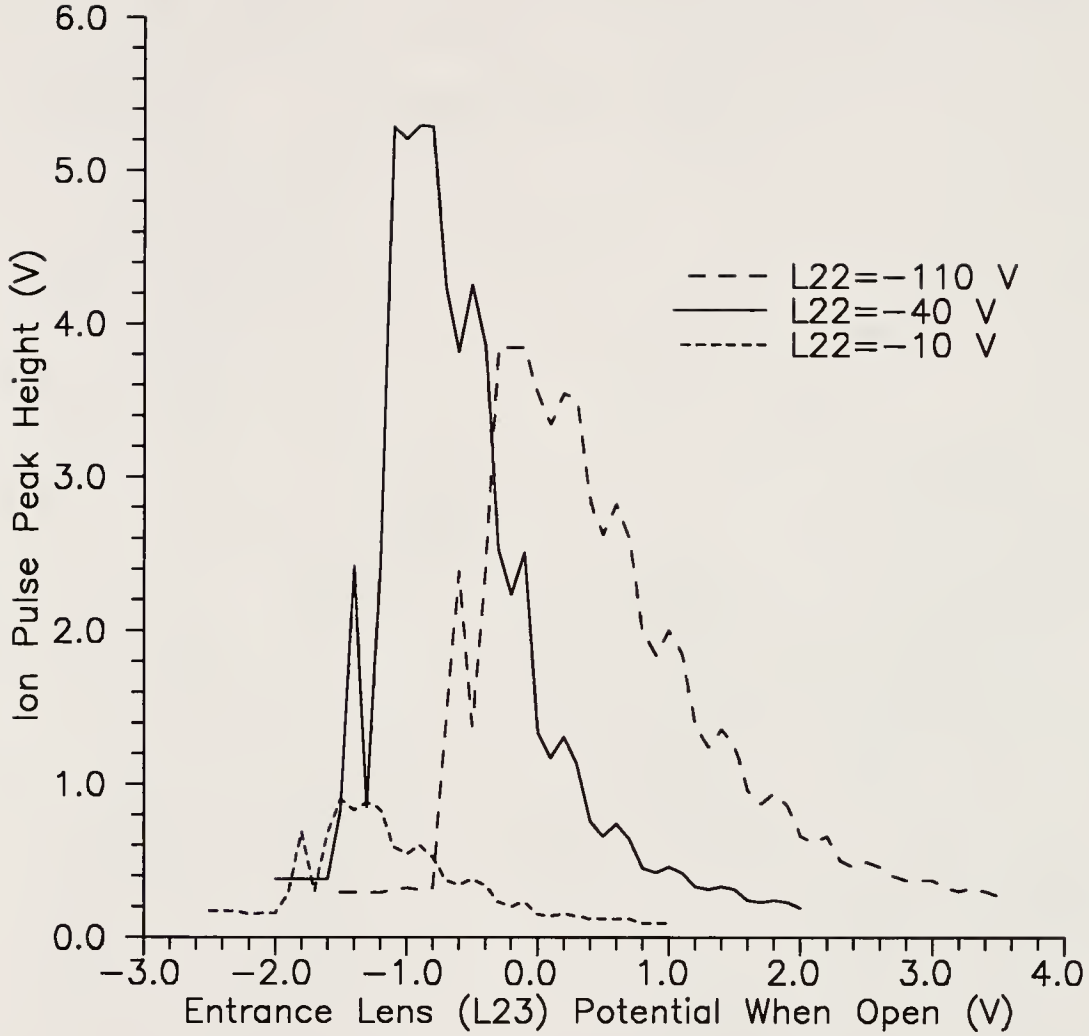

Figure 4-21: Relationship between the potentials applied to lens L22 and the entrance lens, L23, (when injecting ions into Q2) with ion trapping ability. 6.0 mTorr indicated pressure of helium in the collision cell. Q1 offset = -1.5 V, Q2 offset = -2 V.

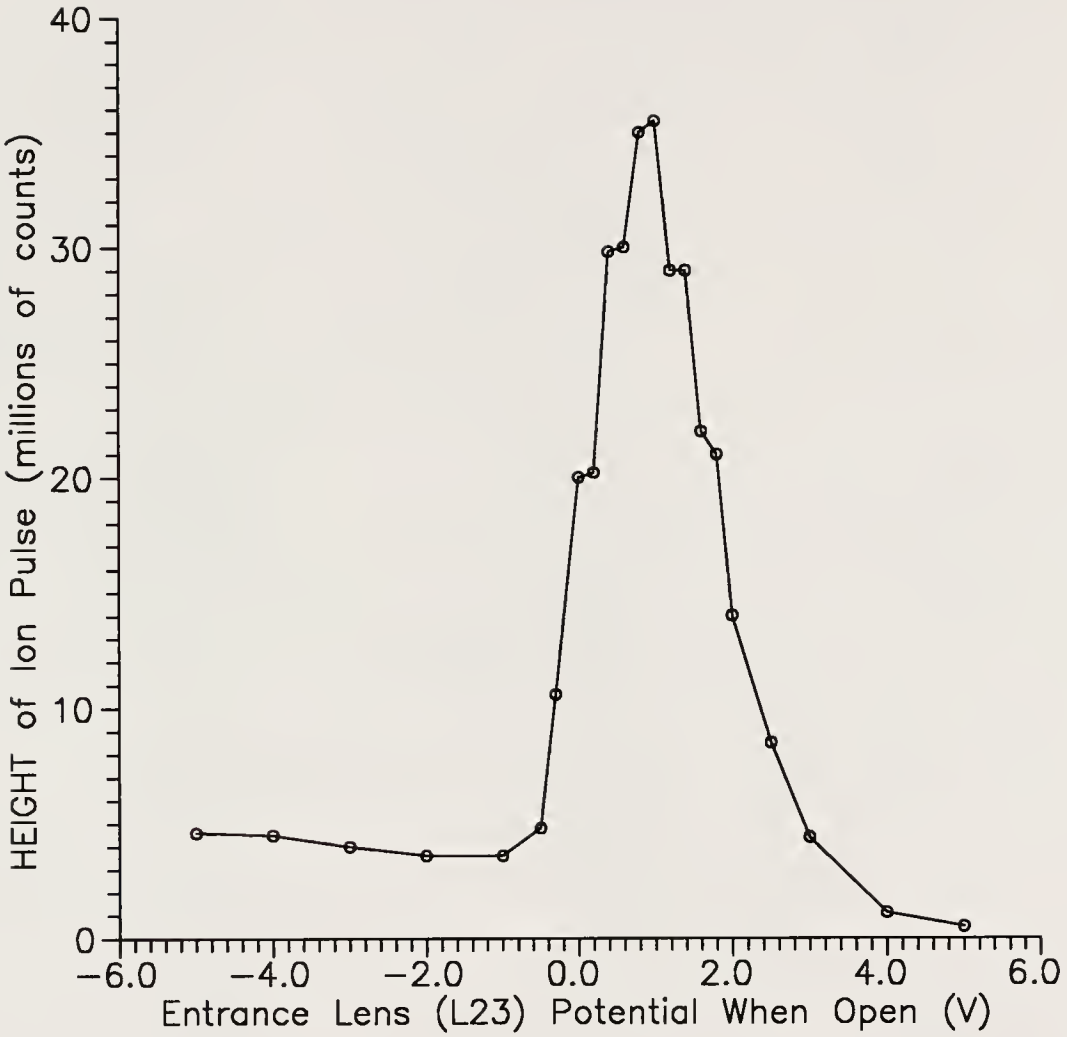

Figure 4-22: Effect of entrance lens, L23, potential (when injecting ions into Q2) on ion trapping ability. No helium in the collision cell. Q1 offset = -1.5 V, Q2 offset = -2 V.

vary depending on whether or not helium is used in the collision cell; more negative voltages are optimum when buffer gas is utilized. This means that, when helium is used, a more negative lens L23 potential can be employed while the Q2 potential well required to confine the ions is still realized (i.e., with lens L23 still being more positive than the Q2 offset).

Collision (Q2) Offset Potential

Like the lens L23 voltage, the offset potential applied to the octopole collision cell greatly affects the ability to trap ions therein. The importance of this parameter is depicted in Figure 4-23. The plot shows that when trapping ions of m/z 69 in the collision cell (using helium), ion intensity is maximized at a collision offset voltage of approximately -6 V. The curve profile can be explained as follows. The Q2 offset voltage must be negative enough so that a potential gradient exists between Q1 and Q2 in order for ions to have sufficient energy to enter Q2. At the same time, though, the DC potential applied to Q2 must not be too negative so that ions (with correspondingly higher kinetic energies) are lost due to scattering, CID, or inefficient trapping in the curved octopole. Furthermore, when ions are ejected from Q2, the potentials applied to the lenses immediately after Q2 (L31, L32 and L33), as well as the Q3 offset voltage, must be more negative than the Q2 offset voltage so that ions can traverse through Q3 and be detected. The optimum Q2 offset potential also depends on whether or not helium buffer gas is utilized in Q2. Optimum values for collision offset potentials with and without buffer gas have been determined to be

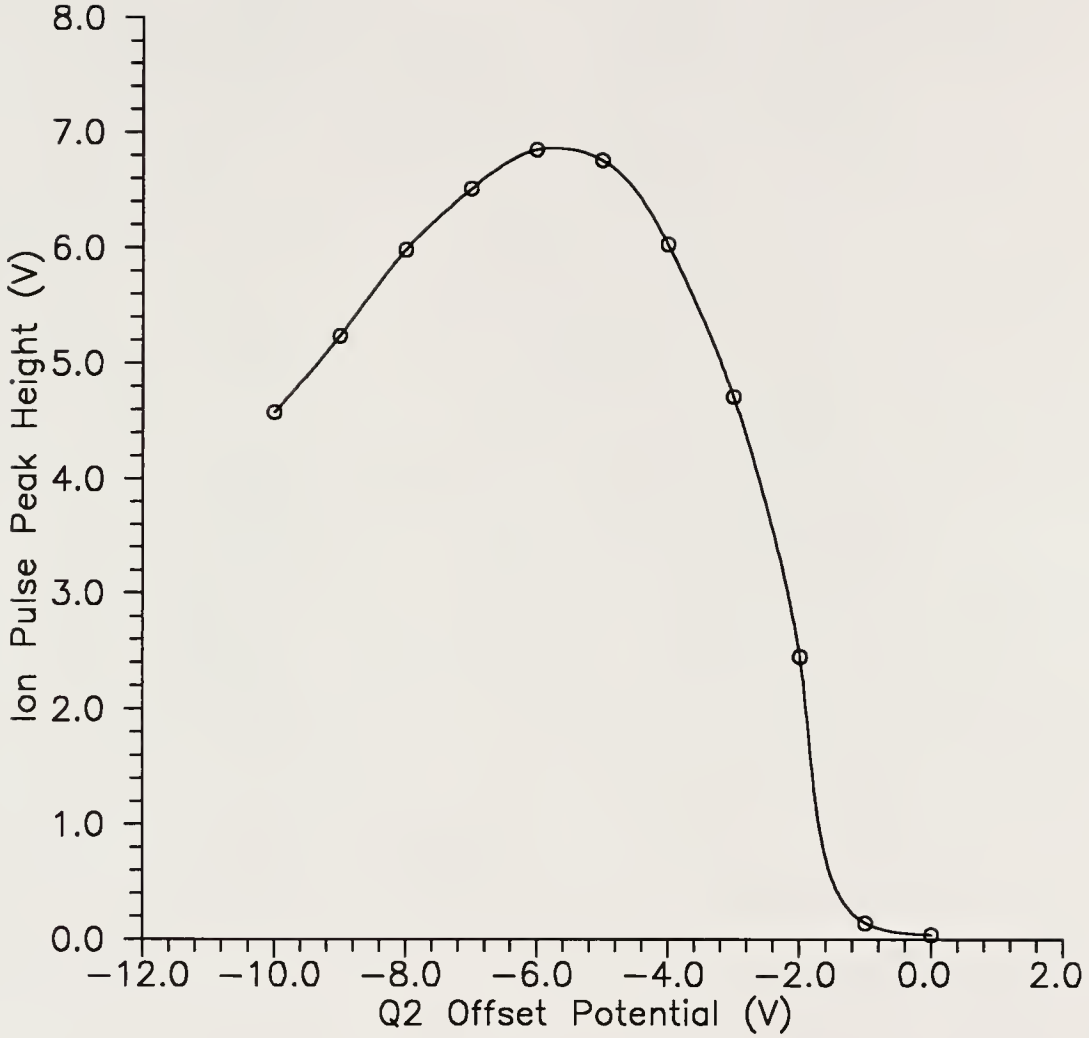

Figure 4-23: Effect of Q2 offset potential on ion trapping ability. 6.0 mTorr indicated pressure of helium in the collision cell. Q1 offset = -2 V.

-6 V and -2 V, respectively. These results are not surprising since helium acts to slow down ions as they enter the collision cell and, thus, can effectively contain ions with higher initial translational energies.

Instrument Tuning for Q2 Ion Trapping

Clearly, satisfactory performance of the Q2 ion trapping system requires the optimization of many ion optical components of the TSQ70 mass spectrometer. This entails careful tuning of the instrument under the special conditions required to trap ions in the collision cell. In this vein, special tuning guidelines and procedures have been developed to facilitate optimization of the mass spectrometer for Q2 ion trapping.

General instructions for tuning the TSQ70 mass spectrometer for use in Q2 ion trapping are outlined in Appendix A. Additionally, two ICL procedures have been written that specifically optimize parameters critical to Q2 ion trapping performance. These procedures, TTRAPOPT and TTRAPTUNE, are listed in Appendix B along with their associated subprograms. The two procedures are essentially similar in that they both automatically optimize the potentials applied to lenses L22 and L23 for trapping in Q2. Furthermore, they set the collision offset voltage to either -6 V or -2 V depending on whether or not helium buffer gas is utilized. The most notable difference between the two procedures is that TTRAPOPT performs the optimizations for only one m/z of interest, while

TTRAPTUNE automatically optimizes lenses L22 and L23 for multiple ions (m/z 69, 131, 219, 414 and 502) of the PFTBA calibration compound.

Figures 4-24 and 4-25 show the results that are obtained upon execution of TTRAPTUNE. It is immediately apparent that the tuning of lenses L22 and L23 are mass dependent under Q2 ion trapping conditions, both with and without helium buffer gas. Upon further inspection, several other conclusions can be drawn. Comparing Figures 4-24a and 4-25a, it is obvious that the optimum L22 potential becomes more negative for higher masses. This is due to the increased kinetic energies that are required for higher mass ions to enter Q2, and is reflective of these how lenses behave under normal tuning conditions. It can also be seen, though, that optimum lens L22 voltages are less negative when helium is not used compared to when helium is utilized. This is explained by noting that helium acts to slow down ions as they enter and reside in Q2. Thus, when using buffer gas, ions may have higher kinetic energies as they enter the collision cell and still be effectively confined.

Comparison of Figures 4-24b and 4-25b is also interesting. The curves have very similar shapes, but the values in Figure 4-24b (helium) are consistently approximately three volts more negative than the potentials in Figure 4-25b (no helium). These differences can be attributed to the distinct collision offset voltages used in each case. If one considers that collision offsets of -6 V and -2 V were used for Figures 4-24b and 4-25b, respectively, it is evident that the optimum values for lens L23 are all roughly 3-4 V more positive that the corresponding Q2 offsets. In

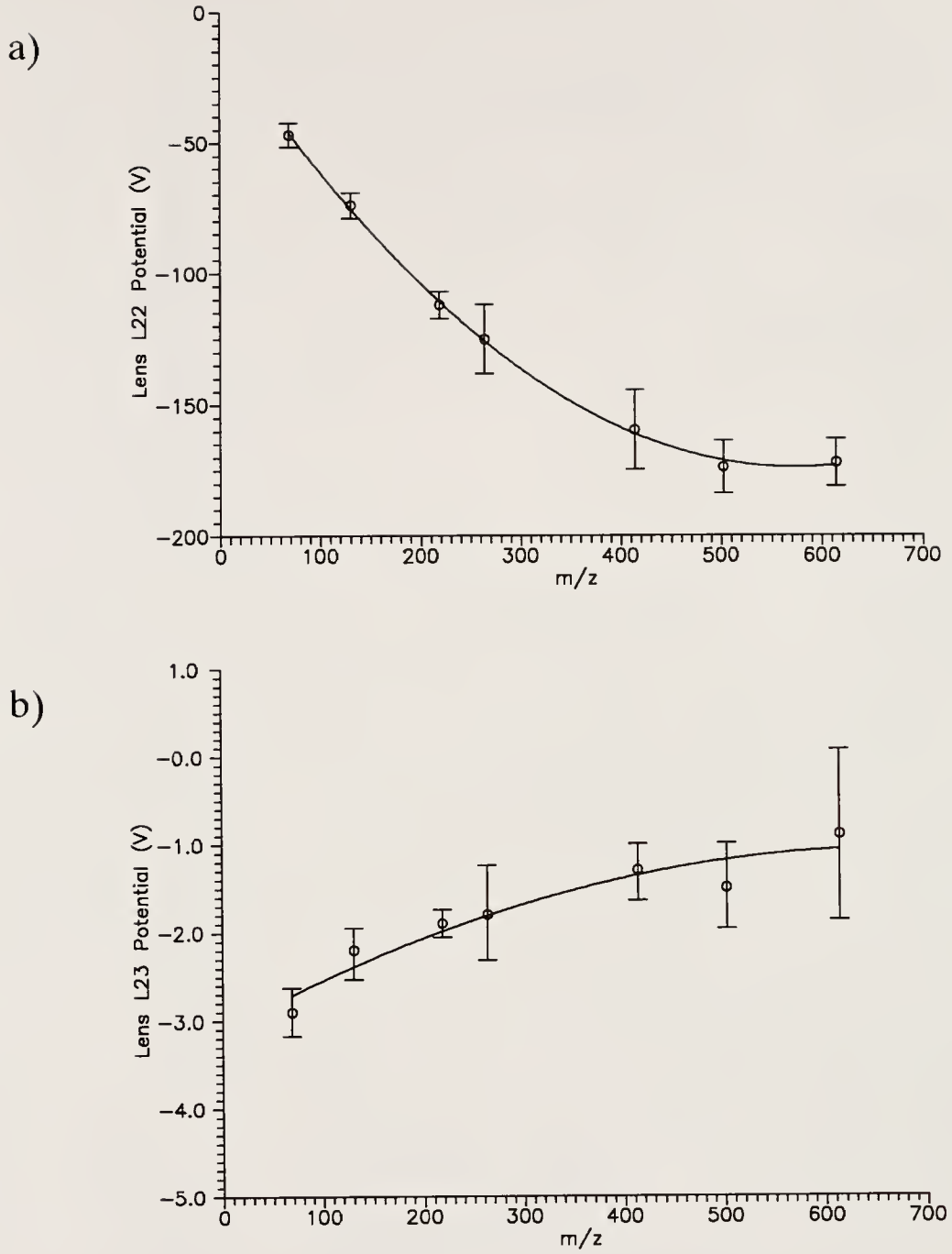

Figure 4-24: Dependence of optimum potentials of lenses a) L22 and b) L23 (when injecting ions into Q2) on m/z when trapping ions in the collision cell with 6.0 mTorr indicated pressure of helium buffer gas. Q2 offset = -6 V. Error bars represent the standard deviation of the results of five executions of the program TTRAPOPT at each m/z.

a)

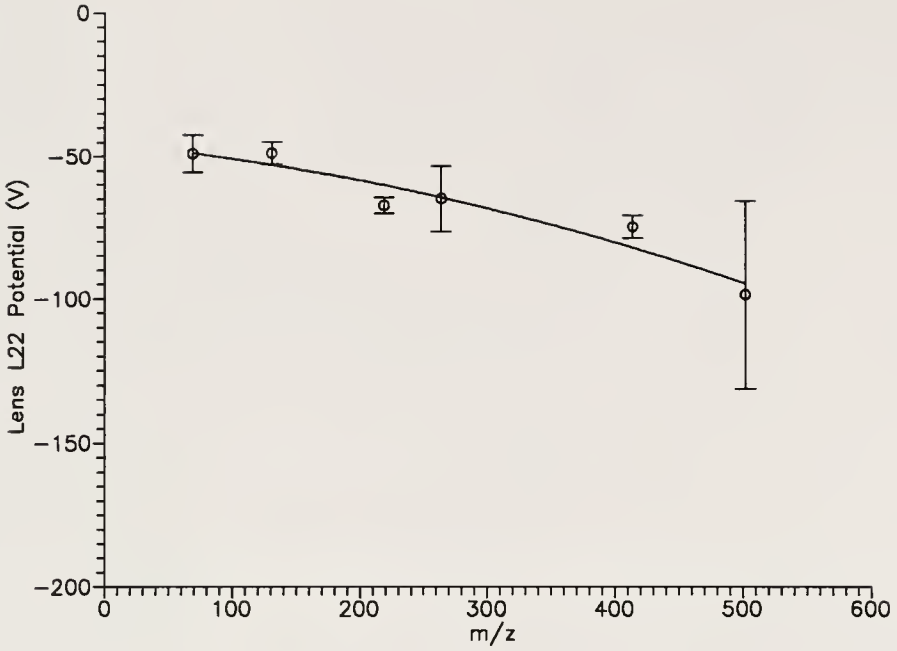

b)

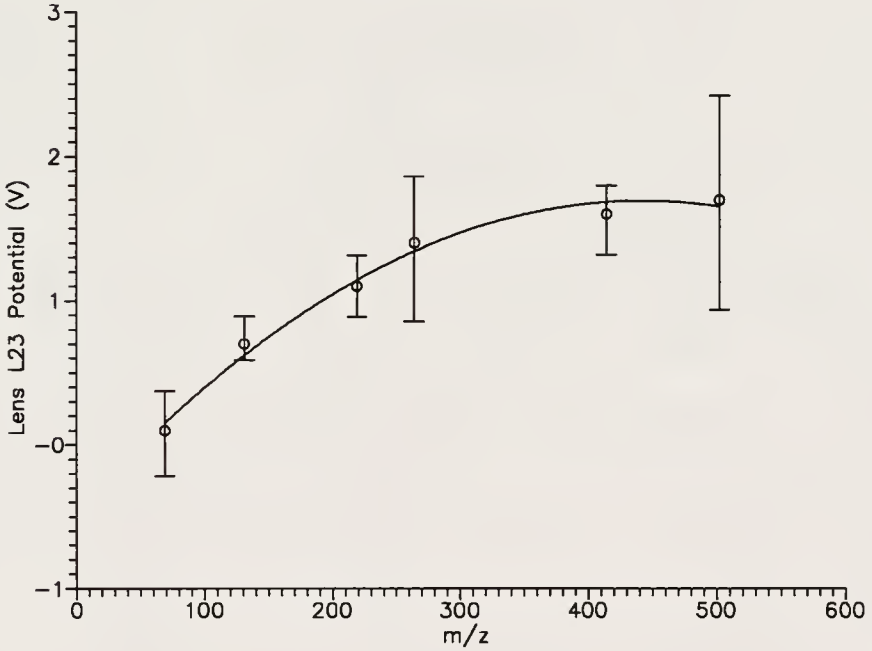

Figure 4-25: Dependence of optimum potentials of lenses a) L22 and b) L23 (when injecting ions into Q2) on m/z when trapping ions in the collision cell without helium buffer gas. Q2 offset = -2 V. Error bars represent the standard deviation of the results of five executions of the program TTRAPOPT at each m/z.

this way, the Q2 potential well necessary for effective ion trapping is preserved in each case.

Conclusions

A system for trapping ions in the collision cell of the TSQ70 triple quadrupole mass spectrometer has been developed and characterized. The technique is easily performed via incorporation of a simple lens control circuit and implementation of Instrument Control Language (ICL) procedures that have been specially designed to control the Q2 trapping experiment.

Parameters significant to the performance of the system have been investigated. It was discovered that the presence of helium buffer gas in the collision cell greatly improves ion trapping efficiencies by slowing down ions as they enter and reside in Q2 and then confining them to the center of the octopole. The number of ions that are ultimately detected as a percentage of those ions that were initially injected into Q2, %(Out/In), increases substantially when helium is used. Calculated values ranged from as little as 0.1%, when trapping ions of m/z 69 without helium, to 91.2%, when trapping m/z 414 ions with helium buffer gas.

Specific ion optical components have also been optimized for Q2 trapping. In particular, the potential applied to the entrance lens, L23, when filling the collision cell with ions has a dramatic effect on ion trapping efficiency. It was also determined that the collision offset voltage affects the ability of Q2 to confine ions. Furthermore, the optimum values for Q2 offset voltage vary depending on whether

or not helium buffer gas is used, and this, in turn, affects the optimum lens L23 potentials. Guidelines have been developed to aid in tuning the instrument for Q2 ion trapping. Moreover, ICL procedures have been devised that automatically tune ion optical components of the TSQ70 that are crucial for effective Q2 ion trapping.

It has been demonstrated that ions can be successfully trapped in the collision cell of the TSQ70 mass spectrometer. The technique allows execution of experiments that are normally impractical, or impossible, to perform on standard tandem quadrupole instruments. In the following chapter, applications and examples of the ion trapping system will be presented. Furthermore, it will be shown that the technique is useful for the study of associative ion-molecule reactions.

CHAPTER 5
INVESTIGATIONS OF ION TRAPPING: FUNDAMENTAL STUDIES AND APPLICATIONS FOR ENHANCEMENT OF ASSOCIATIVE ION-MOLECULE REACTIONS

Introduction

Ion trapping in the collision cell of a triple quadrupole mass spectrometer is an unusual and distinctive technique. As such, there are several characteristics of Q2 ion trapping that make it unique and, in some cases, superior to other ion trapping methods, such as the ease with which ions can be trapped for extended time periods (i.e, hours). Some characteristics of the technique, however, make it less useful than other ion trapping methods. For instance, Q2 ion trapping allows for only two stages of mass spectrometry, while the quadrupole ion trap (QITMS) can perform multiple stages of mass analysis. Furthermore, while the QITMS can acquire data over the entire mass range for each trapping cycle, multiple trapping experiments must be performed with the Q2 ion trap to obtain a full-scan mass spectrum. In this chapter, some of the attributes of Q2 ion trapping are described and their relationships to the Q2 ion trapping process are examined. Furthermore, applications of Q2 ion trapping are presented that demonstrate the power and utility, as well as the limitations, of the technique.

Two of the more significant parameters of the Q2 ion trapping system are the fill time and the trapping time. The fill time can be related to the number of ions that the collision cell holds before becoming saturated. This concept of pumping ions into the confinement zone is somewhat unique when compared to the ionization processes of other ion trapping methods. In a typical quadrupole ion trap mass spectrometer, ionization and reaction take place within the same region of space. Only when external ionization [89-94] is utilized can ions be subsequently injected into the ion trap. The ability to ionize in a different region than where reactions take place has distinct advantages, and provides several interesting effects. The ion confinement characteristics of the Q2 ion trapping system are also quite different from those of other ion trapping devices. In particular, it is very easy to trap ions for extended periods of time. Similar results have been obtained using quadrupole ion traps with superimposed weak octopole fields [95]. It was found that ion storage could be accomplished for several hours without any measurable ion losses. Furthermore, storage of ions for long time periods allows for studies of slow ion-molecule reactions, fragmentation energy thresholds, photochemical ion reactions, high atmosphere ion chemistry under effect of UV radiation, and interactions in the ion cloud.

Experimental

All experiments were performed on a Finnigan MAT (San Jose, CA) TSQ70 triple quadrupole mass spectrometer modified with an octopole collision cell and a

20 kV conversion dynode. Data were acquired with both the data system of the TSQ70 and a LeCroy (Chestnut Ridge, NY) 9400 Digital Storage Oscilloscope (DSO). Characterization studies were performed using perfluorotributylamine (PFTBA) calibration compound. PFTBA was introduced into an EI ion volume in the ion source via a specially designed probe, constructed in house, which allowed for precise metering of the PFTBA vapor pressure. Studies were performed under EI conditions at an electron energy of 70 eV and an emission current of 200 μA. The manifold temperature was maintained at temperatures ranging from 70-100 °C while the ion source temperature was held at 170°C.

For the Q2 ion trapping studies, electron multiplier potentials ranging from -600 to -1400 V were utilized. In general, experiments that were conducted with helium in the collision cell and with Q3 in the RF-only mode used electron multiplier voltages on the order of -700 V. On the other hand, studies that were performed without helium buffer gas in Q2 or with Q3 in the RF/DC mode employed electron multiplier voltages upward of -1000 V. In all cases, the preamplifier gain was set at 10^8 V/A and the conversion dynode was held at -5 kV.

The mass spectrometer was tuned with PFTBA to optimize ion transmission and calibrate the mass assignment using tuning procedures written by Hail [71]. Additionally, further tuning operations were performed using either of the two sets of tuning guidelines discussed in Chapter 4 (see Appendix A).

Experiments involving Q2 ion trapping were regulated by appropriate Instrument Control Language procedures listed in Appendix C. In addition to

utilizing these specially written procedures, several other parameters were optimized for Q2 ion trapping. For all studies, the prescan voltage settling time, SETTIM, was set to its minimum value, 0.1 ms, to minimize the time required for the trapping cycles to execute. Also, the DC offset potential applied to the octopole collision cell was optimized at -6 or -2 V, respectively, depending on whether or not helium buffer gas was employed. For experiments where helium was utilized as a buffer gas, it was introduced into Q2 via a Negretti (Hampshire, England) fine-metering valve to an indicated pressure (with a Granville Phillips Convectron gauge) of approximately 6.0 mTorr. Furthermore, the mode in which Q3 was operated was varied. For experiments where the entire ion pulse (without mass analysis) was to be detected, Q3 was operated in the RF-only mode by turning off the Q3 rods DC potentials using the DDOFF command. If, however, mass analysis was to be performed on the pulse of ions as it exited the collision cell, Q3 was operated in the normal RF/DC mass filter mode.

Parameters important to, or defined by, the Q2 ion trapping process were also carefully controlled. Scan times varied from study to study and typically ranged between 0.001 s and 0.1 s, depending on the nature of the investigation. Similarly, scan range widths varied from 0.1-0.5 amu for detection of trapped ion pulses. The period of time that the collision cell was allowed to fill with ions, the fill time, was typically on the order of 0.1 to 1 s. However, trapping times ranged from several hundred milliseconds to several minutes or more, depending on the particular experiment. In many cases, studies were performed to examine the effects of these,

and other, parameters on the Q2 ion trapping process. Therefore, specific values for scan times, scan ranges, fill times, trapping times and other variables are stated in the text when the situation warrants.

Investigations of the associative ion-molecule reactions of DNA/RNA base ions and allyl chloride under Q2 ion trapping conditions were also undertaken. The DNA/RNA bases adenine, cytosine, thymine and uracil were purchased from Sigma Chemical Company (St. Louis, MO); allyl chloride was acquired form Aldrich Chemical Company (Milwaukee, WI). The bases, contained in capped aluminum vials, were introduced into the ion source via a heated solids probe. The solids probe temperature was precisely adjusted in each case to give an ion current of constant intensity via electron ionization. Simultaneously, allyl chloride was introduced into the collision cell via a Negretti fine-metering valve until approximately 0.5 mTorr was indicated. Helium was then added through a tee in the line to an indicated pressure of approximately 6.5 mTorr.

Optimization of Mass Scanning Parameters

Under normal operation, the triple quadrupole mass spectrometer performs mass scans on a continuous ion beam. Thus, it is possible to change mass scanning parameters to widen the detected mass range or to increase the data throughput by decreasing the scan time. When the triple quadrupole mass spectrometer is operated in the Q2 ion trapping mode, however, the instrument must scan over discrete ion pulses. Since the TSQ70 was not designed to operate in the pulsed mode, the

determination of appropriate mass scanning parameters is critical. Subsequently, it is important to understand how changes in mass scanning parameters affect instrument performance and data acquisition under Q2 ion trapping conditions. The characteristics of a mass scan can be defined adequately by knowing the scan range and scan time utilized. As such, these two parameters were studied to determine their effects on the Q2 ion trapping system.

Much of the ion trapping data presented in this work was acquired using Q3 in the RF-only mode. Under these conditions, the scan range that Q3 is operated over is irrelevant as long as the low-mass cutoff of the device is below the m/z of any ions of interest in the ion pulse. When Q3 is operated as a mass filter in the RF/DC mode, however, it is advantageous to scan over the appropriate m/z for the majority of the ion pulse. This indicates that a very narrow mass range should be used for maximum sensitivity. This also dictates that mass calibration must be accurately adjusted so that ions of interest are stable in the narrow mass range. Another point to consider is that, when viewing centroid data on the TSQ70, observed ion intensities decrease dramatically at scan ranges below 1 amu. This occurs under normal operation as well as when performing Q2 trapping experiments. This would seem to suggest that wider mass ranges are better when scanning over an ion pulse. This assumption is incorrect, however, because centroid peak area calculations depend on the width of the peak as well as its height. Thus, ion intensities decrease significantly when only the apex of the peak is scanned over. This has no net effect, though, if a specific narrow scan range is consistently used. Although the absolute

numbers of counts may be lower, the relative numbers of counts will still compare well. For most of the work presented here, a mass range of 0.2 amu centered around the peak was utilized. This value is a good compromise since excessive ions are not lost due to incorrect mass calibration, and excellent sensitivity is still achieved.

Presumably, the optimum scan time for detection of ions trapped in Q2 would be on the order of the time constant of the ion pulse, so that maximum sensitivity could be obtained. This period is typically 5-10 ms, depending on experimental conditions. However, when studies were initially performed (using the LeCroy DSO for ion detection) to evaluate scan time with respect to detection of ion pulses arising from Q2 trapping, interesting results were obtained. As can be seen in Figure 5-1, ion pulse peak heights increased dramatically at very short scan times. Peak height was greatly enhanced at scan times less than 10 ms, and it seemed that the optimum scan time would be limited to the minimum value allowed by the instrument. It was unclear at first what was occurring at these short scan times, but it was later surmised that ions were accumulating in the collision cell from pulse to pulse. It has been confirmed that this is the case. This subject is discussed, and several examples of the effect are shown in the next section.

Ion Accumulation in the Collision Cell

Looking at Figure 5-1, it is clear that the ion pulse peak heights increase at shorter scan times. Actually, the first pulse (scan/cycle number one) at a short scan

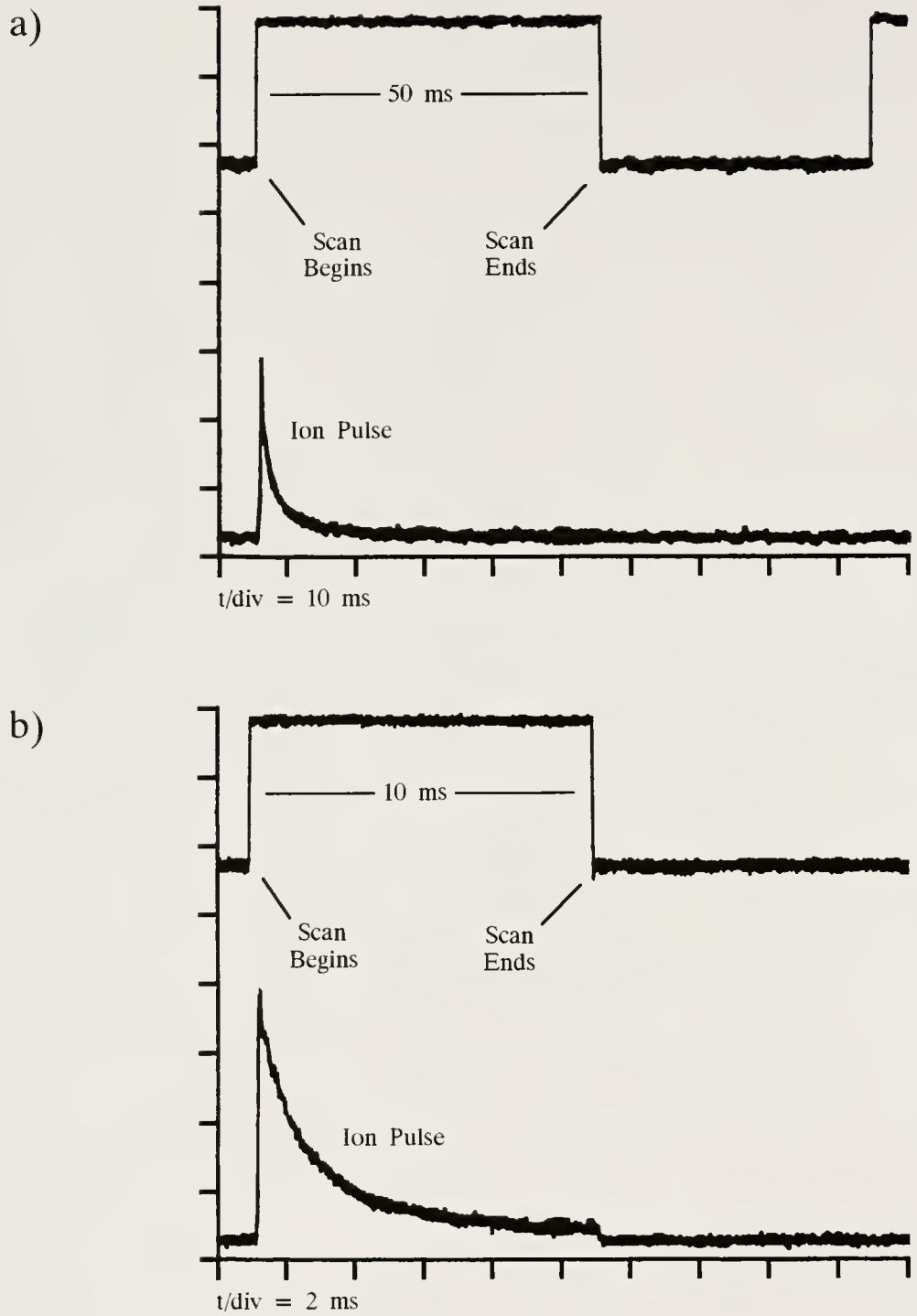

Figure 5-1: Ion pulses observed (when peak height ceases to increase after several scans) at scan times of a) 50 ms and b) 10 ms. Running TQ2FILL51 with 6.0 mTorr helium in Q2. Scanning Q3 (RF/DC) over a 0.2 amu window around m/z 69. Y-axis scale is constant.

c)

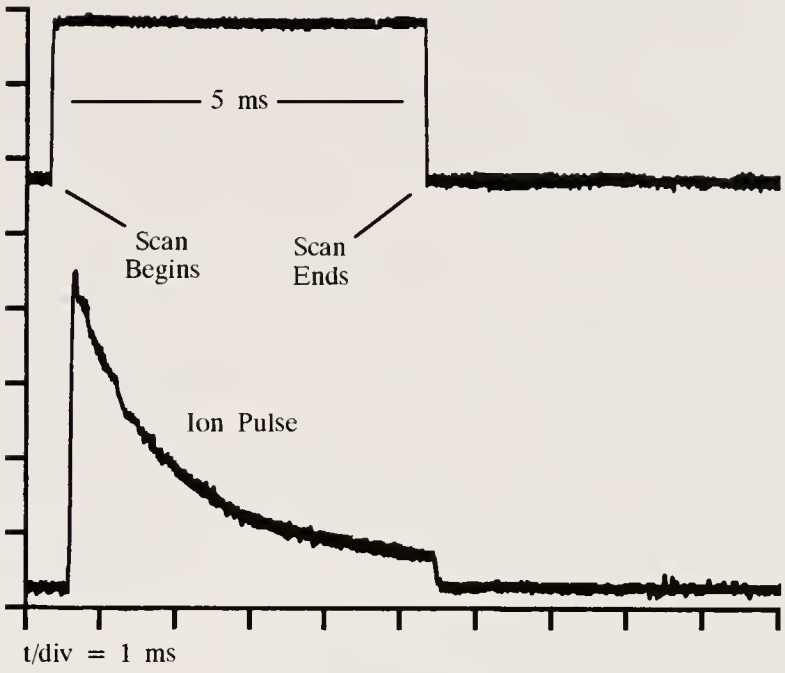

d)

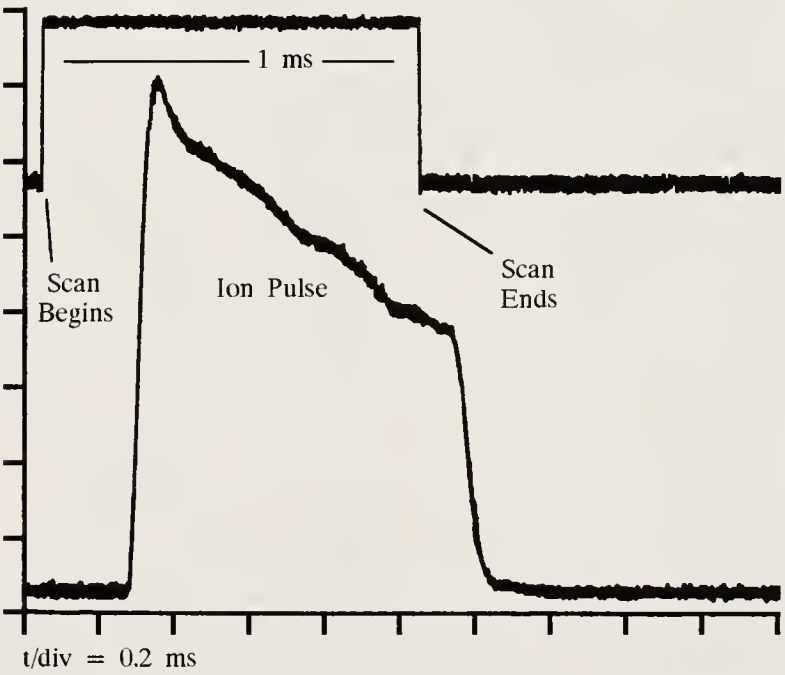

Figure 5-1: (continued) Ion pulses observed (when peak height ceases to increase after several scans) at scan times of c) 5 ms and d) 1 ms. Running TQ2FILL5I with 6.0 mTorr helium in Q2. Scanning Q3 (RF/DC) over a 0.2 amu window around m/z 69. Y-axis scale is constant.

time is not any larger than a pulse observed using a longer scan time. However, as the experiment progresses (and the trapping cycle count increases) peak heights are observed to increase until they reach a plateau. It is also readily apparent that, at scan times less than 10 ms, much of the ion pulse is cut off; the exit lens, L31, closes before many of the ions in the pulse are allowed to escape the collision cell. This means that, over several scans, ions are built up in Q2 and increases in ion pulse intensities are observed.

Several other examples of this phenomenon have been noted that provide strong evidence that ion accumulation is the cause of increased ion intensities at short scan times. Figure 5-2 shows that ion intensities increase up to a plateau when trapping m/z 69 ions of PFTBA in the collision cell without helium buffer gas. Ion accumulation effects are more pronounced when helium buffer gas is not used because ion pulses tend to be longer and more diffuse. Therefore, more ions are left in the collision cell in between cycles. For both of these plots, the scan time was 10 ms and the fill time was fixed at 0.1 s so that the number of ions injected from cycle to cycle was constant. Looking at Figure 5-2a, it is clear that it takes several trap and pulse cycles to reach a "steady state" where the number of ions injected during each fill time is equivalent to the number of ions ejected upon opening of the exit lens. After this point (approximately 1 s), ion losses due to increased trapping times become significant, and ion intensities start to decrease. Similar results are seen in Figure 5-2b. Even though the differences in trapping times, from cycle to cycle, are different in Figure 5-2b than in Figure 5-2a, the absolute number of cycles

a)

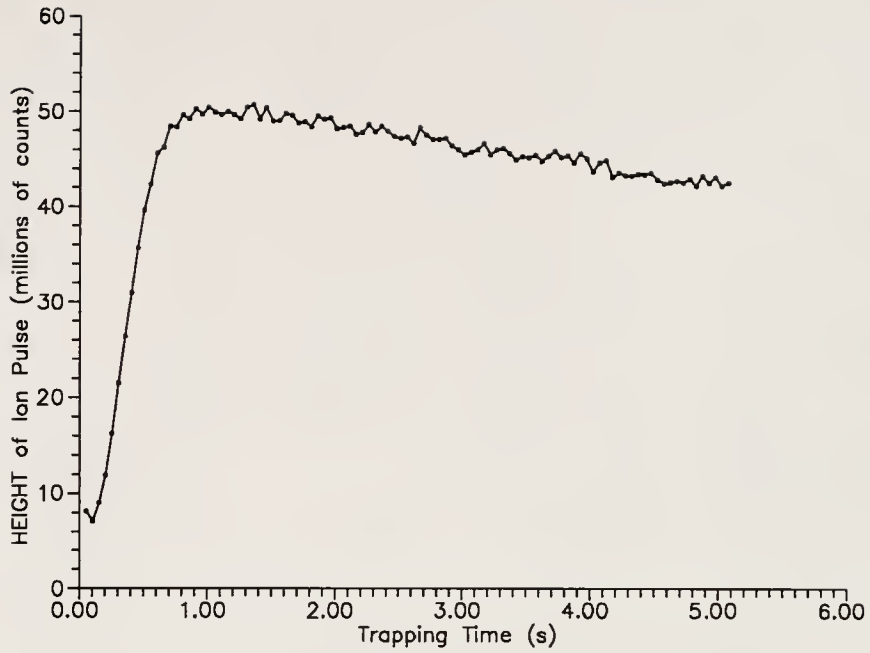

b)

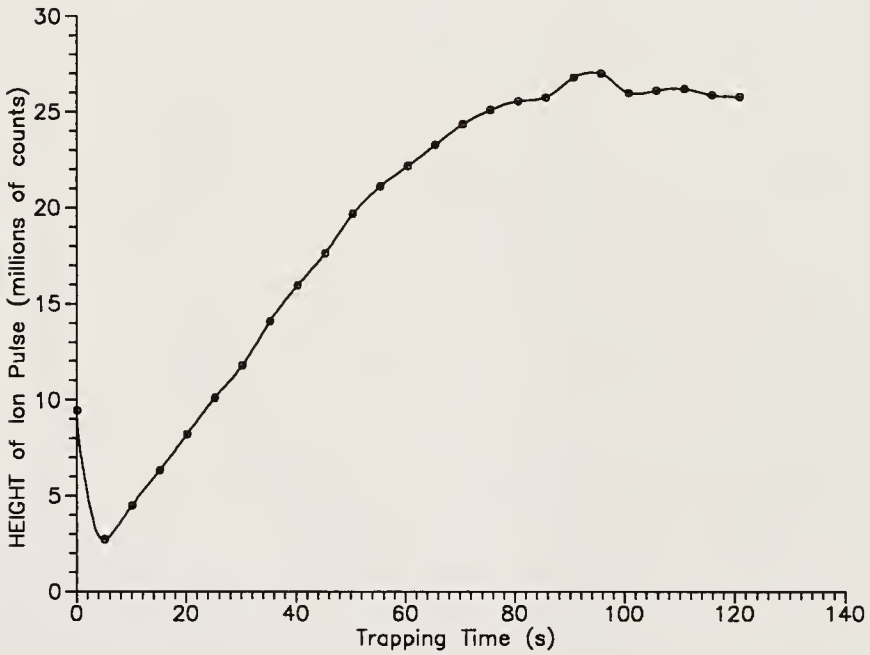

Figure 5-2: Increasing ion pulse intensities resulting from ion accumulation in the collision cell for trapping times of a) 0-5 s and b) 0-120 s. Notice that approximately 20 cycles are required to reach a plateau regardless of the absolute trapping times used in each experiment. No helium buffer gas was used.

(approximately 20) needed to reach a "steady state" is approximately the same; the effect is independent of trapping time. The only explanation for this is that ions are accumulating in the collision cell between cycles.

Figure 5-3 provides more evidence that ion accumulation in Q2 occurs under some circumstances. In these cases, the Q2 ion trapping ICL procedure TQ2FILL5I was modified so that two ion pulses are detected after trapping ions in Q2. The reason that lens L31 opens at two different negative potentials is that the first opening is controlled by the lens control circuit (see Chapter 4) while the second opening is controlled by the instrument firmware. Nonetheless, the differences in the two potentials have essentially no affect on the intensities of the observed ion pulses. It is obvious, especially in comparing Figures 5-3a and 5-3c, that the second ion pulse increases in intensity with decreasing scan time. Moreover, for all three cases, the second ion pulse essentially starts at the level at which the first ion pulse left off. Figure 5-4 is a summary of a similar experiment which shows that the area of the second ion pulse relative to the area of the first ion pulse increases substantially at very short scan times. These observations provide undisputable proof that ions are being accumulated in the collision cell from cycle to cycle.

Clearly, the accumulation of ions in the collision cell is not conducive to studies involving ion-molecule reactions and kinetics. The very nature of these types of studies demands that ions and molecules be allowed to react for known periods of time in order for subsequent observations to be meaningful. If ions are continually amassed in the reaction region, absolute reaction times can never be

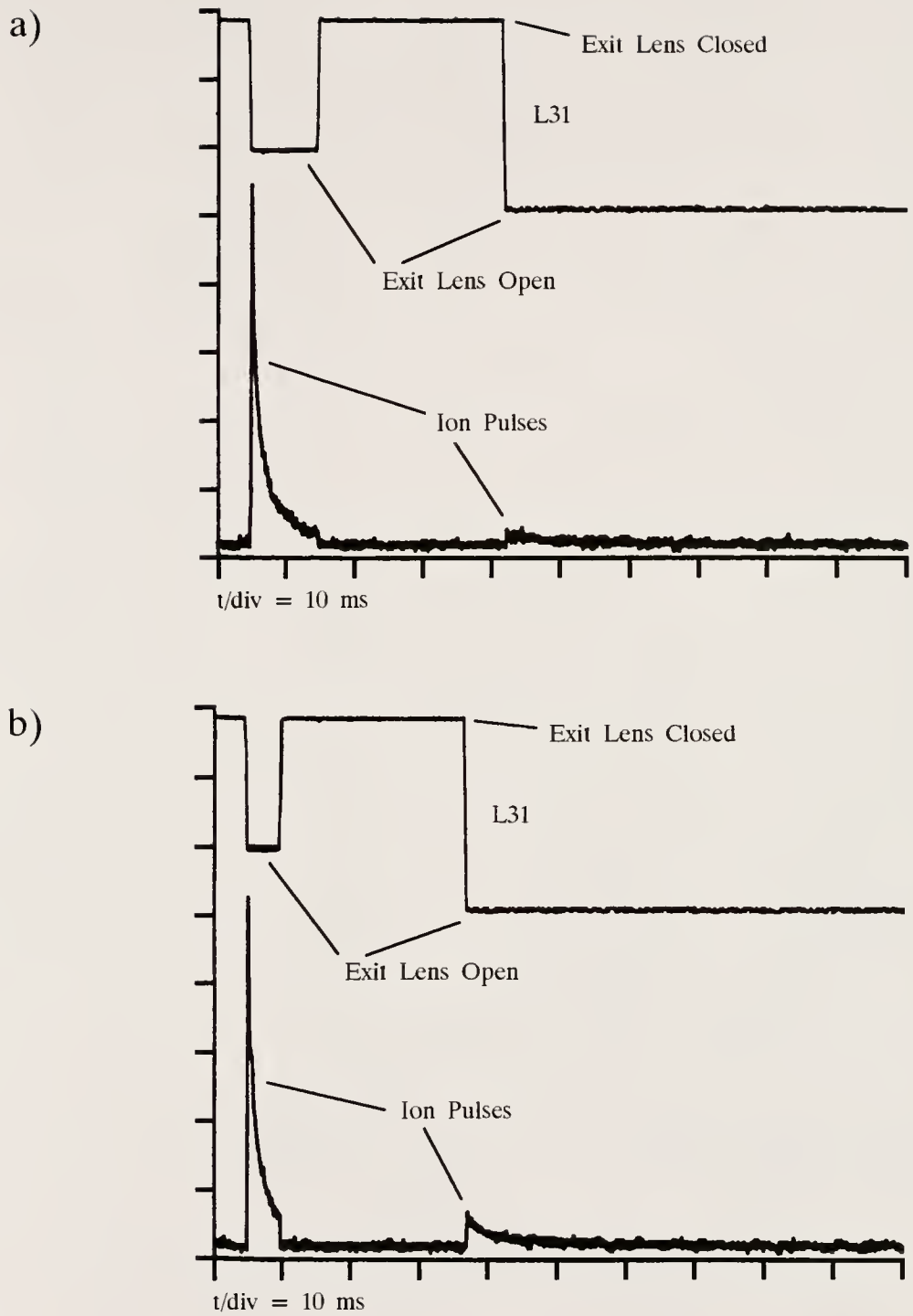

Figure 5-3: DSO traces of ion pulses observed when the exit lens, L31, is opened twice in succession after each trapping period. Scan times are a) 10 ms and b) 5 ms. Running TQ2FILL5I (modified so that lens L31 opens twice each cycle) with 6.0 mTorr helium in Q2. Scanning Q3 (RF-only) over a 0.2 amu window around m/z 69.

c)

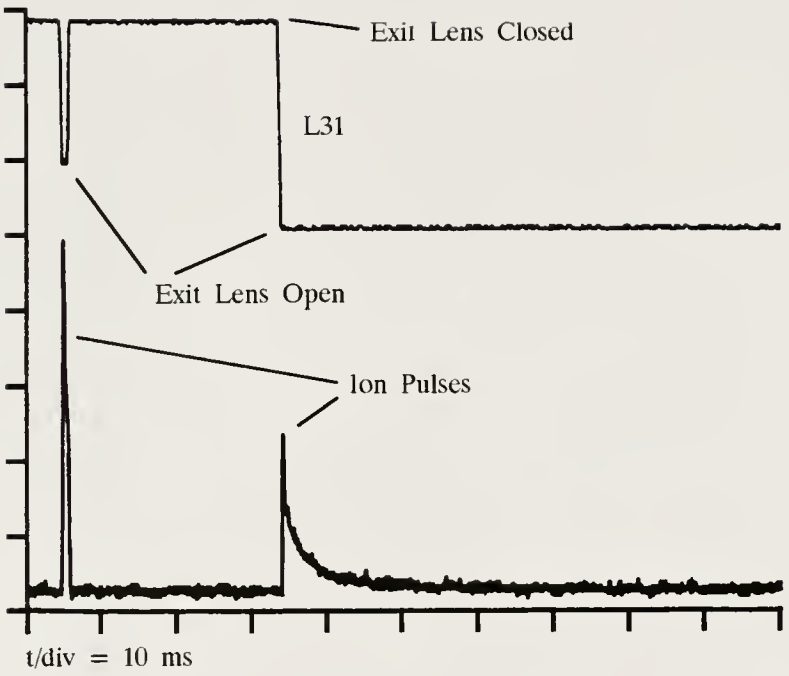

Figure 5-3: (continued) DSO trace of ion pulses observed when the exit lens, L31, is opened twice in succession after each trapping period. Scan time is 1 ms. Running TQ2FILL5I (modified so that lens L31 opens twice each cycle) with 6.0 mTorr helium in Q2. Scanning Q3 (RF-only) over a 0.2 amu window around m/z 69.

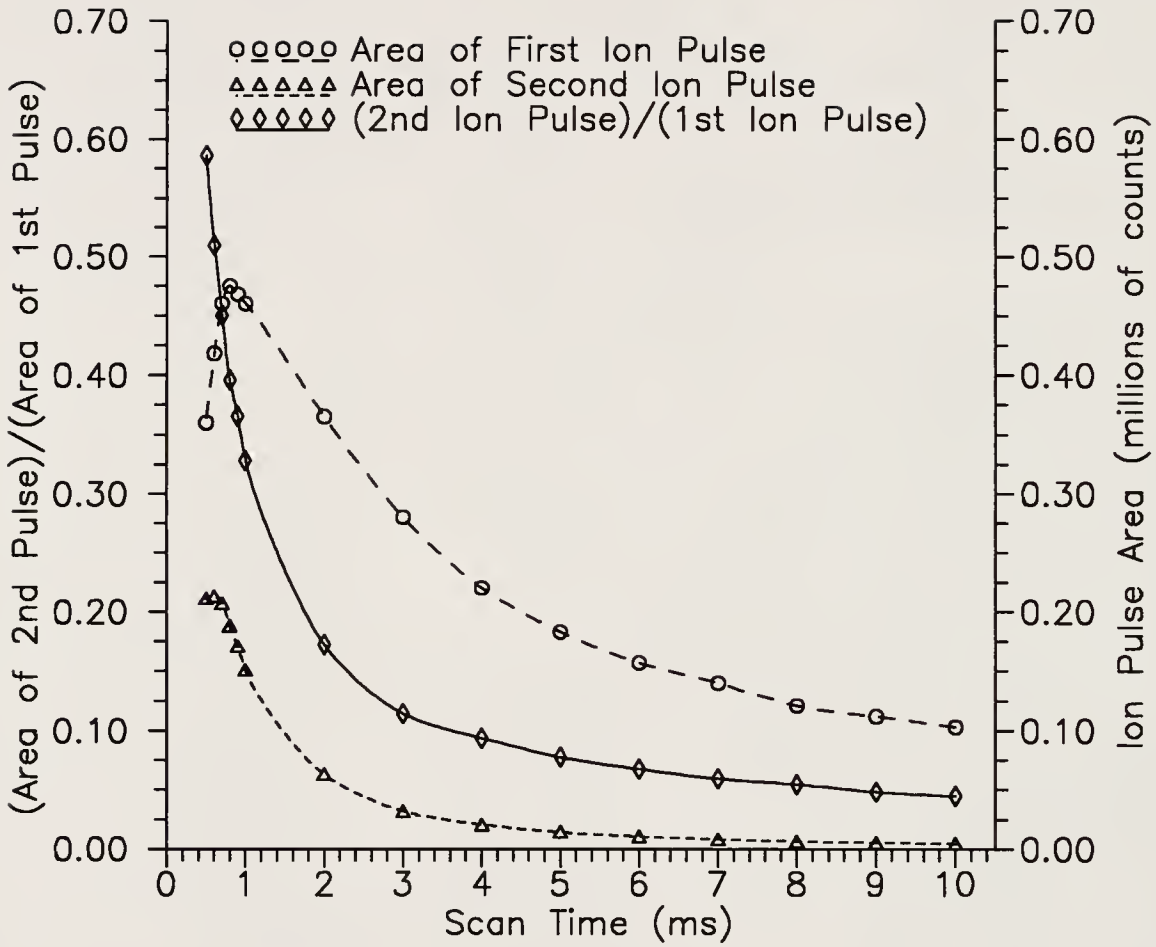

Figure 5-4: Effect of scan time (equivalent to the time that the exit lens, L31, is open) on the areas of the second and first ion pulses (and their ratio) detected after each trapping cycle. 6.0 mTorr helium in Q2, scanning Q3 (RF-only) over a 0.2 amu window around m/z 69.

accurately measured since some ions may be allowed to react for times equivalent to several cycles. For this reason, a method was needed to disperse ions from the collision cell between trap and pulse cycles so that Q2 is always free of ions before ions are injected into it.

There are, practically, two techniques that can be used to eliminate ions from the collision cell after each cycle. The most obvious approach is to have a long period (0.1 s or more) after the initial ion pulse is detected when the exit lens, L31, is allowed to remain open long enough to ensure that any ions trapped can diffuse out of Q2. This, in fact was the technique used to acquire the data shown in Figure 5-3. There are several disadvantages to this method. The most obvious problem is that this technique contributes significantly to the overhead time of each trap and pulse cycle. Thus, a full-length experiment can be prolonged by 10-20% or more. Another more serious drawback is that all the ions left in the collision cell may not be expelled. It is very likely that, in some cases, ion diffusion alone can not force out all of the ions left over from a trapping cycle. This is especially true for higher mass ions since they diffuse at slower rates than do less massive ions. This means that, no matter how long lens L31 is left open, some ions may still be left in the collision cell resulting in ion accumulation.

A more direct approach is to make all the ions in the collision cell unstable so that they are no longer confined in the octopole field. By doing this, ions can be effectively flushed out of the collision cell. This can be done by elevating the RF potential applied to the octopole to a level such that the low-mass cutoff of the

device is above the m/z values of any ions that may be present in Q2. On the TSQ70, the RF potential applied to the octopole is controlled by a parameter called the collision RF potential (CRFP). Since the voltage and frequency specifications of the potential applied to the collision cell of the TSQ70 are Finnigan proprietary information, the CRFP cannot be related to a specific RF voltage without knowledge of appropriate conversion factors. However, it is known that the CRFP is directly related to the RF potential; an increase in the CRFP increases the RF potential of the octopole. Thus, by increasing the CRFP, the low mass cutoff of the octopole is increased and successively more massive ions become unstable and are ejected.

Table 5-1 shows that increasing the CRFP can effectively eliminate ions from the collision cell under Q2 ion trapping conditions. For this experiment, trapping times were kept constant at 0.05 s and Q3 was set to pass all ions (RF-only). Also, the electron multiplier voltage was adjusted for each m/z to achieve maximum ion signals. It is clear that successively more massive ions become unstable as the CRFP is increased. Indeed, other experiments have been performed which confirm that no ions are left in the collision cell if the CRFP is pulsed to a high enough value.

This concept of pulsing the CRFP to eliminate ions from the collision cell is implemented in the Q2 ion trapping ICL procedure TQ2FILL5K. The listing of the program in Appendix C shows that it is identical to TQ2FILL5I except that the CRFP is pulsed to 100 for approximately the time required for one scan (default is approximately 10 ms) after each trap and pulse cycle. Comparing this CRFP of 100 to those listed in Table 5-1, it is apparent that TQ2FILL5K generates a low-mass

Table 5-1: Effect of collision cell RF potential (CRFP) on ejection of ions from the octopole collision cell under Q2 ion trapping conditions.

m/z of Parent Ion[a]	CRFP Required to Flush Out Q2[b]
18	1.6
69	6.5
219	20.5
414	39.0
502	47.3
614	58.0

Note: Running TQ2FILL51 with a fill time of 0.1 s and a trapping time of 0.05 s while using helium buffer gas. Q3 is in RF-only mode and electron multiplier was set for each m/z to maximize ion detection.

[a] Ions of this m/z were mass selected by Q1 and injected into the collision cell to be trapped.

[b] The CRFP that was required so that ion signals were undetectable.

cutoff high enough so that any ions that may accumulate in the collision cell will be efficiently flushed out. This is demonstrated in Figure 5-5, which shows that, at short scan times, ion pulse peak heights, as measured using a DSO, do not increase at all due to ion accumulation when the CRFP is pulsed to 100 after each trapping cycle. Furthermore, pulsing the CRFP to 100 is accomplished very quickly so that the net increase in overhead time is insignificant. Thus, TQ2FILL5K is an effective Q2 ion trapping procedure that allows the collision cell to be free of ions before each individual trapping cycle.

Fill Time Studies

Since the RF field defined by the octopole collision cell is of finite dimensions, the number of ions that can be confined to it is limited. For this reason, it is interesting to examine how the relative numbers of ions injected into the collision cell affect the ultimate numbers of ions detected.

Figure 5-6 shows that fill time has a great effect on ion pulse intensities. This is obvious since, as fill times increase, more ions are injected into the collision cell and more ions are available to be detected as they escape from Q2 when lens L31 opens. Other observations can also be made looking at the two graphs. Upon examination of Figure 5-6a, it is clear that ion pulse intensities begin to level off at fill times somewhat less than 10 s. This is due to saturation of the collision cell with ions (space charge). At the plateau, any increase in the flux of ions being injected into the collision cell is offset by the increased loss of ions due to imperfect ion

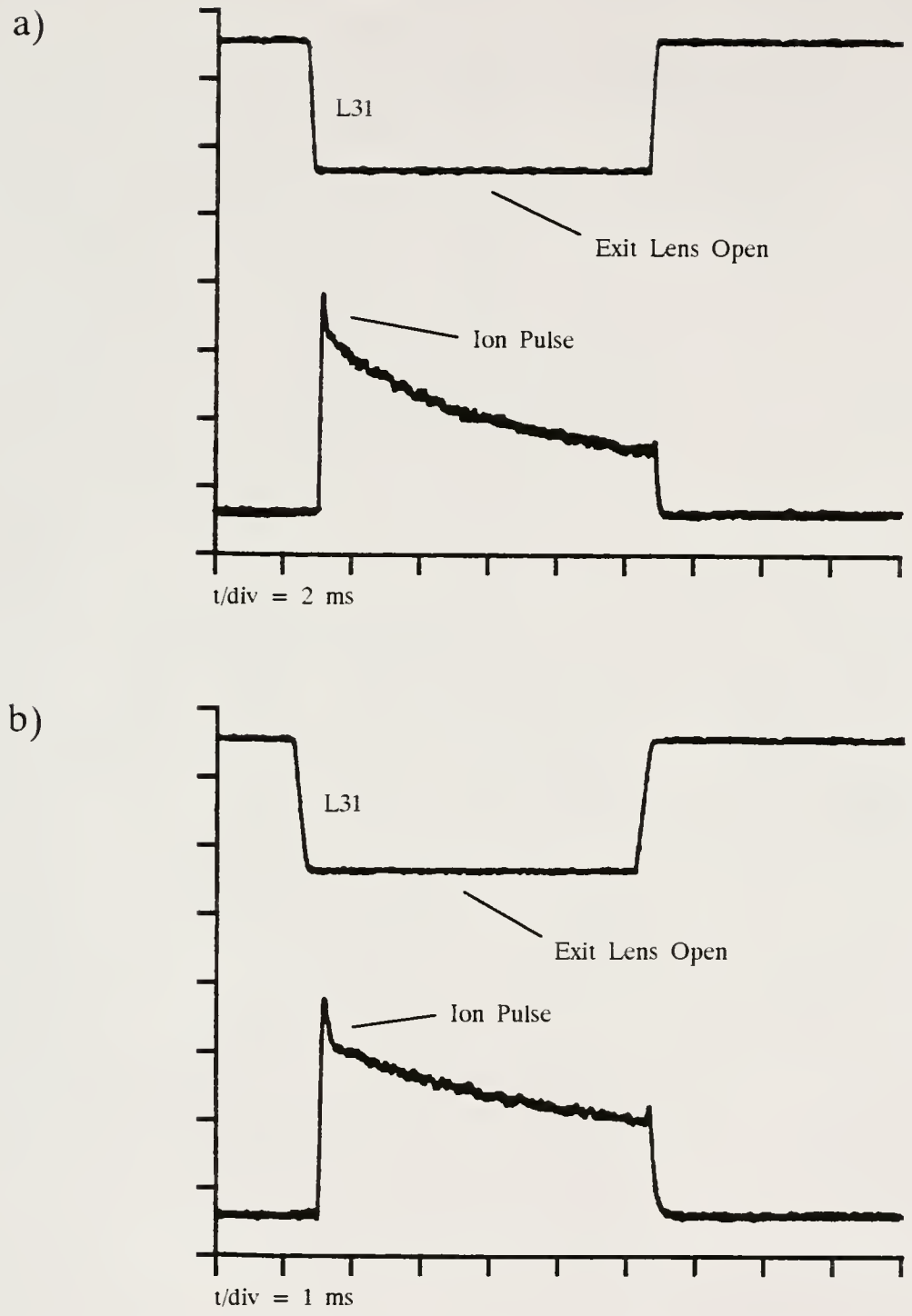

Figure 5-5: Ion pulses observed (after several scans) at scan times of a) 10 ms and b) 5 ms. Running TQ2FILL5K with 6.0 mTorr helium in Q2. Scanning Q3 (RF-only) over a 0.2 amu window around m/z 502. Y-axis scale is constant.

c)

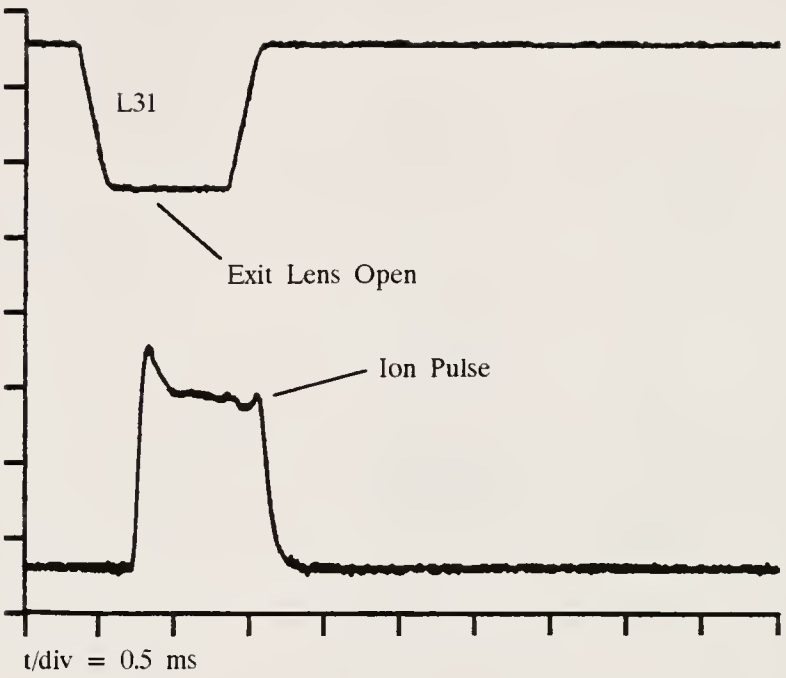

Figure 5-5: (continued) Ion pulse observed (after several scans) at a scan time of 1 ms. Running TQ2FILL5K with 6.0 mTorr helium in Q2. Scanning Q3 (RF-only) over a 0.2 amu window around m/z 502. Y-axis scale is constant.

a)

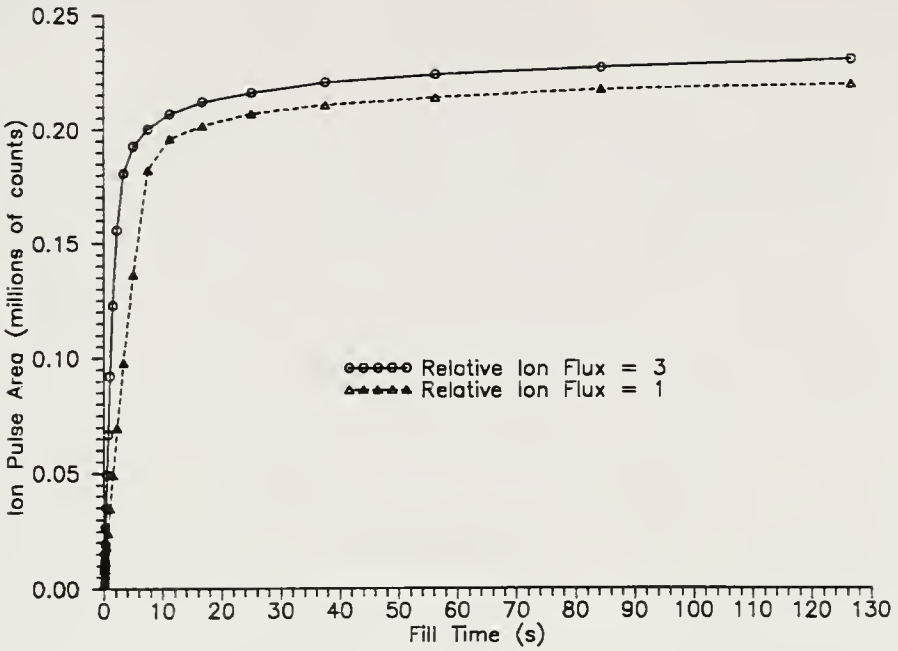

b)

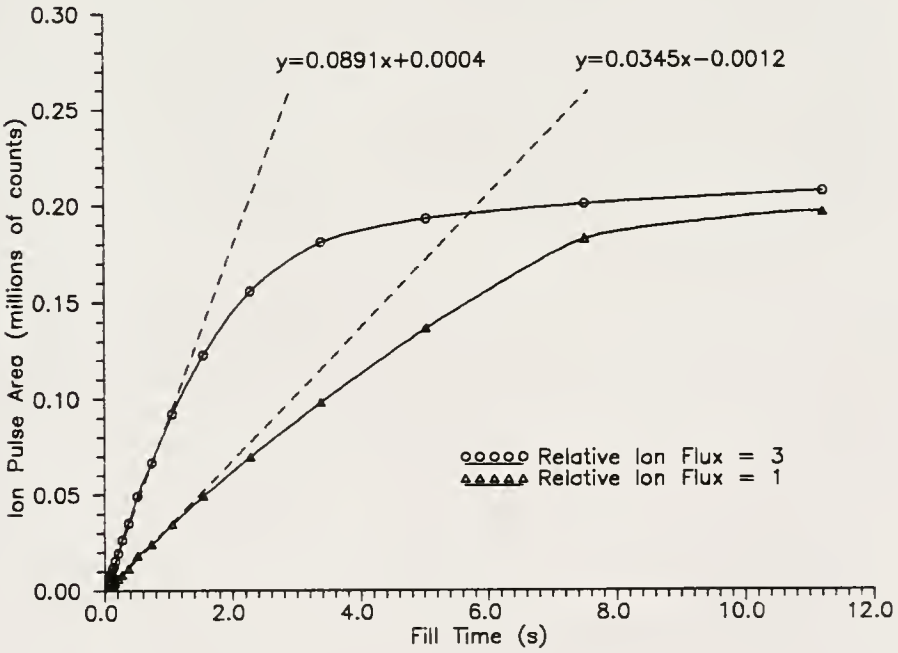

Figure 5-6: Dependence of ion pulse intensities on the number of ions injected into the collision cell. Plots show fill times of a) 0-127 s and b) 0-17 s. Trapping time is 0.05 s, 6.0 mTorr helium in Q2, scanning Q3 (RF-only) over a 0.2 amu window around m/z 69.

containment arising from ion-ion repulsions. Thus, even though more ions are injected into the collision cell at longer fill times, the numbers of ions that are detected in the ion pulse remain about the same. It can also be observed in Figure 5-6a that, for a 3X larger ion flux, the curve levels off at a 5% higher value; meaning that more ions are detected in the ion pulse when the ion flux into Q2 is larger. After a trap time of only 50 ms, the greater flux of ions injected is still reflected in a modestly increased number of ions still present.

Figure 5-6b shows that several other observations can be made when looking at only the first parts of the curves (at relatively short fill times). The most obvious point is that the collision cell fills up faster when a higher flux of ions is injected into Q2. Furthermore, the ratio of the slopes of the linear portions of each curve (approximately 2.6) is approximately equal to the ratio of the two ion fluxes (3). This makes sense since one would expect Q2 to fill up faster when more ions are being pumped into it. Additionally, it is clear that the y-intercepts for each curve are zero. This reflects the fact that an ion pulse is not observed when no ions are initially injected into the collision cell.

Trapping Time Studies

As Figure 5-7 shows, using the ICL procedure TVARTT (Appendix C), ions can be trapped in the collision cell of the TSQ70 mass spectrometer for long periods of time. In this case, PFTBA ions of m/z 69 are trapped in Q2, with helium buffer gas, for up to two minutes with immeasurable ion losses after the first few seconds

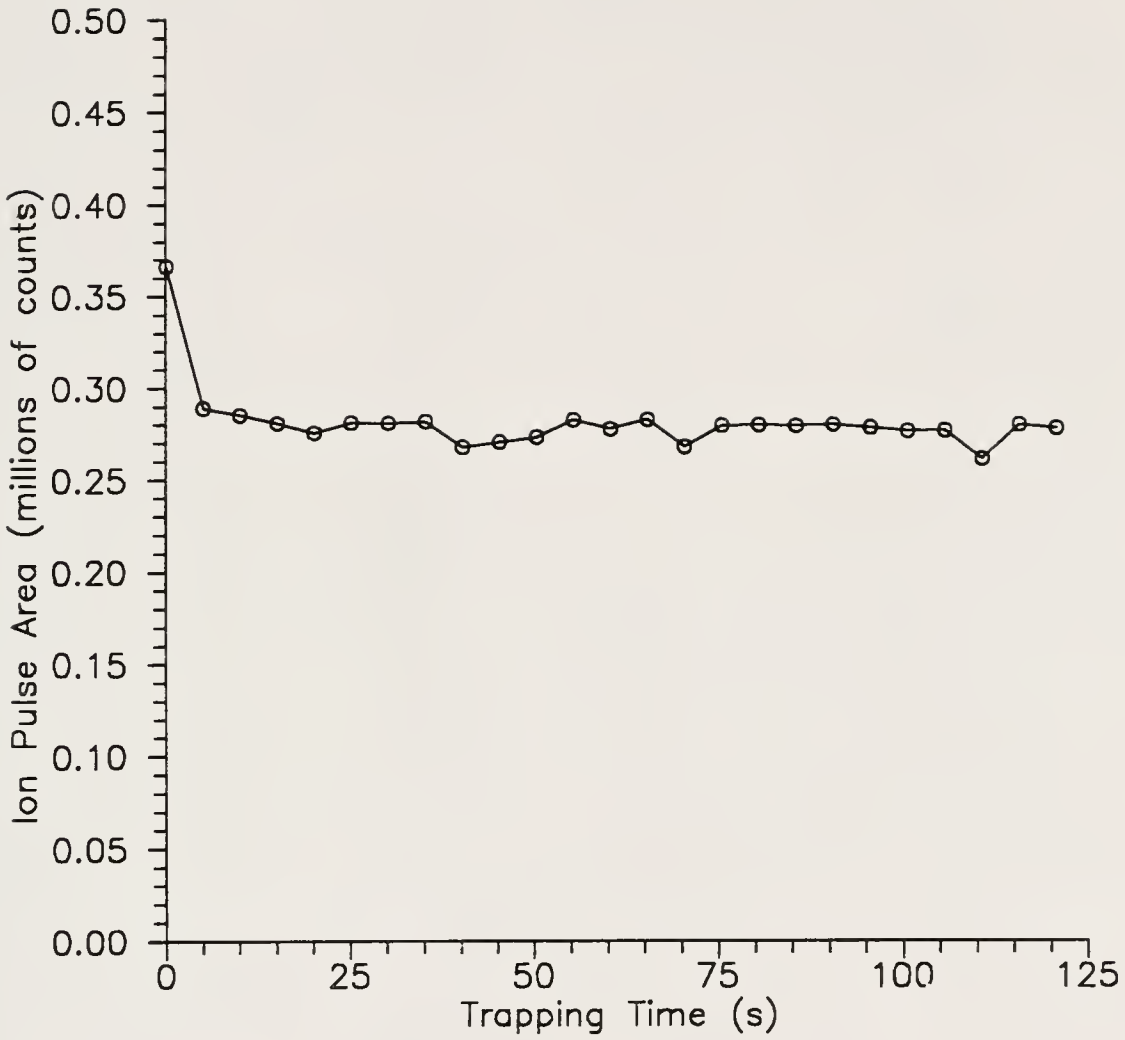

Figure 5-7: Effect of trapping time on trapping efficiency for m/z 69 ions of PFTBA. 6.0 mTorr helium in Q2, scanning Q3 (RF-only) over a 0.2 amu window around m/z 69.

of confinement. Ion intensities decrease somewhat in the first five seconds or so until the ions are thermalized and their orbits become well established. Similar results have been obtained without helium buffer gas when trapping ions of PFTBA. It has been observed, however, that trapped ion pulse intensities are much lower when helium is not used (see Chapter 4) since it is more difficult to slow down and contain ions as they enter the collision cell. Nonetheless, trapping times of several minutes have been noted when trapping ions without helium, provided that the collision offset and lens potentials are carefully optimized.

An extraordinary example of the ability of the Q2 ion trapping system is shown in Figure 5-8. The first ion pulse was observed after a trapping time of one second. The flat top of the peak is due to data system saturation. The second ion pulse, produced under conditions identical to the first, was observed after a trapping time of fifteen hours. It is clear that many of the ions originally injected into the collision cell were contained for the full fifteen hours. In fact, comparing the areas of the two pulses, ion losses were only approximately 40% over the fifteen hour confinement time. Furthermore, of this 40% ion loss, it was determined that 30% of those losses occurred within the first ten minutes. This illustrates that, after they are initially thermalized, ions can be trapped in the collision cell for incredibly long periods of time. Trapping times of this length could be useful for studies involving ion-molecule reactions in the atmosphere or troposphere, photodissociation of ions or photochemically induced ion-molecule reactions.

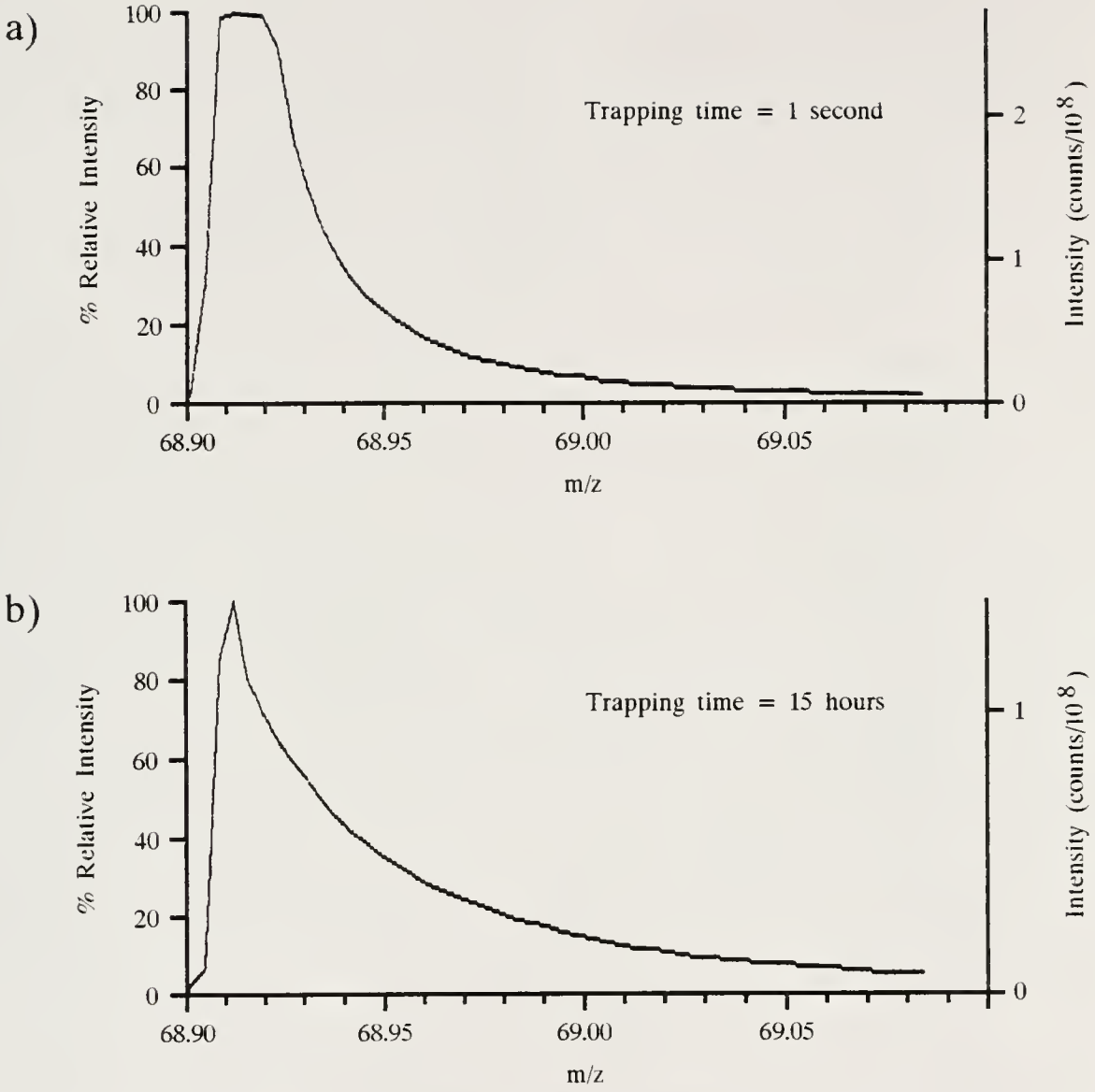

Figure 5-8: Ion pulses detected after trapping times of a) 1 s and b) 15 hr. Except for trapping times, conditions were identical for both experiments. 6.0 mTorr helium in Q2, scanning Q3 (RF-only) over a 0.2 amu window around m/z 69. Fill time = 0.2 s.

In the course of these studies of ion trapping, it was observed that the mode in which Q3 is operated can greatly affect how long ions of PFTBA can be confined to the collision cell and efficiently detected. Originally, it was thought that this effect was due to ion physics or instrumental phenomena. It was speculated that trapped ions, which are likely to be thermalized over long trapping times, were being overly resolved by Q3 when it was operated in the RF/DC mode. Since, when lens L31 is opened, the ions would be moving very slowly (primarily due to diffusion), they may have experienced too many RF cycles when passing through Q3. This would cause overresolution and reduced transmission. Ion losses could also arise from the decreased ion acceptance of Q3 when operated as a mass filter (RF/DC). Although both of these arguments are feasible, neither is wholly correct. The principal reason that the mode of operation of Q3 affects ion pulse detection when trapping ions of PFTBA can be attributed to ion chemistry.

Looking at Figure 5-9, it is clear that the mode in which Q3 is operated has a large effect on the numbers of ions that are detected in the ion pulses. Comparing the traces for Q3 RF-only (low-mass cutoff of 54) and Q3 RF/DC (scanning over m/z 69), it is not surprising that ion intensities drop off when Q3 is operated as a mass filter. It is unexpected, however, that the intensities decrease by so much, especially at longer trapping times. Ion losses due to overresolution in Q3 and decreased ion acceptance cannot account for such large losses. The trace for Q3 RF-only with a low-mass cutoff of 72 provides evidence that ion losses observed when Q3 is RF/DC are due to ion-molecule reactions of m/z 69, CF_3^+. This trace shows that ions with

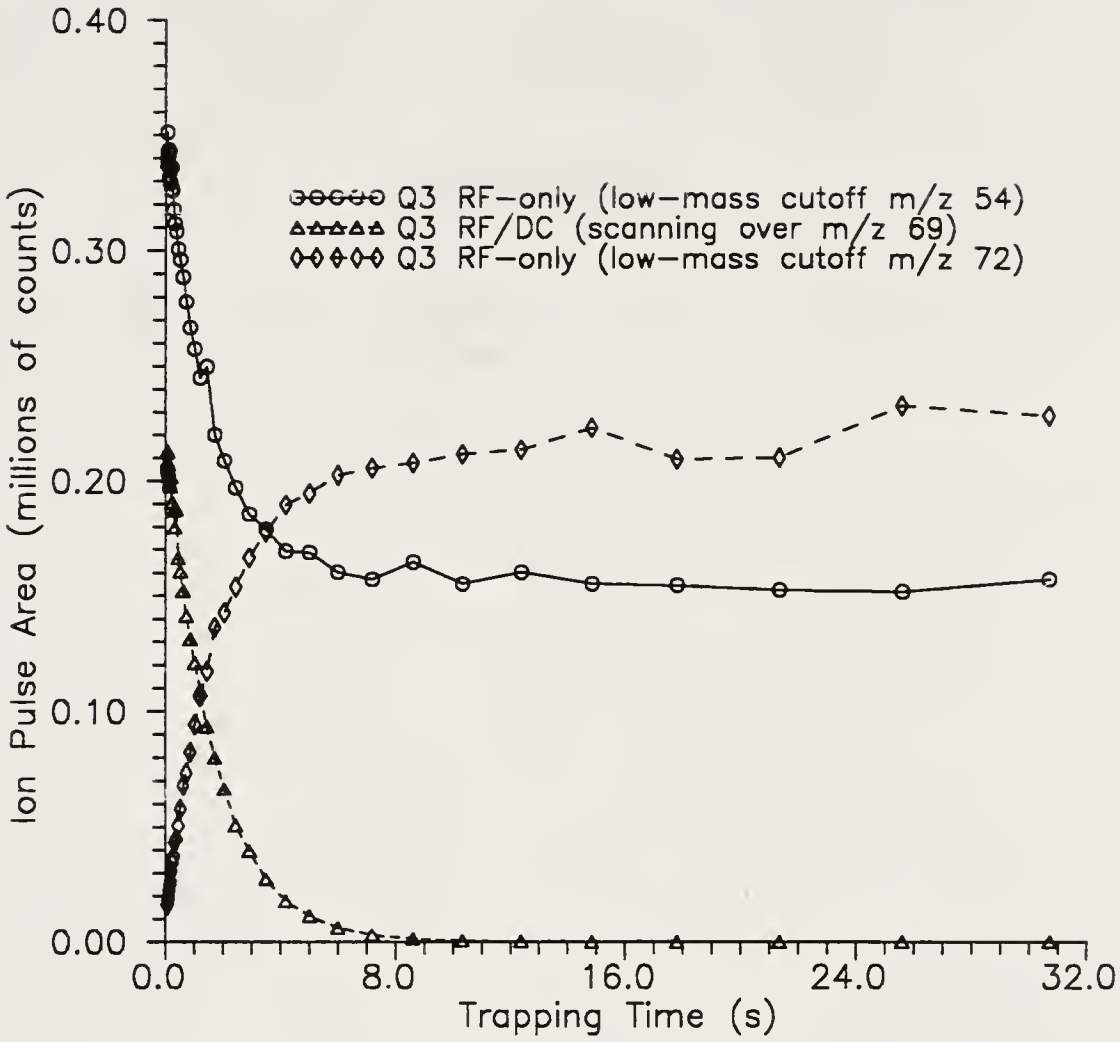

Figure 5-9: Effects of trapping time and Q3 scan mode on detection of ions trapped in the collision cell. Ions injected into Q2 were m/z 69 fragments of PFTBA. 6.0 mTorr helium in Q2.

masses above m/z 72 are continually being formed at longer trapping times. It has been determined that m/z 69 reacts (with PFTBA neutrals which have diffused from the ion source into Q2) primarily to form ions of m/z 414, $C_8F_{16}N$. This explains why, when Q3 is operated in the RF/DC mode scanning over m/z 69, ion intensities decrease rapidly as trapping times increase; ions of m/z 69 are reacting with neutrals to form more massive species that are not detected. The most likely reaction is the dissociative charge exchange between m/z 69 and PFTBA molecules ($(C_4F_9)_3N$, M.W. 671) to form m/z 414 corresponding to loss of neutrals totalling C_4F_{11}. Reactions of some PFTBA ions with other neutrals such as H_2O or O_2 may also be important.

Analogous data are shown in Figures 5-10 and 5-11 for two other fragment ions of PFTBA. Q2 ion trapping of m/z 131, $C_3F_5^+$, is illustrated in Figure 5-10. This plot looks similar to Figure 5-9, except that the drop in m/z 131 intensity (and thus the changes in the other two curves) takes place over longer trapping times. This indicates that m/z 131 also reacts extensively with neutrals in the collision cell to produce more massive ions that go undetected when Q3 is in the RF/DC mode scanning over just m/z 131. Moreover, the fact that the curves level off at longer trapping times dictates that the ion-molecule reactions are slower than the corresponding reactions of m/z 69. Figure 5-11 shows the effects of trapping time on ion pulse detection for m/z 414, $C_8F_{16}N^+$. Comparing the traces for Q3 RF-only (low-mass cutoff of 54) to Q3 RF/DC (scanning over m/z 414), it is immediately apparent that many of the 414^+ ions undergo ion-molecule reactions to form other species and thus are not detected in the Q3 RF/DC mode. This is supported upon

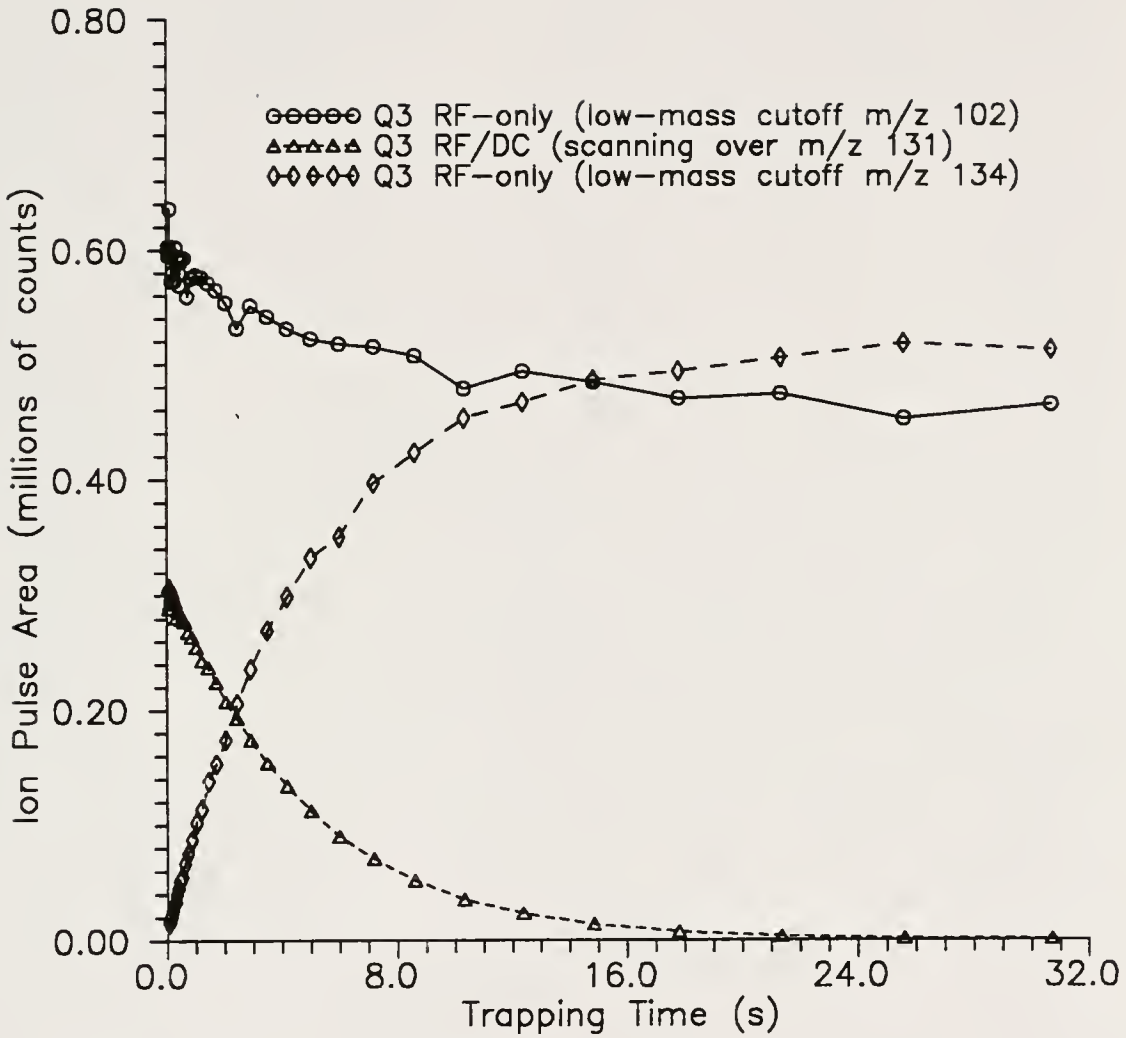

Figure 5-10: Effects of trapping time and Q3 scan mode on detection of ions trapped in the collision cell. Ions injected into Q2 were m/z 131 fragments of PFTBA. 6.0 mTorr helium in Q2.

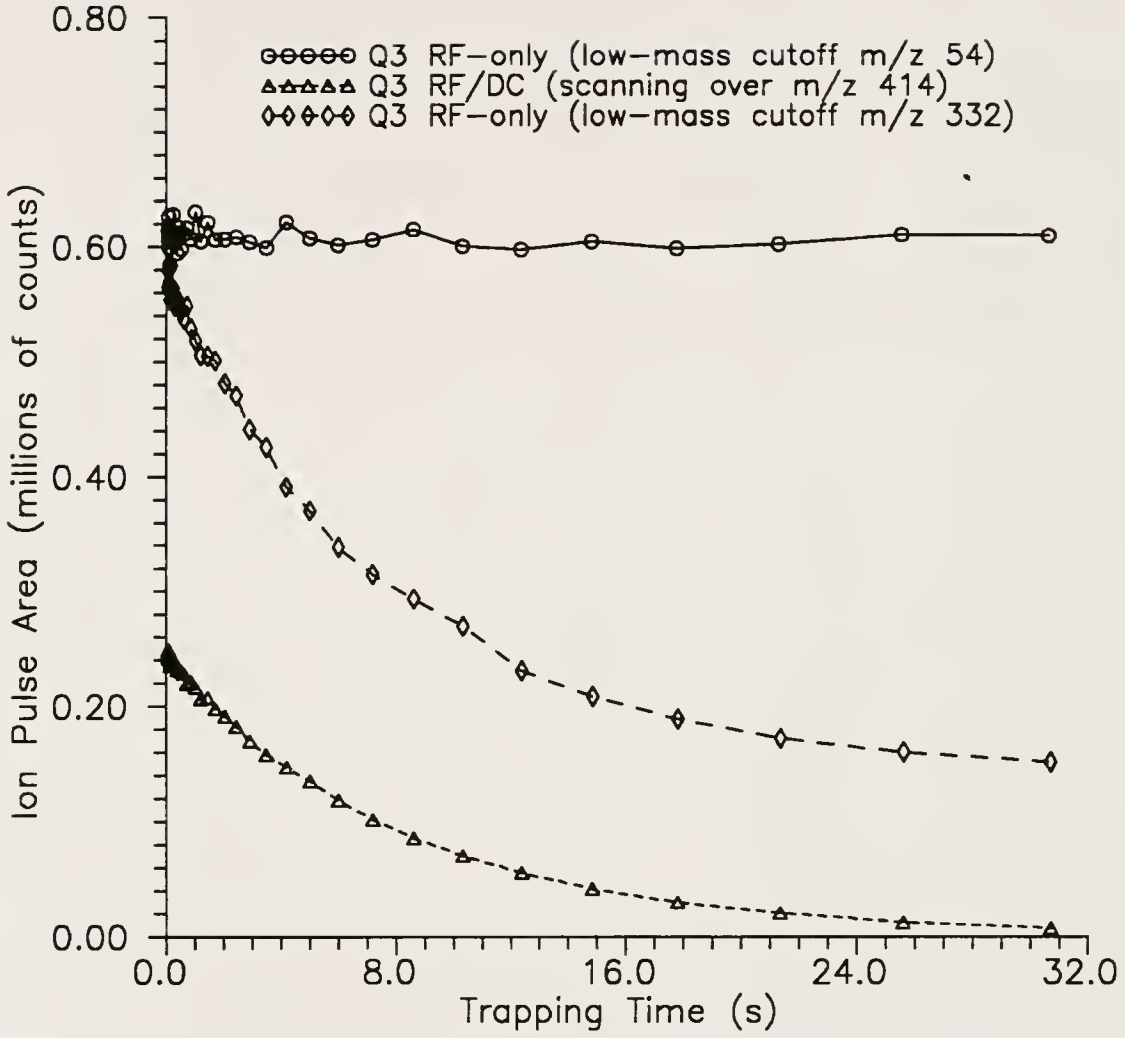

Figure 5-11: Effects of trapping time and Q3 scan mode on detection of ions trapped in the collision cell. Ions injected into Q2 were m/z 414 fragments of PFTBA. 6.0 mTorr helium in Q2.

inspection of the trace representing data taken with Q3 in the RF-only mode with a low-mass cutoff of m/z 332. Comparing this trace to the top trace (RF-only, low-mass cutoff of 54), it is clear that an abundance of ions are formed with m/z values between 54 and 332. These ions may be due to ion-molecule reactions with PFTBA or background gases, or possibly CID. Likewise, looking at the bottom two traces it is clear that some ions (other than m/z 414) are formed (due to CID or ion-molecule reactions) with m/z values greater than 332.

Full Scan Data while Trapping Ions in Q2

One of the disadvantages of the Q2 ion trapping technique is that selected reaction monitoring (SRM), monitoring only a single parent/daughter ion combination for each trapping period, is the only possible method for ion detection. Since ion pulses are normally on the order of 5-10 ms in duration, it is not feasible to perform data acquisition scans over wide mass ranges. Even if one were to perform a narrow-range mass scan over an ion pulse, mass discrimination would be evident due to the exponential decay of the ion pulse during the scan.

The solution to this problem is to perform several trapping experiments in succession, at a constant trapping time, while incrementing the Q3 scan range between trapping cycles. The individual spectra that result can then be linked together by the data system to obtain a "full scan" spectrum. This approach has been utilized by others [56] who have studied ion trapping in a linear quadrupole;

however, the technique is especially suited to the TSQ70 mass spectrometer since no modifications to the data system are necessary for implementation.

The ICL procedure TVARSR (Appendix C) was written to perform the operations necessary to acquire full scan mass spectra under Q2 ion trapping conditions, as described above. The length of time required to obtain a full scan mass spectrum using this technique depends on both the trapping time and the mass range which is scanned. Because of this, the times required to perform experiments of this type vary widely, with durations commonly ranging from several seconds to several minutes. Clearly, experiments of this length are not conducive to routine analyses. However, if one or more specific product ions were chosen for detection, execution times could be drastically reduced by selectively scanning over only these ions, and the technique would become much more practical.

Figures 5-12 and 5-13a depict two full scan mass spectra that were obtained, using TVARSR, when trapping fragment ions of PFTBA in the collision cell. The mass spectrum shown in Figure 5-12 results when ions of m/z 219, $C_4F_9^+$, are trapped in the collision cell for 0.25 s. Several product ions are present in the spectrum including ions at m/z 69, 131 and 197. The ions at m/z 69 and 131 (CF_3^+ and $C_3F_5^+$) correspond to commonly observed fragments of PFTBA and, thus, are probably just daughter ions arising from CID of m/z 219. The peak at m/z 197, on the other hand, is due to the reaction of m/z 219 ions with small amounts of water in the collision cell to form adduct ions of m/z 237, which then lose two HF groups to form m/z 197 ($C_4F_7O^+$). It is interesting to note that ions of m/z 197 are also commonly observed

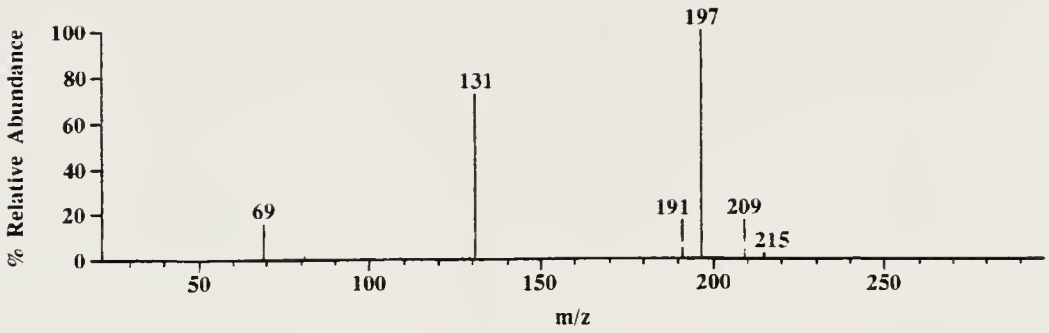

Figure 5-12: Full scan mass spectrum acquired, using TVARSR, when trapping m/z 219 fragment ions of PFTBA in Q2 for 0.25 s.

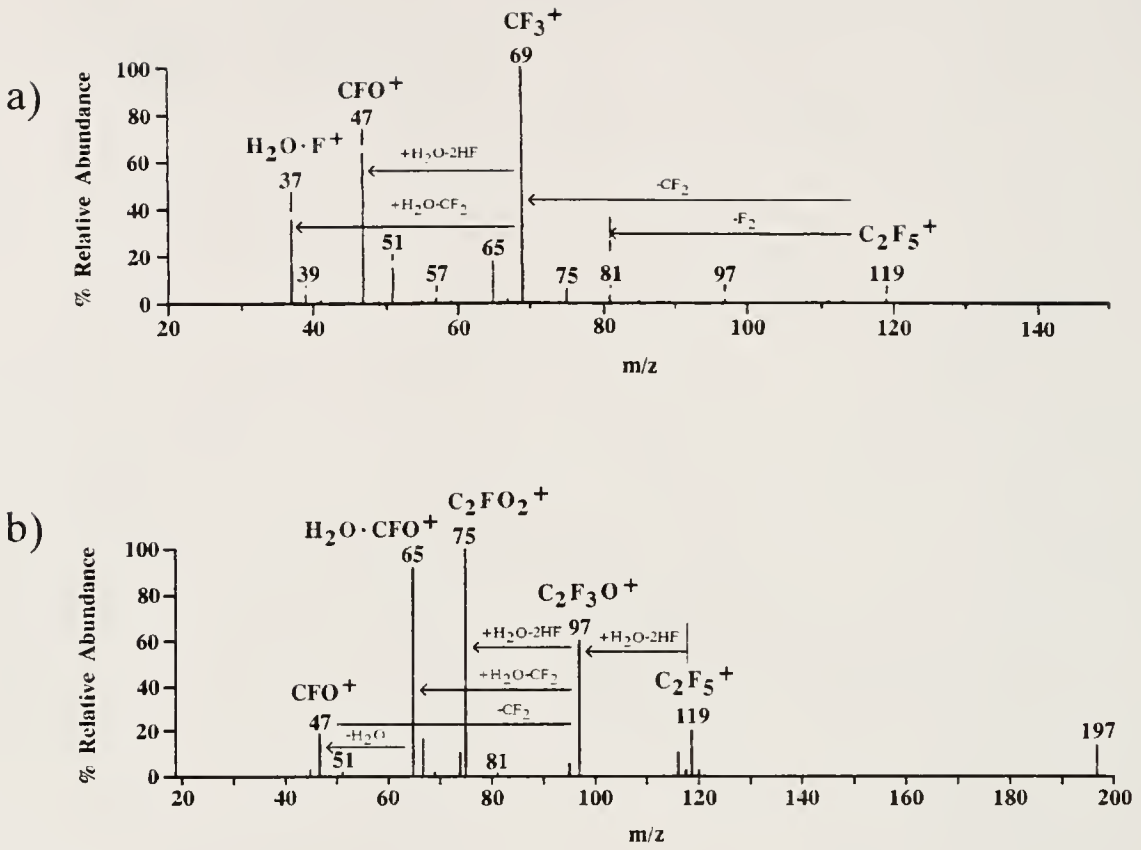

Figure 5-13: a) Full scan mass spectrum acquired, using TVARSR, when trapping m/z 119 fragment ions of PFTBA in Q2 for 0.15 s. b) Mass spectrum obtained with the Finnigan MAT ion trap mass spectrometer (ITMS) when trapping m/z 119 fragment ions of PFTBA for 0.1 s at a q_z value of 0.3.

in the quadrupole ion trap mass spectrometer (QITMS) when PFTBA is ionized by electron ionization and the ions are trapped for relatively long storage times.

Figure 5-13a shows the mass spectrum that results, using TVARSR, when PFTBA fragment ions of m/z 119, $C_2F_5^+$, are trapped in the collision cell for 0.15 s. The mass spectrum that is observed when m/z 119 is stored in the QITMS for 0.1 s is shown in Figure 5-13b. Comparing the mass spectra from these two instruments, it is clear that many ions are common to both, albeit with varying intensities. In particular, product ions at m/z 47, 51, 65, 67, 69, 75, 81, and 97 can be seen in both spectra. Many of these ions can be easily interpreted by considering the possible neutral losses, as indicated in Figure 5-13. The base peak for the Q2 ion trapping spectrum is m/z 69 (CF_3^+, arising from CID); this ion is only approximately 2% of the base peak in the QITMS spectrum. The base peak in the QITMS spectrum, however, is m/z 75, $C_2FO_2^+$, arising from ion-molecule reactions (addition of two H_2O and loss of four HF); this ion is only 6% of the base peak in the Q2 ion trapping spectrum. These differences are due to the ways that ions are introduced into the storage regions. For Q2 ion trapping, ions are injected into the collision cell at approximately 6 eV, whereas ions formed within the ion trap have little translational energy. Thus, ions formed via CID, such as m/z 69, dominate the spectrum observed when trapping ions in Q2, whereas ions arising from ion-molecule reactions with background water neutrals, such as m/z 97, 75, and 65, dominate the QITMS spectrum. Note that the m/z 69 ion, CF_3^+, base peak in the Q2 trapping spectrum, is quite stable to further fragmentation; the lower mass ions observed arise

from ion-molecule reactions of 69^+ with H_2O. Finally, notice that m/z 37 ($H_2O{\cdot}F^+$) is observed in the Q2 trapping spectrum, but not in the QITMS spectrum since the ion trap was operated at a low-mass cutoff of m/z 40 (corresponding to a $q_z = 0.3$). This means that ions with m/z values less that 40 were unstable within the trap and, thus, were not detected.

Reactions of DNA/RNA Base Ions with Allyl Chloride under Ion Trapping Conditions

Reactions of DNA/RNA base ions with allyl halides in the collision cell were discussed extensively in Chapter 2. It was pointed out that, for many of the reactions, product ion intensities were very small and sometimes were not detected at all. This is illustrated in Figure 2-6. It is clear that adenine ions are quite unreactive toward the allyl halides, especially allyl chloride. Likewise, thymine ions produce few or no product ions upon reaction with allyl chloride. While these low reactivities reflect in part the thermodynamic tendencies for these reactions, they are affected by the kinetics of the reactions. Studies were therefore initiated to investigate how these types of reactions behave under Q2 ion trapping conditions. By trapping DNA/RNA ions in the collision cell in the presence of allyl halides, longer reaction times are possible which could allow kinetically slow reactions to approach equilibrium. This, in turn, would maximize the quantities of product ions that are formed, increasing the sensitivity of the method.

Figure 5-14 illustrates how trapping time affects product ion distributions for the reaction of adenine molecular ions ($N^{+\cdot}$) and allyl chloride in the collision cell.

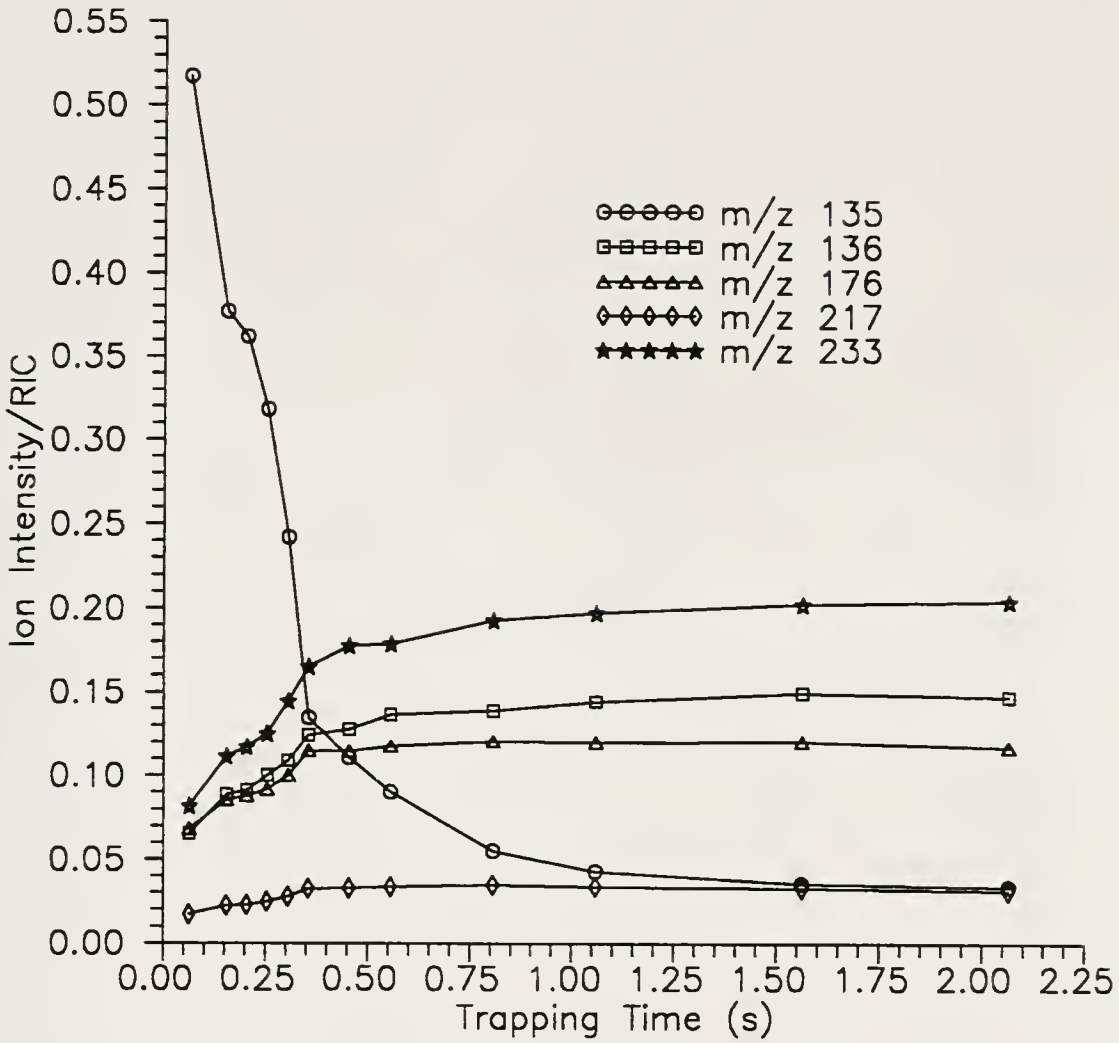

Figure 5-14: Effect of trapping time on reaction of adenine $N^{+\cdot}$ ions. m/z 135, with allyl chloride in the collision cell. 0.5 mTorr allyl chloride was used with helium added to an indicated pressure of 6.5 mTorr.

Additionally, representative daughter spectra obtained at trapping times of 0.06 s and 0.46 s are shown in Figures 5-15a and 5-15b, respectively. It is obvious that trapping time greatly enhances the formation of, among others, P^+ (or $[N+E]^+$) product ions (m/z 176), which correspond to addition of the allyl group to the adenine. Other ions which are observed in the spectra are the adenine molecular ions themselves ($N^{+\cdot}$, m/z 135) and protonated adenine ($[N+H]^+$, m/z 136), as well as the $[P+E-X]^+$ species (m/z 217) arising from addition of a second allyl group. It is unclear what the identity of the most abundant product ion (m/z 233) is, but it clearly dominates the spectra at long trapping times. The ion may arise from some impurity in the collision cell; it was not seen in previous adenine/allyl chloride reactions (see Chapter 2). The reaction reaches equilibrium after about one second, as indicated by the levelling off of the product ion intensities. This equilibration time is quite long and explains why the reaction takes place to only a small extent under normal ion-molecule reaction conditions, with residence times in Q2 on the order of only 100 μs.

The effects of trapping time for reactions of other DNA/RNA base ions with allyl chloride are shown in Figures 5-16 through 5-18. Figure 5-16 shows how the reactions of thymine ions, m/z 126, and allyl chloride progress as trapping time is increased. Several ions can be identified including thymine molecular ions ($N^{+\cdot}$, m/z 126) and protonated molecules ($[N+H]^+$, m/z 127), and thymine-allyl adducts (P^+, m/z 167, and $[P-H]^+$, m/z 166). The observation that $[P-H]^+$ is significantly more abundant than P^+ is unexpected as the $[P-H]^+$ species was not seen in previous thymine/allyl chloride reactions (see Chapter 2). Ions corresponding to m/z 181 have

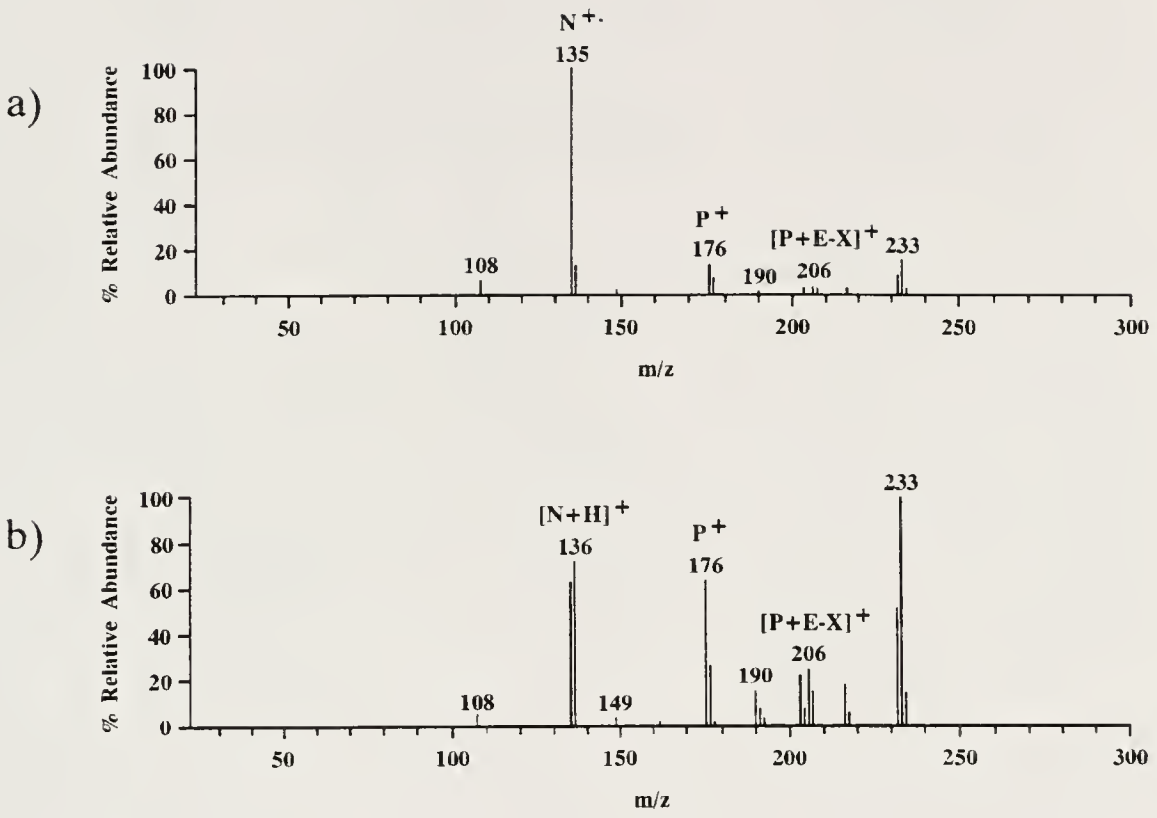

Figure 5-15: Full scan mass spectra resulting from reactions of adenine $N^{+\cdot}$ ions, m/z 135, with allyl chloride in the collision cell. Reaction times are a) 0.06 s and b) 0.46 s. Running TVARSR with 0.5 mTorr (indicated) allyl chloride in Q2. Helium was added to increase the indicated pressure to 6.5 mTorr.

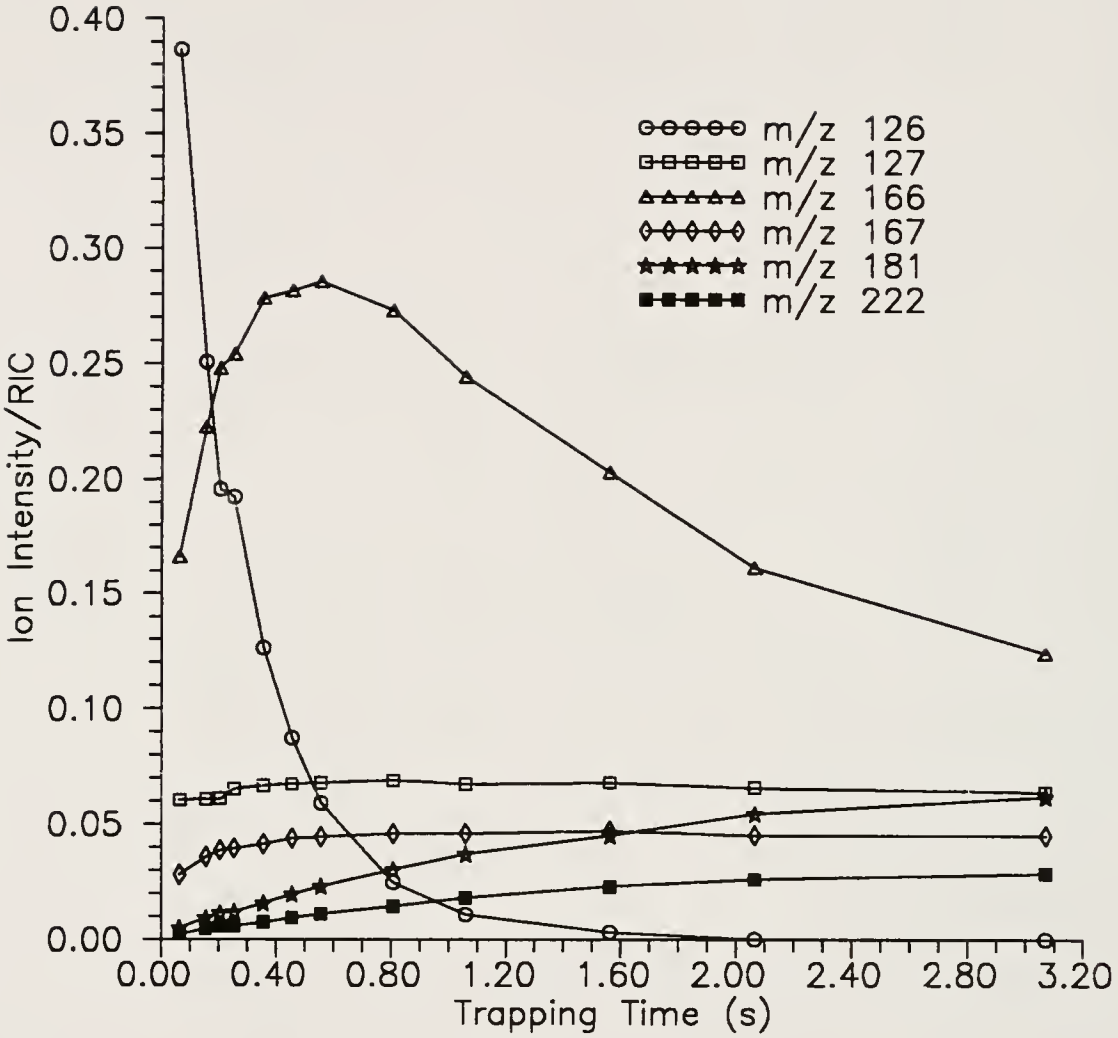

Figure 5-16: Effect of trapping time on reaction of thymine $N^{+\cdot}$ ions, m/z 126, with allyl chloride in the collision cell. 0.5 mTorr allyl chloride was used with helium added to an indicated pressure of 6.5 mTorr.

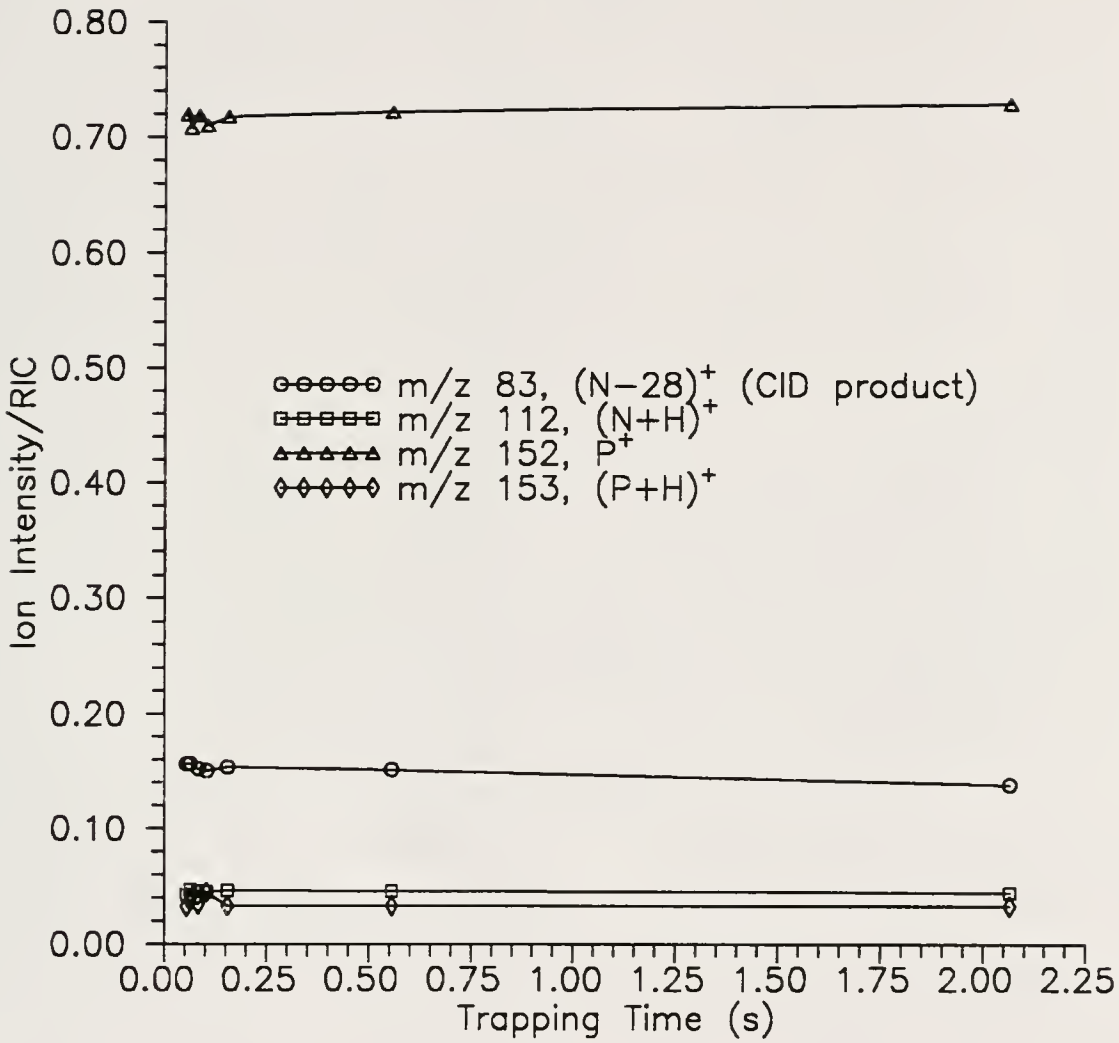

Figure 5-17: Effect of trapping time on reaction of cytosine $N^{+\cdot}$ ions, m/z 111, with allyl chloride in the collision cell. 0.5 mTorr allyl chloride was used with helium added to an indicated pressure of 6.5 mTorr. Note that the m/z 111 ions are less than 0.001 in normalized intensity at even the shortest trapping times.

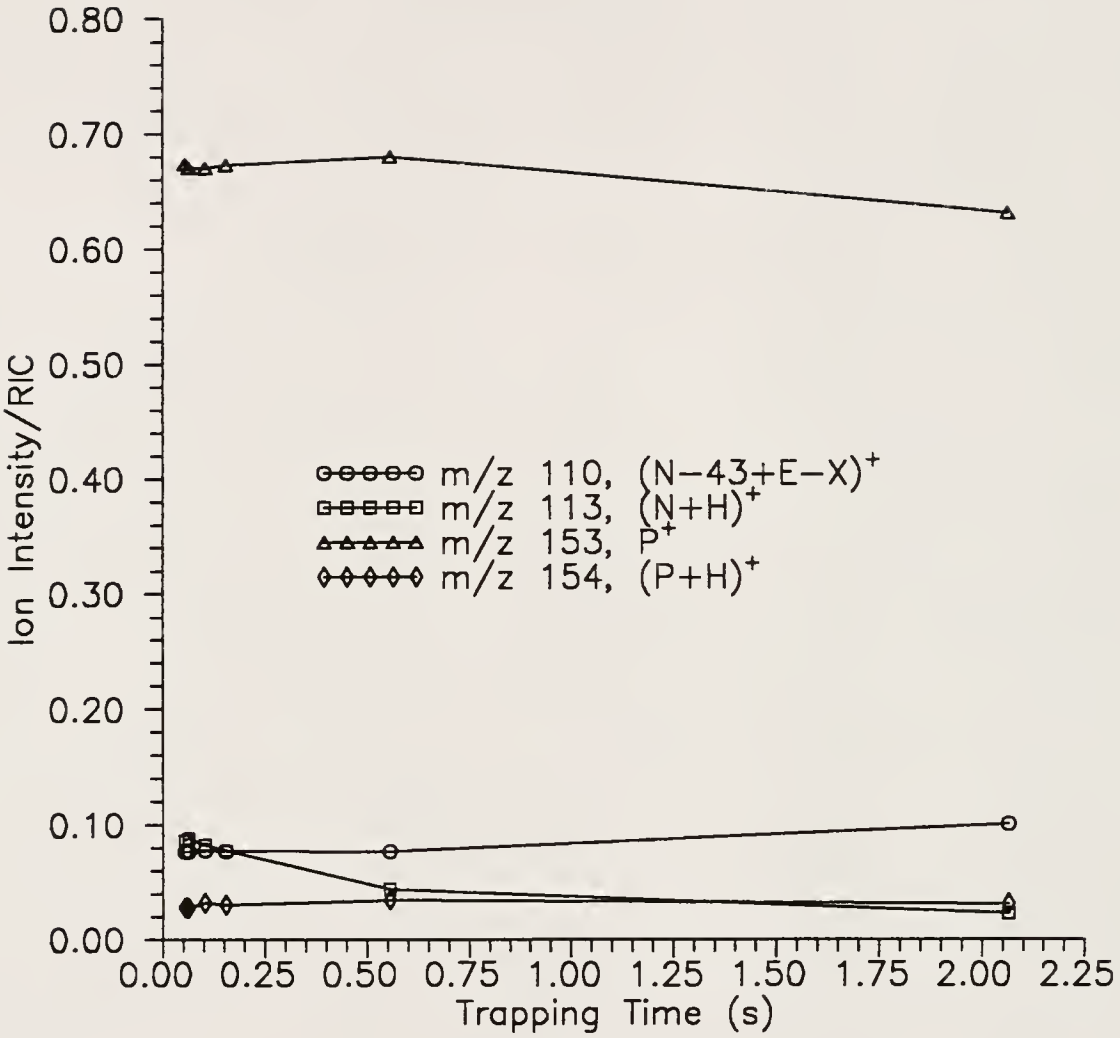

Figure 5-18: Effect of trapping time on reaction of uracil $N^{+\cdot}$ ions, m/z 112, with allyl chloride in the collision cell. 0.5 mTorr allyl chloride was used with helium added to an indicated pressure of 6.5 mTorr. Note that the m/z 112 ions are less than 0.001 in normalized intensity at even the shortest trapping times.

not been characterized, but apparently their production is dependent on reaction time. It appears that 181^+ (and 222^+) increases in intensity at the expense of $[P-H]^+$ (but not P^+ or $[N+H]^+$). It is likely that 181^+ corresponds to the extraction of a $\cdot CH_3$ from another allyl chloride neutral by the $[P-H]^+$ species. This type of reaction has not been observed before for P^+, but it is plausible for $[P-H]^+$. Positive identification of 181^+ could be achieved using a QITMS to isolate $[P-H]^+$ (m/z 166) for further reaction with allyl chloride. Alternatively, parent scans (to find the parent ions of m/z 181 and 222) could be executed on a TQMS while thymine and allyl chloride react in the ion source (with allyl chloride also in Q2). The allyl adduct of the m/z 181 species is observed at m/z 222. Clearly, trapping time has an effect on the relative product ion intensities for the reaction. Furthermore, it appears, from the plot, that equilibrium for the reaction is not established even after more than three seconds. Thus, ion trapping allows the reaction to proceed to a much greater extent than is possible by conventional ion-molecule reactions in the collision cell.

Figures 5-17 and 5-18 show the relative ion intensities that are observed when two kinetically favorable reactions are studied using Q2 ion trapping. As is apparent in Figure 2-6, cytosine and uracil $N^{+\cdot}$ ions react with allyl chloride readily under conditions normally employed for Q2 ion-molecule reactions. Thus, it is not surprising that essentially no dependence on reaction time is noticed when these processes are investigated using Q2 ion trapping. Indeed, for each case, the intensity of the molecular ion of the base (m/z 111 for cytosine, and m/z 112 for uracil)

sharply reduced at even the shortest reaction times. Furthermore, formations of product ions (P^+) corresponding to allyl adducts are constant for each reaction, regardless of trapping time. These plots demonstrate that Q2 ion trapping is not needed for these reactions since, due to fast reaction kinetics, maximum product ion intensities are obtained after a very short confinement times.

Conclusions

Studies have been performed employing the Q2 ion trapping system. Processes directly related to the mechanism of ion confinement, and characteristics particular to the method have been evaluated. Furthermore, applications of ion trapping for enhancement of associative ion-molecule reactions have been demonstrated. The results of these studies have illustrated the utility of the technique and provided a better understanding of the Q2 ion trapping system.

Since ions exit the collision cell as discrete pulses when performing Q2 trapping, mass scanning parameters were optimized for detection. It was found that scan times equivalent to the time constants of the ion pulses, approximately 5-10 ms, were optimum so that maximum sensitivities were realized. Furthermore, very narrow mass ranges (e.g., 0.2 amu) were utilized so that ions of the particular m/z of interest were stable over the entire scan.

It has been discovered that, when using short scans, ions can accumulate in the collision cell from cycle to cycle due to incomplete ion ejection. This effect was evident in several experiments that were performed. Since ion accumulation does

not allow for satisfactory investigations of ion-molecule reactions, a means has been developed to purge ions from the collision cell between trap and pulse cycles. This method, which involves ramping the RF potential applied to the octopole between cycles, causes the remaining ions to be flushed out of the collision cell before the beginning of the next cycle. This technique has been implemented in several of the ICL procedures used for various Q2 ion trapping experiments so that the effects of ion accumulation can be eliminated.

Studies of fill time and trapping time have been performed. It has been determined that a finite number of ions can be contained in the collision cell before ion-ion repulsions become significant enough to cause excessive ion losses. Furthermore, the flux of ions that are injected into Q2 determines the maximum fill time that can be used before the number of ions detected reaches a plateau. Experiments have also shown that ions can be efficiently trapped in the collision cell for several hours or more, with most of the ion losses occurring within the first few minutes of confinement.

Selected reaction monitoring (SRM) is the only amenable method of ion detection when utilizing the Q2 ion trapping technique. Nonetheless, full scan mass spectra have been acquired by performing successive trapping experiments and then linking the individual mass spectra. Even though a typical experiment may take over a minute to complete, obtaining complete spectra is advantageous in that all ions can be monitored when trapping times are varied.

Utilizing the Q2 ion trapping method with full scan data acquisition, reactions of DNA/RNA base ions with allyl chloride have been investigated. It was determined that product ion intensities for the reactions that proceed to a small extent under normal ion-molecule reaction conditions can be dramatically enhanced when ion trapping is employed. In contrast, ion trapping had no noticeable effects on product ion formation for those reactions that are kinetically favorable. The studies demonstrated that ion trapping can be helpful for some slow ion-molecule reactions, but that it may not be required for some reactions that are kinetically fast.

CHAPTER 6
CONCLUSIONS AND FUTURE WORK

Conclusions

The work presented in this dissertation has demonstrated that reactions of DNA/RNA base and nucleoside ions with allyl halides in the collision cell of a triple quadrupole mass spectrometer (TQMS) are complex, but often produce correlating product ions via a variety of reaction mechanisms. The results also indicate that the method has the potential for real-time determination of carcinogens or mutagens. In addition, it has been shown that the Finnigan MAT TSQ70 TQMS can be utilized as an ion trapping device for the study of associative ion-molecule reactions such as those described above.

Relative reactivities of DNA/RNA base and nucleoside ions toward allyl halides have been determined based on the production of allyl-nucleophile adduct ions, P^+. It was found that the molecular ions, $N^{+\cdot}$, and/or protonated molecules, $[N+H]^+$, of all the nucleophiles studied are reactive, with the DNA/RNA base ions being more reactive, in general, than the corresponding nucleoside ions. Side reaction products, due to charge exchange processes, have also been observed for many of the reagent combinations. Significant intensities of side reaction products are typically observed only when allyl iodide is used as the electrophile (due to its

relatively low ionization energy); in many cases the abundance of side reaction products distorts the relative reactivity as measured by P^+ production. For this reason, side reaction products have been identified and correlated so that results can be meaningfully interpreted.

Selection of the nucleophile in large part determines the sensitivity that is ultimately realized for these reactions. Unfortunately, a trade-off exists in that the more reactive nucleophiles such as uracil tend to have more extensive side reactions, thus decreasing the sensitivity of the reaction (for the product ion $[N+41]^+$, or P^+). Nonetheless, reactions of ionized DNA/RNA bases (such as uracil) are still much more sensitive than reactions of the corresponding nucleoside ions. Furthermore, whereas the nucleosides require a soft ionization process (e.g., benzene charge exchange) to produce molecular ions for reaction, the DNA/RNA bases can be ionized via electron ionization, a much easier and more reproducible method.

It has been determined that the pressure of allyl halide in the collision cell has a large effect on product ion distribution. Typically, higher-order reactions become prominent at higher allyl halide pressures. Furthermore, at very high pressures, ion intensities start to decrease due to increased ion scattering in the collision cell. Calibration curves for reactions of each DNA/RNA base ion with allyl halides are generally not linear; limits of detection for the most reactive DNA/RNA base ion, uracil, are on the order of 10-100 femtomoles of allyl halide in the single reaction monitoring (SRM) mode. These studies show that it is very difficult to determine reactivities, and thus mutagenicities, by solely monitoring production of

the P^+ ($[N+41]^+$) ion unless reaction conditions are carefully controlled and remain consistent from analysis to analysis.

A system for trapping ions in the collision cell of the TSQ70 triple quadrupole mass spectrometer has been developed and characterized. The technique is easily performed via incorporation of a simple lens control circuit and implementation of Instrument Control Language (ICL) procedures that have been specially designed to control the Q2 trapping experiment. Parameters significant to the performance of the system have been investigated. It has been discovered that the presence of helium buffer gas in the collision cell greatly improves ion trapping efficiencies by slowing down ions as they enter Q2 and then confining them to the center of the octopole. Specific ion optical components have also been optimized for Q2 trapping. In particular, the potential applied to the entrance lens, L23, when filling the collision cell with ions has a dramatic effect on the number of ions that can be confined to Q2. It has also been determined that the collision offset voltage (Q2 offset) affects Q2 ion trapping efficiency. Furthermore, the optimum values for Q2 offset voltage vary depending on whether or not helium buffer gas is used, and this, in turn, affects the optimum lens L23 potentials. Guidelines have been developed to aid in tuning the instrument for Q2 ion trapping. Moreover, ICL procedures have been devised that automatically tune ion optical components of the TSQ70 that are crucial for effective Q2 ion trapping. Through these studies, the technique has been well characterized and can be utilized for experiments (such as kinetics studies of

ion-molecule reactions) that are normally impractical, or impossible, to perform on standard tandem quadrupole instruments.

Investigations have been performed employing the Q2 ion trapping system. It has been discovered that, when using short scan times, ions can accumulate in the collision cell from cycle to cycle due to incomplete ion ejection. A means has been developed to purge ions from the collision cell between trap and pulse cycles and has been implemented in procedures written to control various types of Q2 ion trapping experiments. It has been determined that a finite number of ions can be contained in the collision cell before ion-ion repulsions cause excessive ion losses. Furthermore, the flux of ions that are injected into Q2 determines the maximum fill time that can be used before the number of ions detected reaches a plateau. Experiments have also shown that ions can be efficiently trapped in the collision cell for several hours or more, with most of the ion losses occurring within the first few minutes of confinement. Full scan mass spectra have been acquired by performing successive trapping experiments and then linking the individual mass spectra. Even though a typical experiment may take over a minute to complete, the resulting spectra are advantageous in that several ions can be monitored when trapping times are varied. Utilizing the technique, reactions of DNA/RNA base ions with allyl chloride have been investigated. It is clear that product ion intensities for reactions that proceed to a small extent under normal ion-molecule reaction conditions can be dramatically enhanced when ion trapping is employed. On the contrary, ion trapping has no noticeable effects on product ion formation for those reactions that are

kinetically favorable. The studies have demonstrated that ion trapping can be helpful for some slow ion-molecule reactions, but that it may not be required for some reactions that are kinetically fast. The results of these investigations have illustrated the utility of the technique and have provided a better understanding of the Q2 ion trapping system.

Suggestions for Future Work

Reactions of Other Nucleophile Ions

It would be interesting to investigate reactions of other larger nucleophile ions with allyl halides. By using an atmospheric pressure ionization source (API) such as electrospray (ESI), studies of this type could be extended to utilize actual DNA fragments. This would allow ionized nucleotides or oligonucleotides to react with allyl halides or other electrophiles in the collision cell. Ion-molecule reactions of larger DNA sections may provide more insight into the way that mutagens such as the allyl halides react with DNA in vivo; the sites of these reactions might also be determined. Furthermore, reactivities of solvated ions produced by the ESI process toward allyl halides could be evaluated. Correlation of the reactivities of solvated and unsolvated ions would make for interesting comparisons to solution-phase reactions.

Comparison of Quadrupole and Octopole Collision Cells

As was discussed in Chapter 4, the ion confinement characteristics of quadrupole and octopole devices are quite different. Experiments could be performed to evaluate ion trapping with the original quadrupole collision cell for comparison to those results obtained with the octopole collision cell. Many groups that have studied multipole devices with two-dimensional electric fields [58,80-84] have found that, in some cases, higher-order multipoles can be more effective than quadrupoles in the RF-only mode for guiding and transporting low-energy ions, such as in a collision cell. The enhanced ion containment characteristics of octopoles have been attributed to somewhat extended stability regions, which lead to wider mass ranges and more uniform transmission qualities. It is not clear, however, how these properties would affect ion trapping in the RF-only quadrupole and octopole. Since ions can be confined to the collision cell for upwards of several minutes, it may be that any peculiarities in the ion motions specific to each individual device will become amplified over the trapping time. Thus, any deficiencies (or advantages) of the confinement characteristics of the quadrupole collision cell may become more apparent when attempting to trap ions.

Radial Detection of Stored Ions via RF Ramping

As was discussed in Chapter 5, due to the nature of this technique, one of the drawbacks of Q2 ion trapping is that selected reaction monitoring is the only possible method for ion detection. This limitation can be overcome to some extent by linking

spectra acquired from several trapping experiments performed consecutively while detecting ions over successive mass ranges. However, this method is very time-consuming, especially at long trapping times, and does not produce true full scan spectra. In particular, this problem is most pronounced when the neutral reactant (electrophile) is transient in Q2 such as when GC or on-line sample introduction is utilized.

It may be possible to detect stored ions in the collision cell by ramping the RF potential applied to Q2 so that the low-mass cutoff of the device acts to eject ions of successively higher masses. By doing this, acquisition of full scan data with a single trapping experiment would be facilitated. As is shown in Figure 6-1, when plotted in (RF,DC) space, the regions of stability for ions at m/z 69, 131 and 219 in a quadrupole are quite different. Since the collision cell is an RF-only device (DC=0 V), only the RF component determines whether or not ions are stable within Q2. It is clear from Figure 6-1 that more massive ions are stable over wider ranges of RF voltage. In particular, only m/z 219 is stable above an RF potential of approximately 375 V. By ramping the Q2 RF potential, which is related to the collision RF potential (CRFP), consecutively more massive ions become unstable in the radial direction (analogous to the mass-selective instability scan mode employed with the quadrupole ion trap mass spectrometer [43]). These ions could then be detected by a separate continuous dynode electron multiplier adjacent to the side of the collision cell between one pair of the rods. However, this means that at best only 1/4 of the ejected ions will be detected. Furthermore, given the length of the rods

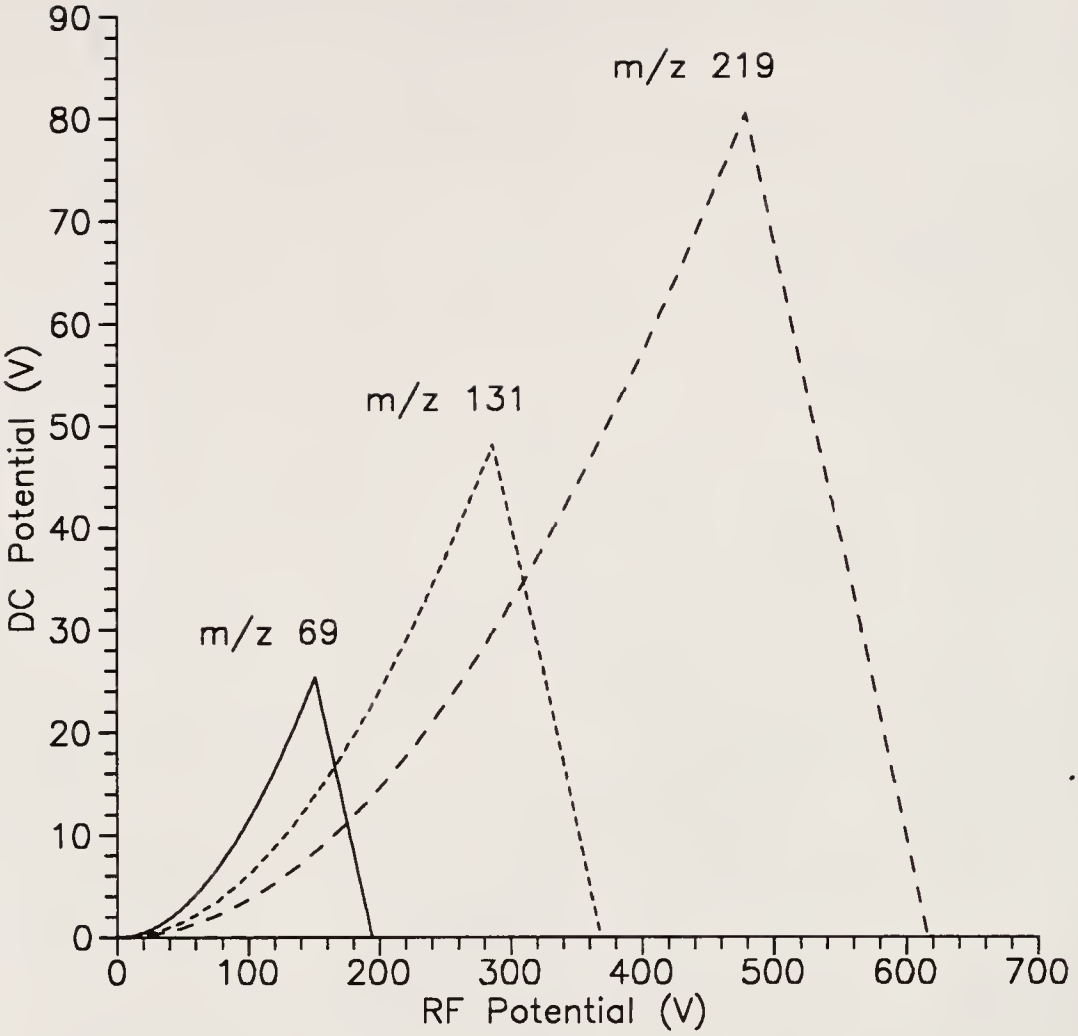

Figure 6-1: Stability diagrams in (RF,DC) space for m/z 69, 131 and 219. Curves were calculated using the Mathieu equation for a quadrupole mass filter with r_0=0.5 cm and an RF frequency of 1.1 MHz.

in comparison to the size of the electron multiplier, and the fact that most of the ions will probably hit the rods, the process may be very inefficient.

Besides the practical problems of ion detection with this method, there may be some fundamental limitations that make the technique infeasible when using an octopole collision cell. It has been shown [58,80-82] that stability diagrams of multipole devices (third order and above) are very diffuse and not well defined. In addition, since ion forces are non-linear functions of displacement for the higher-order multipoles, initial positions of the ions as they enter the device also influence ion stabilities. This means that it may be impossible to reliably determine when and what ions are being "scanned" out of Q2 when ramping the RF potential. Furthermore, even if this problem can be overcome, poor mass resolution may limit the utility of the technique. Utilization of the quadrupole collision cell may help alleviate these problems and allow adequate performance of the method.

Replacement of Q3 with a Quadrupole Ion Trap (Q-Q-ITMS)

A different approach that could be taken to achieve true full scan spectra of trapped ions in Q2 would be to replace the mass filter (Q3) after the collision cell with a quadrupole ion trap. In fact, an instrument of this general design has been constructed [96-98]. The presence of the ion trap was shown to enhance ion abundances while the RF/DC quadrupole acted as a mass filter for external ion selection and injection into the trap, providing a means for collision-induced dissociation processes and ion-molecule reactions. In this design, the RF-only

quadrupole was used as simply a beam transfer device to connect the two mass analyzers. Similar instruments have been developed where the RF-only collision cell is replaced by a quadrupole ion trap [99-101]. Again, though, the quadrupoles were used only as mass filters while ions were trapped solely in the quadrupole ion traps.

It is proposed here that the octopole collision cell of the TSQ70 be utilized as the primary ion trapping device, in order to exploit it's excellent ion confinement characteristics. In turn, the quadrupole ion trap following Q2 would act primarily as a simple mass analyzer to produce a mass spectrum of the pulse of ions that exit the collision cell. By doing this, the very high sensitivities obtained with the Q2 ion trapping method would be realized and acquisition of full scan data would be facilitated.

Resonance Excitation in Q2

Collision-induced dissociation (CID) in a TQMS is normally controlled by varying the axial kinetic energy of the parent ion in Q2. Many times, for species that are especially stable, very high collision energies are required for acceptable fragmentation patterns. It has been reported [71], however, that high collision energies often result in reduced ion transmission efficiencies and require special tuning considerations. Alternatively, it may be more effective to increase parent ion oscillatory kinetic energy via resonance excitation, thus inducing CID. This would be accomplished by utilizing a supplementary RF voltage applied to the Q2 rods at the fundamental resonant frequency of the parent ion of interest. This, in turn,

would increase the orbital radius and kinetic energy of the ion, and would cause fragmentation through collisions with neutral gases present in the collision cell.

The theory behind resonance-enhanced collision-induced dissociation (RECID) has been described by Paul and coworkers [102], and has been implemented in several mass spectrometer designs. A process similar to RECID is used on the ion trap mass spectrometer (ITMS) to initiate CID. This technique, termed axial modulation or "tickling," has proven to be a very efficient method for CID [44]. Furthermore, resonance excitation has also been applied to RF-only quadrupoles [103-104] in order achieve notch rejection of particular ionic species. The technique has shown to be useful for selective ejection of reaction ions that may cause undesired side reactions during studies of ion-molecule reactions.

Unlike notch rejection, where ion motions become so large that ions are ejected from the collision cell, RECID would amplify ion orbits only enough to induce CID. Furthermore, by utilizing RECID on trapped ions in Q2, the length of time the ions are confined to the collision cell would effectively determine the extent of CID. It is unlikely, however, that RECID would be easily achieved on the TSQ70 due to the nature of ion motions in the octopole collision cell. It has been shown [84] that an ion's secular frequency in an RF-only octopole depends on the initial position of the ion as it enters the octopole (entry angle and ion displacement from the central point between the rods) as well as the octopole dimensions and the applied RF frequency and amplitude. This means that ions of the same m/z may have distinct secular frequencies if their entry conditions are different. Thus, it may

be difficult to excite all the ions of a particular m/z with only one resonance frequency. Utilization of the quadrupole collision cell would presumably eliminate this problem since ion forces are linear functions of displacement for second-order multipoles, and are thus independent of initial conditions.

APPENDIX A
TUNING GUIDELINES FOR LOW-ENERGY ION-MOLECULE REACTIONS AND ION TRAPPING IN THE COLLISION CELL OF THE TSQ70

The following procedures outline the steps required to tune the TSQ70 mass spectrometer for low-energy ion-molecule reactions in the collision cell. The method was developed by Jody A. Freeman and subsequently modified by Anthony P. Annacchino.

Note: The tune table file should be saved (under a name other than INIT) periodically during the tuning process to insure that the file is not lost.

1. Check RF TUNE and coarse calibration, and tune if necessary.
2. Using PPOLN, PPOLR, DPOLN and DPOLR, set the polarities of Q1 and Q3 for maximum ion transmission.
3. Tune Q1 and Q3 normally with MTUNEQ1 and MTUNEQ3 using perfluorotributylamine (PFTBA) calibration compound.
4. Set all correction factors, including MSMSC, to zero.
5. Retune by hand any tuning parameters that were incorrectly optimized by MTUNEQ1 and MTUNEQ3.
6. In the Q3MS mode, make the tune tables for all lenses after Q2 (L31, L32, L33) flat, so that the lens voltages are constant over the entire mass range.

7. In the DAUGHTER mode, set up user tables (instead of tune tables) for lenses L31, L32 and L33. This is done in the TUNE view by typing N* (* is a number between 1 and 9) for each lens. Each table may have to be cleared (using CA) since flat tables are required. Before proceeding, recheck to make sure that all correction factors are set to zero.

8. In the Q3MS mode, make sure that all the set points for the daughter offset (DOFF) potential are approximately -2 or -3 volts. In the DAUGHTER mode, the collision offset (COFF) potential should be approximately -2 volts.

9. Using PFTBA in the DAUGHTER mode, tune lenses L31, L32 and L33 over a mass range that encompasses the mass range of the products of the ion-molecule reaction. Normally, this can be accomplished by tuning for daughters of m/z 219 (69, 131, 169, 197 and 219) using DAC scans, for each of the three lenses. Concurrently, place set points in each user table corresponding to each daughter mass.

Tuning for the specific ion-molecule reaction is then undertaken. In this example, tuning is performed for the reaction of adenine $N^{+\cdot}$ ions (m/z 135) and allyl chloride to form product ions at m/z 176.

10. In the Q1MS mode, observe the peak shape and intensity of the adenine molecular ion (m/z 135). For suitable ion-molecule reactions, the m/z 135 intensity should at least be comparable to the intensities typically observed for air (m/z 28) and water (m/z 18).

11. In the DAUGHTER mode (daughters of m/z 135), introduce allyl chloride into Q2 via a leak valve until the peak at m/z 176 is maximized.
12. Using DAC scans in the DAUGHTER mode, tune lenses L31, L32 and L33 for m/z 176. Concurrently, place set points in each user table corresponding to the product ion mass.
13. If necessary, in the DAUGHTER mode optimize the collision offset potential for the ion-molecule reaction using DAC scans.
14. Repeat steps 10-13 for each combination of parent and product ions.
15. Save the final tune table file.

The following procedures outline the steps required to tune the TSQ70 mass spectrometer for ion trapping in the collision cell. The method was developed by Anthony P. Annacchino.

Note: The tune table file should be saved (under a name other than INIT) periodically during the tuning process to insure that the file is not lost.

1. Check RF TUNE and coarse calibration, and tune if necessary.
2. Using PPOLN, PPOLR, DPOLN and DPOLR, set the polarities of Q1 and Q3 for maximum ion transmission.
3. Set the prescan settling time (SETTIM) to 0.0001 second.
4. Tune Q1 and Q3 normally with MTUNEQ1 and MTUNEQ3 using perfluorotributylamine (PFTBA) calibration compound.

5. Set all correction factors, including MSMSC, to zero.

6. Set user outputs 1 and 2 (UO1 and UO2) to 2 volts. This is done so that the lens L31 control circuit is protected.

7. Retune by hand any tuning parameters that were incorrectly optimized by MTUNEQ1 and MTUNEQ3. In particular, make sure that the mass resolution and calibration values are satisfactory.

8. In the Q3MS mode, make the tune tables for all lenses after Q2 (L31, L32, L33) flat, so that the lens voltages are constant over the entire mass range.

9. In the DAUGHTER mode, set up user tables (instead of tune tables) for lenses L31, L32 and L33. This is done in the TUNE view by typing N* (* is a number between 1 and 9) for each lens. Each table may have to be cleared (using CA) since flat tables are required. Before proceeding, recheck to make sure that all correction factors are set to zero.

10. In the Q3MS mode, make sure that all the set points for the daughter offset (DOFF) potential are approximately -2 or -3 volts. In the DAUGHTER mode, the collision offset (COFF) potential should be approximately -2 volts.

11. Using PFTBA in the DAUGHTER mode, tune lenses L32 and L33. This is accomplished by tuning for daughters of m/z 219 (69, 131, 169, 197 and 219) using DAC scans, for each lens. Concurrently, place set points in each user table corresponding to each daughter mass.

12. Set lens L31 to a flat -10 volts without using any set points. In order for TTRAPTUNE to run correctly, set points must not be used when setting the lens L31 voltage.

13. Determine whether or not helium buffer gas will be used for Q2 ion trapping. If buffer gas is being used, leak helium into the collision cell at an indicated pressure of approximately 6 mTorr.

14. Run the tuning procedure TTRAPTUNE. This procedure sets the correct collision offset potential and optimizes lenses L22 and L23 for Q2 ion trapping. The procedure takes several minutes to run.

15. Recheck mass resolution and calibration and adjust if necessary.

16. Save the final tune table file.

APPENDIX B
INSTRUMENT CONTROL LANGUAGE (ICL) PROCEDURES USED TO FACILITATE TUNING FOR ION TRAPPING IN THE COLLISION CELL OF THE TSQ70

The following ICL procedures were written by Anthony P. Annacchino to optimize the potentials applied to lenses L22 and L23 under Q2 ion trapping conditions. TTRAPOPT performs the optimizations for one m/z of interest while TTRAPTUNE automatically optimizes lenses L22 and L23 for multiple ions of PFTBA calibration compound.

```
TTRAPOPT.ICL
#Written by Tony Annacchino on 7/8/92.
#This program optimizes lenses L22 and L23 for ion trapping
#in Q2.  The user may specify whether or not helium buffer
#gas is being used.  The program accepts one variable as the
#mass of interest.
IF %1=0;%1=69;END;TMASS=%1
REPEAT 200;BEEP;END
.#Please make sure that the L31 control circuit is on.
DOZE(2)
DAU(TMASS);INL23=0;URESP=0
WHILE (URESP=0)
  DOZE (2);BEEP;BEEP
  .#Is He being used in Q2? --> type .HELIUM or .NOHELIUM
END
TOPT1;OFF
GO;STOP;REPEAT 100;BEEP;END
..#L22 and L23 are optimized for Q2 trapping of m/z;.TMASS
ABORT
```

```
TTRAPTUNE.ICL
#Written by Tony Annacchino on 7/10/92.
#This program optimizes lenses L22 and L23 for ion trapping
#in Q2 for several masses. The user may specify whether
#or not helium buffer gas is being used.
REPEAT 200:BEEP:END
.#Please make sure that the L31 control circuit is on.
DOZE(2)
DAU;INL23=0;URESP=0
WHILE (URESP=0)
  DOZE (2);BEEP:BEEP
  .#Is He being used in Q2? --> type .HELIUM or .NOHELIUM
END
TL31=L31:IEMULT=EMULT:CLR(20,1):CLR(15,1)
TTRAPMASS
OFF;GO;STOP:REPEAT 100:BEEP:END
..#L22 and L23 have been optimized for Q2 trapping
ABORT
```

The following ICL procedure was written by Anthony P. Annacchino and is a subprogram of TTRAPOPT.

```
TOPT1.ICL
#Written by Tony Annacchino on 7/8/92.
#This is a subroutine of TTRAPOPT.
SN=0;PROF;SM=TMASS;FM=(TMASS-.1);LM=(TMASS+.1);ST=.01
UO2=.5;TL23=L23:TL31=L31:PL23=50:L31=45:UO1=5.3
GO;STOP;DDOFF;MAXL22=0;MAXNL23=0;HITEMAX=0
NL23=INL23;L22=-190:HIGHL22=20:L22INC=10
TL22
L22=MAXL22;NL23=MAXNL23;THEIGHT=HITEMAX
TEMULT
NL23=INL23;L22=-190:HIGHL22=20:L22INC=5
TL22
L22=MAXL22;NL23=-10:HIGHNL23=10;NL23INC=.2
TNL23
NL23=MAXNL23;L22=(MAXL22-20);HIGHL22=(MAXL22+20);L22INC=.5
TL22
L22=MAXL22;NL23=(MAXNL23-2);HIGHNL23=(MAXNL23+2);NL23INC=.1
```

```
TNL23
L22=MAXL22;L23=MAXNL23  #SET L22 AND L23 TO OPTIMUM VALUES
L31=TL31;UO1=2;UO2=2;DDON
RETURN
```

The following ICL procedures were written by Anthony P. Annacchino and are subprograms of TTRAPTUNE.

```
TTRAPMASS.ICL
#Written by Tony Annacchino on 7/10/92.
#This is a subroutine of TTRAPTUNE.
TMASS=69;TOPT2
TMASS=131;TOPT2
TMASS=219;TOPT2
TMASS=414;TOPT2
TMASS=502;TOPT2
L31=TL31;UO1=2;UO2=2;DDON
RETURN
```

```
TOPT2.ICL
#Written by Tony Annacchino on 7/10/92.
#This is a subroutine of TTRAPMASS.
SN=0;PROF;SM=TMASS;FM=(TMASS-.1);LM=(TMASS+.1);ST=.01
UO2=.5;PL23=50;L31=45;UO1=5.3
GO;STOP;DDOFF;MAXL22=0;MAXNL23=0;HITEMAX=0
NL23=INL23;L22=-190;HIGHL22=20;L22INC=10
TL22
L22=MAXL22;NL23=MAXNL23;THEIGHT=HITEMAX
TEMULT
NL23=INL23;L22=-190;HIGHL22=20;L22INC=5
TL22
L22=MAXL22;NL23=-10;HIGHNL23=10;NL23INC=.2
TNL23
NL23=MAXNL23;L22=(MAXL22-20);HIGHL22=(MAXL22+20);L22INC=.5
TL22
L22=MAXL22;NL23=(MAXNL23-2);HIGHNL23=(MAXNL23+2);NL23INC=.1
TNL23
LTAB(20,TMASS)=MAXL22;LTAB(15,TMASS)=MAXNL23
```

```
EMULT=IEMULT:HITEMAX=0:NL23=INL23
RETURN
```

The following ICL procedures were written by Anthony P. Annacchino and are subprograms of both TTRAPOPT and TTRAPTUNE.

```
HELIUM.ICL
#Written by Tony Annacchino on 7/6/92.
#This is a subroutine of several programs.
#It sets COFF and EMULT for trapping conditions with
#helium buffer gas.
URESP=1
.#Optimizing L22 and L23 for Q2 trapping with helium.
COFF=-6:INL23=-3
ECURR=200:EMULT=600
RETURN
```

```
NOHELIUM.ICL
#Written by Tony Annacchino on 7/6/92.
#This is a subroutine of several programs.
#It sets COFF and EMULT for trapping conditions without
#helium buffer gas.
URESP=1
.#Optimizing L22 and L23 for Q2 trapping without helium.
COFF=-2:INL23=0
ECURR=200:EMULT=1000
RETURN
```

```
TL22.ICL
#Written by Tony Annacchino on 7/8/92.
#This is a subroutine of several programs.
N=1
WHILE L22<HIGHL22
  DOZE(.1) #FILL Q2 WITH IONS
  L23=PL23:GO:STOP  #CLOSE FRONT DOOR TO Q2
  DOZE(0)  #TRAP IONS IN Q2 BRIEFLY
  UO2=10:GO:STOP  #EMPTY Q2 AND DETECT ION PULSE
```

```
  IF HEIGHT>HITEMAX
    MAXL22=L22:MAXNL23=NL23:HITEMAX=HEIGHT
  END
  IF N=1:HITEMAX=0:N=2:END
  TQ2RF=CRFP:CRFP=100:GO:STOP:CRFP=TQ2RF:GO:STOP
  UO2=.5:L22=(L22+L22INC):L23=NL23:GO:STOP
                    #BEGIN FILLING Q2
END
RETURN


TEMULT.ICL
#Written by Tony Annacchino on 7/8/92.
#This is a subroutine of several programs.
N=1
WHILE THEIGHT<50000000
  DOZE(.1) #FILL Q2 WITH IONS
  L23=PL23:GO:STOP  #CLOSE FRONT DOOR TO Q2
  DOZE(0)  #TRAP IONS IN Q2 BRIEFLY
  UO2=10:GO:STOP  #EMPTY Q2 AND DETECT ION PULSE
  THEIGHT=HEIGHT
  IF N=1:THEIGHT=0:N=2:END
  EMULT=EMULT+50:DOZE(.2)
  IF EMULT>1750:THEIGHT=60000000:END
  TQ2RF=CRFP:CRFP=100:GO:STOP:CRFP=TQ2RF:GO:STOP
  UO2=.5:L23=NL23:GO:STOP  #BEGIN FILLING Q2
END
RETURN


TNL23.ICL
#Written by Tony Annacchino on 7/8/92.
#This is a subroutine of several programs.
N=1
WHILE NL23<HIGHNL23
  DOZE(.1) #FILL Q2 WITH IONS
  L23=PL23:GO:STOP  #CLOSE FRONT DOOR TO Q2
  DOZE(0)  #TRAP IONS IN Q2 BRIEFLY
  UO2=10:GO:STOP  #EMPTY Q2 AND DETECT ION PULSE
  IF HEIGHT>HITEMAX
    MAXL22=L22:MAXNL23=NL23:HITEMAX=HEIGHT
  END
  IF N=1:HITEMAX=0:N=2:END
  TQ2RF=CRFP:CRFP=100:GO:STOP:CRFP=TQ2RF:GO:STOP
```

```
  UO2=.5:NL23=(NL23+NL23INC):L23=NL23:GO:STOP
                    #BEGIN FILLING Q2
END
RETURN
```

APPENDIX C
INSTRUMENT CONTROL LANGUAGE (ICL) PROCEDURES USED TO PERFORM ION TRAPPING IN THE COLLISION CELL OF THE TSQ70

The following ICL procedures were written by Anthony P. Annacchino to perform ion trapping in the collision cell of the TSQ70 mass spectrometer. Each procedure is somewhat different as indicated in the program comments and the main text of the dissertation.

```
TQ2FILL5F.ICL
#Written by Tony Annacchino on 4/9/92.
#This is a generic trapping program.  It allows control of
#all trapping parameters such as ion m/z that is trapped
#(SM, FM, LM), collision offset (COFF), PROF or CENT data,
#scan time (ST), fill time (FT), trap time (TT), Q3DC on or
#off (DDON, DDOFF) and entrance and exit lens voltages (PL23,
#PL31, NL23, NL31).  Parameters are set to default values, but
#may be changed at any time on the fly.
SN=0:PROF:DAU:SM=69:FM=68.5:LM=69.5:ST=.01:COFF=-6
FT=.1:TT=0:TL23=L23:TL31=L31:PL23=40:PL31=25:NL23=L23
ISOURCE 1:NL31=L31:L31=PL31:GO:STOP:DDOFF
WHILE EMULT>200
  DOZE(FT)  #FILL Q2 WITH IONS
  L23=PL23:GO:STOP   #CLOSE FRONT DOOR TO Q2
  DOZE(TT)  #TRAP IONS IN Q2
  ISOURCE 2:L31=NL31:GO:STOP  #EMPTY Q2 AND DETECT ION PULSE
  ISOURCE 1:L31=PL31:L23=NL23:GO:STOP  #BEGIN FILLING Q2
END:L31=TL31:L23=TL23  #RESET LENSES TO TUNE TABLE VALUES
..#DONE
OFF:ASTOP:GO:STOP:ABORT
```

```
TQ2FILL5H.ICL
#Written by Tony Annacchino on 4/30/92.
#This is a generic trapping program.  It allows control of
#all trapping parameters such as ion m/z that is trapped
#(SM, TFM, TLM), collision offset (COFF), PROF or CENT data,
#scan time (ST), fill time (FT), trap time (TT), Q3DC on or
#off (DDON,DDOFF) and entrance lens voltages (PL23, NL23).
#Exit lens voltages are set in the tune table.  Parameters
#are set to default values, but may be changed at any time.
SN=0;PROF;DAU;SM=69;TFM=68.5;TLM=69.5;ST=.01;COFF=-6
FT=.1;TT=0;TL23=L23;PL23=40;NL23=L23
ISOURCE 1:PFM=10:PLM=11:GO(PFM,PLM);STOP;DDOFF
WHILE EMULT>200
  DOZE(FT)  #FILL Q2 WITH IONS
  L23=PL23:GO:STOP   #CLOSE FRONT DOOR TO Q2
  DOZE(TT)  #TRAP IONS IN Q2
  ISOURCE 2:GO(TFM,TLM):STOP  #EMPTY Q2 AND DETECT ION PULSE
  ISOURCE 1;L23=NL23;GO(PFM,PLM);STOP  #BEGIN FILLING Q2
END;L23=TL23  #RESET LENSES TO TUNE TABLE VALUES
..#DONE
OFF;ASTOP;GO;STOP;ABORT


TQ2FILL5I.ICL
#Written by Tony Annacchino on 5/13/92.
#This is a generic trapping program.  It allows control of
#all trapping parameters such as ion m/z that is trapped
#(SM, FM, LM), collision offset (COFF), PROF or CENT data,
#scan time (ST), fill time (FT), trap time (TT), Q3DC on or
#off (DDON, DDOFF) and entrance lens voltages (PL23, NL23).
#Parameters are set to default values, but may be changed at
#any time on the fly.  L31 is controlled by an external
#circuit where "L31" controls L31 except during the scan
#where the ion pulse is detected, where "UO1" controls L31.
#These parameters must be calibrated to L31.
#The subroutine T5ISUB actually contains the code for this
#entire program.
T5ISUB
OFF:ASTOP;GO;STOP;ABORT


TQ2FILL5K.ICL
#Written by Tony Annacchino on 7/3/92.
#This is a generic trapping program.  It allows control of
```

```
#all trapping parameters such as ion m/z that is trapped
#(SM, FM, LM), collision offset (COFF), PROF or CENT data,
#scan time (ST), fill time (FT), trap time (TT), Q3DC on or
#off (DDON, DDOFF) and entrance lens voltages (PL23, NL23).
#CRFP is pulsed to +100V to flush ions out of Q2 between
#successive cycles.
#Parameters are set to default values, but may be changed at
#any time on the fly.  L31 is controlled by an external
#circuit where "L31" controls L31 except during the scan
#where the ion pulse is detected, where "UO1" controls L31.
#These parameters must be calibrated to L31.
#The subroutine T5KSUB actually contains the code for this
#entire program.
T5KSUB
OFF;ASTOP;GO;STOP;ABORT
```

The following ICL procedures were written by Anthony P. Annacchino and are subprograms of TQ2FILL5I and TQ2FILL5K, respectively.

```
T5ISUB.ICL
#Written by Tony Annacchino on 5/13/92.
#This is a subroutine of TQ2FILL5I.  See that program for
#details.
SN=0;UCLR;PROF;DAU;SM=69;FM=68.9;LM=69.1;ST=.01;COFF=-6
UO2=.5;FT=.1;TT=0;TL23=L23;TL31=L31;PL23=50;NL23=L23
ISOURCE 1;L31=45;UO1=5.3;GO;STOP;DDON;N1=1
WHILE EMULT>200
  DOZE(FT)  #FILL Q2 WITH IONS
  L23=PL23;GO;STOP   #CLOSE FRONT DOOR TO Q2
  DOZE(TT)  #TRAP IONS IN Q2
  UO2=10;ISOURCE 2;GO;STOP  #EMPTY Q2 AND DETECT ION PULSE
  ULIST N1,1 = SN;ULIST N1,2 = TIC;N1=N1+1
  UO2=.5;ISOURCE 1;L23=NL23;GO;STOP  #BEGIN FILLING Q2
END;L31=TL31;L23=TL23  #RESET LENSES TO TUNE TABLE VALUES
UO1=2;UO2=2
RETURN
```

```
T5KSUB.ICL
#Written by Tony Annacchino on 7/3/92.
#This is a subroutine of TQ2FILL5K.  See that program for
#details.
SN=0:PROF:DAU:SM=69:FM=68.9:LM=69.1:ST=.01:COFF=-6
UO2=.5:FT=.1:TT=0:TL23=L23:TL31=L31:PL23=50:NL23=L23
ISOURCE 1:L31=45:UO1=5.3:GO:STOP:DDON
WHILE EMULT>200
  DOZE(FT)  #FILL Q2 WITH IONS
  L23=PL23:GO:STOP   #CLOSE FRONT DOOR TO Q2
  DOZE(TT)  #TRAP IONS IN Q2
  UO2=10:ISOURCE 2:GO:STOP  #EMPTY Q2, DETECT ION PULSE
  ISOURCE 1:TQ2RF=CRFP:CRFP=100:GO:STOP:CRFP=TQ2RF:GO:STOP
  UO2=.5:L23=NL23:GO:STOP  #BEGIN FILLING Q2
END:L31=TL31:L23=TL23  #RESET LENSES TO TUNE TABLE VALUES
UO1=2:UO2=2
RETURN
```

The following ICL procedure and subprogram were written by Anthony P. Annacchino to successively vary the trapping time for an experiment performed under Q2 ion trapping conditions.

```
TVARTT.ICL
#Written by Tony Annacchino on 5/15/92.
#This program varies the trapping time (TT) for a CID or
#ion-molecule rxn in Q2.  It accepts variables for the set
#mass (%1), the daughter mass (%2), the fill time (%3), the
#initial trapping time (%4), and the final trap time (%5).
#It calls a subroutine (TVARTTSUB) which actually controls
#most of the experiment.
IF %1=0; %1=219; END
IF %2=0; %2=131; END
IF %3=0; %3=0.2; END
IF %4=0; %4=0; END
IF %5=0; %5=1; END
SN=0:CENT:DAU:SM=%1:TDAU=%2:FM=SM-.1:LM=SM+.1:ST=.01
COFF=-6:UO2=.5:FT=%3:TT=%4:FTT=%5:TL23=L23:TL31=L31
PL23=50:NL23=L23:ISOURCE 1:L31=45:UO1=5.3
```

```
TVARTTSUB
OFF:ASTOP:GO:STOP:ABORT


TVARTTSUB.ICL
#Written by Tony Annacchino on 5/15/92.
#This is a subroutine of TVARTT.  See TVARTT for details.
#This program alternates b/w scanning over the set mass and
#the daughter mass.
GO:STOP:DDON:UCLR:N1=1
WHILE TT<FTT+0.01
  N2=2:ULIST N1.1 = TT
  WHILE N2<4
    DOZE(FT) #FILL Q2 WITH IONS
    L23=PL23:GO:STOP #CLOSE FRONT DOOR TO Q2
    DOZE(TT) #TRAP IONS IN Q2
    UO2=10:ISOURCE 2:GO:STOP #EMPTY Q2 AND DETECT IONS
    ULIST N1.N2 = TIC:UO2=0.5:ISOURCE 1
    TQ2RF=CRFP:CRFP=100:GO:STOP:CRFP=TQ2RF:GO:STOP
    IF N2=2:FM=TDAU-.1:LM=TDAU+.1
    ELSE:FM=SM-.1:LM=SM+.1:END
    L23=NL23:N2=N2+1:GO:STOP #BEGIN FILLING Q2
  END:TT=TT+.02:N1=N1+1
END:L31=TL31:L23=TL23:UO1=2:UO2=2
RETURN
```

The following ICL procedure and subprogram were written by Anthony P. Annacchino to successively vary the scan range for an experiment performed under Q2 ion trapping conditions to obtain a full-scan mass spectrum.

```
TVARSR.ICL
#Written by Tony Annacchino on 2/9/93.
#This program varies the scan range for a CID or ion-
#molecule rxn in Q2.  It accepts variables for the set
#mass (%1), the first daughter mass (%2), the last
#daughter mass (%3), the fill time (%4), and the trapping
#time (%5).  It calls a subroutine (TVARSRSUB) which
#controls some of the experiment.
```

```
IF %1=0; %1=219; END
IF %2=0; %2=20; END
IF %3=0; %3=400; END
IF %4=0; %4=.1; END
IF %5=0; %5=.2; END
SN=0;CENT;DAU;SM=%1;FDAU=%2;FM=FDAU-.5
LM=FDAU+.5;LDAU=%3
ST=.01;COFF=-6;UO2=.5;FT=%4;TT=%5;TL23=L23;TL31=L31
PL23=50;NL23=L23;ISOURCE 1;L31=45;UO1=5.3
TVARSRSUB
OFF;ASTOP;GO;STOP;ABORT


TVARSRSUB.ICL
#Written by Tony Annacchino on 2/9/93.
#This is a subroutine of TVARSR.  See TVARSR for details.
GO;STOP;DDON
WHILE FDAU<LDAU+.1
  DOZE(FT) #FILL Q2 WITH IONS
  L23=PL23;GO;STOP #CLOSE FRONT DOOR TO Q2
  DOZE(TT) #TRAP IONS IN Q2
  UO2=10;ISOURCE 2;GO;STOP #EMPTY Q2 AND DETECT IONS
  ISOURCE 1;TQ2RF=CRFP;CRFP=100;GO;STOP;CRFP=TQ2RF;GO;STOP
  UO2=0.5;FDAU=FDAU+1;FM=FDAU-.5;LM=FDAU+.5
  L23=NL23;GO;STOP #BEGIN FILLING Q2
END;L31=TL31;L23=TL23;UO1=2;UO2=2
RETURN
```

LITERATURE CITED

1. Freeman, J.A. Ph.D. Dissertation, University of Florida, 1991.

2. Hermens, J.; Busser, F.; Leeuwanch, P.; Musch, A. *Toxicol. Environ. Chem.* **1985**, *9*, 219-236.

3. Agarwal, S.C.; Van Duren, B.L.; Solomon, J.J.; Kline, S.A. *Environ. Sci. Technol.* **1980**, *14*, 1249-1253.

4. Chen, A.M.; Carlson, R.E. *Anal. Chem.* **1981**, *53*, 1001-1006.

5. Gothe, R.; Calleman, C.J.; Ehrenberg, L.; Wachtmeister, C.A. *Ambio* **1974**, *3*, 234-236.

6. Devanesan, P.D.; RamaKrishna, N.V.S.; Todorovic, R.; Rogan, E.G.; Cavalieri, E.L.; Jeong, H.; Jankowiak, R.; Small, G.J. *Chem. Res. Toxicol.* **1992**, *5*, 302-309.

7. Schram, K.H. *Trends Anal. Chem.* **1988**, *7*, 28-32.

8. Tondeur, Y.; Moschel, R.C.; Dipple, A.; Koepke, S.R. *Anal. Chem.* **1988**, *58*, 1316-1324.

9. Crow, F.W.; Tomer, K.B.; Gross, M.L.; McCloskey, J.A.; Bergstrom, D.E. *Anal. Biochem.* **1984**, *139*, 243-262.

10. Cavalieri, E.L.; Rogan, E.G.; Devanesan, P.D.; Cremonesi, P.; Cerny, R.L.; Gross, M.L.; Bodell, W.J. *Biochemistry* **1990**, *29*, 4820-4827.

11. Annan, R.S.; Giese, R.W.; Vouros, P. *Anal. Biochem.* **1990**, *191*, 86-95.

12. Bryant, M.S.; Lay, J.O. Jr.; Chiarelli, M.P. *J. Am. Soc. Mass Spectrom.* **1992**, *3*, 360-371.

13. Aberth, W.; Straub, K.W.; Burlingame, A.L. *Anal. Chem.* **1982**, *54*, 2029-2034.

14. Hardin, E.D.; Fan, T.P.; Blakely, C.R.; Vestal. M.L. *Anal.Chem.* **1984**, *56*, 2-7.

15. Wolf, S.M.; Vournos, P.; Norwood, C.; Jackim, E. *J. Am. Soc. Mass Spectrom.* **1992**, *3*, 757-761.

16. Teffera, Y.; Baird, W.M.; Smith, D.L. *Anal. Chem.* **1991**, *63*, 453-456.

17. Rogan, E.G.; Cavalieri, E.L.; Tibbels, S.R.; Cremonesi, P.; Warner, C.D.; Nagel, D.L.; Tomer, K.B.; Cerny, R.L.; Gross, M.L. *J. Amer. Chem. Soc.* **1988**, *110*, 4023-4029.

18. RamaKrishna, N.V.S.; Gao, F.; Padmavathi, N.S.; Cavalieri, E.L.; Rogan, E.G.; Cerny, R.L.; Gross, M.L. *Chem. Res. Toxicol.* **1992**, *5*, 293-302.

19. RamaKrishna, N.V.S.; Cavalieri, E.L.; Rogan, E.G.; Dolnikowski, G.; Cerny, R.L.; Gross, M.L.; Jeong, H.; Jankowiak, R.; Small, G.J. *J. Am. Chem. Soc.* **1992**, *114*, 1863-1874.

20. Davioli, E.; Cerny, R.L.; Gross, M.L. *Adv. Mass Spectrom.* **1989**, *11A*, 268-269.

21. Yost, R.A.; Enke, C.G.; McGilvery, D.C.; Smith, D.; Morrison, J.D. *Int. J. Mass Spectrom. Ion Phys.* **1979**, *30*, 127-136.

22. McLuckey, S.A. *J. Am. Soc. Mass Spectrom.* **1992**, *3*, 599-614.

23. Porter, C.J.; Proctor, C.J.; Beynon, J.H. *Org. Mass Spectrom.* **1981**, *16*, 62-67.

24. van Koppen, P.A.M.; Illies, A.J.; Liu, S.; Bowers, M.T. *Org. Mass Spectrom.* **1982**, *17*, 399-402.

25. Schroder, E. *Org. Mass Spectrom.* **1989**, *24*, 205-210.

26. Kostiainen, R. *Biomed. Environ. Mass Spectrom.* **1989**, *18*, 116-121.

27. Meyerhoffer, W.J.; Bursey, M.M. *Org. Mass Spectrom.* **1989**, *24*, 169-175.

28. Meyerhoffer, W.J.; Bursey, M.M. *Org. Mass Spectrom.* **1989**, *24*, 246-252.

29. Dolnikowski, G.G.; Allison, J.; Watson, J.T. *Org. Mass Spectrom.* **1990**, *25*, 119-123.

30. White, E.L.; Bursey, M.M. *Biomed. Environ. Mass Spectrom.* **1989**, *18*, 413-415.

31. Pachuta, R.R.; Kenttämaa, H.I.; Cooks, R.G.; Zennie, T.M.; Ping, C.; Chang, C.; Cassady, J.M. *Org. Mass Spectrom.* **1988**, *23*, 10-15.

32. Kinter, M.T.; Bursey, M.M. *Biomed. Environ. Mass Spectrom.* **1988**, *15*, 583-588.

33. Busch, K.L.; Kruger, T.L.; Cooks, R.G. *Anal. Chim. Acta* **1980**, *119*, 153-156.

34. Berberich, D.W.; Hail, M.E.; Johnson, J.V.; Yost, R.A. *Int. J. Mass Spectrom. Ion Proc.* **1989**, *94*, 115-147.

35. Hail, M.E.; Berberich, D.W.; Yost, R.A. *Anal. Chem.* **1989**, *61*, 1874-1879.

36. Schmit, J.P.; Dawson, P.H.; Beaulieu, N. *Org. Mass Spectrom.* **1985**, *20*, 269-275.

37. Fetterolf, D.D. Ph.D. Dissertation, University of Florida, 1983.

38. Schmit, J.P.; Beaudet, S.; Brisson, A. *Org. Mass Spectrom.* **1986**, *21*, 493-498.

39. Heath, T.G.; Allison, J.; Watson, J.T. *J. Am. Soc. Mass Spectrom.* **1991**, *2*, 270-277.

40. Freeman, J.A.; Johnson, J.V.; Hail, M.E.; Yost, R.A.; Kuehl, D.W. *J. Amer. Soc. Mass Spectrom.* **1990**, *1*, 110-115.

41. Eder, E.; Henschler, D.; Neudecker, T. *Xenobiotica* **1982**, *12*, 831-848.

42. Ames, B.N. *Science* **1979**, *204*, 587-592.

43. Stafford, G.C.; Kelley, P.E.; Syka, J.E.P.; Reynolds, W.E.; Todd, J.F.J. *Int. J. Mass Spectrom. Ion. Proc.* **1984**, *60*, 85-98.

44. Louris, J.N.; Cooks, R.G.; Syka, J.E.P.; Kelley, P.E.; Stafford, G.C.; Todd, J.F.J. *Anal. Chem.* **1987**, *59*, 1677-1685.

45. Cooks, R.G.; Kaiser, R.E. *Acc. Chem. Res.* **1990**, *23*, 213-219.

46. Lawson, G.; Todd, J.F.J. *Chem. Brit.* **1972**, *8*, 373-380.

47. Campana, J.E. *Int. J. Mass Spectrom. Ion Phys.* **1980**, *33*, 101-117.

48. Miller, P.E.; Denton, M.B. *J. Chem. Ed.* **1986**, *63*, 617-622.

49. Wanczek, K.P. *Int. J. Mass Spectrom. Ion Proc.* **1984**, *60*, 11-60.

50. Gross, M.L.; Rempel, D.L. *Science* **1984**, *226*, 261-268.

51. Yost, R.A. *Triple Quadrupole MS/MS for Mixture Analysis*, proposal to the National Science Foundation, 1982.

52. Beaugrand, C.; Devant, G.; Jaouen, D.; Mestdagh, H.; Rolando, C. *Proceedings of the 35th ASMS Conference on Mass Spectrometry and Allied Topics* **1987**, 345-346.

53. Beaugrand, C.; Devant, G.; Jaouen, D.; Mestdagh, H.; Rolando, C. *Spectros. Int. J.* **1987**, *5*, 265-272.

54. Beaugrand, C.; Devant, G.; Jaouen, D.; Mestdagh, H.; Rolando, C. *Proceedings of the 36th ASMS Conference on Mass Spectrometry and Allied Topics* **1988**, 811-812.

55. Beaugrand, C.; Jaouen, D.; Mestdagh, H.; Rolando, C. *Anal. Chem.* **1989**, *61*, 1447-1453.

56. Dolnikowski, G.G.; Kristo, M.J.; Enke, C.G.; Watson, J.T. *Int. J. Mass Spectrom. Ion. Proc.* **1988**, *82*, 1-15.

57. Dolnikowski, G.G.; Heath, T.G.; Watson, J.T.; Scrivens, J.H.; Rolando, C.H. *J. Am. Soc. Mass Spectrom.* **1990**, *1*, 481-488.

58. Hägg, C.; Szabo, I. *Int. J. Mass Spectrom. Ion. Proc.* **1986**, *73*, 277-294.

59. Harrison, A.G. *Chemical Ionization Mass Spectrometry*; CRC Press, Inc.: Boca Raton, Florida, 1983.

60. Cerney, R.L.; Gross, M.L.; Grotjahn, L. *Anal. Biochem.* **1986**, *156*, 424-435.

61. Cerny, R.L.; Tomer, K.B.; Gross, M.L.; Grotjahn, L. *Anal. Biochem.* **1987**, *165*, 175-182.

62. Tomer, K.B.; Gross, M.L.; Deinzer, M.L. *Anal. Chem.* **1986**, *58*, 2527-2534.

63. Covey, T.R.; Bonner, R.F.; Shushan, B.I.; Henion, J.D. *Rapid Commun. Mass Spectrom.* **1988**, *2*, 249-256.

64. Smith, R.D.; Loo, J.A.; Edmonds, C.G.; Barinaga, C.J.; Udseth, H.R. *Anal. Chem.* **1990**, *62*, 882-899.

65. McLuckey, S.A.; Van Berkel, G.J.; Glish, G.L. *J. Am. Soc. Mass Spectrom.* **1992**, *3*, 60-70.

66. Hettich, R.L.; Buchanan, M.V. *J. Am. Soc. Mass Spectrom.* **1991**, *2*, 402-412.

67. Spengler, B.; Pan, Y.; Cotter, R.J.; Kan, L.-S. *Rapid Commun. Mass Spectrom.* **1990**, *4*, 99-102.

68. Huth-Fehre, T.; Gosine, J.N.; Wu, K.J.; Becker, C.H. *Rapid Commun. Mass Spectrom.* **1992**, *6*, 209-213.

69. Subba Rao, S.C.; Fenselau, C. *Anal. Chem.* **1978**, *50*, 511-515.

70. Allgood, C.; Ma, Y.-C.; Munson, B. *Anal. Chem.* **1991**, *63*, 721-725.

71. Hail, M.E. Ph.D. Dissertation, University of Florida, 1989.

72. Abbatt, J.A.; Harrison, A.G. *Org. Mass Spectrom.* **1986**, *21*, 557-563.

73. Lias, S.G.; Bartmess, J.E.; Liebman, J.F.; Holmes, J.L.; Levin, R.D.; Mallard, W.G. *J. of Phys. and Chem. Reference Data*; Lide, D.R. Jr., Ed.; **1988**, *17*, Supplement 1.

74. Fasman, G.D., Ed. *Handbook of Biochemistry and Molecular Biology, Physical and Chemical Data*, Volume 1, 3rd Edition; CRC Press, Inc.: Cleveland, Ohio, 1976; pp 330-331.

75. van Sittert, N.J. In *Monitoring Human Exposure to Carcinogenic and Mutagenic Agents*; Berlin, A.; Draper, M.; Hemminki, K.; Vainio, H., Eds.; IARC Scientific Publications: Lyons, France, 1983; pp 153-168.

76. Montesano, R. *J. Supramol. Structure Cellular Biochem.* **1981**, *17*, 259-273.

77. Coopersmith, B.I.; Yost, R.A., unpublished results, **1993**.

78. Syka, J.E.P.; Schoen, A.E.; Ceja, P.C.; Smith, R.M. *Proceedings of the 34th ASMS Conference on Mass Spectrometry and Allied Topics* **1986**, 718-719.

79. Syka, J.E.P.; Schoen, A.E. *Int. J. Mass Spectrom. Ion. Proc.* **1990**, *96*, 97-109.

80. Szabo, I. *Int. J. Mass Spectrom. Ion. Proc.* **1986**, *73*, 197-235.

81. Hägg, C.; Szabo, I. *Int. J. Mass Spectrom. Ion. Proc.* **1986**, *73*, 237-275.

82. Hägg, C.; Szabo, I. *Int. J. Mass Spectrom. Ion. Proc.* **1986**, *73*, 295-312.

83. Syka, J.E.P.; Szabo, I. *Proceedings of the 36th ASMS Conference on Mass Spectrometry and Allied Topics* **1988**, 1328-1329.

84. Davis, S.C.; Wright, B. *Rapid Commun. Mass Spectrom.* **1990**, *4*, 186-197.

85. Dahl, D.A.; Delmore, J.E. *Proceedings of the 35th ASMS Conference on Mass Spectrometry and Allied Topics* **1987**, 257-258.

86. Dehmelt, H.G. *Advances At. Mol. Phys.* **1967**, *3*, 53-72.

87. Johnson, J.V.; Yost, R.A., unpublished results, **1987**.

88. Douglas, D.J.; French, J.B. *J. Am. Soc. Mass Spectrom.* **1992**, *3*, 398-408.

89. Kishore, M.N.; Ghosh, P.K. *Int. J. Mass Spectrom. Ion. Phys.* **1979**, *29*, 345-350.

90. Schwartz, J.C.; Cooks, R.G. *Proceedings of the 36th ASMS Conference on Mass Spectrometry and Allied Topics* **1988**, 634-635.

91. Louris, J.N.; Brodbelt-Lustig, J.S.; Kaiser, R.E.; Cooks, R.G. *Proceedings of the 36th ASMS Conference on Mass Spectrometry and Allied Topics* **1988**, 968-969.

92. Louris, J.N.; Amy, J.W.; Ridley, T.Y.; Cooks, R.G. *Int. J. Mass Spectrom. Ion. Proc.* **1989**, *88*, 97-112.

93. Pedder, R.E.; Yost, R.A.; Weber-Grabau, M. *Proceedings of the 37th ASMS Conference on Mass Spectrometry and Allied Topics* **1989**, 468-469.

94. Williams, J.D.; Reiser, H.-P.; Kaiser, R.E.; Cooks, R.G. *Int. J. Mass Spectrom. Ion. Proc.* **1991**, *108*, 199-220.

95. Franzen, J.; Gabling, R.-H. *Proceedings of the 40th ASMS Conference on Mass Spectrometry and Allied Topics* **1992**, 1009-1010.

96. Morand, K.L.; Horning, S.R.; Cooks, R.G. *Int. J. Mass Spectrom. Ion. Proc.* **1991**, *105*, 13-29.

97. Cooks, R.G.; Morand, K.L. *Proceedings of the 38th ASMS Conference on Mass Spectrometry and Allied Topics* **1990**, 1460-1461.

98. Pinkston, J.D.; Delaney, T.E.; Morand, K.L.; Cooks, R.G. *Proceedings of the 39th ASMS Conference on Mass Spectrometry and Allied Topics* **1991**, 160-161.

99. Gabling, R.-H.; Romanowski, G.; Wanczek, K.-P. *Int. J. Mass Spectrom. Ion. Proc.* **1986**, *69*, 153-162.

100. Kofel, P.; Reinhard, H.; Schlunegger, U.P. *Proceedings of the 38th ASMS Conference on Mass Spectrometry and Allied Topics* **1990**, 886-887.

101. Kofel, P.; Reinhard, H.; Schlunegger, U.P. *Proceedings of the 38th ASMS Conference on Mass Spectrometry and Allied Topics* **1990**, 1462-1463.

102. Paul, W.; Reinhard, H.P.; von Zahn, U. *Zeitschrift für Physik* **1958**, *152*, 143-182.

103. Reinsfelder, R.E.; Denton, M.B. *Int. J. Mass Spectrom. Ion Phys.* **1981**, *37*, 241-250.

104. Miller, P.E.; Denton, M.B. *Int. J. Mass Spectrom. Ion Proc.* **1990**, *96*, 17-26.

BIOGRAPHICAL SKETCH

Anthony Peter Annacchino, Jr., son of Anthony P. Annacchino and Linda L. Annacchino, was born in Syracuse, New York, on July 20, 1965. Tony grew up in Baldwinsville, New York, and graduated from Charles W. Baker High School in 1983.

From 1983 to 1987, Tony attended the State University of New York at Binghamton with a four year New York Board of Regents academic scholarship. During his time there, he spent a year performing undergraduate research under the direction of Dr. Carmen Huie. He graduated with honors in May 1988 with a B.S. degree in chemistry.

In January 1988, Tony began his graduate work in analytical chemistry at the University of Florida under the direction of Dr. Richard A. Yost. During his free time, he was a member of many jazz and R&B bands around Gainesville. In particular, he was a featured saxophone soloist with the University of Florida Jazz Band, and he received the Directors Award in April 1990.

Upon completion of his graduate studies, Tony will begin work at the Corporate Research Center of International Paper in Tuxedo, New York. He and his fiancée, Jennifer Ann Buckingham, plan to marry in the spring of 1994.

I certify that I have read this study and that in my opinion it conforms to acceptable standards of scholarly presentation and is fully adequate, in scope and quality, as a dissertation for the degree of Doctor of Philosophy.

Richard A. Yost, Chairman
Professor of Chemistry

I certify that I have read this study and that in my opinion it conforms to acceptable standards of scholarly presentation and is fully adequate, in scope and quality, as a dissertation for the degree of Doctor of Philosophy.

James D. Winefordner
Graduate Research Professor of Chemistry

I certify that I have read this study and that in my opinion it conforms to acceptable standards of scholarly presentation and is fully adequate, in scope and quality, as a dissertation for the degree of Doctor of Philosophy.

David H. Powell
Associate Scientist of Chemistry

I certify that I have read this study and that in my opinion it conforms to acceptable standards of scholarly presentation and is fully adequate, in scope and quality, as a dissertation for the degree of Doctor of Philosophy.

John R. Eyler
Professor of Chemistry

I certify that I have read this study and that in my opinion it conforms to acceptable standards of scholarly presentation and is fully adequate, in scope and quality, as a dissertation for the degree of Doctor of Philosophy.

Charles L. Beatty
Professor of Materials Science
and Engineering

This dissertation was submitted to the Graduate Faculty of the Department of Chemistry in the College of Liberal Arts and Sciences and to the Graduate School and was accepted as partial fulfillment of the requirements for the degree of Doctor of Philosophy.

December 1993

_____

Dean, Graduate School